

**CYTOKININS IN *Dictyostelium discoideum*: NEW INSIGHTS FOR EXPANDED
ROLES DURING THE LIFE CYCLE OF THE SOCIAL AMOEBAS**

A dissertation submitted to the Committee of Graduate Studies
in partial fulfillment of the requirements
for the degree of
Doctor of Philosophy
in the Faculty of Arts and Science

Trent University

Peterborough, Ontario, Canada

©Copyright by Megan Marie Aoki, 2023

Environmental and Life Sciences Ph.D. Graduate Program

May 2023

ABSTRACT

CYTOKININS IN *Dictyostelium discoideum*: NEW INSIGHTS FOR EXPANDED ROLES DURING THE LIFE CYCLE OF THE SOCIAL AMOEBEA

Megan Marie Aoki

Cytokinins (CKs) are a pervasive group of growth-promoting signaling molecules spanning every kingdom of life. Their roles are best known in plants, where they act as phytohormones controlling nearly all aspects of plant growth and development. CKs continue to be detected in new organisms, posing questions about their roles in such widespread forms of life. The research presented in this thesis, therefore, investigated CK dynamics in a non-plant system using the simple eukaryotic model, *Dictyostelium discoideum*. Prior to this thesis, CKs were established as key intercellular signals necessary for proper development of *D. discoideum* – specifically in the induction of sporulation and maintenance of spore dormancy. However, there were no documented roles of CKs prior to the late stages of multicellular development. Comprehensive mass spectrometric screening for CKs detected six novel CK forms during all stages of *D. discoideum* growth and development. Based on these findings, a model was proposed that mapped CK biosynthesis in *D. discoideum*. The CK profiles indicate that there are differing dominant CK forms during vegetative growth and early development compared to those detected during late multicellular development. This led to the hypothesis that CKs have different roles during the distinctive life cycle stages of *D. discoideum*. This hypothesis was tested by generating knockout and overexpression strains of the key, primary CK biosynthesis gene, *iptA*, to investigate potential expanded roles for CKs during growth and the early stages of *D. discoideum* development. *iptA*-deficiency resulted in cytokinesis defects and

both *iptA*-deficiency and overexpression caused altered mitochondrial morphology, dysregulated TCA cycle and amino acid metabolism, as well as increased levels of the energy metabolite, AMP. These combined phenotypes were suggestive of mitochondrial-associated dysfunction in vegetative growth and provided the first evidence of expanded roles of CKs during the *D. discoideum* life cycle. This was the first metabolomics-based evidence of CKs influencing mitochondrial function in *D. discoideum*. Lastly, a key CK-activating enzyme was functionally characterized, *DdLOG*, and additional CK biosynthesis enzymes were identified for future examination. Together, the findings of this thesis provide insights into: CK biosynthesis in a non-plant associated model; new roles for CKs during the *D. discoideum* life cycle; and CK interactions with mitochondria. The methods established as part of this thesis can be used as a foundation for characterizing further CK biosynthesis enzymes and as a guide for detecting subtle sub-cellular phenotypes related to CK metabolism in *D. discoideum* and other CK-producing organisms.

KEYWORDS: cytokinins, *D. discoideum*, cytokinin biosynthesis, mass spectrometry, metabolomics, adenylate isopentenyltransferase, IptA, Lonely Guy, CK-phosphoribohydrolase, *DdLOG*, mitochondrial-associated dysfunction

PREFACE

This thesis is presented in manuscript format. Content from Chapters 1 and 2 are derived from a published review. Chapter 3 initiates the first experimental chapter - which is also published. Chapters 4 and 5 are experimental chapters that will be submitted for publication once the thesis is finalized. Co-authors and their contributions are listed in the preface of each chapter. Permissions from copyright holders for published chapters are presented in Appendix I.

Additional publications not included in thesis

Aoki, M. M., Kisiala, A. B., Rahman, T., Morrison, E. N., and Emery, R. J. N. (2021). Cytokinins are pervasive among common in vitro culture media: An analysis of their forms, concentrations and potential sources. *J Biotechnol.* 334, 43-46. doi: 10.1016/j.jbiotec.2021.05.005.

Kisiala, A., Kambhampati, S., Stock, N. L., **Aoki, M. M.**, and Emery, R. J. N. (2019). Quantification of cytokinins using high-resolution accurate-mass orbitrap mass spectrometry and parallel reaction monitoring (PRM). *Analytical Chemistry* 91, 15049-15056. doi: 10.1021/acs.analchem.9b037.

Aoki, M. M., Seegobin, M., Kisiala, A., Noble, A., Brunetti, C., and Emery, R.J.N. (2019). Phytohormone metabolism in mammals – Cytokinins are taken up and inter-converted in HeLa cell culture. *FASEB BioAdvances.* 1, 320-331. doi: 10.1096/fba.2018-00032.

Jorge, G. L. Kisiala, A., Morrison, E., **Aoki, M. M.**, Nogueira, A. P. O., and Emery, R. J. N. (2019). Endosymbiotic *Methylobacterium oryzae* mitigates the impact of limited water availability in lentil (*Lens culinaris* Medik.) by increasing plant cytokinin levels. *Environmental and Experimental Botany.* 162: 525-540. doi: 10.1016/j.envexpbot.2019.03.028.

ACKNOWLEDGEMENTS

I have never been a person who has felt a true calling in life towards a particular career, but rather I have always been interested in everything – always wondering what career path I'd someday find myself on. In my early undergraduate career at Trent, I so fondly remember my professor Dr. Craig Brunetti (and now supervisor) discussing his research and inviting students to volunteer in his lab. Sparked by his enthusiasm, I was quick to join and to see for myself what research was all about. I quickly found myself fascinated with the unknown and the prospect of discovery. Moreover, the environment was infectious – a vibrant group of hardworking and positive individuals all striving towards something. Therefore, I decided to pursue graduate school, not solely for the level up in nerd status, but rather, for the opportunity to continue to work with so many amazing individuals. As such, I have many incredible people to acknowledge and thank for supporting me along the way.

I, first, would like to sincerely thank my three supervisors, Dr. Neil Emery, Dr. Robert Huber, and Dr. Craig Brunetti. I feel so incredibly fortunate to have you all as my supervisors. First and foremost, I will always be grateful for your genuine positivity and relentless support. Further, your diverse research backgrounds allowed me to learn a broader skillset – challenging me from different angles and ultimately providing me with a greater understanding of research as a whole. I want to thank you for the freedom and independence you granted me throughout my research, allowing me to pursue many exciting areas while also knowing when to subtly redirect my over-zealous ambitions in order to keep me on track with my current research!

Neil, I am in awe of your leadership skills and your ability to promote such a positive working environment. Your humble and unassuming manner paired with your quirky sense of humour brings out the best in each of your students. You have a way with words and an uncanny ability to break down challenging concepts in mere seconds – a skill I aspire to someday achieve. I appreciate the way you always made yourself available when I was in need of instantaneous life advice and for simply listening when I needed to talk. Lastly, a special thank you to your family members – Jill, Laurence, Frances, and Elise – for welcoming me into your home with open and warm arms. Rob, you are an inspiring researcher. I got to witness you start up the Huber Lab at Trent and to grow it successfully into what it is today – a hub for new *Dicty* enthusiasts. Your attention to detail, work-ethic, and overall scientific acumen have been an incredible example for me to follow. The way you communicate your work and captivate your audience seems effortless. But most importantly, you have always encouraged me – and for this I am so grateful. Craig, I can clearly remember your lectures as an undergraduate student, specifically your enthusiasm and excitement when explaining new and exciting research (and as mentioned earlier, this is what sparked my interest in research). You have an excitement for science that is infectious, which I have always appreciated. Your relentless approach and affinity for fine details has made me a better researcher. You have been pivotal in bettering my scientific writing and developing “the story”. The skills you have instilled in me will undoubtedly carry over into many other areas of my life. Neil, Rob, and Craig – it has been an honour to be your student. Thank you.

To the amazing past and present lab mates in the Emery, Huber, and Brunetti Labs, I owe you my sanity. I am grateful for the friendships I have made in the three labs I am a

part of, which includes a long list of amazing humans I have had the privilege of getting to know and suffer alongside while our cells control our lives. A huge thank you to the following past and present members of the Emery Lab: Mark Seegobin, Zeynab Azimychetabi, Kim (Kimchi) Molina Bean, Erin Morrison, Anna Kisiala, Peter Andreas, Ainsely Lewis, Alex Kuhne, Vedanti Ghatwala, Daniel Palberg, Emma Kaszecki, Malaika Persaud, Stacy James, Ewart Smith, Navindra Soodoo, Dev Seneviratne, Imesha Perera, Nourhene Grich, Tamzida Rahman, Jared Treverton, Benjamin Greene, Cody Butler, Hai Nguyen, Thien Nguyen, Shaojun Li, and Zhiyong Zhang. A huge thank you to the past and present members of the Huber and Brunetti Labs: Meagan McLaren, Elicia Yap, Morgan Wilson-Smillie, Aruban Thanabalasingam, Saby Mathavarajah, Adam Remtulla, Joshua Gray, William Kim, Samantha Logan, and Haley MacLeod.

I owe a special thanks to several of these individuals whose friendships I have relied on over the course of my Ph.D. To Mark Seegobin, the individual who taught me everything I know and whom I admire as a researcher and human. You have been through every step of my thesis mentoring me, making me delicious foods (along with Care of course too), out-researching me, and just overall contributing to my life in the most positive of ways. I am grateful for your friendship, and I am excited to see how your future unfolds with that bright mind of yours! To my nice girls, Zeynab Azimychetabi and Kimchi Molina Bean, thank you for coming into my life and making it explode with happiness and laughter. You two have made the last part of my thesis so incredibly joyful, and I will always cherish the memories we have made together. To Erin Morrison, one of the only individuals who could calm me when it seemed like my thesis was falling apart – you have one of the brightest minds I have ever encountered, and you are a role model to me. Thank

you for your unending support and our fun tea parties and walks. To Anna Kisiala, thank you for always being willing to talk science with me and for showing me how to become a good researcher. I will always appreciate our early days when we actually had time to go on walks and have teas. Your friendship means a lot to me, and I cannot thank you enough for all of the time you have spent training me and coaching me on how to be a better scientist and writer! To Alex Kuhne, my travel partner extraordinaire, I will always treasure our 17-day conference adventures in Europe and can't wait for the next one! To Ainsely Lewis, thank you for always checking in on me and for teaching me so much about metabolomics! To Meagan McLaren, my 'imaginary' friend, you are an absolute ray of sunshine. I am so grateful to have gotten to science beside you and turn the lab into our own doctor's office on occasion. To Philip Siambi, thank you for always helping me out with my weird equipment requests and for being a walking ray of sunshine and positivity. I will miss most definitely miss our weird hallway chats. To my Huber gang - Elicia Yap, Morgan Wilson-Smillie, and Aruban Thanabalasingam – you have literally saved my sanity, and I couldn't imagine being suffering alongside of a better group of humans. Thank you for all of our fun food runs, wildly bizarre conversations, and venting sessions. To Emilee Storfie, thank you for supporting and participating in our workaholic mentality and for always being ready to vent when our cells were not behaving. I am so proud of what you accomplished, and you have provided an immense amount of joy and free therapy sessions to me, for which I am incredibly grateful. To Saby Mathavarajah and Scott Farrow, while you don't know each other, you are both phenomenal humans and researchers. For both of you, science is your language, and you have both provided me with endless feedback and help with my research, as well as a constant supply of excessively nerdy

conversations, for which I am very grateful. To Haley MacLeod, thanks for always rooting me on from afar and checking in - you are an exceptional human and friend! To my friend, Caitlyn Battelle, thank you for not giving up on me during my lapses in communication during times when my work was consuming me. Your encouragement and regular phone calls during my commutes have kept me grounded, and I appreciate and rely on our friendship so much. I am truly grateful and humbled by the incredible friendships I have made over the course of my Ph.D.

I would also like to extend my sincere thanks to several members of the ENLS Graduate program, the Biology department, and the Graduate Office. To Linda Cardwell, my fellow equalitist - you are an inspiration and a true joy to be around. Thank you for your weekly encouragement and for making my ENLS graduate experience such a positive one. I am beyond grateful for your friendship and support! To Smolly Coulson, you have been such a positive force during my time at Trent and while TAing your courses. Thank you for teaching me how to sew, and for always helping me when I asked no matter what my question was! To Debbie Lietz and Tracy Ross, thank you for being so kind and for always being willing to help. To Angela Sikma, thank you for your life-saving knowledge regarding nitric acid and for always greeting me in the hall with a smile. To Naomi Stock, thank you for all of your technical help with mass spectrometry! To Mary Lynn Scriver and Erin Davidson thank you for your administrative support! To Jane Rennie, thank you for providing me with helpful feedback to my excessive emails and for pushing me to make each scholarship application better. You have been an invaluable support when applying to scholarships, and I owe my success to you!

Throughout the course of my Ph.D., I have been very fortunate to be supported by the Natural Sciences and Engineering Research Council of Canada, the Queen Elizabeth II Graduate Scholarship in Science and Technology, and the Environmental and Life Sciences Graduate Curtin and French American Charitable Trust Scholarships. The support received by these various sources allowed me to dedicate myself fully to my Ph.D., and I am very grateful.

I lastly want to thank my family for their constant support allowing me the ability to completely immerse myself in my research for the last five years. Without your support, none of this would have been possible, and my words cannot fully convey how beyond grateful I am to each of you for cheering me on and allowing me the opportunity to challenge and grow myself through this pursuit. To my mom, Michelle Arnoldussen, thank you for always talking me to school or home on my daily commutes and allowing me to explain my research or de-stress after a long day. You have been my biggest cheerleader, and I could not have done this without your constant showering of love and support! To my sister and her family, Hillary, Josh, Silas, and Margo Busch – you have all been my biggest encouragers! Hill, experiencing graduate school together has been so fun, despite being a country apart. Thank for always letting me vent and for celebrating my successes. I am very much so looking forward to celebrating your graduation soon! To my sister and her family – Kelley, Chris, Justine, and Eric Gravedoni – and my brothers and their families - Tyler, Megan, and Archer Arnoldussen - and Adam and Braedon Arnoldussen – thank you for always rooting for me and checking in with me – your support and love means so much to me! To Mike and Joyce Christianson, my second parents, you both mean the world to me, and I am so appreciative of your phone calls to check in and root for me along this

journey. To Uncle Kevin and Aunt Nancy Green, you have always supported me to whatever end, and I am so incredibly grateful for that – it means the world to me! To my brother-in-law and family, Naoto, Jen, Ryden, and Brynlee – thank you all for encouraging me and rooting me on – a special thanks to Rydie for participating in science adventures with me! To my in-laws, Jodi and Naomichi Aoki, you have been such a source of encouragement and I cannot thank you both enough. Your daily support has allowed me to pursue this incredibly challenging path in life – I could not have done this without your constant support and care.

To my husband and friend, Yoshi Aoki, my sincerest thank you and endless words of appreciation will never be enough to express how grateful I am for the support you have provided me with each day of this five-year endeavor. But I will try, nonetheless. For every accompanying high and low of my Ph.D., you have been there for me celebrating the successes and encouraging through the challenges. You have spent countless hours listening to me talk about my research and offering feedback on every presentation and written work. You have challenged me to communicate my research more effectively and actively participated in every part of this journey – for which I am so grateful. Thank you for being creative in ways we can spend time together while also simultaneously working at the same time. Through this all, you have been my greatest support. Thank you for your unconditional love and for continuing to love me even after my bad science days!

To my most favourite beings, Moes (my horse) and Belle Aoki (my dog), thank you for your sweet nuzzles and sloppy wet kisses of encouragement every day. Your demands for my attention were much needed to pull me out of my world of chaos and bring me back to the present!

DEDICATION

To my dad, Daniel Hilary Arnoldussen – Growing up, you always told me that “education is important” in such a quiet and matter of fact way. You were the first person to celebrate your children and grand-children’s accomplishments in school – no matter how big or small. I was able to bear witness to your incredible work ethic growing up and your relentless striving to be the best version of yourself for 17 amazing years. I owe my success in my Ph.D. to you, for gifting me with your stubbornness to succeed and to push harder in the face of challenges – a trait I learned is very necessary in the field of Molecular Biology. Through the course of my Ph.D., I heard your words in my head whenever I encountered challenges reassuring me that “education was important”, and I have come to cherish those words. I truly understand now how important education is, not solely for the acquisition of knowledge but for the character-building that comes as part of the journey.

TABLE OF CONTENTS

TITLE PAGE.....	i
ABSTRACT	ii
KEYWORDS	iii
PREFACE.....	iv
ACKNOWLEDGEMENTS	v
DEDICATION	xii
TABLE OF CONTENTS	xiii
LIST OF TABLES	xv
LIST OF FIGURES.....	xvi
LIST OF ABBREVIATIONS	xviii
 CHAPTER 1 – General introduction	
PREFACE.....	1
CYTOKININS.....	2
THE DICTYOSTELIA	5
RESEARCH OBJECTIVES.....	6
FIGURES	10
REFERENCES	12
 CHAPTER 2 – Cytokinins in Dictyostelia – A unique model for studying the functions of signaling agents from species to kingdoms	
PREFACE.....	16
ABSTRACT	17
CYTOKININS IN DICTYOSTELIA.....	18
CYTOKININ BIOSYNTHESIS AND METABOLISM	19
CK SECRETION AND TRANSLOCATION	29
CK SIGNAL TRANSDUCTION.....	31
FUTURE DIRECTIONS.....	36
CONCLUSION	39
TABLES AND FIGURES.....	41
REFERENCES	46
 CHAPTER 3 – Cytokinin detection during the <i>Dictyostelium discoideum</i> life cycle: Profiles are dynamic and affect cell growth and spore germination	
PREFACE.....	56
ABSTRACT	57
INTRODUCTION	59
MATERIALS AND METHODS	62
RESULTS.....	70
DISCUSSION.....	74
CONCLUSION	79
TABLES AND FIGURES.....	81
SUPPLEMENTARY MATERIALS	86
REFERENCES	91

CHAPTER 4 – From biosynthesis and beyond – Loss or overexpression of the cytokinin synthesis gene, *iptA*, alters cytokinesis and mitochondrial and amino acid metabolism in *Dictyostelium discoideum*

PREFACE.....	96
ABSTRACT	97
INTRODUCTION.....	99
MATERIALS AND METHODS	102
RESULTS.....	115
DISCUSSION.....	122
CONCLUSION	131
FIGURES	133
SUPPLEMENTARY MATERIALS	142
REFERENCES.....	156

CHAPTER 5 – Functional characterization of a Lonely Guy protein in *Dictyostelium discoideum*

PREFACE.....	163
ABSTRACT	164
INTRODUCTION.....	166
MATERIALS AND METHODS	168
RESULTS AND DISCUSSION.....	174
CONCLUSION	180
TABLES AND FIGURES.....	182
SUPPLEMENTARY MATERIALS	188
REFERENCES.....	190

CHAPTER 6 – General discussion

GENERAL DISCUSSION.....	195
THE <i>Dictyostelium discoideum</i> CK BIOSYNTHESIS PATHWAY.....	195
PLEIOTROPIC ROLES OF CYTOKININS	198
FUTURE DIRECTIONS.....	200
CONCLUSIONS	202
REFERENCES.....	204

APPENDIX I – Permission from copyright holders

CHAPTER 1/2.....	206
CHAPTER 3.....	207

LIST OF TABLES

Table 2.1.	Sequence similarity of equilibrative nucleoside transporter (ENT) proteins in <i>D. discoideum</i>	41
Table 3.1.	Endogenous and ² H-labeled cytokinins (CKs) scanned for by High-performance liquid chromatography-positive electrospray ionization-high resolution tandem mass spectrometry (HPLC-(ESI+)-HRMS/MS) in <i>Dictyostelium discoideum</i> intracellular (IC) and extracellular (EC) samples	81
Table 5.1.	Free base (FB) products and their respective labeled internal standard compounds scanned for by high-performance liquid chromatography-positive electrospray ionization-high resolution tandem mass spectrometry (HPLC-(ESI+)-HRMS/MS) in all enzyme assay samples	181

LIST OF FIGURES

Figure 1.1. Common isoprenoid cytokinin (CK) structures and model of isoprenoid CK biosynthesis derived from plant, fungi, and bacterial models	10
Figure 1.2. The <i>D. discoideum</i> life cycle showing the transition from single-celled amoebae to a multicellular organism	11
Figure 2.1. Gene expression analysis of known and putative CK biosynthesis genes in <i>D. discoideum</i>	41
Figure 2.2. Proposed cytokinin (CK) biosynthesis pathway based on the CKs detected throughout all stages of the <i>D. discoideum</i> life cycle	42
Figure 2.3. Reaction scheme for discadenine (DA) biosynthesis	43
Figure 2.4. <i>Dictyostelium discoideum</i> has a putative <i>LOG</i> gene	44
Figure 2.5. A model for the induction of sporulation by CK proposed by Anjard and Loomis (2008)	45
Figure 3.1. Cytokinin (CK) production (pmol/10 ⁶ cells) detected by high-performance liquid chromatography-positive electrospray ionization-high resolution tandem mass spectrometry (HPLC-(ESI+)-HRMS/MS) during five stages of the <i>Dictyostelium discoideum</i> life cycle	82
Figure 3.2. <i>Dictyostelium discoideum</i> germination rate (%) and cytokinin (CK) production over a 72-hour time course	83
Figure 3.3. Effect of 100 nM <i>N</i> ⁶ -isopentenyladenine (iP) treatment on AX3 cell proliferation in HL5 medium over a 144-hour growth period	84
Figure 3.4. Proposed model of cytokinin (CK) biosynthesis in <i>Dictyostelium discoideum</i> consisting of two activation pathways— <i>de novo</i> and tRNA degradation.....	85
Figure 4.1. Knockout of <i>iptA</i> results in a 99% reduction of total cytokinin (CK) levels and fruiting bodies with small sori and thin stalks.....	132
Figure 4.2. <i>iptA</i> -deficiency results in aberrant developmental morphology	133
Figure 4.3. <i>iptA</i> -deficiency does not affect vegetative growth or pinocytosis	134
Figure 4.4. Loss of <i>iptA</i> impairs cytokinesis	135

Figure 4.5. <i>iptA</i> -deficiency alters the morphology and numbers of mitochondria during vegetative growth	136
Figure 4.6. <i>iptA</i> -deficiency (<i>iptA</i> ⁻) and overexpression (<i>GFP-iptA</i>) dysregulates the tricarboxylic acid (TCA) cycle in vegetative amoebae	137
Figure 4.7. <i>iptA</i> -deficiency and overexpression affect energy metabolite levels (AMP/ADP/ATP) but do not affect NAD ⁺ /NADH levels	139
Figure 4.8. Amino acid and derivatives decrease in abundance in <i>iptA</i> -deficient and overexpression strains in vegetative growth and 24-hour development	140
Figure 5.1. Structural and conserved features of <i>DdLOG</i>	182
Figure 5.2. Consensus cladogram of the highly conserved LOG protein family	183
Figure 5.3. SDS-PAGE and western blot of purified <i>DdLOG</i> protein from <i>Escherichia coli</i> culture	184
Figure 5.4. <i>in vitro</i> characterization of purified and desalted recombinant <i>DdLOG</i> using iPMP as a substrate	184
Figure 5.5. Reaction scheme and relative phosphoribohydrolase activity of <i>DdLOG</i>	185
Figure 5.6. Enzyme kinetics of <i>DdLOG</i>	186

LIST OF ABBREVIATIONS

μg	microgram
μL	microliter
μm	micrometer
2-MeSiP	2-methylthio- <i>N</i> ⁶ -isopentenyladenine
aa	amino acid
AcaA	adenylyl cyclase of aggregation protein
AcgA	adenylyl cyclase of germination protein
AcrA	adenylate cyclase with response regulator domain protein
ade	adenine
ADP	adenosine diphosphate
AGC	automatic gain control
AMP	adenosine 5'-monophosphate
AMPK	5'-AMP-activated protein kinase
ANOVA	analysis of variance
ATP	adenosine triphosphate
BA	<i>N</i> ⁶ -benzyladenine
BAMP	<i>N</i> ⁶ -benzyladenosine-5'-monophosphate
BLAST	Basic local alignment search tool
bp	base pair(s)
C	celsius
cAMP	3', 5'-cyclic adenosine monophosphate
CHASE	cyclases/histidine kinases associated sensory extracellular
CK	cytokinin
CKX	cytokinin oxidase
CRISPR/Cas9	clustered regularly interspaces short palindromic repeats/CRISPR-associated protein 9
<i>cZ</i>	<i>cis</i> -zeatin
DA	discadenine
<i>Dd</i> LOG	<i>D. discoideum</i> Lonely guy protein/CK-phosphoribohydrolase
DhkA	histidine kinase A protein
DhkB	histidine kinase B protein
DMAPP	dimethylallyl pyrophosphate
EC	extracellular
ENT	equilibrative nucleoside transporter
FB	free base
FITC-dextran	fluorescein isothiocyanate-dextran
FM	FM minimal medium
FM-AL	FM minimal medium without arginine and lysine
FM-AA	FM minimal medium without amino acids
FS	full scan
FTICR	Fourier transform ion cyclotron resonance mass spectrometer
G418	geneticin

<i>g</i>	units of gravity
g	gram
GFP	green fluorescent protein
<i>gpdA</i>	glyceraldehyde-3-phosphate dehydrogenase
h	hour
HK	histidine kinase
HP	histidine phosphotransfer protein
HPLC	high-performance liquid chromatography
HPLC-(ESI+)- HRMS/MS	high-performance liquid chromatography-positive electrospray ionization-high resolution tandem mass spectrometry
HPLC-(HRAM)-FS-MS	high performance liquid chromatography-high resolution accurate mass-full scan mass spectrometry
IC	intracellular
iP	<i>N</i> ⁶ -isopentenyladenine
IPP	isopentenyl pyrophosphate
iPR	<i>N</i> ⁶ -isopentenyladenine-9-riboside
iPMP	<i>N</i> ⁶ -isopentenyladenine-9-riboside-5' phosphate
IPT	adenylate isopentenyltransferase
<i>iptA</i>	<i>D. discoideum</i> adenylate isopentenyltransferase gene
IptA	<i>D. discoideum</i> adenylate isopentenyltransferase protein
ItpA	inosine triphosphate pyrophosphatase
KO	knockout
LCD	lysine decarboxylase
LF	Lo-Flo medium
<i>m/z</i>	mass-to-charge ratio
MEP	methylerythritol phosphate
ms	millisecond
mm	millimeter
MVA	mevalonate
n.d.	not detected
NAD ⁺	oxidized nicotinamide adenine dinucleotide
NADH	reduced nicotinamide adenine dinucleotide
NCE	normalized collision energy
ng	nanogram
nM	nanomolar
NO	nitric oxide
NT	nucleotide
OE	overexpression
OXPPOS	oxidative phosphorylation
P	phosphate
PBS	phosphate buffered saline
PCR	polymerase chain reaction
pmol	picomole
ppm	parts per million
PRH	phosoribohydrolase

PRM	parallel reaction monitoring
PUP	purine uptake permease
RdeA	rapid development protein
RegA	cAMP phosphodiesterase
RLU	relative light units
<i>rnlA</i>	mitochondrial large subunit rRNA
RT-qPCR	quantitative reverse transcription polymerase chain reaction
SDF-1	spore differentiation factor 1
SDF-2	spore differentiation factor 2
SEM	standard error of the mean
sgRNA	single guide RNA
SM	Sussman Maurice
SPE	solid phase extraction
TCA cycle	tricarboxylic acid cycle
TCS	two-component signaling
TEM	transmission electron microscopy
tRNA	transfer RNA
tRNA-IPT	tRNA-isopentenyltransferase
WT	wild-type; AX3 strain in this thesis

CHAPTER 1

PREFACE

The general introduction content and figures in this chapter are adapted from a review publication (see below). Chapter 2 contains the remaining portion of this review and includes the abstract and keywords used for publication.

Title: Cytokinins in Dictyostelia – A unique model for studying the functions of signaling agents from species to kingdoms.

Authors: Megan M. Aoki, R. J. Neil Emery, Christophe N. Anjard, Craig R. Brunetti, Robert J. Huber

Reference: Published in *Frontiers in Cell and Developmental Biology* (2020), 8: 511. doi: 10.3389/fcell.2020.00511

Copyright: See APPENDIX I.

Contributions: M.A. and N.E. wrote the first draft of the manuscript. C.A. provided critical feedback and expanded the CK secretion and translocation section. All authors contributed to manuscript revisions and approved the submitted version.

CHAPTER 1

GENERAL INTRODUCTION

CYTOKININS

The cytokinins (CKs) encompass a group of evolutionarily significant molecules, most well known for their roles in signaling, where they orchestrate all levels of plant growth and development (Mok and Mok, 2001). Chemically, these molecules are N^6 adenine derivatives, and they exhibit a broad phylogenetic occurrence from bacteria to humans sharing both common and diverging roles, such as growth promotion and virulence, among others (Figure 1.1A) (Akiyoshi et al., 1984; Golovko et al., 2000; see reviews by Spíchal, 2012 and Kabbara et al., 2020). Recent genetic and molecular analyses have led to an explosion of research on the pleiotropic effects of these hormones in plant species (see reviews Kieber and Schaller, 2014; Durán-Medina et al., 2017). The early and simple documented roles of CKs at the single-cell level, such as the promotion of cell growth and differentiation, have now expanded to more complex roles involving whole-plant organization and beyond, such as: shoot initiation, leaf senescence, vascular and embryonic development, and nutrient uptake, among others (Kieber and Schaller, 2014). In concert, the elucidation of key elements in CK biosynthesis, perception, and signal transduction pathways have been pivotal to the understanding of these hormones on a molecular level.

In plants, biosynthesis of the most abundant CK type, the isoprenoid-type CKs, occurs through two different pathways: the methylerythritol phosphate pathway (MEP; *de novo* pathway) and the mevalonate pathway (MVA; tRNA-degradation pathway) (Figure 1.1B). Isoprenoid- (iP), *trans*-zeatin- (*tZ*), and dihydrozeatin-type CKs (DZ) are

predominately derived from the *de novo* biosynthesis pathway through adenylyl-isopentenyl transferases (IPTs) (Sakakibara, 2006). In contrast to the *de novo* pathway, the MVA or tRNA-degradation pathway is responsible for the production of *cis*-zeatin-type CKs (*cZ*) through tRNA-isopentenyltransferases (tRNA-IPTs) (Figure 1.1) (Miyawaki et al., 2006). In fungi and mammals, there is evidence that iP- and methyl-thiolated-type (2MeS-) CKs are also derived from the tRNA degradation pathway (Morrison et al., 2017; Seegobin et al., 2018). In both pathways, IPTs facilitate N-prenylation of the adenosine molecule at the N^6 terminus (Figure 1.1B) (Kakimoto, 2001; Takei et al., 2001; Sakakibara, 2006). When the isoprenoid donor dimethylallyl pyrophosphate (DMAPP) acts with IPT, isopentenyladenine-type (iP-type) CKs are formed. From iP-type CKs, other CKs can be generated (e.g., *tZ*, *DZ*) through modifications of the side chain. Specifically, adenylyl-IPTs catalyze the transfer of the isoprenoid moiety to adenine through the rate limiting reaction to form iP nucleotides (either mono-, di-, or tri-phosphate; iPRPs). Therefore, the production of all other isoprenoid CK types is dependent upon the initial presence of IPT to facilitate iPRP production. In the case of tRNA-IPTs, prenylation occurs on tRNA molecules at position A37, and upon degradation, the tRNA-derived CKs contribute to the pool of unbound CKs in the organism (Gajdosová et al., 2011). From plant CK biosynthesis pathways, it is well-known that there are various CK types, and they are distinguished by their characteristic side-chain attachments at the N^6 position of the adenine (e.g., iP or *tZ*) (Figure 1.1A) (Kamada-Nobusada and Sakakibara, 2009). Within each CK-type, there are various structural derivatives or forms that exist which determine the level of biological activity within the organism, such as: free bases, ribosides and nucleotides, and conjugates with glucose, xylose, or amino acid residues (Figure 1.1A). Generally, the nucleotide forms

are considered inactive precursors from which the more biologically active riboside and free base forms can be created.

Recently, an increasing amount of attention has been placed on uncovering the roles of CKs outside of the plant kingdom. In fact, these signaling molecules and or components of their biosynthesis pathways are present in organisms of all kingdoms. There is a possibility that CKs have roles in the growth and development of all organisms that produce them. Owing to their ubiquitous presence in all kingdoms, CKs are viewed as primary candidates for the study of interkingdom, hormone-like, signaling molecules (Kabbara et al., 2018). Recent evidence involving CKs opens many new doors for research beyond the plant kingdom. The human pathogen, *Mycobacterium tuberculosis*, secretes CKs that induce transcriptional changes affecting both the metabolome and staining properties of *M. tuberculosis* (Samanovic et al., 2018). These findings clearly demonstrate strong evidence of the involvement of CKs as signaling molecules on an interkingdom level. A phytopathogenic bacterial receptor was identified revealing a conserved mechanism by which bacteria can respond to CK in order to defend themselves against their host innate immune response (Wang et al., 2017; Chen et al., 2019). Moreover, a possible role for CKs in animal-microbiota relationships with implications for human health was explored in a recent review (Chanclud and Lacombe, 2017). In the apicomplexan parasite, *Toxoplasma gondii*, CKs regulate growth, the cell cycle, and apicoplast (a vestigial plastid involved in lipid synthesis) proliferation (Andrabi et al., 2018). The thermophilic archaeon, *Sulfolobus islandicus* REY15A, was the first archaeal species identified to possess a CK-activating enzyme, lonely guy (LOG) (Mayaka et al., 2019). Furthermore, the detection of six additional CK forms, beyond the one previously

identified (*N*⁶-isopentenyladenine-9-riboside), were reported in mammalian tissues (Seegobin et al., 2018). Among these various examples of CK production or activity in non-plant biota, there is a common theme of CKs exhibiting biological functions in many kingdoms of life. Exogenous application of CKs on mammalian cancer cell lines show that CKs have anticancer activity (Voller et al., 2010). Moreover, CKs affect growth and germination in the social amoeba, *Dictyostelium discoideum* and in the biotrophic fungus, *Claviceps purpurea* (Anjard and Loomis, 2008; Hinsch et al., 2015; Aoki et al., 2019). In the coming years, it is likely that we will continue to see increasing roles of CKs beyond the plant kingdom as research continues to use organisms from all kingdoms of life.

THE DICTYOSTELIA

The Dictyostelids are soil-dwelling, amoeboid protozoans belonging to the Amoebozoa phylum (Raper, 1984; Romeralo et al., 2011). These eukaryotes are often referred to as social amoebae, owing to their unique life cycle, which consists of two mutually exclusive states: vegetative growth (single-celled amoebae) and development (multicellular organism) (Figure 1.2). Individual amoeboid cells grow asexually and divide mitotically, feeding upon soil bacteria and/or decaying leaf litter until resources are depleted. Starvation triggers the developmental program through the secretion of a chemical messenger, cAMP, which acts as a chemoattractant initiating the migration of neighboring amoebae (i.e. chemotaxis) to form an aggregate of cells (Konijn et al., 1967). These aggregates are collectively known as mounds. Tens of thousands of aggregated cells then undergo morphogenesis to form a multicellular pseudoplasmodium (slug), which migrates towards light and warmth (see review by Schaap, 2011). Cells within the slug

terminally differentiate into either stalk or spores to form the final life cycle stage, a fruiting body, which consists of specialized stalk cells and a droplet of spores that sits atop the stalk (Schilde and Schaap, 2013; Loomis, 2014).

The most well-known organism of the Amoebozoa phylum is *Dictyostelium discoideum*, hereafter referred to as *D. discoideum*. The genome of *D. discoideum* was the first free-living protozoan to be sequenced (Eichinger et al., 2005). Prior to sequencing, over five decades of intensive research on this social amoeba led to increased understanding of various cellular processes, such as chemotaxis and differentiation. Uniquely situated at the juncture of plants and animals, sharing many traits between the two kingdoms, the Dictyostelids offer a matchless platform to assess a wide variety of cellular and developmental processes. The unique life cycle of Dictyostelid species, paired with its position in phylogeny and possession of CK biosynthetic and signal transduction components, highlights how Dictyostelids can be used as models to study the role of CKs beyond the plant kingdom. This is expanded upon in Chapter 2 and the rest of the thesis.

RESEARCH OBJECTIVES

The primary focus of this research was to use *D. discoideum* as a model to expand our understanding of the roles of CKs outside of plants. Initial research exploring CKs in *D. discoideum* was from the early 1970's, when researchers discovered the presence of a novel CK and spore germination inhibitor, known as discadenine (DA) (Obata et al., 1973; Taya et al., 1978a). Around the same time, the first evidence of a *de novo* CK biosynthetic pathway initiated by an adenylate-isopentenyltransferase (IPT) was documented in *D. discoideum* (Taya et al., 1978b). This early work established CKs as key signals during the

later developmental stages of the *D. discoideum* life cycle. This was later expanded upon by Anjard and Loomis (2008) who showed that CKs were essential intercellular signals for triggering sporulation and maintaining spore dormancy. This combined research piqued my interest and established the initial focus, which was 1) to map the CK biosynthesis pathway in *D. discoideum*, comprehensively screening for all naturally occurring forms of CKs during the *D. discoideum* life cycle, and 2) to determine if CK biosynthesis is truly restricted to the later developmental stages of *D. discoideum*.

Comprehensive screening of CK profiles in *D. discoideum* revealed the presence of six novel CK forms (four more than were previously identified in *D. discoideum*). Moreover, CKs were detected during every life cycle stage from vegetative growth to late multicellular development. These findings posed many new questions regarding the roles of CK throughout the life cycle and are reported in Chapter 3. Of particular interest, the dominant CK profiles were strikingly different in vegetative growth and early development compared to those found in later development. This led to the hypothesis that CKs have expanded functions in growth and development of *D. discoideum*. Therefore, knockout and overexpression strains were generated for the primary CK biosynthesis gene, *iptA*, to investigate potential roles of CKs in vegetative amoebae and their early development through biochemical analyses and metabolomics (Chapter 4). Loss or overexpression of *iptA* revealed unexpected findings, including impaired cytokinesis, altered mitochondrial morphology, and decreased levels of TCA cycle metabolites and amino acids. The combined results support the hypothesis that CKs and/or IptA have expanded roles in early growth and late development (Chapter 4). Lastly, the attention was brought back to CK biosynthesis, for which a candidate CK-activating enzyme in *D. discoideum*,

DDB0305758, was functionally characterized through recombinant expression of the candidate protein in *Escherichia coli* (Chapter 5). In plants, CK-specific phosphoribohydrolases, known as LOGs, are the enzymes responsible for converting CKs to their most biologically active free base forms (Kurakawa et al., 2007; Kuroha et al., 2009). Bioinformatic analyses paired with biochemical characterization suggested that the encoded product of the uncharacterized gene, *DDB_G0281309*, exhibits phosphoribohydrolase activity and converts both CK-nucleotides and the non-CK nucleotide, AMP, into their respective free base products (Chapter 5). The *Dd*LOG protein has a higher rate of turnover for CK-nucleotides than the non-CK nucleotide, AMP, exhibiting a broader specificity for substrates than LOGs found in plants. Collectively, the results of this Ph.D. thesis revealed novel insights into the biosynthesis of CKs and expanded our understanding of the pleiotropic nature of CK dynamics during the life cycle of *D. discoideum*.

This thesis is presented in manuscript-style and consists of a compilation of four chapters prefaced by this general introduction and concluded with a general discussion. The detailed breakdown of the chapters is as follows: 1) this general introduction – which includes a section from a review published in *Frontiers in Cell and Developmental Biology* (Aoki et al., 2020), 2) a literature review on the present knowledge of CK biosynthesis, signal transduction, and CK-small molecule interactions in *D. discoideum* – which contains the remaining portion of the review published in *Frontiers in Cell and Developmental Biology* (Aoki et al., 2020), 3) a data chapter profiling CKs during the *D. discoideum* life cycle – which was published in *Biomolecules* (Aoki et al., 2019), 4) a data chapter investigating the role of CKs in vegetative growth and early development through knockout

and overexpression of *iptA* – which will be submitted for publication following the Ph.D. defence, 5) a data chapter characterizing a CK-activating enzyme in *D. discoideum* – which will be submitted for publication following the Ph.D. defense, and 6) a general discussion summarizing insight gained from this research along with accompanying future directions.

FIGURES

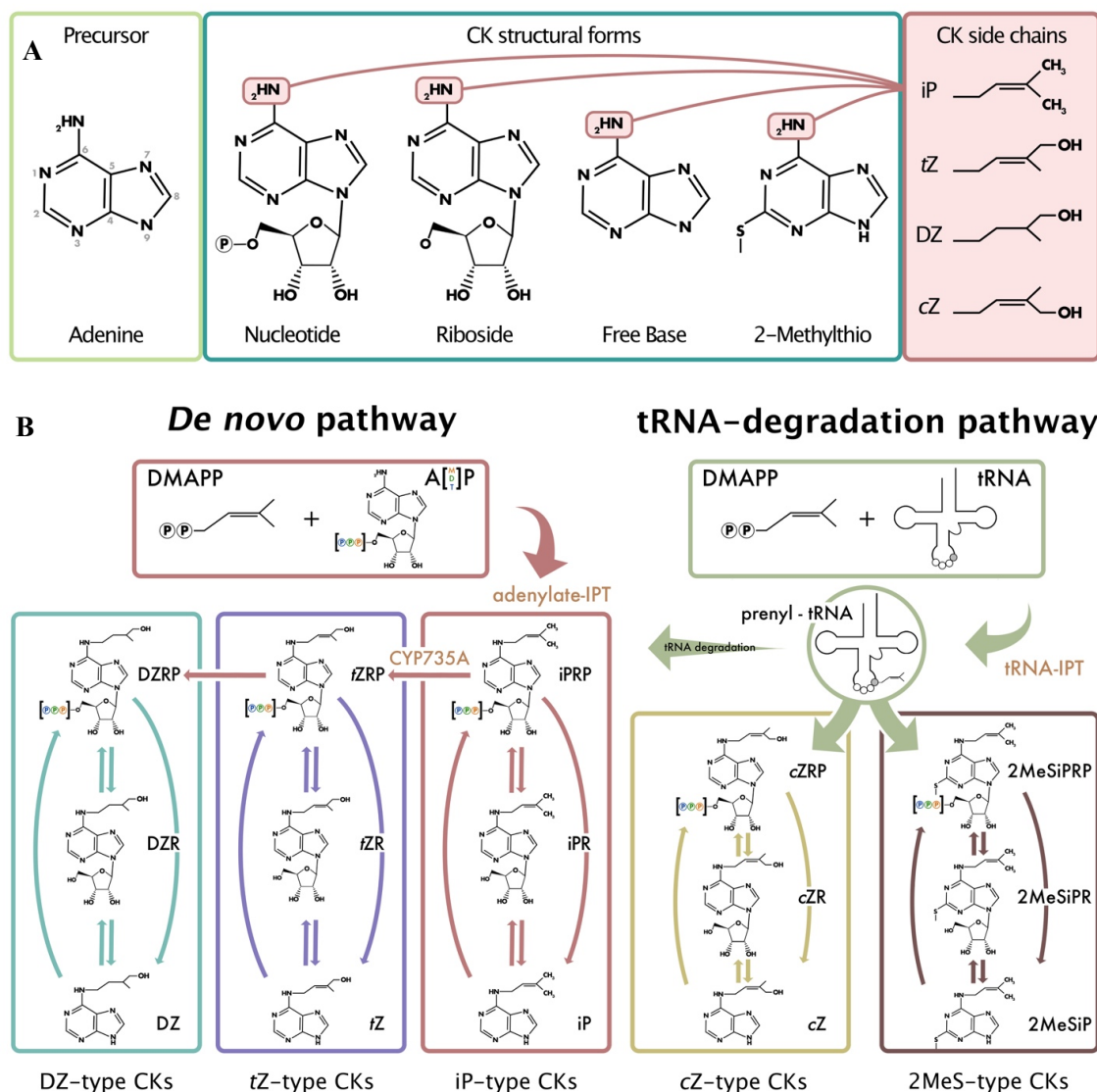


Figure 1.1 Common isoprenoid cytokinin (CK) structures and model of isoprenoid CK biosynthesis derived from plant, fungi, and bacterial models. (A) Depicts the numbering system used in CK nomenclature, the common CK structural forms, and the various isoprenoid side chains (iP, tZ, DZ, and cZ) that can be attached to the N^6 position of the adenine. **(B)** Depicts the two different pathways from which isoprenoid CKs can be formed: the methylerythritol phosphate pathway (*de novo* pathway) and the mevalonate pathway (tRNA-degradation pathway). Arrows are representative of the various enzymes that convert between the different CK types and structural derivatives. Orange font indicates specific enzymes. The 2MeS-type CKs shown as a product of tRNA degradation all possess 2MeSiP-type side chains; however, 2MeStZ- and 2MeScZ-type are also possible. Note that not all CK structural forms and enzymes responsible for CK biosynthesis and metabolism are depicted (e.g., glucosides or cytokinin oxidase, etc.). Adapted from: Kamada-Nobusada and Sakakibara, 2009; Spíchal, 2012; Morrison et al., 2015; Morrison et al., 2017).

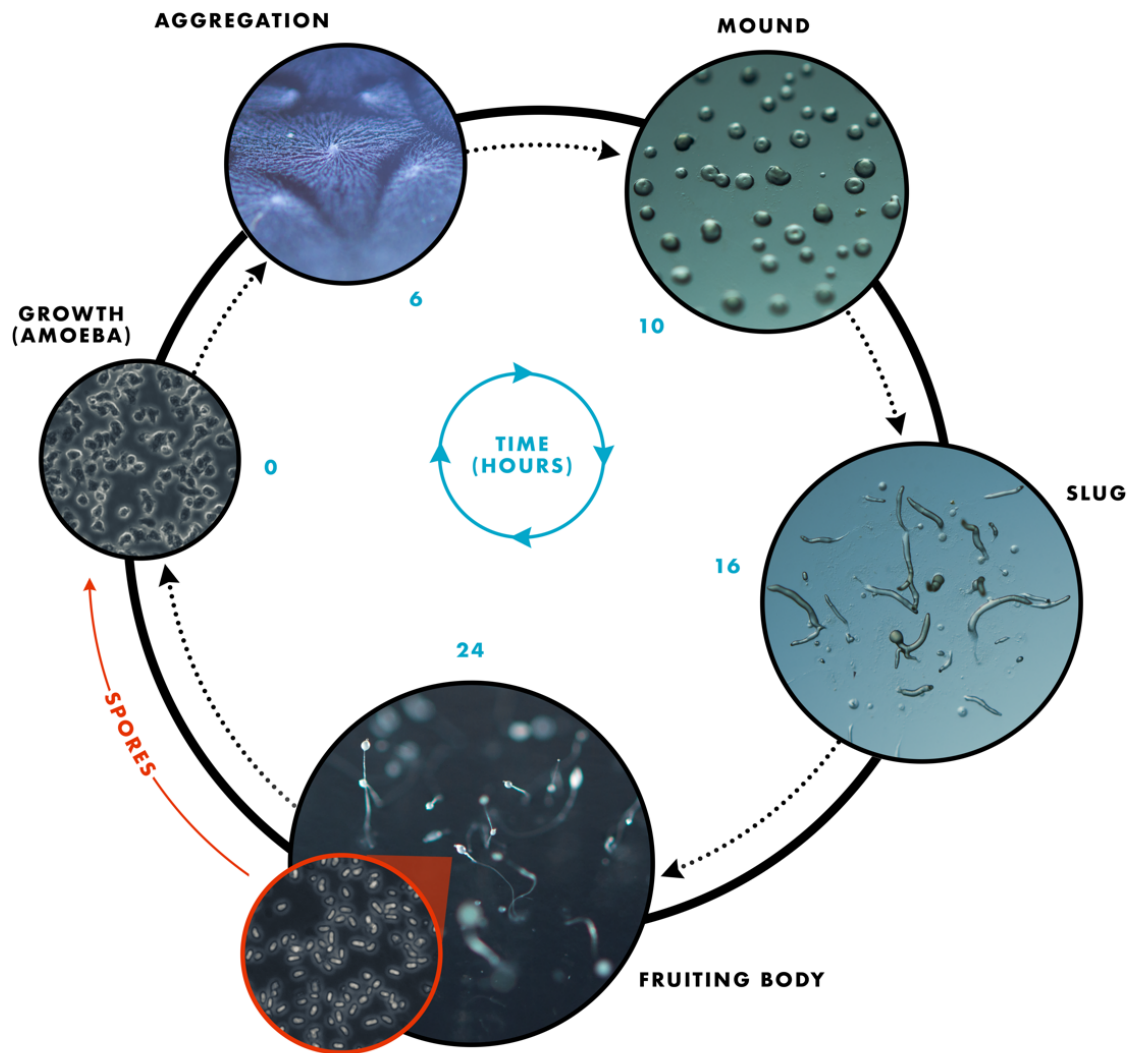


Figure 1.2. The *D. discoideum* life cycle showing the transition from single-celled amoebae to a multicellular organism. Upon starvation, the developmental program is initiated so that single-celled amoebae aggregate towards a central location, as depicted in the aggregation image. The cells continue to aggregate to form the mound structure, which occurs after approximately 10 hours starvation. Transition from the mound to the slug life cycle stage take approximately 6 to 8 hours. Finally, culmination generates a fruiting body consisting of a slender stalk and mass of spores (sorus) that forms 24 hours after the onset of starvation. Each spore gives rise to single amoeba upon germination when food resources are available. To appreciate the different scales, the average sizes of the various stages are as follows: vegetative amoebae are 10-20 μm , mounds and slugs range from 0.1-2 mm, and fruiting bodies are approximately 1.5 mm tall (sorus is between 150-300 μm and the individual spores in the sorus are 6-9 μm long by 3 μm wide).

REFERENCES

- Akiyoshi, D. E., Klee, H., Amasino, R. M., Nester, E. W., and Gordon, M. P. (1984). T-DNA of *Agrobacterium tumefaciens* encodes an enzyme of cytokinin biosynthesis. *Proc. Natl. Acad. Sci. U.S.A.* 81, 5994–5998. doi: 10.1073/pnas.81.19.5994.
- Andrabi, S. B. A., Tahara, M., Matsubara, R., Toyama, T., Aonuma, H., Sakakibara, H., et al. (2018). Plant hormone cytokinins control cell cycle progression and plastid replication in apicomplexan parasites. *Parasitol. Int.* 67, 47–58. doi: 10.1016/j.parint.2017.03.003.
- Anjard, C. and Loomis, W. F. (2008). Cytokinins induce sporulation in *Dictyostelium*. *Development* 135, 819–827. doi: 10.1242/dev.018051.
- Aoki, M. M., Emery, R. J. N., Anjard, C., Brunetti, C. R., and Huber, R. J. (2020). Cytokinins in Dictyostelia – A unique model for studying the functions of signaling agents from species to kingdoms. *Front. Cell Dev. Biol.* 8, 511. doi: 10.3389/fcell.2020.00511.
- Aoki, M. M., Kisiala, A. B., Li, S., Stock, N. L., Brunetti, C. R., Huber, R. J., et al. (2019). Cytokinin detection during the *Dictyostelium discoideum* life cycle: Profiles are dynamic and affect cell growth and spore germination. *Biomolecules* 9, 702. doi: 10.3390/biom9110702.
- Chanclud, E., and Lacombe, B. (2017). Plant Hormones: Key players in gut microbiota and human diseases? *Trends Plant Sci.* 22, 754–758. doi: 10.1016/j.tplants.2017.07.003.
- Chen, P., Jiao, X., Zhang, Y., Wu, L., Tang, D. J., Li, P., et al. (2019). The crystal structure of the phytopathogenic bacterial sensor PcrK reveals different cytokinin recognition mechanism from the plant sensor AHK4. *J. Struct. Biol.* 208, 69–76. doi: 10.1016/j.jsb.2019.08.001.
- Durán-Medina, Y., Díaz-Ramírez, D., and Marsch-Martínez, N. (2017). Cytokinins on the Move. *Front. Plant Sci.* 8, 146. doi: 10.3389/fpls.2017.00146.
- Eichinger, L., Pachebat, J. A., Glöckner, G., Rajandream, M.-A., Sucgang, R., Berriman, M., et al. (2005). The genome of the social amoeba *Dictyostelium discoideum*. *Nature* 435, 43–57. doi: 10.1038/nature03481.
- Gajdosová, S., Spíchal, L., Kamínek, M., Hoyerová, K., Novák, O., Dobrev, P. I., et al. (2011). Distribution, biological activities, metabolism, and the conceivable function of *cis*-Zeatin-type cytokinins in plants. *J. Exp. Bot.* 62, 2827–2840. doi: 10.1093/jxb/erq457.
- Golovko, A., Hjälml, G., Sitbon, F., and Nicander, B. (2000). Cloning of a human tRNA isopentenyl transferase. *Gene* 258, 85–93. doi: 10.1016/S0378-1119(00)00421-2.

- Hinsch, J., Vrabka, J., Oeser, B., Novák, O., Galuszka, P., and Tudzynski, P. (2015). *De novo* biosynthesis of cytokinins in the biotrophic fungus *Claviceps purpurea*. *Environ. Microbiol.* 17, 2935–2951. doi: 10.1111/1462-2920.12838.
- Kabbara, S., Schmülling, T., and Papon, N. (2018). CHASEing cytokinin receptors in plants, bacteria, fungi, and beyond. *Trends Plant Sci.* 23, 179–181. doi: 10.1016/j.tplants.2018.01.001.
- Kakimoto, T. (2001). Identification of plant cytokinin biosynthetic enzymes as dimethylallyl diphosphate:ATP/ADP isopentenyltransferases. *Plant Cell Physiol.* 42, 677–685. doi: 10.1093/pcp/pce112.
- Kamada-Nobusada, T. and Sakakibara, H. (2009). Molecular basis for cytokinin biosynthesis. *Phytochemistry* 70, 444–449. doi: 10.1016/j.phytochem.2009.02.007.
- Kieber, J. J., and Schaller, G. E. (2014). Cytokinins. *Arab. B.* 12, e0168. doi: 10.1199/tab.0168.
- Konijn, T. M., Van De Meene, J. G., Bonner, J. T., and Barkley, D. S. (1967). The acrasin activity of adenosine-3',5'-cyclic phosphate. *Proc. Natl. Acad. Sci. U.S.A.* 58, 1152–1154. doi: 10.1073/pnas.58.3.1152.
- Loomis, W. F. (2014). Cell signaling during development of *Dictyostelium*. *Dev. Biol.* 391, 1–16. doi: 10.1016/j.ydbio.2014.04.001.
- Mayaka, J. B., Huang, Q., Xiao, Y., Zhong, Q., Ni, J., and Shen, Y. (2019). The Lonely Guy (LOG) homologue SiRe_0427 from the thermophilic archaeon *Sulfolobus islandicus* REY15A is a phosphoribohydrolase representing a novel group. *Appl. Environ. Microbiol.* 85. doi: 10.1128/AEM.01739-19.
- Miyawaki, K., Tarkowski, P., Matsumoto-Kitano, M., Kato, T., Sato, S., Tarkowska, D., et al. (2006). Roles of *Arabidopsis* ATP/ADP isopentenyltransferases and tRNA isopentenyltransferases in cytokinin biosynthesis. *Proc. Natl. Acad. Sci. U.S.A.* 103, 16598–16603. doi: 10.1073/pnas.0603522103.
- Mok, D. W., and Mok, M. C. (2001). Cytokinin metabolism and action. *Annu. Rev. Plant Physiol. Plant Mol. Biol.* 52, 89–118. doi: 10.1146/annurev.arplant.52.1.89.
- Morrison, E. N., Emery, R. J. N., and Saville, B. J. (2017). Fungal derived cytokinins are necessary for normal *Ustilago maydis* infection of maize. *Plant Pathol.* 66, 726–742. doi: 10.1111/ppa.12629.
- Morrison, E. N., Knowles, S., Hayward, A., Thorn, R. G., Saville, B. J., and Emery, R. J. N. (2015). Detection of phytohormones in temperate forest fungi predicts consistent abscisic acid production and a common pathway for cytokinin biosynthesis.

- Mycologia* 107, 245–257. doi: 10.3852/14-157.
- Obata, Y., Abe, H., Tanaka, Y., Yanagisawa, K., and Uchiyama, M. (1973). Isolation of a spore germination inhibitor from a cellular slime mold *Dictyostelium discoideum*. *Agric. Biol. Chem.* 37, 1989–1990. doi: 10.1080/00021369.1973.10860941.
- Raper, K. B. (1984). *The Dictyostelids*. Princeton, New Jersey: Princeton University Press.
- Romeralo, M., Cavender, J. C., Landolt, J. C., Stephenson, S. L., and Baldauf, S. L. (2011). An expanded phylogeny of social amoebas (Dictyostelia) shows increasing diversity and new morphological patterns. *BMC Evol. Biol.* 11, 84. doi: 10.1186/1471-2148-11-84.
- Sakakibara, H. (2006). Cytokinins: Activity, biosynthesis, and translocation. *Annu. Rev. Plant Biol.* 57, 431–449. doi:10.1146/annurev.arplant.57.032905.105231.
- Samanovic, M. I., Hsu, H. C., Jones, M. B., Jones, V., McNeil, M. R., Becker, S. H., et al. (2018). Cytokinin signaling in *Mycobacterium tuberculosis*. *MBio* 9. doi: 10.1128/mBio.00989-18.
- Schaap, P. (2011). Evolution of developmental cyclic adenosine monophosphate signaling in the Dictyostelia from an amoebozoan stress response. *Dev. Growth Differ.* 53, 452–462. doi: 10.1111/j.1440-169X.2011.01263.x.
- Schilde, C., and Schaap, P. (2013). “The Amoebozoa,” in (Humana Press, Totowa, NJ), 1–15. doi: 10.1007/978-1-62703-302-2_1.
- Seegobin, M., Kisiala, A., Noble, A., Kaplan, D., Brunetti, C., and Emery, R. J. N. (2018). *Canis familiaris* tissues are characterized by different profiles of cytokinins typical of the tRNA degradation pathway. *FASEB J.* 32, 6575–6581. doi: 10.1096/fj.201800347.
- Spíchal, L. (2012). Cytokinins - recent news and views of evolutionally old molecules. *Funct. Plant Biol.* 39, 267. doi: 10.1071/FP11276.
- Takei, K., Sakakibara, H., and Sugiyama, T. (2001). Identification of genes encoding adenylate isopentenyltransferase, a cytokinin biosynthesis enzyme, in *Arabidopsis thaliana*. *J. Biol. Chem.* 276, 26405–26410. doi: 10.1074/jbc.M102130200.
- Taya, Y., Tanaka, Y., and Nishimura, S. (1978a). Cell-free biosynthesis of discadenine, a spore germination inhibitor of *Dictyostelium discoideum*. *FEBS Lett.* 89, 326–328. doi: 10.1016/0014-5793(78)80247-6
- Taya, Y., Tanaka, Y., and Nishimura, S. (1978b). 5'-AMP is a direct precursor of cytokinin in *Dictyostelium discoideum*. *Nature* 271, 545–547. doi: 10.1038/271545a0.
- Voller, J., Zatloukal, M., Lenobel, R., Doleal, K., Bére, T., Krytof, V., et al. (2010).

Anticancer activity of natural cytokinins: A structure-activity relationship study.
Phytochemistry 71, 1350–1359. doi: 10.1016/j.phytochem.2010.04.018.

Wang, F. F., Cheng, S. T., Wu, Y., Ren, B. Z., and Qian, W. (2017). A bacterial receptor PcrK senses the plant hormone cytokinin to promote adaptation to oxidative stress.
Cell Rep. 21, 2940–2951. doi: 10.1016/j.celrep.2017.11.017.

CHAPTER 2

PREFACE

The content in this chapter includes the remaining portion of my published review, which has been updated in a few sections to reflect new findings obtained over the course of my Ph.D. following its initial publication.

Title: Cytokinins in Dictyostelia – A unique model for studying the functions of signaling agents from species to kingdoms.

Authors: Megan M. Aoki, R. J. Neil Emery, Christophe N. Anjard, Craig R. Brunetti, Robert J. Huber

Reference: Published in *Frontiers in Cell and Developmental Biology* (2020), 8: 511. doi: 10.3389/fcell.2020.00511

Copyright: See APPENDIX I.

Contributions: M.A. and N.E. wrote the first draft of the manuscript. C.A. provided critical feedback and expanded the CK secretion and translocation section. All authors contributed to manuscript revisions and approved the submitted version.

CHAPTER 2

Cytokinins in Dictyostelia – A unique model for studying the functions of signaling agents from species to kingdoms.

Published in: *Frontiers in Cell and Developmental Biology* (2020), 8: 511.

doi: 10.3389/fcell.2020.00511

ABSTRACT

Cytokinins (CKs) are a diverse group of evolutionarily significant growth-regulating molecules. While the CK biosynthesis and signal transduction pathways are the most well-understood in plant systems, these molecules have been identified in all kingdoms of life. This review follows the recent discovery of an expanded CK profile in the social amoeba, *Dictyostelium discoideum*. A comprehensive review on the present knowledge of CK biosynthesis, signal transduction, and CK-small molecule interactions within members of Dictyostelia will be summarized. In doing so, the utility of social amoebae will be highlighted as a model system for studying the evolution of these hormone-like signaling agents, which will set the stage for future research in this area.

KEYWORDS: cytokinins, Dictyostelia, *Dictyostelium discoideum*, cytokinin biosynthesis, cytokinin signaling, development

CYTOKININS IN DICTYOSTELIA

Overview

The first papers published on the presence of CK in Dictyostelids involved the discovery of a novel CK in *D. discoideum*, known as discadenine (DA) (Obata et al., 1973; Tanaka et al., 1975; Abe et al., 1976). DA was discovered in the spore mass and was characterized as a potent inhibitor of spore germination. A notable discovery involving CKs in Dictyostelids by Taya et al. (1978a) revealed the existence of a CK biosynthetic pathway unrelated to the tRNA CK degradation pathway. Moreover, 5'-AMP was shown to be the acceptor molecule for the isopentenyl group forming the precursor molecule, isopentenyl adenine nucleotide (iPRP). Collectively, this early work in Dictyostelids laid the foundation for the CK biosynthesis pathway to be mapped in *Arabidopsis thaliana* (see reviews by Sakakibara, 2006; Kamada-Nobusada and Sakakibara, 2009). Following the initial discovery of an alternate biosynthetic pathway in Dictyostelids, the presence of *N*⁶-isopentenyladenine (iP) was identified at the start of fruiting body formation, also known as culmination, and iP was shown to be the precursor molecule to DA (Tanaka et al., 1978). Further analysis revealed a developmental regulation of CK in *D. discoideum*, as both iP and DA were detected following the onset of culmination (Ihara et al., 1980). This early evidence of the developmental role of CK in *D. discoideum* was later confirmed and expanded upon by Anjard and Loomis (2008). More recently, a comprehensive scan of 30 potential CKs in *D. discoideum* revealed that six different CKs are synthesized and secreted during growth, development, and germination (Aoki et al., 2019). Total levels of CK production were highest in the fruiting body and during germination, followed by aggregation and single-celled growth. Interestingly, iP-type CKs were the dominant CK

forms during single-celled growth and aggregation, and DA was not present during these early life cycle stages. We detected high levels of DA following the onset of culmination, which is consistent with previous research (Ihara et al., 1980; Anjard and Loomis, 2008). Exogenous application of iP affected single-celled growth by prolonging the stationary phase of cultures (Aoki et al., 2019). Together, these results indicate a greater role for CKs during the *D. discoideum* life cycle, and they laid the foundation for this thesis. The remainder of this chapter reviews CK biosynthesis, metabolism, signal transduction, and CK-small molecule interactions that are specific to *D. discoideum*. Examples using other CK-producing organisms are used to provide additional context for CK function.

CYTOKININ BIOSYNTHESIS AND METABOLISM

IptA – adenylyl isopentenyltransferase

In *D. discoideum*, there are three identified IPT genes, only one of which has been functionally characterized (Anjard and Loomis, 2008). A phylogenetic analysis of the corresponding proteins revealed that the *D. discoideum* genome encodes one adenylyl-IPT and two tRNA-IPTs (Anjard and Loomis, 2008). The adenylyl-IPT gene, denoted *iptA*, encodes a 283 amino acid, 32 kDa protein (IptA, DDB0233672) (Anjard and Loomis, 2008). IptA is a developmentally regulated protein, and its activity peaks during the late culmination stage of *D. discoideum* development (Figure 2.1) (Ihara et al., 1980, Ihara et al., 1984; Rot et al., 2009). Purification of IptA reveals that it is highly unstable and loses most of its activity after one day (Ihara et al., 1984). In terms of substrate specificity, 5'-AMP is the most effective substrate for IptA followed by ADP, which is 60-80% as effective. ATP, adenine, and adenosine are not substrates for IptA in *D. discoideum* (Ihara

et al., 1984). The activity of *D. discoideum* IptA is dependent upon divalent metal cations (Zn^{2+} , Mg^{2+} , Mn^{2+}), which is consistent with other prenyl-transfer reactions (Durbecq et al., 2001). The K_m values of *D. discoideum* IptA, under optimum conditions (pH 7.0, 1 mM Zn^{2+} , and 25°C) for both 5'-AMP and isopentenylpyrophosphate are 1.0×10^{-7} M and 2.2×10^{-6} M respectively (Ihara et al., 1984). While the role of IptA in *D. discoideum* is consistent with plants and other CK-producing biota, the aforementioned properties of the enzyme (K_m , substrate specificity, etc.) are variable among CK-producing organisms, such as *A. thaliana*, and the plant-pathogenic bacterium, *Agrobacterium tumefaciens* (Kakimoto, 2001; Sugawara et al., 2008). For instance, the adenylate-IPT from *D. discoideum* and *A. tumefaciens* use AMP as the prenyl acceptor molecule, while *A. thaliana* adenylate-IPTs preferentially use ADP or ATP (Taya et al., 1978a; Kakimoto, 2001).

Disruption of *iptA*, through homologous recombination in the AX4 parental strain of *D. discoideum*, reduced total CK production and impaired spore viability (Anjard and Loomis, 2008). The rate of CK accumulation in *iptA*⁻ cells was 90% less than that observed in wild-type cells when developed from vegetative cells on filters over a 30-hour period (CK production was assessed every 2 hours starting from 20 hours to 30 hours). Developing *iptA*⁻ cells with 10% wild-type cells resulted in improved sporulation, indicating a non-cell autonomous phenotype (Anjard, unpublished). A threshold concentration of CK was calculated to determine the amount of endogenous CK necessary to fully induce spore formation, which was 10 nM. *iptA*⁻ cells took 30 hours to reach this concentration, roughly 6-8 hours longer than wild-type cells. As a result, these findings support the conclusion that CKs play a significant role in sporulation in *D. discoideum* (Anjard and Loomis, 2008).

Although IptA is responsible for catalyzing the reaction for the synthesis of isopentenyl adenine-type (iP-type) CKs, organisms do not usually display a full complement of CK forms and this likely reflects the different pathways present and relative enzyme activities therein. Thus far, six CK forms have been identified in *D. discoideum*: *cis*-zeatin (*cZ*), DA, iP, *N*⁶-isopentenyladenine-9-riboside (iPR), *N*⁶-isopentenyladenine-9-riboside-5' phosphate (iPRP), and 2-methylthio-*N*⁶-isopentenyladenine (2MeSiP) (Figure 2.2) (Abe et al., 1976; Tanaka et al., 1978; Taya et al., 1978b; Aoki et al., 2019). Of these identified CK forms, the most well-studied are iP and DA; DA will be discussed at greater lengths in a following section entitled discadenine synthase. The biosynthesis of iP-type CKs in *D. discoideum* appears to be similar to other CK-producing organisms, as the traditional CK forms of iP (nucleotide, riboside, and free base) have been identified throughout the life cycle (Aoki et al., 2019). Of the iP-type CKs identified in *D. discoideum*, the free base fraction, iP, is the most prevalent CK form detected (Anjard and Loomis, 2008; Aoki et al., 2019). Other than higher plants, only a handful of other CK-producing species contain adenylate-IPT genes: the plant pathogenic bacteria, *Agrobacterium tumefaciens* (Akiyoshi et al., 1984) and *Rhodococcus fascians* (Crespi et al., 1992); the land moss, *Physcomitrella patens* (Lindner et al., 2014); the cyanobacterium, *Nostoc sp.* (Frébortová et al., 2015); and the social amoebae, *D. discoideum* and *D. purpureum* (Anjard and Loomis, 2008; Sucgang et al., 2011; <http://www.dictybase.org>).

IptB and IptC – putative tRNA isopentenyltransferases

In *D. discoideum*, there are two putative tRNA-IPTs: *iptB* and *iptC*. In the commonly used AX3 and AX4 strains of *D. discoideum*, there is a large duplication on chromosome 2, which affects *iptC* resulting in two copies of this gene, denoted *iptC-1* and

iptC-2 (Bloomfield et al., 2008). From phylogenetic analyses, IptB and IptC cluster with tRNA-IPTs that are closely related to bacterial and eukaryotic tRNA-IPTs respectively; however, there has been no functional characterization to date (Anjard and Loomis, 2008; Lindner et al., 2014; Nishii et al., 2018). Despite tRNA-IPTs being the most abundant IPT-type conserved across kingdoms of life, much less is known about it compared to adenylate-IPTs in terms of CK biosynthesis (Schäfer et al., 2015). *iptB* encodes a predicted 522 amino acid, 61 kDa protein (IptB, DDB0233673), and *iptC* encodes a predicted 413 amino acid, 48 kDa protein (IptC, DDB0233671). While these proteins have not been previously studied, it is likely that IptB and IptC contribute to the collective pool of CKs in *D. discoideum*, as the disruption of *iptA* leads to a drastic reduction of CK levels, but not a complete elimination of CK biosynthesis (Anjard and Loomis, 2008). In support of this idea, the recent CK profiles of *D. discoideum* follow a similar trend to what is found in CK-producing organisms with dominant tRNA-IPT CK pathways, possessing mostly iP-type CKs (Figure 2.2) (Aoki et al., 2019). Therefore, the peak in expression at the 16-hour stage of development (slug stage) could coincide with preparing the cells for the encapsulation of spores, where tRNA-bound CKs could be degraded to contribute to the pool of free CKs required for encapsulation at the 20-hour time point (Figure 2.1; <http://www.dictybase.org>). In *D. discoideum*, there is little known about tRNA modification. Total tRNA transcript abundance does not increase during development, but tRNA modifications do (Palatnik et al., 1977; Rosengarten et al., 2017). The peak in expression of *iptB* and *iptC* throughout development aligns with these studies, which further support the putative roles of tRNA modification assigned to both of these gene products (Figure 2.1).

Beyond the role of CK biosynthesis, tRNA-IPTs are involved in many other functions, such as translation fidelity (in yeast and humans), *in vitro* growth and gene expression (in bacteria), and tRNA-gene mediated silencing (tgm) and drug resistance under environmental stress (in yeast), among others (Tolerico et al., 1999; Ericson and Bjork, 1986; Spinola et al., 2005; Suzuki et al., 2012; Pratt-Hyatt et al., 2013; Yu et al., 2017; see review by Dabravolski, 2020). Dabravolski (2020) summarizes that the roles of tRNA-IPTs can be broken up into different categories: 1) tRNA-isopentenylolation-related, 2) tRNA-isopentenylolation-unrelated, and 3) CK production upon tRNA degradation. Interestingly, a secondary zinc finger domain in addition to the IPP transferase domain (Pfam: IPPT) is required for the tgm role of certain tRNA-IPTs (Dabravolski, 2020 and references therein). IptB contains both of these domains, but IptC does not. Therefore, perhaps IptB has a secondary role involving tgm. With this in mind, more work with *iptB* and *iptC* knockout strains is necessary to determine the extent to which tRNA-IPTs contribute to CK production in *D. discoideum* and to other roles.

Discadenine synthase

Unlike both adenylate-IPTs and tRNA-IPTs, discadenine synthase (or synthetase) is unique to members of Dictyostelia (Taya et al., 1980; Abe et al., 1981). Discadenine synthase is responsible for catalyzing the reaction that creates the novel CK and potent spore germination inhibitor, DA (Taya et al., 1978b; Ihara et al., 1980, Abe et al., 1981; Ihara et al., 1986). Specifically, DA is synthesized through direct transfer of the 3-amino-3-carboxy-propyl moiety of S-adenosylmethionine (SAM) to iP (Figure 2.3) (Taya et al., 1978b). While the gene encoding discadenine synthase remains unidentified, various properties of the protein have been studied in *D. discoideum* (Taya et al., 1978b; Ihara et

al., 1980, Ihara et al., 1986). We conducted protein BLAST and HMMER searches in *D. discoideum* using known 3-amino-3-carboxypropyl transferases from other organisms, such as tRNA-uridine aminocarboxylpropyl transferase in *Escherichia coli*, to identify potential DA-synthase gene candidates, but none were found. Furthermore, we performed co-expression analyses with *iptA* as a reference using publicly available *D. discoideum* RNA-seq datasets and created a size-exclusion range based on papers that purified discadenine synthase from *D. discoideum* in the 1970's (Ihara et al., 1986; Kin et al., 2018; Aoki, unpublished). This narrowed our search to one candidate gene, *DDB_G0267868*. We successfully cloned the putative candidate into several different *E. coli* strains for recombinant protein expression, but the protein would not express. We then employed a different expression system and infiltrated *Nicotiana benthamiana* with *Agrobacterium* to transiently express the candidate discadenine synthase gene; however, the protein of interest could still not be detected. Therefore, it remains to be determined whether the candidate is indeed the discadenine synthase gene.

The activity of DA synthase increases during *D. discoideum* development (Ihara et al., 1980). The protein is active earlier than IptA and continually increases in activity following aggregation, which includes a brief hold in activity after 16-hours of development (slug stage), followed by a major peak at 26 hours (post-fruiting body development) and a final smaller peak at 31 hours. Considering that iP is the precursor to DA, it is puzzling that the activity of IptA peaks 10 hours later than DA synthase (Ihara et al., 1980). The sharp rise in IptA activity near the onset of sporulation may indicate that large amounts of iP are rapidly converted to DA allowing for the precipitous encapsulation and dormancy of spores. In support of the incongruent enzymatic activities of IptA and DA

synthase, similar findings were observed in *D. discoideum* between the developmentally regulated enzymes UDP-glucose epimerase and UDP-galactose polysaccharide transferase (Telser and Sussman, 1971).

The CK produced through DA synthase is unlike all other known naturally occurring CKs. Structurally, DA is an adenine derivative and is recognized as the first natural purine to possess an α -amino acid residue on the *N3* position of the adenine (Figure 2.3) (Nomura et al., 1977). Unlike its precursor, iP, DA does not promote cell proliferation (at concentrations between 1 nM and 1 μ M), nor does it prolong the stationary phase of single-celled growth (Aoki et al., 2019; data not shown). However, when tested using the classical cytokinin assay, (i.e. tobacco callus cell division bioassay), DA exhibits CK activity at concentrations tested between 0.5 μ M and 16 μ M (Nomura et al., 1977). More rigorous testing of DA as a CK was performed using several classical cytokinin and ligand-binding assays designed to assess CK activity in other organisms (Mik et al., 2017). The CK-like activity of DA was confirmed through the tobacco callus (cell division), *Amaranthus* (anthocyanin production), and detached wheat leaf (senescence) bioassays, and the activities were compared to that of a known potent, aromatic CK, benzyladenine (BA). The tobacco callus bioassay demonstrated most clearly the CK activity of DA, as the proliferation of CK-dependent callus cells was stimulated in a dose-dependent manner (at concentrations between 1 nM and 100 μ M). Interestingly, the same concentration at which BA exerted cytotoxicity (10 μ M) did not affect callus cell growth for cells treated with 10 μ M DA. In fact, DA-treated callus cells continued to proliferate at this concentration. While *N3*-substituted CK derivatives (i.e. *N3*-methylated BA) have been shown to reduce CK activity, the *N3*- α -amino acid residue in DA was shown to decrease the cytotoxicity of

the molecule compared to BA. As further confirmation of the CK-like activity, DA reduced the binding of isotopically labeled *tZ* in the *A. thaliana* receptors, AHK3 and CRE1/AHK4 (Mik et al., 2017). Of the two receptors, a higher affinity of DA occurred for CRE1/AHK4. Moreover, in a bacterial receptor assay, where the activation of the *A. thaliana* CK receptors results in the expression of the β -galactosidase reporter gene, DA elicited expression in both receptors, also in a dose-dependent manner (Mik et al., 2017). Therefore, DA possesses growth-promoting properties as a CK (in other organisms), as well as growth-inhibiting properties as an inhibitor of spore germination (in *D. discoideum*).

The proposed activities for DA may reflect a specific functionality within certain members of the *Dictyostelium* genus. A correlation between acrasins, or chemotactic agents, and spore germination inhibitors was noted between various Dictyostelid species (Taya et al., 1980; Abe et al., 1981). Of the six Dictyostelid species tested in these studies, DA and discadenine synthase were detected in only three species (namely *D. discoideum*, *D. purpureum*, and *D. mucoroides*). These three species were the only species tested that use cAMP as their chemotactic agent for aggregation. Furthermore, inhibition of spore germination was achieved through treatment with 2 μ M DA in these same three species, but not in the other three tested Dictyostelid species that utilize other chemotactic agents besides cAMP for aggregation (*D. minutum*, *D. lacteum*, and *Polysphondylium violaceum*). Based on these findings, it was postulated that spore germination inhibitors, including DA, may be both biochemically and evolutionarily linked with the chemotactic agent (Taya et al., 1980). This link with cAMP and DA will be discussed further in the CK-small molecule functional interactions section.

LOG – CK phosphoribohydrolase or Lonely Guy

CK phosphoribohydrolase (LOG) is responsible for the direct conversion of CK nucleotides into their most biologically active forms, the free bases (Kurakawa et al., 2007). This enzyme was first discovered in rice (*Oryza sativa*) where a loss of function mutant resulted in decreased floral organs and flowers with only one stamen; accordingly, it was wryly named ‘lonely guy’ (LOG). Since this discovery, LOG orthologs have been characterized in other plant species as well as bacteria, fungi, and archaea (Kuroha et al. 2009; Hinsch et al., 2015; Samanovic et al., 2015; Seo and Kim, 2017; Mayaka et al., 2019; Moramarco et al., 2019). A Protein BLAST search revealed a putative LOG ortholog (DDB0305758) in *D. discoideum* that presents strong homology with known LOG genes from plants and bacteria (Figure 2.4A). Interestingly, there are two peaks in the expression of the putative *LOG* gene: during vegetative growth and late development, both of which coincide with a time when CK accumulation and biological effects have been observed in *D. discoideum* (Figure 2.4B) (Anjard and Loomis, 2008; Rot et al., 2009; Aoki et al., 2019). *LOG* knockout and overexpression analyses in *A. thaliana* reveal pleiotropic effects on plant growth and development, leading to the conclusion that LOG plays a fundamental role in the regulation of CK across all developmental stages of *A. thaliana* (Kuroha et al., 2009). As an update since publication of this review (Aoki et al., 2020), we have experimentally confirmed that this LOG candidate is a CK-activating phosphoribohydrolase in *D. discoideum*, a result which forms the basis of Chapter 5.

CKX – Cytokinin oxidase/dehydrogenase

Cytokinin oxidase/dehydrogenase (CKX) inactivates CKs through oxidative cleavage of the N^6 side chain from the adenine ring (Frébert et al., 2011). While CKX-

activity has been identified primarily in plant species, similar enzymatic activities have been demonstrated in both *D. discoideum* and *S. cerevisiae* (Van Kast and Laten, 1987; Armstrong and Firtel, 1989). An enzyme with CKX-like activity was assayed by Armstrong and Firtel (1989) throughout all stages of *D. discoideum* growth and development. There was a peak in enzyme activity from growth to aggregation and then a steady decline throughout the remainder of *D. discoideum* development. The purified enzyme catalyzed the cleavage of the N^6 side chain from iP to adenine, and for this reason, was discussed as being similar to CKX in higher plants. However, Protein BLAST searches for both *D. discoideum* and *S. cerevisiae* do not reveal CKX-related sequences. Considering this point, Schmülling et al. (2003) speculates that CK breakdown via CKX is not conserved across all CK-producing organisms. In fact, the radish plant, *Raphanus sativus*, inactivates CKs solely through N-conjugation (Parker and Letham, 1973). The regulatory enzymes responsible for CK deactivation through N- or O- conjugation with a sugar moiety, commonly glucose, are known as uridine diphosphate glycosyltransferases (Šmehilová et al., 2014). A brief search on dictyBase revealed five characterized glucosyltransferases, four of which contained annotations for N-linked glucosylation. In our previous CK profiling experiments, we did not detect CK-glucosides at any stage of the *D. discoideum* life cycle; however, we did not search all possible conjugate alternatives (Aoki, unpublished). It is likely that the observed CKX-like activity in *D. discoideum* occurs through a non-CK specific degrading enzyme, such as one of the mentioned *D. discoideum* glucosyltransferases. Further work is necessary to determine 1) if *D. discoideum* produces any CK-conjugates and 2) if so, what enzyme is responsible for CK deactivation.

CK SECRETION AND TRANSLOCATION

Like most hormones, CKs are synthesized intracellularly before being secreted into the extracellular space. Transporter proteins play a key role in the inter- and intracellular distribution of CKs. This topic has yet to be explored in *D. discoideum*, so we will draw on what is known in plant systems. In *A. thaliana*, the transmembrane ABC transporter, ABCG14, is responsible for the active transport of CKs from the roots to the shoots via the xylem (Ko et al., 2014; Zhang et al., 2014). This ATPase transporter localizes to the plasma membrane of root cells, and its inactivation prevents the translocation of CKs. Experiments using radioactively labeled CKs show that *AtABCG14* acts as a CK exporter rather than an importer (Zhang et al., 2014). Potential regulation of CK secretion at the level of the ABC transporter is possible but has not been investigated. The *AtABCG14* protein is characterized as a half-transporter, composed of both an ATPase binding domain and a transmembrane domain. To be functional, half-transporters must associate with another polypeptide containing both a binding domain and a transmembrane domain to form a homo- or heterodimer. Alternatively, genes encoding full ABCG transporters, with all four domains (2 binding domains and 2 transmembrane domains) residing on a single polypeptide, are found in plants but not animals. Clear homologs of *AtABCG14* are found across the plant kingdom and likely play a similar role in CK transport. The *D. discoideum* genome possesses a wide variety of ABC transporters encompassing 71 different genes, which includes 24 for the G family (8 half transporters and 16 full transporters) (Anjard et al., 2002; see also update in <http://www.dicthybase.org>).

A sequence comparison shows that *AtABCG14* presents strong homology with members of the *D. discoideum* ABCG family, especially *DdABCG22*. A null mutant of

DdABCG22 was generated during a systematic study of ABC transporters (Miranda et al., 2013). This null strain presented delayed development and reduced spore viability – a phenotype that would be expected in the case of impaired CK secretion. However, the CK production of this strain was not evaluated. Furthermore, *DdABCG22* was also found to influence vegetative cell dispersion during a screening for mutants reverting the dispersive phenotype of the *ami8-* mutant (Nagasaki and Uyeda, 2008). As CKs were recently shown to have a role during vegetative cell stage, such results are not unexpected (Aoki et al., 2019). Therefore, assessing CK production and secretion in the *DdABCG22* null strain would give insight into whether this protein is involved in active transport of CKs or if its phenotype is unrelated to CK.

Two other protein families play a dominant role in CK transport in plants – the purine uptake permease (PUP) transporter family and the equilibrative nucleoside transporter (ENT) family. Certain members of the PUP transporter family allow for CK import into plant cells, specifically CK-nucleotides (Liu et al., 2019). The CK-specific PUP permeases appear to have evolved during terrestrial plant colonization between the bryophytes and the lycophytes from the pre-existing nucleotide sugar permease precursor (Jelesko, 2012). Thus, it is not surprising that homologs of PUP permease cannot be found in the *D. discoideum* genome. However, we cannot exclude the existence of a permease with similar function that would have evolved independently within Dictyostelids. The ENT family of transporters are also responsible for CK import into plant cells – specifically CK-ribosides (Liu et al., 2019). Out of the four ENT gene products in rice, one, *OsENT2* was shown to transport CK-ribosides, as well as adenosine (Hirose et al., 2005). *D. discoideum* possesses three uncharacterized ENT genes similar to *OsENT2* but also to

other ENTs, making it impossible to predict their substrate specificity without further experimentation (Table 2.1).

CK SIGNAL TRANSDUCTION

The canonical CK signal transduction pathway in plants involves a multi-step phosphorelay system that interacts through a complex form of the two-component signaling (TCS) pathway (Hwang and Sheen, 2001). TCS pathways are dominant in prokaryotes, especially bacteria, where they comprise the basic stimulus-response regulatory network allowing organisms to sense and respond to nearly all environmental stimuli (Stock et al., 2000). It is important to note that not all CK-producing organisms that respond to CK possess TCS elements. This is the case in several mammalian studies where CKs act as agonists to the adenosine receptors A_{2A} and A_3 (Blad et al., 2011; Lee et al., 2012; Lappas, 2015). However, the remainder of this section will focus on components of the TCS CK signaling pathway, as are present in *D. discoideum*. Classically, the TCS pathway involves a histidine kinase (HK), which acts as the receptor, and a response regulator protein (RR), which, once activated, elicits a specific response through downstream effectors. This is slightly modified in land plants, where the CK signal transduction pathway involves a series of sequential phosphorylation events that alternate between His and Asp residues initiated by HKs, are perpetuated by histidine phosphotransfer proteins (HPs), and finished by RRs (Kieber and Schaller, 2018). A conserved extracellular loop of the HK transmembrane receptors belonging to the cyclase/histidine kinase-associated sensory extracellular (CHASE) domain-containing histidine kinase family is responsible for the initiation of CK signaling (Anantharaman and

Aravind, 2001). Interestingly, the number of reported CK-producing organisms that possess conserved CHASE domains in recent years has expanded and will be described below (Kabbara et al., 2018).

DhkA and AcgA

In *D. discoideum*, there are two CHASE-domain containing proteins that are both involved in encystation and sporulation – the histidine kinase, DhkA, and the adenylyl cyclase of germination stage protein, AcgA (Alvarez-Curto et al., 2007; Anjard and Loomis, 2008). Neither of these proteins appear to be a CK receptor in *D. discoideum*, as null mutants for both proteins have a normal response to CK treatment (Anjard and Loomis, 2008). However, a *dhkA* and *acgA* double knockout has yet to be tested for definitive confirmation that neither of these proteins function as the CK receptor in *D. discoideum*. While CK was shown to act independently of DhkA, DhkA is still thought to regulate spore germination (Anjard and Loomis, 2008). In pre-spore cells, the peptide, spore differentiation factor 2 (SDF-2), binds to the CHASE domain in DhkA, which leads to the dephosphorylation of the cAMP phosphodiesterase, RegA, resulting in its inactivation. In this same time frame, the CK signaling pathway in *D. discoideum* (discussed below) converges to facilitate spore formation by inducing cAMP production (Figure 2.5) (Anjard and Loomis, 2008).

DhkB and AcrA

The CK signal transduction pathway leading to the induction of sporulation is dependent on the histidine kinase, DhkB, and the adenylate cyclase with response regulator domain, AcrA (Anjard and Loomis, 2008). *dhkB* encodes a 1,969 amino acid, 219 kDa protein (DhkB, DDB0215358), whereas *acrA* encodes a 2,123 amino acid, 243 kDa protein

(AcrA, DDB0191294). *dhkB* is one of 13 functional histidine kinase genes in the *D. discoideum* genome that encodes a HK protein possessing several potential transmembrane domains and extracellular loops (Anjard and Loomis, 2003). Because of the large size of both of these transmembrane proteins, they were tested in a CK binding assay to determine if they were CK receptors (Anjard and Loomis, 2008). Wild-type cells (22-hours) undergoing development were tested for their ability to bind ³H-labeled iP in the presence of 1 mM adenine to minimize non-specific background binding. Wild-type cells had a binding affinity for ³H-iP of 6 nM. Furthermore, specific binding of ³H-iP in vegetative and 22-hour developed wild-type cells and 22-hour developed *dhkB*⁻ and *acrA*⁻ cells was determined for each of the respective cell types. Developed 22-hour wild-type, *dhkB*⁻, and *acrA*⁻ cells all bound similar levels of ³H-iP indicating that DhkB and AcrA are unlikely to be CK receptors. Vegetative wild-type cells bound 8-times less CK in comparison to the three tested developed cell types suggesting that the receptor is developmentally regulated. Zinda and Singleton (1998) reported that *dhkB*⁻ null cells develop into fruiting bodies within 22 to 24 hours. However, precocious germination of spores quickly ensues as the mutant *dhkB*⁻ spores fail to respond to the spore germination inhibitor, DA. The germinated amoebae within the spore head quickly dehydrate owing to the high osmolarity maintained in the spore mass, and the majority of the cells are non-viable. *dhkB*⁻ cells with partially constitutive PKA activity (*dhkB*⁻/*K*), developed at low densities and failed to differentiate into spores when treated with DA or other CKs; however, they could differentiate when treated with the spore inducers SDF-1, SDF-2, and GABA at levels similar to those found in wild-type cells (Anjard and Loomis, 2008). AcrA carries two response regulatory regions, which were suggested as potential targets for the interaction between DhkB and

AcrA (Anjard et al., 2001; see reviews by Kriebel and Parent, 2004 and Loomis, 2014). Like *dhkB*⁻ cells, *acrA*⁻ spores germinated precociously resulting in almost no viable cells (Söderbom et al., 1999). An abnormal phenotype was observed in *acrA*⁻ cells, in which the knockout strain formed fruiting bodies with abnormally thin stalks and glassy, translucent spore masses. Interestingly, this phenotype was also observed in the *dhkB*⁻ and *dhkA*⁻ knockout strains (Zinda and Singleton, 1998; Wang et al., 1999). Consistent with *dhkB*⁻ cells, *acrA*⁻ cells also failed to differentiate into spores following treatment with DA, iP, or *tZ*, but differentiated normally in response to other sporulation inducers (Anjard and Loomis, 2008).

AcaA, RdeA, and RegA

Several other known proteins affecting *D. discoideum* development were studied to determine whether they were involved in the induction of sporulation by CKs (Anjard and Loomis, 2008). The adenylyl cyclase of aggregation protein, AcaA, was identified as a possible candidate for interaction with CK owing to its similarity to AcrA. *acaA*⁻ cells responded well to CKs, SDF-2, and GABA, indicating that the SDF-2 induction of spore encapsulation is not dependent upon a specific source of cAMP derived from this adenylyl cyclase (Anjard and Loomis, 2008). The rapid development protein, RdeA, and the previously mentioned cAMP phosphodiesterase, RegA, were tested to rule out any indirect effects of CK sporulation induction through stimulation of these proteins in the SDF-2 pathway. As mentioned earlier, spore induction through both the SDF-2 and CK signaling pathways occurs at precisely the same time during development. Previous work on spore induction pathways indicated that the peptide, SDF-2, generated from the Acyl-CoA binding protein, AcbA, acts on the receptor histidine kinase DhkA, which is present on

both pre-spore and pre-stalk cells (Anjard and Loomis, 2005). The binding of SDF-2 to DhkA inhibits phosphorelay between RdeA and RegA. As such, the unphosphorylated response regulation region of RegA results in an accumulation of cAMP through AcrA, which increases the activity of PKA triggering rapid encapsulation of spores (Wang et al., 1999). Cells lacking RdeA and RegA responded to CK normally but were unable to respond to SDF-2 or GABA, thus leading to the conclusion that these proteins are not required for the induction of sporulation by CKs (Anjard and Loomis, 2008). While there have been no direct interactions observed between these three mentioned proteins and CKs, their combined roles lead to increased cAMP production, which is essential for encapsulation (Schaap and Schilde, 2018).

In summary, the signal transduction pathway for the induction of sporulation by CK is dependent upon DhkB and AcrA. CK signaling acts indirectly with the proteins involved in the SDF-2 signal transduction pathway, DhkA, RdeA, and RegA resulting in increased cAMP signaling. Furthermore, the other adenylyl cyclases, AcaA and AcgA, do not appear to directly interact with the CK pathway, unlike AcrA. However, there is an underlying connection with CK and cAMP in *D. discoideum* that will be discussed in the CK-small molecule functional interaction section. Potential cross-talk with CKs and other signaling pathways is likely and is common in other systems (e.g., CKs and auxin in plants); therefore, this would be an area of interest for future studies. Currently, there are no recognized receptors in *D. discoideum* that respond to CK, so further investigation is necessary to identify how CKs enact their effects. A candidate gene was found during systematic screening for developmental mutants after REMI mutagenesis. The mutant, DGG1110, presented a strikingly similar phenotype to the *acrA* null strain. Both strains

develop normally but form spores that fail to remain dormant in the spore mass, leading to the death of the emerging amoebae. Differentiation assays with cells recovered from the culminant show that DGG1110 cells, like *acrA* null cells, form spores in response to SDF-1, GABA or SDF-2 but not to *trans*-zeatin (Anjard and Loomis, 2006, unpublished). The gene inactivated in the DGG1110 strain (*DDB_G0269128*), encodes a predicted 544 amino acid protein with no clear homology to a known gene. However, this sequence presents a potential extracellular domain flanked by two transmembrane regions with a similar size and topology to the CHASE domain. While the homology with such domain is low, the mere presence of a potential extracellular loop in addition to the lack of response to CK in the null mutant make this gene a strong candidate for being the unidentified CK receptor in *D. discoideum*.

FUTURE DIRECTIONS – CK-SMALL MOLECULE FUNCTIONAL INTERACTIONS

CK-cAMP interactions

cAMP is considered a universal second messenger controlling a wide variety of biological processes in all kingdoms of life (McDonough and Rodriguez, 2012). Among Dictyostelia, cAMP plays a dominant role in developmental signaling (Schaap, 2011). In the evolution of Dictyostelids, the roles of cAMP progressed from those involved in biological processes relating to stress to those regulating chemotactic aggregation, morphogenesis, and differentiation (Schaap, 2016). While the links between cAMP and the developmental program of *D. discoideum* have been extensively studied, intriguing suggestions of interactions between cAMP and CK have appeared over the last half century and remain largely unexplored.

Early studies on the role of CK in *D. discoideum* report an interesting correspondence between chemoattractants and spore germination inhibitors (Taya et al., 1980; Abe et al., 1981). As mentioned above, only the species that use cAMP as their acrasin also produce and respond to the spore germination inhibitor, DA. Moreover, during CK synthesis, the acceptor molecule of the isopentenyl side chain, 5'-AMP, which is catalyzed by IPT to create iP nucleotides, can be derived from cAMP through hydrolysis from cAMP phosphodiesterase (Taya et al., 1980). This evolutionary link between cAMP and CK among Dictyostelia was further confirmed through recent molecular phylogenetic analyses where all members of the most recently diverged species of Dictyostelia, group 4, use cAMP as their acrasin despite the use of various other chemoattractants among members belonging to the earlier diverged species of Dictyostelia in groups 1-3 (Schaap et al., 2006; Schaap, 2011). Therefore, it is likely that the earlier diverged species of Dictyostelia in groups 1-3 do not possess the enzyme to synthesize DA unlike the species belonging to group 4 who use cAMP as their chemoattractant.

Among other CK-producing organisms, links between cAMP and CK have been established. In *A. thaliana*, Plakidou-Dymock et al. (1998) identified seven potential seven transmembrane-spanning G-protein coupled receptors candidates. One of the candidates, *GCR1*, was isolated owing to its high similarity to other characterized seven-transmembrane proteins. Interestingly, the GCR1 protein is most closely related to the *D. discoideum* cAMP receptors, CarA-D. Transcriptome analysis of *GCR1* in *A. thaliana* revealed new evidence that this protein is involved in hormonal responses, including CK biosynthesis and response, among many other functions (Chakraborty et al., 2015). Therefore, it would be of high interest to study the Car receptors in *D. discoideum* as

potential CK receptors. In *E. coli*, CKs have a growth-promoting effect by modulating the activity of enzymes responsible for cAMP biosynthesis and degradation (Judewicz et al., 1973; Coppola et al., 1976). A similar effect is seen in mammalian cells where exogenously added CKs act as competitive inhibitors of cAMP phosphodiesterase (Hecht et al., 1974). While a link between cAMP and CK is suggested through the reported studies, much remains to be understood between the functional interplay between these two molecules. Considering the dominant role cAMP plays throughout the *D. discoideum* life cycle, *D. discoideum* provides an excellent system to further unravel the interaction between CKs and cAMP.

CK-NO interactions

Like cAMP, nitric oxide (NO) is prevalent among all kingdoms and is one of the most common signaling molecules among living organisms (Schmidt and Walter, 1994; Lamattina et al., 2003; Moncada and Higgs, 2006). In *D. discoideum*, endogenous production of NO acts as a regulator of differentiation during development (Tao et al., 1997). NO-releasing compounds, such as sodium nitroprusside, inhibit *D. discoideum* aggregation by affecting the ability of cells to generate cAMP pulses (Tao et al., 1992, 1996). On the contrary, treatment with NO-scavengers, such as oxyhemoglobin (oxyHb), stimulates *D. discoideum* aggregation (Tao et al., 1997). Combining these respective results, a working model for the action of NO was proposed in *D. discoideum*: NO inhibits cAMP production in vegetative cells; upon starvation, the cells overcome the NO-inhibiting effects through cAMP pulses initiating the developmental program of *D. discoideum*. Interestingly, preliminary data involving treatment of starved *D. discoideum* cells with different CKs (iP and BA) inhibits NO production, leading to precocious

aggregation (Mathavarajah & Aoki, unpublished). Moreover, total endogenous CK concentrations increase as cells transition from growth to aggregation (Aoki et al., 2019). These findings are consistent with the results regarding the treatment of cells with NO-scavengers. Therefore, CKs may have a secondary role in regulating NO levels in *D. discoideum*, specifically in the initiation of the developmental program.

Considering the preliminary evidence that CKs affect NO in *D. discoideum*, it is likely that future research will continue to elucidate further interactions between these two signaling molecules both in *D. discoideum* and other CK-producing organisms. Furthermore, the strong interactions between CK and NO, as demonstrated in plants and other CK-producing organisms, could be used to elucidate candidate genes in *D. discoideum* involving NO synthesis and regulation (Husain et al., 2010; Feng et al., 2013; Liu et al., 2013; Samanovic and Darwin, 2015).

CONCLUSION

The Dictyostelid system is unlike any other model organism utilized to assess the evolution of CKs as signaling agents among and between kingdoms of life. In fact, many new emerging areas of *D. discoideum* research encompass interactions with organisms in other kingdoms. These emerging areas include topics such as, *D. discoideum* as farmers of symbiotic bacteria, host defense against pathogenic bacteria and nematodes, and interactions with spore-dispersing organisms – all of which are influenced by interkingdom signaling, and perhaps CKs (Bozzaro and Eichinger, 2011; Brock et al., 2013; Smith et al., 2014; Novohradská et al., 2017). While there is accumulating evidence documenting the conservation of CK biosynthetic and signal transduction pathways among Dictyostelia

species, much remains to be understood about the role of CK within this clade. Considering the widespread occurrence of CKs in both single-celled and multicellular organisms, Dictyostelids offer a unique opportunity to assess how CKs have evolved from roles at the cellular level to roles in controlling complex events during multicellular development. Furthermore, the dominant role that cAMP and NO play in various aspects of *D. discoideum* development expand the utility of this organism for studying not only the evolution of CKs beyond the plant kingdom, but also CK interactions with other signaling molecules. An additional promising small molecule to be investigated in the future for CK interactions is inorganic polyphosphate (poly P). Several studies highlight the drastic accumulation of poly P throughout the course of *D. discoideum* development, and *ppk1*⁻ cells have developmental defects in germination similar to those described for the CK-dependent *dhkB*⁻ and *acrA*⁻ null cells (Zhang et al., 2005; Livermore et al., 2016). Utilizing this model system, specific functions of CKs can be observed at the single cell level and beyond into multicellular organization and development. This gives insight into the pleiotropic nature of CKs and the mechanisms by which they facilitate physiological interactions among and between various kingdoms of life.

TABLES AND FIGURES

Table 2.1. Sequence similarity of equilibrative nucleoside transporter (ENT) proteins in *D. discoideum*. The sequence similarity of three uncharacterized equilibrative nucleoside transporter (ENT) proteins in *D. discoideum* are compared to the known cytokinin transporter protein, *OsENT2*, in *Oryza sativa*.

<i>D. discoideum</i> Gene ID	<i>D. discoideum</i> Protein ID	Length (aa)	Identity (%)	Positives (%)	E-value
DDB_G0283439	DDB0273810	430	22	43	5.00E-13
DDB_G0281515	DDB0237816	522	21	41	8.00E-12
DDB_G0281513	DDB0237815	482	22	41	7.00E-11

The amino acid sequence of *OsENT2* (Accession: BAG95361.1) was inputted into the BLASTp server of dictyBase with the following parameters: E-value, 0.1; Matrix, BLOSUM62; Filter, no (<http://www.dictybase.org>).

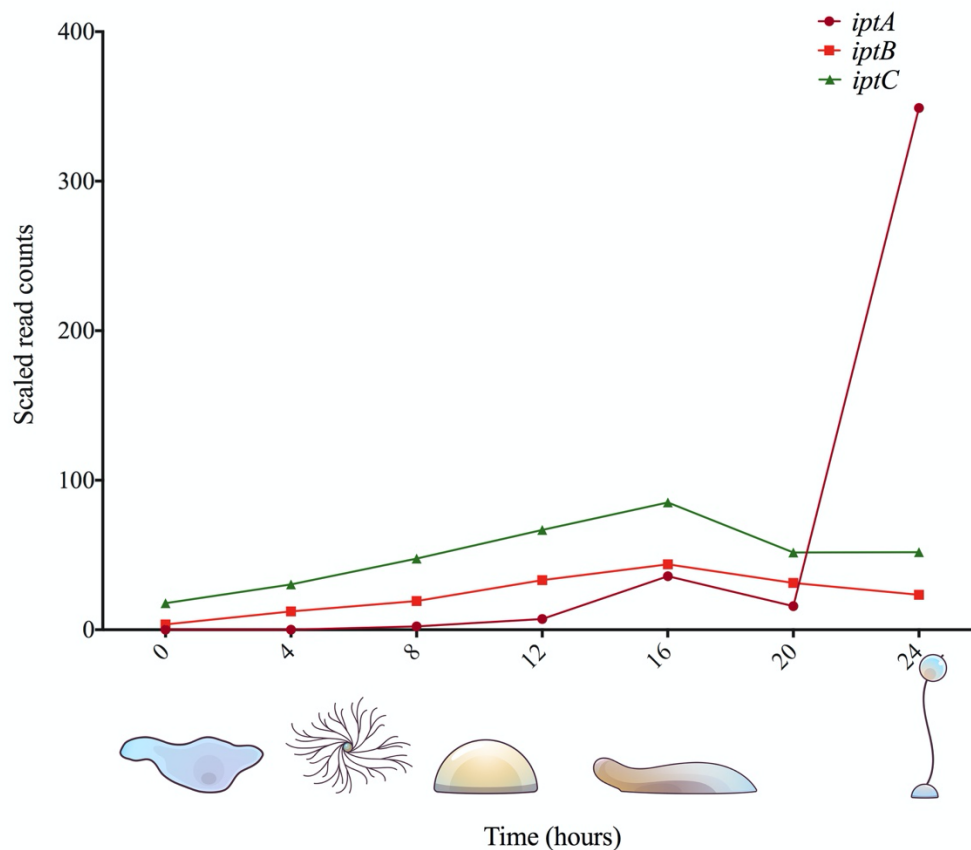


Figure 2.1. Gene expression analysis of known and putative CK biosynthesis genes in *D. discoideum*. RNA-Seq data was obtained from dictyExpress (www.dictyexpress.biolaab.si) (Rot et al., 2009).

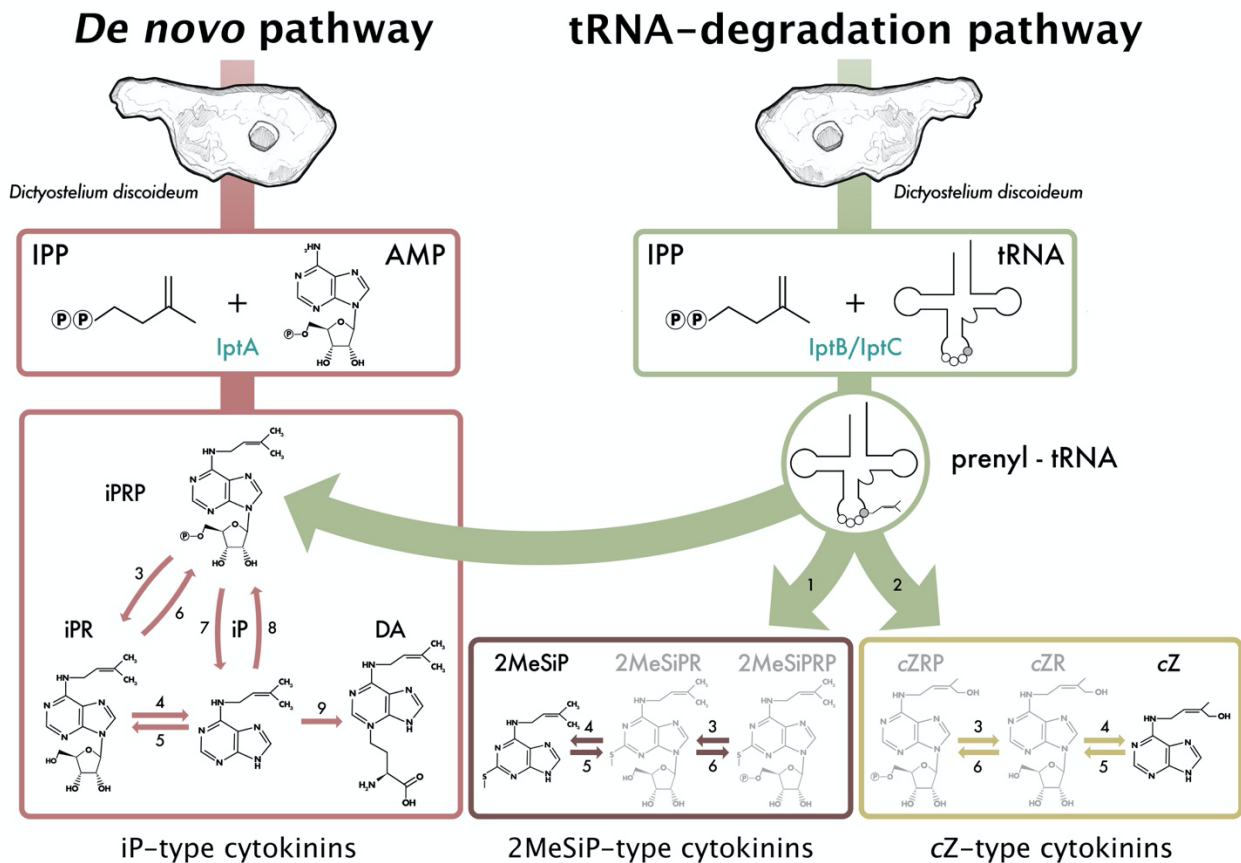


Figure 2.2. Proposed cytokinin (CK) biosynthesis pathway based on the CKs detected throughout all stages of the *D. discoideum* life cycle. Black CK structures denote CKs that have been previously detected in *D. discoideum*, and greyed CK structures are indicative of common CK forms detected in other CK-producing biosynthetic pathways. Numbers represent known or inferred enzymes from previous *D. discoideum*, plant, fungi, and bacteria studies and are as follows: 1. *cdk5rap1*-like ortholog (*DDB_G0287079*); 2. cis-hydroxylase; 3. 50-ribonucleotide phosphohydrolase; 4. adenosine nucleosidase; 5. purine nucleoside phosphorylase; 6. adenosine kinase; 7. CK phosphoribohydrolase (LOG-like ortholog, *DDB_G0281309*); 8. adenine phosphoribosyltransferase; 9. discadenine synthase (Taya et al., 1978a, 1978b; Anjard and Loomis, 2008; Kamada-Nobusada and Sakakibara, 2009; Spíchal, 2012; Morrison et al., 2015; Morrison et al., 2017; Nishii et al., 2018). Reproduced with permission from Aoki et al. (2019).

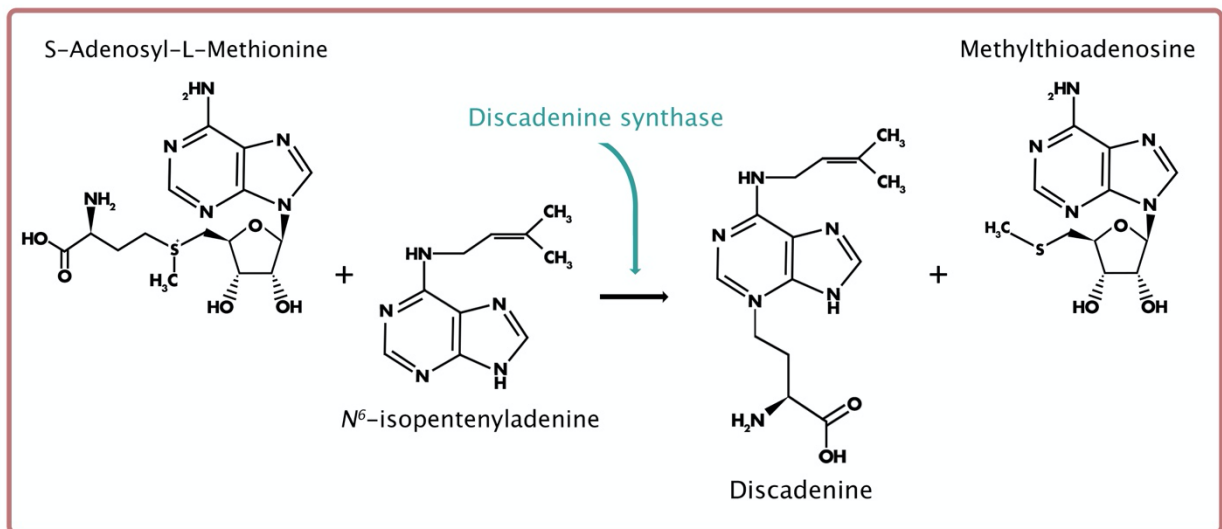


Figure 2.3. Reaction scheme for discadenine (DA) biosynthesis. DA is derived from N^6 -isopentenyladenine (iP) and catalyzed by discadenine synthase.

A

Species	Gene name	Length (aa)	Accession	Identities (%)	Positives (%)	E-value
<i>A. thaliana</i>	<i>At_log3</i>	191	OAP11690.1	53	67	2.00E-47
<i>O. sativa</i>	<i>Os_log</i>	242	Q5ZC82.1	47	62	3.00E-48
<i>R. fascians</i>	<i>fasF</i>	198	AET25218.1	38	59	1.00E-32
<i>M. tuberculosis</i>	<i>Mt_log</i>	187	O05306.1	35	58	6.00E-25
<i>C. purpurea</i>	<i>cpur_02269</i>	240	CCE28582.1	38	52	1.00E-28
<i>B. pertussis</i>	<i>Bp1253</i>	209	Q7VYQ7	24	48	4.00E-11

The amino acid sequences of LOG proteins from various CK-producing species were inputted into the BLASTp server of dictyBase with the following parameters: E-value, 0.1; Matrix, BLOSUM62; Filter, no (<http://www.dictybase.org>).

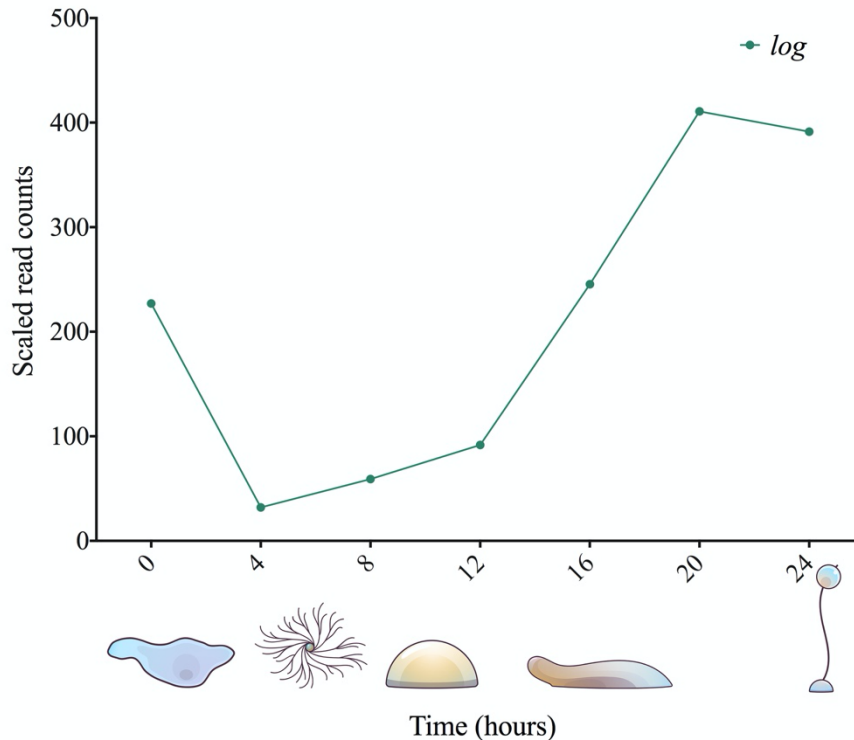
B

Figure 2.4. *Dictyostelium discoideum* has a putative LOG gene (*DDB_G0281309*). (A) LOG orthologs from several organisms. Protein BLASTs were performed using the dictyBase BLAST server to assess sequence similarity of LOG orthologs to the encoded product of the putative LOG gene, *DDB_G0281309* (<http://www.dictybase.org>). (B) Gene expression profile of the putative LOG gene using RNA-Seq data obtained from dictyExpress (www.dictyexpress.biolab.si) (Rot et al., 2009).

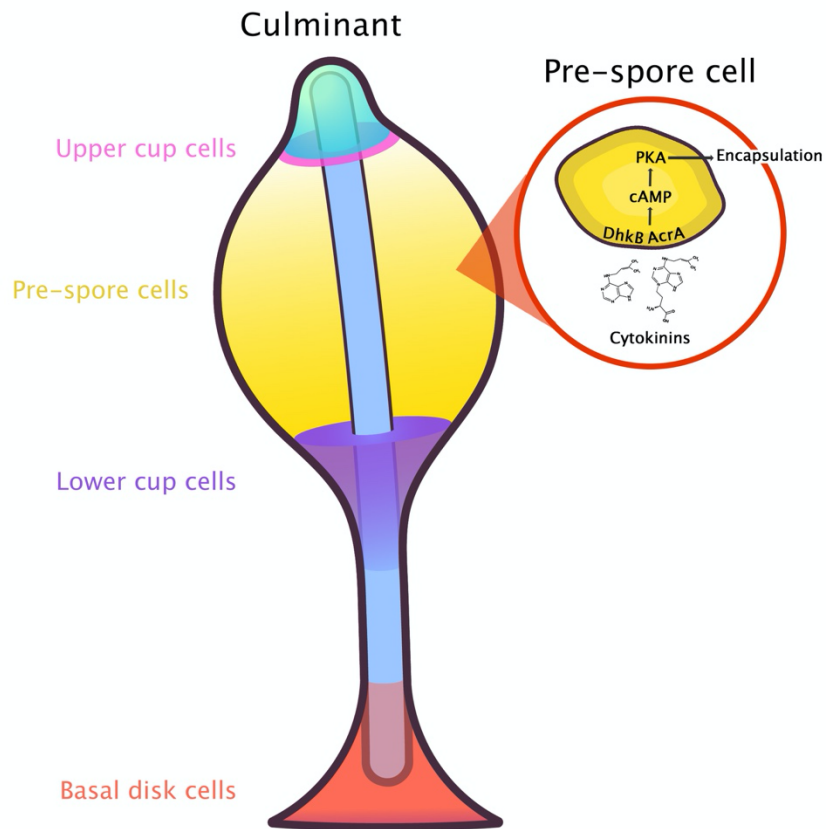


Figure 2.5. A model for the induction of sporulation by CK proposed by Anjard and Loomis (2008). Cytokinin is perceived by an unknown receptor and initiates a downstream phosphorelay through interaction of the histidine kinase, DhkB, and the adenylyl cyclase, AcrA. This, in turn, leads to an increase in intracellular cAMP where the CK pathway and the SDF-2 signaling pathway (not shown) converge at the level of PKA activation. An increase in PKA activity then leads to rapid encapsulation of spores.

REFERENCES

- Abe, H., Hashimoto, K., and Uchiyama, M. (1981). Discadenine distribution in cellular slime molds and its inhibitory activity on spore germination. *Agric. Biol. Chem.* 45, 1295–1296. doi:10.1080/00021369.1981.10864699.
- Abe, H., Uchiyama, M., Tanaka, Y., Saito, H. (1976). Structure of discadenine, a spore germination inhibitor from the cellular slime mold *Dictyostelium discoideum*. *Tetrahedron Lett.* 17, 3807–3810. doi: 10.1016/S0040-4039(00)93115-0.
- Akiyoshi, D. E., Klee, H., Amasino, R. M., Nester, E. W., and Gordon, M. P. (1984). T-DNA of *Agrobacterium tumefaciens* encodes an enzyme of cytokinin biosynthesis. *Proc. Natl. Acad. Sci. U.S.A.* 81, 5994–5998. doi: 10.1073/pnas.81.19.5994.
- Alvarez-Curto, E., Saran, S., Meima, M., Zobel, J., Scott, C., and Schaap, P. (2007). cAMP production by adenylyl cyclase G induces differentiation in *Dictyostelium* slugs. *Development* 134, 959-966. doi: 10.1242/dev.02775.
- Anantharaman, V. and Aravind, L. (2001). The CHASE domain: A predicted ligand-binding module in plant cytokinin receptors and other eukaryotic and bacterial receptors. *Trends Biochem. Sci.* 26, 579–582. doi: 10.1016/S0968-0004(01)01968-5.
- Anjard, C. and Loomis, W. F. (2003). “Histidine Kinases of *Dictyostelium*,” in *Histidine Kinases in Signal Transduction*, eds. M. Inouye and R. Dutta (San Diego: Academic Press), 421–438. doi: 10.1016/B978-012372484-7/50021-7.
- Anjard, C. and Loomis, W. F. (2005). Peptide signaling during terminal differentiation of *Dictyostelium*. *Proc. Natl. Acad. Sci. U.S.A.* 102, 7607–7611. doi: 10.1073/pnas.0501820102.
- Anjard, C. and Loomis, W. F. (2008). Cytokinins induce sporulation in *Dictyostelium*. *Development* 135, 819-827. doi: 10.1242/dev.018051.
- Anjard, C., Loomis, W. F., and *Dictyostelium* Sequencing Consortium (2002). Evolutionary analyses of ABC transporters of *Dictyostelium discoideum*. *Eukaryot. Cell* 1, 643–652. doi: 10.1128/ec.1.4.643-652.2002.
- Anjard, C., Söderbom, F., and Loomis, W. F. (2001). Requirements for the adenylyl cyclases in the development of *Dictyostelium*. *Development* 128, 3649–3654.
- Aoki, M. M., Emery, R. J. N., Anjard, C., Brunetti, C. R., and Huber, R. J. (2020). Cytokinins in Dictyostelia – A unique model for studying the functions of signaling agents from species to kingdoms. *Front. Cell Dev. Biol.* 8, 511. doi: 10.3389/fcell.2020.00511.
- Aoki, M. M., Kisiala, A. B., Li, S., Stock, N. L., Brunetti, C. R., Huber, R. J., et al. (2019). Cytokinin detection during the *Dictyostelium discoideum* life cycle: Profiles are

- dynamic and affect cell growth and spore germination. *Biomolecules* 9, 702. doi: 10.3390/biom9110702.
- Armstrong, D. J. and Firtel, R. A. (1989). Cytokinin oxidase activity in the cellular slime mold, *Dictyostelium discoideum*. *Dev. Biol.* 136, 491–499. doi: 10.1016/0012-1606(89)90274-1.
- Blad, C. C., von Frijtag Drabbe Künzel, J. K., de Vries, H., Mulder-Krieger, T., Bar-Yehuda, S., Fishman, P., et al. (2011). Putative role of the adenosine A₃ receptor in the antiproliferative action of N⁶-(2-isopentenyl)adenosine. *Purinergic Signal.* 7, 453-462. doi: 10.1007/s11302-011-9244-9.
- Bloomfield, G., Tanaka, Y., Skelton, J., Ivens, A., and Kay, R. R. (2008). Widespread duplications in the genomes of laboratory stocks of *Dictyostelium discoideum*. *Genome Biol.* 9. doi: 10.1186/gb-2008-9-4-r75.
- Bozzaro, S. and Eichinger, L. (2011). The professional phagocyte *Dictyostelium discoideum* as a model host for bacterial pathogens. *Curr. Drug Targets* 12, 942–954. doi: 10.2174/138945011795677782.
- Brock, D. A., Read, S., Bozhchenko, A., Queller, D. C., and Strassmann, J. E. (2013). Social amoeba farmers carry defensive symbionts to protect and privatize their crops. *Nat. Commun.* 4, 2385. doi: 10.1038/ncomms3385.
- Chakraborty, N., Sharma, P., Kanyuka, K., Pathak, R. R., Choudhury, D., Hooley, R. A., et al. (2015). Transcriptome analysis of *Arabidopsis* GCR1 mutant reveals its roles in stress, hormones, secondary metabolism and phosphate starvation. *PLoS One* 10, e0122423. doi: 10.1371/journal.pone.0117819.
- Coppola, S., Marino, P., and Zoina, A. (1976). Cytokinin contents and cAMP metabolism during growth of *Escherichia coli*. *Experientia* 32, 566–567. doi: 10.1007/BF01990164.
- Crespi, M., Messens, E., Caplan, A. B., van Montagu, M., and Desomer, J. (1992). Fasciation induction by the phytopathogen *Rhodococcus fascians* depends upon a linear plasmid encoding a cytokinin synthase gene. *EMBO J.* 11, 795-804. doi: 10.1002/j.1460-2075.1992.tb05116.x.
- Dabravolski, S. (2020). Multi-faceted nature of the tRNA isopentenyltransferase. *Funct. Plant Biol.* 47, 475-485. doi: 10.1071/FP19255.
- Durbecq, V., Sainz, G., Oudjama, Y., Clantin, B., Bompard-Gilles, C., Tricot, C., et al. (2001). Crystal structure of isopentenyl diphosphate:dimethylallyl diphosphate isomerase. *EMBO J.* 20, 1530–1537. doi: 10.1093/emboj/20.7.1530.
- Ericson, J. U. and Bjork, G. R. (1986). Pleiotropic effects induced by modification

- deficiency next to the anticodon of tRNA from *Salmonella typhimurium* LT2. *J. Bacteriol.* 166, 1013–1021. doi: 10.1128/jb.166.3.1013-1021.1986.
- Feng, J., Wang, C., Chen, Q., Chen, H., Ren, B., Li, X., et al. (2013). S-nitrosylation of phosphotransfer proteins represses cytokinin signaling. *Nat. Commun.* 4, 1529. doi: 10.1038/ncomms2541.
- Frébort, I., Kowalska, M., Hluska, T., Frébortová, J., and Galuszka, P. (2011). Evolution of cytokinin biosynthesis and degradation. *J. Exp. Bot.* 62, 2431–2452. doi: 10.1093/jxb/err004.
- Frébortová, J., Greplová, M., Seidl, M. F., Heyl, A., and Frébort, I. (2015). Biochemical characterization of putative adenylate dimethylallyltransferase and cytokinin dehydrogenase from *Nostoc sp.* PCC 7120. *PLoS One* 10, e0138468. doi: 10.1371/journal.pone.0138468.
- Hecht, S. M., Faulkner, R. D., and Hawrelak, S. D. (1974). Competitive inhibition of beef heart cyclic AMP phosphodiesterase by cytokinins and related compounds. *Proc. Natl. Acad. Sci. U.S.A.* 71, 4670–4674. doi: 10.1073/pnas.71.12.4670.
- Hinsch, J., Vrabka, J., Oeser, B., Novák, O., Galuszka, P., and Tudzynski, P. (2015). *De novo* biosynthesis of cytokinins in the biotrophic fungus *Claviceps purpurea*. *Environ. Microbiol.* 17, 2935–2951. doi: 10.1111/1462-2920.12838.
- Hirose, N., Makita, N., Yamaya, T., and Sakakibara, H. (2005). Functional characterization and expression analysis of a gene, OsENT2, encoding an equilibrative nucleoside transporter in rice suggest a function in cytokinin transport. *Plant Physiol.* 138, 196–206. doi: 10.1104/pp.105.060137.
- Husain, M., Jones-Carson, J., Song, M., McCollister, B. D., Bourret, T. J., and Vázquez-Torres, A. (2010). Redox sensor SsrB Cys203 enhances *Salmonella* fitness against nitric oxide generated in the host immune response to oral infection. *Proc. Natl. Acad. Sci. U.S.A.* 107, 14396–14401. doi: 10.1073/pnas.1005299107.
- Hwang, I. and Sheen, J. (2001). Two-component circuitry in *Arabidopsis* cytokinin signal transduction. *Nature* 413, 383–389. doi: 10.1038/35096500.
- Ihara, M., Tanaka, Y., Yanagisawa, K., Taya, Y., and Nishimura, S. (1986). Purification and some properties of discadenine synthase from *Dictyostelium discoideum*. *BBA - Gen. Subj.* 881, 135–140. doi: 10.1016/0304-4165(86)90106-6.
- Ihara, M., Taya, Y., and Nishimura, S. (1980). Developmental regulation of cytokinin, spore germination inhibitor discadenine and related enzymes in *Dictyostelium discoideum*. *Exp. Cell Res.* 126, 273–278. doi: 10.1016/0014-4827(80)90265-7.
- Ihara, M., Taya, Y., Nishimura, S., and Tanaka, Y. (1984). Purification and some properties

- of $\Delta 2$ -isopentenylpyrophosphate:5'AMP $\Delta 2$ -isopentenyltransferase from the cellular slime mold *Dictyostelium discoideum*. *Arch. Biochem. Biophys.* 230, 652–660. doi: 10.1016/0003-9861(84)90446-6.
- Jelesko, J. G. (2012). An expanding role for purine uptake permease-like transporters in plant secondary metabolism. *Front. Plant Sci.* 3, 1–5. doi: 10.3389/fpls.2012.00078.
- Judewicz, N. D., De Robertis, E. M., and Torres, H. N. (1973). Inhibition of *Escherichia coli* growth by cyclic adenosine 3', 5'-monophosphate. *Biochem. Biophys. Res. Commun.* 52, 1257–1262. doi: 10.1016/0006-291X(73)90636-0.
- Kabbara, S., Schmülling, T., and Papon, N. (2018). CHASEing cytokinin receptors in plants, bacteria, fungi, and beyond. *Trends Plant Sci.* 23, 179–181. doi: 10.1016/j.tplants.2018.01.001.
- Kakimoto, T. (2001). Identification of plant cytokinin biosynthetic enzymes as dimethylallyl diphosphate:ATP/ADP isopentenyltransferases. *Plant Cell Physiol.* 42, 677–685. doi: 10.1093/pcp/pce112.
- Kamada-Nobusada, T. and Sakakibara, H. (2009). Molecular basis for cytokinin biosynthesis. *Phytochemistry* 70, 444–449. doi: 10.1016/j.phytochem.2009.02.007.
- Kieber, J. J. and Schaller, G. E. (2018). Cytokinin signaling in plant development. *Development* 145, dev149344. doi: 10.1242/dev.149344.
- Kin, K., Forbes, G., Cassidy, A., and Schaap, P. (2018). Cell-type specific RNA-Seq reveals novel roles and regulatory programs for terminally differentiated *Dictyostelium* cells. *BMC Genomics.* 19, 764. doi: 10.1186/s12864-018-5146-3.
- Ko, D., Kang, J., Kiba, T., Park, J., Kojima, M., Do, J., et al. (2014). *Arabidopsis* ABCG14 is essential for the root-to-shoot translocation of cytokinin. *Proc. Natl. Acad. Sci. U.S.A.* 111, 7150–7155. doi: 10.1073/pnas.1321519111.
- Kriebel, P. W. and Parent, C. A. (2004). Adenylyl cyclase expression and regulation during the differentiation of *Dictyostelium discoideum*. *IUBMB Life* 56, 541-546. doi: 10.1080/15216540400013887.
- Kurakawa, T., Ueda, N., Maekawa, M., Kobayashi, K., Kojima, M., Nagato, Y., et al. (2007). Direct control of shoot meristem activity by a cytokinin-activating enzyme. *Nature* 445, 652–655. doi: 10.1038/nature05504.
- Kuroha, T., Tokunaga, H., Kojima, M., Ueda, N., Ishida, T., Nagawa, S., et al. (2009). Functional analyses of LONELY GUY cytokinin-activating enzymes reveal the importance of the direct activation pathway in *Arabidopsis*. *Plant Cell* 21, 3152–3169. doi: 10.1105/tpc.109.068676.

- Lamattina, L., García-Mata, C., Graziano, M., and Pagnussat, G. (2003). Nitric oxide: The versatility of an extensive signal molecule. *Annu. Rev. Plant Biol.* 54, 109–136. doi: 10.1146/annurev.arplant.54.031902.134752.
- Lappas, C. M. (2015). The plant hormone zeatin riboside inhibits T lymphocyte activity via adenosine A_{2A} receptor activation. *Cell Mol. Immunol.* 12, 107–112. doi: 10.1038/cmi.2014.33.
- Lee., Y-C., Yang, Y-C., Huang, C-L., Kuo, T-Y., Lin, J-H., Yang, D-M., and Huang, N-K. (2012). When cytokinin, a plant hormone, meets the adenosine A_{2A} receptor: A novel neuroprotectant and lead for treating neurodegenerative disorders? *PLoS One* 7, e38865. doi: 10.1371/journal.pone.0038865.
- Lindner, A. C., Lang, D., Seifert, M., Podlešáková, K., Novák, O., Strnad, M., et al. (2014). Isopentenyltransferase-1 (IPT1) knockout in *Physcomitrella* together with phylogenetic analyses of IPTs provide insights into evolution of plant cytokinin biosynthesis. *J. Exp. Bot.* 65, 2533–2543. doi: 10.1093/jxb/eru142.
- Liu, W. Z., Kong, D. D., Gu, X. X., Gao, H. B., Wang, J. Z., Xia, M., et al. (2013). Cytokinins can act as suppressors of nitric oxide in *Arabidopsis*. *Proc. Natl. Acad. Sci. U.S.A.* 110, 1548–1553. doi: 10.1073/pnas.1213235110.
- Liu, C. J., Zhao, Y., and Zhang, K. (2019). Cytokinin transporters: Multisite players in cytokinin homeostasis and signal distribution. *Front. Plant Sci.* 10, 1–9. doi: 10.3389/fpls.2019.00693.
- Livermore, T. M., Chubb, J. R., Saiardi, A. (2016). Developmental accumulation of inorganic polyphosphate affects germination and energetic metabolism in *Dictyostelium discoideum*. *Proc. Natl. Acad. Sci. U.S.A.* 113, 996–1001. doi: 10.1073/pnas.1519440113.
- Loomis, W. F. (2014). Cell signaling during development of *Dictyostelium*. *Dev. Biol.* 391, 1–16. doi: 10.1016/j.ydbio.2014.04.001.
- Mayaka, J. B., Huang, Q., Xiao, Y., Zhong, Q., Ni, J., and Shen, Y. (2019). The Lonely Guy (LOG) homologue SiRe_0427 from the thermophilic archaeon *Sulfolobus islandicus* REY15A is a phosphoribohydrolase representing a novel group. *Appl. Environ. Microbiol.* 85. doi: 10.1128/AEM.01739-19.
- McDonough, K. A. and Rodriguez, A. (2012). The myriad roles of cyclic AMP in microbial pathogens: From signal to sword. *Nat. Rev. Microbiol.* 10, 27–38. doi: 10.1038/nrmicro2688.
- Mik, V., Mičková, Z., Doležal, K., Frébort, I., and Pospíšil, T. (2017). Activity of (+)-discadenine as a plant cytokinin. *J. Nat. Prod.* 80, 2136–2140. doi: 10.1021/acs.jnatprod.6b01165.

- Miranda, E. R., Zhuchenko, O., Toplak, M., Santhanam, B., Zupan, B., Kuspa, A., et al. (2013). ABC transporters in *Dictyostelium discoideum* development. *PLoS One* 8. doi: 10.1371/journal.pone.0070040.
- Moncada, S. and Higgs, E. A. (2006). The discovery of nitric oxide and its role in vascular biology. *Br. J. Pharmacol.* 147, S193-201. doi: 10.1038/sj.bjp.0706458.
- Moramarco, F., Pezzicoli, A., Salvini, L., Leuzzi, R., Pansegrau, W., and Balducci, E. (2019). A LONELY GUY protein of *Bordetella pertussis* with unique features is related to oxidative stress. *Sci. Rep.* 9, 1–12. doi: 10.1038/s41598-019-53171-9.
- Morrison, E. N., Emery, R. J. N., and Saville, B. J. (2017). Fungal derived cytokinins are necessary for normal *Ustilago maydis* infection of maize. *Plant Pathol.* 66, 726–742. doi: 10.1111/ppa.12629.
- Morrison, E. N., Knowles, S., Hayward, A., Thorn, R. G., Saville, B. J., and Emery, R. J. N. (2015). Detection of phytohormones in temperate forest fungi predicts consistent abscisic acid production and a common pathway for cytokinin biosynthesis. *Mycologia* 107, 245–257. doi: 10.3852/14-157.
- Nagasaki, A. and Uyeda, T. Q. P. (2008). Screening of genes involved in cell migration in *Dictyostelium*. *Exp. Cell Res.* 314, 1136–1146. doi: 10.1016/j.yexcr.2007.12.002.
- Nishii, K., Wright, F., Chen, Y. Y., and Möller, M. (2018). Tangled history of a multigene family: The evolution of ISOPENTENYLTRANSFERASE genes. *PLoS One* 13, 1–23. doi: 10.1371/journal.pone.0201198.
- Nomura, T., Tanakat, Y., Abe, H., and Uchiyama, M. (1977). Cytokinin activity of discadenine: A spore germination inhibitor of *Dictyostelium discoideum*. *Phytochemistry* 16, 1819–1820. doi: 10.1016/0031-9422(71)85097-5.
- Novohradská, S., Ferling, I., and Hillmann, F. (2017). Exploring virulence determinants of filamentous fungal pathogens through interactions with soil amoebae. *Front. Cell. Infect. Microbiol.* 7, 497. doi: 10.3389/fcimb.2017.00497.
- Obata, Y., Abe, H., Tanaka, Y., Yanagisawa, K., and Uchiyama, M. (1973). Isolation of a spore germination inhibitor from a cellular slime mold *Dictyostelium discoideum*. *Agric. Biol. Chem.* 37, 1989–1990. doi: 10.1080/00021369.1973.10860941.
- Palatnik, C. M., Katz, E. R., and Brenner, M. (1977). Isolation and characterization of transfer RNAs from *Dictyostelium discoideum* during growth and development. *J. Biol. Chem.* 252, 694–703.
- Parker, C. W., and Letham, D. S. (1973). Regulators of cell division in plant tissues. XVI: Metabolism of zeatin by radish cotyledons and hypocotyls. *Planta* 114, 199–218. doi:

10.1007/BF00389036.

- Plakidou-Dymock, S., Dymock, D., and Hooley, R. (1998). A higher plant seven-transmembrane receptor that influences sensitivity to cytokinins. *Curr. Biol.* 8, 315–324. doi: 10.1016/S0960-9822(98)70131-9.
- Pratt-Hyatt, M., Pai, D. A., Haeusler, R. A., Wozniak, G. G., Good, P. D., Miller, E. L., et al. (2013). Mod5 protein binds to tRNA gene complexes and affects local transcriptional silencing. *Proc. Natl. Acad. Sci. U.S.A.* 110, E3081-9. doi: 10.1073/pnas.1219946110.
- Rosengarten, R. D., Santhanam, B., Kokosar, J., and Shaulsky, G. (2017). The long noncoding RNA transcriptome of *Dictyostelium discoideum* development. *G3 Genes, Genomes, Genet.* 7, 387–398. doi: 10.1534/g3.116.037150.
- Rot, G., Parikh, A., Curk, T., Kuspa, A., Shaulsky, G., and Zupan, B. (2009). dictyExpress: A *Dictyostelium discoideum* gene expression database with an explorative data analysis web-based interface. *BMC Bioinformatics* 10, 265. doi: 10.1186/1471-2105-10-265.
- Sakakibara, H. (2006). Cytokinins: Activity, biosynthesis, and translocation. *Annu. Rev. Plant Biol.* 57, 431–449. doi:10.1146/annurev.arplant.57.032905.105231.
- Samanovic, M. I. and Darwin, K. H. (2015). Cytokinins beyond plants: Synthesis by *Mycobacterium tuberculosis*. *Microb. Cell* 2, 168-170. doi: 10.15698/mic2015.05.203.
- Samanovic, M. I., Tu, S., Novák, O., Iyer, L. M., McAllister, F. E., Aravind, L., et al. (2015). Proteasomal control of cytokinin synthesis protects *Mycobacterium tuberculosis* against nitric oxide. *Mol. Cell* 57, 984-994. doi: 10.1016/j.molcel.2015.01.024.
- Schaap, P. (2011). Evolution of developmental cyclic adenosine monophosphate signaling in the Dictyostelia from an amoebozoan stress response. *Dev. Growth Differ.* 53, 452–462. doi: 10.1111/j.1440-169X.2011.01263.x.
- Schaap, P. (2016). Evolution of developmental signalling in Dictyostelid social amoebas. *Curr. Opin. Genet. Dev.* 39, 29–34. doi: 10.1016/j.gde.2016.05.014.
- Schaap, P. and Schilde, C. (2018). Encystation: the most prevalent and underinvestigated differentiation pathway of eukaryotes. *Microbiology* 164, 727-739. doi: 10.1099/mic.0.000653.
- Schaap, P., Winckler, T., Nelson, M., Alvarez-Curto, E., Elgie, B., Hagiwara, H., et al. (2006). Molecular phylogeny and evolution of morphology in the social amoebas. *Science (80-)*. 314, 661–663. doi: 10.1126/science.1130670.

- Schäfer, M., Brütting, C., Canales, I. M., Großkinsky, D. K., Vankova, R., Baldwin, I. T., and Meldau, S. (2015). The role of *cis*-zeatin-type cytokinins in plant growth regulation and mediating responses to environmental interactions. *J. Exp. Bot.* 66, 4873-4884. doi: 10.1093/jxb/erv214.
- Schmidt, H. H. and Walter, U. (1994). NO at work. *Cell* 78, 919–925. doi: 10.1016/0092-8674(94)90267-4.
- Schmülling, T., Werner, T., Riefler, M., Krupková, E., and Bartrina y Manns, I. (2003). Structure and function of cytokinin oxidase/dehydrogenase genes of maize, rice, *Arabidopsis* and other species. *J. Plant Res.* 116, 241–252. doi: 10.1007/s10265-003-0096-4.
- Seo, H. and Kim, K.-J. (2017). Structural basis for a novel type of cytokinin-activating protein. *Sci. Rep.* 7, 45985. doi: 10.1038/srep45985.
- Šmehilová, M., Dobrušková, J., Novák, O., Takáč, T., and Galuszka, P. (2016). Cytokinin-specific glycosyltransferases possess different roles in cytokinin homeostasis maintenance. *Front. Plant Sci.* 7: 1264. doi: 10.3389/fpls.2016.01264.
- Smith, J., Queller, D. C., and Strassmann, J. E. (2014). Fruiting bodies of the social amoeba *Dictyostelium discoideum* increase spore transport by *Drosophila*. *BMC Evol. Biol.* 14, 105. doi: 10.1186/1471-2148-14-105.
- Söderbom, F., Anjard, C., Iranfar, N., Fuller, D., and Loomis, W. F. (1999). An adenylyl cyclase that functions during late development of *Dictyostelium*. *Development* 126, 5463–5471.
- Spíchal, L. (2012). Cytokinins - recent news and views of evolutionally old molecules. *Funct. Plant Biol.* 39, 267. doi: 10.1071/FP11276.
- Spinola, M., Galvan, A., Pignatiello, C., Conti, B., Pastorino, U., Nicander, B., et al. (2005). Identification and functional characterization of the candidate tumor suppressor gene TRIT1 in human lung cancer. *Oncogene* 24, 5502–9. doi: 10.1038/sj.onc.1208687.
- Stock, A. M., Robinson, V. L., and Goudreau, P. N. (2000). Two-component signal transduction. *Annu. Rev. Biochem.* 69, 183–215. doi: 10.1146/annurev.biochem.69.1.183.
- Sucgang, R., Kuo, A., Tian, X., Salerno, W., Parikh, A., Feasley, C. L., et al. (2011). Comparative genomics of the social amoebae *Dictyostelium discoideum* and *Dictyostelium purpureum*. *Genome Biol.* 12, R20. doi: 10.1186/gb-2011-12-2-r20.
- Sugawara, H., Ueda, N., Kojima, M., Makita, N., Yamaya, T., and Sakakibara, H. (2008).

- Structural insight into the reaction mechanism and evolution of cytokinin biosynthesis. *Proc. Natl. Acad. Sci. U.S.A.* 105, 2734–2739. doi: 10.1073/pnas.0707374105.
- Suzuki, G., Shimazu, N., and Tanaka, M. (2012). A yeast prion, Mod5, promotes acquired drug resistance and cell survival under environmental stress. *Science* 336, 355–359. doi: 10.1126/science.1219491.
- Tanaka, Y., Abe, H., Uchiyama, M., Taya, Y., and Nishimura, S. (1978). Isopentenyladenine from *Dictyostelium discoideum*. *Phytochemistry* 17, 543–544.
- Tanaka, Y.-M., Hashimoto, Y., Yanagisawa, K., Abe, H., and Uchiyama, M. (1975). Partial structure of a spore germination inhibitor from a cellular slime mold, *Dictyostelium discoideum*. *Agric. Biol. Chem.* 39, 1929–1932. doi: 10.1080/00021369.1975.10861883.
- Tao, Y., Howlett, A., and Klein, C. (1992). Nitric oxide stimulates the ADP-ribosylation of a 41-kDa cytosolic protein in *Dictyostelium discoideum*. *Proc. Natl. Acad. Sci. U.S.A.* 89, 5902–5906. doi: 10.1073/pnas.89.13.5902.
- Tao, Y., Howlett, A., and Klein, C. (1996). Nitric oxide inhibits the initiation of cAMP pulsing in *Dictyostelium discoideum* without altering receptor-activated adenylate cyclase. *Cell. Signal.* 8, 26–34. doi: 10.1016/0898-6568(95)02011-x.
- Tao, Y. P., Misko, T. P., Howlett, A. C., and Klein, C. (1997). Nitric oxide, an endogenous regulator of *Dictyostelium discoideum* differentiation. *Development* 124, 3587–3595. doi: 10.1242/dev.124.18.3587.
- Taya, Y., Tanaka, Y., and Nishimura, S. (1978a). 5'-AMP is a direct precursor of cytokinin in *Dictyostelium discoideum*. *Nature* 271, 545–547. doi: 10.1038/271545a0.
- Taya, Y., Tanaka, Y., and Nishimura, S. (1978b). Cell-free biosynthesis of discadenine, a spore germination inhibitor of *Dictyostelium discoideum*. *FEBS Lett.* 89, 326–328. doi: 10.1016/0014-5793(78)80247-6
- Taya, Y., Yamada, T., and Nishimura, S. (1980). Correlation between acrasins and spore germination inhibitors in cellular slime molds. 143, 715–719. doi: 10.1128/jb.143.2.715-719.1980.
- Telser, A. and Sussman, M. (1971). Uridine diphosphate galactose-4-epimerase, a developmentally regulated enzyme in the cellular slime mold *Dictyostelium discoideum*. *J. Biol. Chem.* 246, 2252–2257.
- Tolerico, L. H., Benko, A. L., Aris, J. P., Stanford, D. R., Martin, N. C., and Hopper, A. K. (1999). *Saccharomyces cerevisiae* Mod5p-II contains sequences antagonistic for nuclear and cytosolic locations. *Genetics* 151, 57-75.

- Van Kast, C. A., and Laten, H. M. (1987). Cytokinin utilization by adenine-requiring mutants of the yeast *Saccharomyces cerevisiae*. *Plant Physiol.* 83, 726–727. doi: 10.1104/pp.83.4.726.
- Wang, N., Söderbom, F., Anjard, C., Shaulsky, G., and Loomis, W. F. (1999). SDF-2 induction of terminal differentiation in *Dictyostelium discoideum* is mediated by the membrane-spanning sensor kinase DhkA. *Mol. Cell. Biol.* 19, 4750–4756. doi: 10.1128/mcb.19.7.4750.
- Yu, J. M., Wang, D., Pierson, L. S., and Pierson, E. A. (2017). Disruption of MiaA provides insights into the regulation of phenazine biosynthesis under suboptimal growth conditions in *Pseudomonas chlororaphis* 30-84. *Microbiol. (United Kingdom)* 163, 94–108. doi: 10.1099/mic.0.000409.
- Zhang, H., Gómez-García, M. R., Brown, M. R. W., and Kornber, A. (2005). Inorganic polyphosphate in *Dictyostelium discoideum*: Influence on development, sporulation, and predation. *Proc. Natl. Acad. Sci. U.S.A.* 102, 2731–2735. doi: 10.1073/pnas.0500023102.
- Zhang, K., Novak, O., Wei, Z., Gou, M., Zhang, X., Yu, Y., et al. (2014). *Arabidopsis* ABCG14 protein controls the acropetal translocation of root-synthesized cytokinins. *Nat. Commun.* 5, 3274. doi: 10.1038/ncomms4274.
- Zinda, M. J., and Singleton, C. K. (1998). The hybrid histidine kinase dhkB regulates spore germination in *Dictyostelium discoideum*. *Dev. Biol.* 196, 171–183. doi: 10.1006/dbio.1998.8854.

CHAPTER 3

PREFACE

- Title: Cytokinin detection during the *Dictyostelium discoideum* life cycle:
Profiles are dynamic and affect cell growth and spore germination.
- Authors: Megan M. Aoki, Anna B. Kisiala, Naomi L. Stock, Shaojun Li, Craig
R. Brunetti, Robert Huber, and R. J. Neil Emery.
- Reference: Published in: *Biomolecules* (2019), 9: 702
doi: 10.3390/biom9110702
- Copyright: See APPENDIX I.
- Contributions: Conceptualization, M.M.A., C.R.B., R.J.H., and R.J.N.E.; Formal
analysis, M.M.A. and A.B.K.; Methodology, M.M.A. performed all cell
culture and preparations of samples for mass spectrometry and
metabolomics, A.B.K. assisted with methodology for mass spectrometry
methods, S.L. synthesized discadenine for the mass spectrometry
analyses, and N.L.S. assisted with the FTICR-MS analysis; Supervision,
C.R.B., R.J.H., and R.J.N.E.; Writing—original draft, M.M.A.;
Writing—review and editing, M.M.A., A.B.K., N.L.S, C.R.B., R.J.H.,
and R.J.N.E.

CHAPTER 3

Cytokinin detection during the *Dictyostelium discoideum* life cycle: Profiles are dynamic and affect cell growth and spore germination.

Published in: *Biomolecules* (2019), 9: 702

doi: 10.3390/biom9110702

ABSTRACT

Cytokinins (CKs) are a family of evolutionarily conserved growth regulating hormones. While CKs are well-characterized in plant systems, these N^6 -substituted adenine derivatives are found in a variety of organisms beyond plants, including bacteria, fungi, mammals, and the social amoeba, *Dictyostelium discoideum*. Within *Dictyostelium*, CKs have only been studied in the late developmental stages of the life cycle, where they promote spore encapsulation and dormancy. In this study, we used high-performance liquid chromatography-positive electrospray ionization-high resolution tandem mass spectrometry (HPLC-(ESI+)-HRMS/MS) to profile CKs during the *D. discoideum* life cycle: growth, aggregation, mound, slug, fruiting body, and germination. Comprehensive profiling revealed that *D. discoideum* produces six CK forms (*cis*-zeatin (*cZ*), discadenine (DA), N^6 -isopentenyladenine (iP), N^6 -isopentenyladenine-9-riboside (iPR), N^6 -isopentenyladenine-9-riboside-5'phosphate (iPRP), and 2-methylthio- N^6 -isopentenyladenine (2MeSiP)) in varying abundance across the sampled life cycle stages, thus laying the foundation for the CK biosynthesis pathway to be defined in this organism. Interestingly, iP-type CKs were the most dominant CK analytes detected during growth and aggregation. Exogenous treatment of AX3 cells with various CK types revealed that

iP was the only CK to promote the proliferation of cells in culture. In support of previous studies, metabolomics data revealed that DA is one of the most significantly upregulated small molecules during *D. discoideum* development, and our data indicates that total CK levels are highest during germination. While much remains to be explored in *D. discoideum*, this research offers new insight into the nature of CK biosynthesis, secretion, and function during *D. discoideum* growth, development, and spore germination.

KEYWORDS: high-performance liquid chromatography-positive electrospray ionization-high resolution tandem mass spectrometry (HPLC-(ESI+)-HRMS/MS), cytokinin, cytokinin biosynthesis, *Dictyostelium discoideum*, social amoeba, discadenine, germination

INTRODUCTION

Dictyostelium discoideum is one of the most well-known representatives of the *Amoebozoa* phylum (Schilde and Schaap, 2013). Owing to its unique life cycle, this social amoeba can exist both as a single-cellular and multicellular organism. In its natural environment, *D. discoideum* amoebae feed upon bacteria and decaying leaf litter in the forest soil. However, once food resources are depleted, the developmental programme is initiated through dramatic transcriptional changes, thus enabling *D. discoideum* to adapt to a period of starvation and subsequent transition to multicellularity (Loomis, 2014). cAMP is secreted as a chemical messenger in a pulsatile manner from the population of starved amoebae and acts as a chemoattractant causing the cells to migrate towards a central location (Gerisch and Wich, 1975; Konijn et al., 1967). Thousands of cells form aggregates, referred to as mounds. The cells in the mound continue to secrete cAMP at the apex, which sends a column of cells into the air that eventually topples over forming the pseudoplasmodium or slug (Siegert et al., 1995). Light and temperature guide the migration of the slug towards the top layer of the forest soil, where the fruiting body forms. This final structure consists of a slender tube-like stalk that suspends the spores above the surface for future germination and largely depends on cytokinins (CKs), which are signaling molecules that initiate spore formation and maintain spore dormancy (Obata et al., 1973; Tanaka et al., 1975; Anjard and Loomis, 2008).

CKs are a group of evolutionarily conserved N^6 -substituted adenine derivatives, most commonly known for their widespread signaling effects influencing nearly all aspects of plant growth and development (Mok and Mok, 2001). Within *D. discoideum*, 2 CK types have been identified to date, N^6 -isopentenyladenine (iP) and discadenine (DA) (Abe et al.,

1976; Tanaka et al., 1978). In plants and other CK-producing organisms (e.g., bacteria, fungi, and insects, etc.), iP is the precursor CK from which other CKs are derived (Sakakibara, 2005; Spíchal, 2012). iP is also the precursor molecule to DA, in which direct transfer of the 3-amino-3-carboxy-propyl moiety of *S*-adenosylmethionine (SAM) is added to the *N*3 position of the adenine molecule (Taya et al., 1978a). DA is unique to social amoebae and has only been detected among Dictyostelids that secrete cAMP as their chemoattractant for aggregation (Taya et al., 1980; Abe et al., 1981; Schaap et al., 2006). DA was first discovered for its role as a potent spore germination inhibitor (Obata et al., 1973; Tanaka et al., 1975; Abe et al., 1981) and more recently for its role in inducing sporulation of *D. discoideum* cells, along with iP and other exogenously applied CKs (Anjard and Loomis, 2008). These developmental roles of CK are the only documented roles of CK in *D. discoideum* to date.

Work by Anjard and Loomis (2008) identified the primary CK biosynthesis gene in *D. discoideum*, *iptA*, which is responsible for 90% of the CKs produced within the fruiting body. In CK-producing organisms, isopentenyltransferases (IPTs) are the key enzymes responsible for the formation of isoprenoid-type CKs, such as iP, dihydrozeatin (DZ), *trans*-zeatin (*tZ*), and *cis*-zeatin (*cZ*). There are 2 different forms of IPT: adenylyate-IPTs and tRNA-IPTs (Kamada-Nobusada and Sakakibara, 2009). Adenylyate-IPTs produce free CKs through *de novo* biosynthesis pathway, whereas tRNA-IPTs produce CKs bound to tRNA. Upon tRNA-degradation, the bound CKs are liberated to contribute to the pool of free CKs within the organism. Based on phylogenetic analysis, *D. discoideum* possesses three IPT genes: *iptA*, *iptB*, and *iptC*. *iptA* groups with adenylyate-IPTs, and *iptB* and *iptC* are putative tRNA-IPTs (Anjard and Loomis, 2008; Lindner et al., 2014; Nishii et al.,

2018). Collectively, these three IPT genes appear to be distantly related to plant IPTs and were likely acquired through horizontal gene transfer events, in support of previous phylogenetic analyses (Eichinger et al., 2005; Nishii et al., 2018). The protein product of *iptA* facilitates the formation of iP-type CKs. The enzymes responsible for the synthesis of iP and DA (isopentenyltransferase, IptA; discadenine synthase) are considered to be developmentally regulated, as their peak activities have been identified following the onset of culmination (initiation of fruiting body formation) (Anjard and Loomis, 2008; Ihara et al., 1980; Ihara et al., 1984). While CKs have a significant role in the later developmental stages of the *D. discoideum* life cycle, much remains to be understood regarding the biosynthesis, signal transduction, and roles of CKs across the entire life cycle.

In this study, high-performance liquid chromatography-positive electrospray ionization-high resolution tandem mass spectrometry (HPLC-(ESI+)-HRMS/MS) was used to profile endogenous CKs during the 5 major stages of the *D. discoideum* life cycle: growth, aggregation, mound, slug, fruiting body, and germination. Through comprehensive profiling of 30 naturally occurring CKs, this study reveals that *D. discoideum* produces and secretes six CK forms in varying abundance throughout the life cycle, giving insight into CK biosynthesis among social amoebae. Additionally, the metabolome of each life cycle stage was investigated to identify any significant trends in CK metabolites in comparison to other small molecule metabolites secreted during development. Finally, the effect of CKs on *D. discoideum* growth was determined through exogenous hormone application of three different CK types over a 144-hour growth period. Collectively, these results provide evidence of an expanded role for CKs beyond the previously described functions limited to spore formation and dormancy.

MATERIALS AND METHODS

Strains, buffers, and chemicals

The *D. discoideum* AX3 strain was obtained from the Dicty Stock Center, and it was initially grown and maintained at room temperature (22°C) on SM agar with *Klebsiella aerogenes* (Fey et al., 2007). Subsequent liquid cultures were grown axenically in either HL5 medium or FM minimal medium (Formedium, Hunstanton, Norfolk, UK) supplemented with ampicillin (100 µg/mL) and streptomycin sulfate (300 µg/mL) at 150 rpm and room temperature. All cells used in experiments were harvested in the mid-log phase of growth ($1-5 \times 10^6$ cells/mL). FM minimal medium was used to avoid high background CK levels originating from biological ingredients present in standard nutrient-rich medium (e.g., HL5). KK2 buffer (2.2 g/L KH₂PO₄ and 0.7 g/L K₂HPO₄, pH 6.5) was used as a starvation buffer and for washing cells harvested from petri dishes and agar plates. iP and N⁶-benzyladenine (BA) were purchased from Sigma-Aldrich (Oakville, Ontario, Canada) and were dissolved in a minimal volume of 1M NaOH and diluted with HPLC-grade methanol (CH₃OH) to prepare a stock solution (0.1 mM) for exogenous treatment. DA was synthesized as described by Mik et al. (2017) with slight modifications and was dissolved in 100% DMSO to prepare a stock solution (0.657 mM). The concentrations of methanol and DMSO in the growth medium did not exceed 1%.

Sampling of life cycle stages for CK profiling

Five life cycle stages representative for the key morphological changes exhibited throughout *D. discoideum* growth and development were chosen for CK analysis: growth (single-celled amoeba), aggregation (6-hour starvation in KK2 buffer), mound, slug, and fruiting body. For all life cycle stages, KK2 buffer was separated from the cell pellet by

centrifugation to allow for analysis of intracellular CK retention (IC) and extracellular secretion (EC).

For the growth and aggregation samples, 6.25×10^6 growth-phase cells were plated in polystyrene Petri dishes (100 mm \times 15 mm) and grown overnight at room temperature in 7 mL of FM minimal medium. The following day, the medium from the growth samples was harvested separately from the adherent cells in the Petri dish. The EC samples were centrifuged for 5 min at 986g to remove cell debris, transferred to a new sterile 15 mL tube, and stored immediately at -20°C until CK metabolites were extracted for HPLC-(ESI+)-HRMS/MS analysis. The remaining adherent cells were removed from the Petri dish by pipetting, washed twice with KK2 buffer, pelleted for 1 min at 6,200g, and stored immediately at -20°C . Cell concentration was determined for each replicate using a hemocytometer. For the aggregation samples, the FM minimal medium was discarded and replaced with 7 mL of KK2 buffer for 6 h. After 6 h, the KK2 buffer was collected as the EC samples, and the cells were pelleted, as described for the growth samples to analyze the IC CK content.

For the developmental life cycle stages (mound, slug, and fruiting body), 5×10^7 growth-phase cells suspended in 300 μL of KK2 buffer were spread evenly onto 1% water agar and maintained in the dark in a humidity chamber for 10–24 h. The individual plates were harvested only if there was synchronous development of the respective life cycle stage, where at least 80% of the developmental structures were alike. In general, mounds were observed after 10 h of development, slugs after 16–18 h, and fruiting bodies after 24 h. For all life cycle stages cultured on water agar, the respective structures were harvested by gently scraping the agar surface and washing it with 3 mL of KK2 buffer. The collected

cells and KK2 buffer were centrifuged for 5 min at 986g. The KK2 buffer was carefully transferred to a new sterile 15 mL tube without disturbing the cell pellet and then stored separately at -20°C to be analyzed as the EC samples. The remaining pellet for each developmental life cycle stage was immediately stored at -20°C to be analyzed as the IC samples.

Spore germination

Spore germination was assayed using FM minimal medium and 1% water agar. First, 7.5×10^7 growth-phase cells suspended in 300 μL of KK2 were evenly spread onto water agar and allowed to form fruiting bodies as described above. The spores were harvested by collecting the entire fruiting body structures as follows: (1) the agar surface was washed with 1 mL KK2 buffer and gently scraped with a cell scraper, (2) the KK2 buffer containing the entire fruiting body structure and spores was placed into a sterile microcentrifuge tube, (3) the spore suspension was centrifuged for 5 min at 986g to pellet the samples (a sample was collected prior to centrifugation to determine cell concentration using a hemocytometer), (4) the buoyant cellulose stalks were removed with a pipette tip, and (5) the remaining spores were plated in 7 mL of FM minimal medium. The spores took roughly 72 h to germinate ($> 75\%$). During this timeframe, IC and EC samples were collected separately at three different time points: 24-, 48-, and 72-hour. The 7 mL of medium were separated from the spores and/or germinated amoebae at each of selected time points and were centrifuged for 5 min at 986g. Following centrifugation, the cell-free medium was transferred into separate 15 mL tubes to avoid any contamination from cellular debris and was stored at -20°C to be processed for CK extraction as the EC samples. The remaining spores or amoebae were harvested from the Petri dish using a pipette, washed twice with

KK2 buffer, re-pelleted, and then stored at -20°C to be processed as the IC samples. Images were taken at each of the sampled life cycle stages to determine percent germination for each replicate.

Extraction and purification of *D. discoideum*-derived CKs

A modified protocol of CK hormone extraction and purification optimized to minimize enzymatic activities causing CK nucleotide degradation and CK isomerization was used as described previously (Quesnelle and Emery, 2007; Hoyerová et al., 2006; Farrow and Emery, 2012). One mL of ice-cold (-20°C) modified extraction solvent Bielecki No. 2 ($\text{CH}_3\text{OH}:\text{H}_2\text{O}:\text{HCO}_2\text{H}$ (15:4:1, $v/v/v$)) was added to the EC and IC samples. All samples were consecutively spiked with 10 ng of each of the deuterated internal standards to enable endogenous hormone quantification through isotope dilution. The following standards were added to each sample: $^2\text{H}_6[9\text{RMP}]\text{DZ}$, $^2\text{H}_6[9\text{RMP}]\text{iP}$, $^2\text{H}_5[9\text{R}]\text{tZ}$, $^2\text{H}_3[9\text{R}]\text{DZ}$, $^2\text{H}_6[9\text{R}]\text{iP}$, $^2\text{H}_7[9\text{R}]\text{BA}$, $^2\text{H}_3\text{DZ}$, $^2\text{H}_6\text{iP}$, $^2\text{H}_7\text{BA}$, $^2\text{H}_5\text{tZOG}$, $^2\text{H}_7\text{DZOG}$, $^2\text{H}_5\text{tZROG}$, $^2\text{H}_7\text{DZROG}$, $^2\text{H}_5\text{tZ7G}$, $^2\text{H}_5\text{tZ9G}$, $^2\text{H}_3\text{DZ9G}$, $^2\text{H}_52\text{MeStZ}$, $^2\text{H}_62\text{MeSiP}$, $^2\text{H}_52\text{MeStZR}$, and $^2\text{H}_62\text{MeSiPR}$ (Olchemim Ltd., Olomouc, Czech Republic, Table 3.1). Isotopically-labeled internal standards (IS) were not available for all analytes, so in some cases an IS was used for more than 1 analyte (Table 3.1). In the case of DA, (in which no commercial labeled standard was available), the presence of DA in sample extracts was confirmed by examining the isotopic fine structure in mass spectra obtained with a Bruker Solarix XR, Fourier transform ion cyclotron resonance mass spectrometer (FTICR-MS) (Billerica, MA, USA) equipped with a 7T magnet (Supplementary Figure 3.1). The samples were allowed to passively extract overnight at -20°C in the modified Bielecki No. 2 extraction solvent. The following day, the samples were centrifuged (11,180g for 10 min), and the supernatant

was collected and placed into a new tube. The remaining IC and EC samples were resuspended in an additional 1 mL of the extraction solvent, and the samples were allowed to extract for an additional 30 min at -20°C . Re-extracted samples were centrifuged and both supernatants were pooled and evaporated to in a speed vacuum concentrator (Savant SPD111V, UVS400, Thermo Fisher Scientific, Waltham, MA, USA) at room temperature.

Dried extraction residues from both the EC and IC samples were reconstituted in 1 mL of 1 M HCO_2H (pH 1.4) to ensure complete protonation of all CKs. Each extract was subjected to solid phase extraction (SPE) on a mixed mode, reversed-phase, cation-exchange cartridge (MCX 6cc; 200 mg, Canadian Life Sciences, Peterborough, ON, Canada). Cartridges were activated with 5 mL of CH_3OH and equilibrated with 5 mL of 1M HCO_2H . Each sample was loaded and allowed to pass through the column by gravity and the columns were then washed with 5 mL of 1 M HCO_2H , followed by 5 mL of CH_3OH . The nucleotide fraction was eluted first using 5 mL of 0.35 M NH_4OH to be processed separately from the other CK fractions, which are retained on the column based on charge and their hydrophobic properties. Free bases, ribosides, methylthiols, and glucosides were subsequently eluted together using 5 mL of 0.35 M NH_4OH in 60% CH_3OH . Both eluted fractions were evaporated in a speed vacuum concentrator at room temperature and stored at -20°C until further processing.

Since CK-nucleotides could not be directly analyzed by our LC-MS/MS method, the separately eluted nucleotide samples were dephosphorylated using 3 units of alkaline phosphatase (alkaline phosphatase calf intestine, New England BioLabs, Whitby, ON, Canada) in 1 mL of 0.1 M ethanolamine-HCl (pH 10.4) for 12 h at 37°C (Emery et al., 2000). The resulting ribosides were evaporated in a speed vacuum concentrator at room

temperature. The riboside fraction obtained as a result of this processing reflects the pooled contribution of mono-, di-, and tri-phosphates of each CK type (iPRP, cZRP, tZRP, and DZRP). Samples were reconstituted in 1.5 mL Milli-Q H₂O for further purification on C₁₈ cartridges (C₁₈ 6cc, 500 mg, Canadian Life Sciences; Peterborough, ON, Canada). Cartridges were activated with 3 mL of CH₃OH and equilibrated with 6 mL of Milli-Q H₂O. Samples were loaded onto the C₁₈ cartridge and were allowed to pass through the column by gravity. The residue was washed with 3 mL of Milli-Q H₂O and the ribosides were eluted using 1.25 mL of CH₃OH:H₂O (80:20 v/v). All sample eluents were evaporated, and residues were stored at -20°C until further processing.

Prior to HPLC-(ESI+)-MS/MS analysis, the extracted CK fractions were reconstituted in 1.5 mL of initial mobile phase conditions (95:5 H₂O:CH₃CN) both with 0.08% CH₃CO₂H. Samples were transferred to glass auto-sampler vials and stored at -20°C until analysis.

CK quantification by HPLC-(ESI+)-HRMS/MS

D. discoideum CKs within the EC and IC samples were identified and quantified using HPLC-(ESI+)-HRMS/MS (Kisiala et al., 2019). Briefly, a 25 µl sample volume was injected into the Thermo Ultimate 3000 HPLC coupled to a Thermo Q-Exactive™ Orbitrap mass spectrometer equipped with a heated electrospray ionization (HESI) source (Thermo Scientific, San Jose, CA, USA). Compounds were separated using a reversed-phase C₁₈ column (Kinetex 2.6 µ C18 100 A, 2.1 × 50 mm; Phenomenex, Torrance, CA, USA). All hormone fractions were eluted with a multistep gradient of component A: H₂O with 0.08% CH₃CO₂H mixed with component B: CH₃CN with 0.08% CH₃CO₂H at a flow rate of 0.4 mL/min. The initial conditions were 5% B increasing linearly to 10% B over 2 min

followed by an increase to 95% B over 6.5 min; 95% B was held constant for 1.5 min before returning to starting conditions for 5 min; total run time was 15 min.

The eluate was introduced into the Orbitrap HESI source (capillary temperature of 250°C) and analyzed using parallel reaction monitoring (PRM) at 35,000 resolution. CKs were analyzed in positive ion mode. The HESI source was operated with sheath gas, 30 arbitrary units; auxiliary gas, 8 arbitrary units; max spray current, 100 μ A; auxiliary gas heater temperature, 450°C; S-lens RF level, 60 and spray voltage 3.9 kV. The PRM parameters included the following: automatic gain control (AGC), 1×10^6 ; maximum injection time (IT), 128 ms; m/z 1.2 isolation window and normalized collision energy (NCE) individually optimized for each CK analyte.

All data was analyzed using Thermo Xcalibur (v 3.0.63) software (Thermo Scientific, San Jose, CA, USA), to calculate peak areas. Quantification was achieved through isotope dilution analysis based on recovery of ^2H -labeled internal standards.

Untargeted metabolomics

The samples extracted for CK profiling from the developmental stages were further used for untargeted metabolomics analysis. The extraction protocol used MCX cartridges, which are specific for basic, polar compounds, such as CKs. The metabolomic data were acquired in full scan (FS) mode using the Thermo Q-Exactive[™] Orbitrap mass spectrometer. The samples were injected into the mass spectrometer through the Thermo Ultimate 3000 HPLC system using the parameters described in Section 2.5. For FS analysis, each sample was run in positive ion mode over the mass range of m/z 80–600, at 35,000 resolution, with automatic gain control (AGC) target of 3×10^6 , and maximum injection time (IT) of 128 ms.

The raw data files were uploaded directly to XCMS Online (Tautenhahn et al., 2012; Gowda et al., 2014) to analyze significantly up- or down-regulated *D. discoideum* metabolites (including CKs) across the developmental stages (aggregation, mound, slug, and fruiting body) using the previously described settings with slight modifications (Chen et al., 2017). Metabolite detection was achieved through the centWave method with a tolerance of 2.0 ppm (Tautenhahn et al., 2012). KK2 buffer was used as a negative control to eliminate the metabolites present in the wash buffer from statistical analysis. The pre-filter was set to 6 scans with a minimum of 5000 intensity, the signal to noise threshold was 10, and noise was set to 1×10^6 for positive mode. The obiwarp method was used for retention time correction (Prince and Marcotte, 2006). The 'fillPeaks' function with default settings and remaining zeros were imputed with two-thirds the minimum value on a per mass basis. Compounds produced by *D. discoideum* were identified by accurate mass using the METLIN database.

Growth assays with exogenous CK treatment

Cells in the mid-log phase of growth ($1-5 \times 10^6$ cells/mL) were collected and resuspended to a final concentration of 1×10^6 cells/mL in 5 mL of fresh HL5 medium. The cells were incubated at room temperature and 150 rpm over a 6-day period. Cell concentrations were assessed daily using a hemocytometer. HL5 medium was supplemented with iP, BA, or DA to determine the effect of CKs on cell proliferation at the following concentrations: 0 nM, 1 nM, 10 nM, 100 nM, 500 nM, and 1 μ M. Statistical significance was assessed in GraphPad Prism (GraphPad Software Incorporated, La Jolla, CA, USA) using two-way ANOVA followed by Bonferroni's multiple comparisons test (p values < 0.05 were considered significant; n = the number of biological replicates analyzed).

RESULTS

CKs are detected throughout all stages of the *D. discoideum* life cycle

To determine the ability of *D. discoideum* to synthesize diverse CK forms during its life cycle, a total of 30 naturally occurring CKs were profiled by HPLC-(ESI+)-HRMS/MS during the 5 stages of the *D. discoideum* life cycle: growth (single-celled amoeba), aggregation (induced by 6-hour starvation), mound, slug, and fruiting body. An analysis of *D. discoideum* culture media was conducted prior to the CK profiling experiments to determine which medium contained the lowest background levels of CKs (Supplementary Figure 3.2). From this analysis, FM minimal medium was selected since it contains the lowest levels of background CK levels compared to other more traditional nutrient rich media, such as HL5.

Our CK profiling analysis revealed that *D. discoideum* synthesizes six CK forms in varying concentrations throughout the different life cycle stages: *cZ*, DA, iP, *N*⁶-isopentenyladenosine (iPR), *N*⁶-isopentenyladenine-9-ribose-5' phosphate (iPRP), and 2-methylthio-*N*⁶-isopentenyladenine (2MeSiP) (Figure 3.1A). Among the profiled stages, the fruiting body contained the highest levels of CKs (total IC CK: 29 pmol/10⁶ cells; total EC CK: 88 pmol/10⁶ cells). Here, in addition to detecting iP and DA, we identified the nucleotide form of iP, iPRP, in both the IC and EC samples at concentrations of 16 pmol/10⁶ cells and 0.61 pmol/10⁶ cells, respectively (Figure 3.1A).

During growth and aggregation, the CK profiles were dominated by iP-type CKs: iP, iPR, and iPRP (Figure 3.1B and C). Among the CKs detected in both stages, iP free base was synthesized and detected at the highest concentration in the EC samples. Interestingly, the concentration of iP increased most dramatically from growth (9 pmol/10⁶ cells) to

aggregation (14 pmol/10⁶ cells) in the EC samples (Figure 3.1A). iPR was present at low concentrations (< 0.60 pmol/10⁶ cells) both intracellularly and extracellularly, with a general trend of the EC concentration being three and six times higher than that of the IC concentration in the growth and aggregation stages, respectively (Figure 3.1A). iPRP was only detected in the IC samples during growth and in the EC samples during aggregation. *cZ* and 2MeSiP were also detected in both of these stages. *cZ* was consistently detected in the EC samples in low concentrations (< 0.90 pmol/10⁶ cells), and 2MeSiP was detected at similar IC and EC concentrations (between 0.94 and 1.35 pmol/10⁶ cells). DA was not detected during growth or aggregation.

CKs were detected in the least abundance during the mound and slug life cycle stages (Figure 3.1). The total level of CKs did not exceed a concentration of 3 pmol/10⁶ cells for either the IC or EC samples. *cZ*, DA, and iPRP were present in both the mound and slug stages, whereas iP was only detected in the EC samples during mound formation. The EC values for these stages may be slightly underestimated compared with the other life cycle stages, as these structures were harvested directly off of the agar surface, and the wash buffer was collected as the EC samples.

DA is one of the most up-regulated metabolites during *D. discoideum* development

Following our CK profiling results, we examined the metabolome (all detectable small molecules restricted to our sample preparation conditions) of the *D. discoideum* life cycle. This enabled further identification of trends in CK analytes in comparison to other detected non-CK metabolites using an untargeted, high-resolution Orbitrap LC-MS analysis—followed by XCMS feature detection and multigroup analysis through XCMS Online (Gowda et al., 2014). This dataset has been made available through XCMS Online (ID:

1201031). Within the EC samples collected at the aggregation, mound, slug, and fruiting body stages, a total of 476 common metabolite features were detected. Of these 476 aligned metabolite features, 276 were significantly different among the sampled developmental time points (> 1.5 -fold change, $p < 0.01$). DA was among the most upregulated metabolites during *D. discoideum* development (Supplementary Figure 3.3). Specifically, DA accumulated most dramatically from the slug to fruiting body life cycle stage and was the 31st most significantly changed feature during development ($p = 3.73 \text{ E}^{-12}$). Beyond DA, there were no other CK analytes identified as a feature significantly up- or down-regulated relative to the other small molecule metabolites identified among the analyzed *D. discoideum* life cycle stages (data not shown).

CK levels are highest during germination

Considering the role of CKs to maintain spore dormancy paired with our observation of high CK levels during the fruiting body life cycle stage, we assessed CK synthesis during the process of spore germination over a 72-hour time course. Percent germination was determined over the 72-hour time course, in which $> 75\%$ of the spores germinated by the final 72-hour sampling period (Figure 3.2A). After 24-, 48-, and 72-hour in FM minimal medium, IC and EC samples were harvested to extract CKs. Five CK forms were detected in the IC germination samples (DA, iP, iPR, iPRP, and 2MeSiP; Figure 3.2B). In the EC samples, the same five CK forms were detected plus an additional CK form, *cZ* (Figure 3.2C).

During all sampled life cycle stages, *D. discoideum* secreted more CKs outside of the cell (EC samples) than it retained within the cell (IC samples) (Figures 3.1 and 3.2). During germination, the concentrations of DA and iP were the highest of the six detected CK

analytes (Figure 3.2B and 3.2C). The IC samples were largely dominated by iPRP at the 24-hour sampling period, which slowly decreased by nearly 5-fold over the germination time course (Figure 3.2B). Inversely, 2MeSiP production increased dramatically over the germination period. DA production within the IC samples was highest when approximately 10% of the spores had germinated and slowly decreased as germination progressed. Lastly, IC levels for iP and iPR were relatively low and unchanging (< 3 pmol/ 10^6 cells) over the 72-hour time course (Figure 3.2B).

The EC germination samples contained the highest concentrations of CK in all the sampled life cycle stages (Figure 3.2C). Specifically, iP and DA were the most abundant CK analytes, with concentrations 10- and 19-times higher, respectively, than those observed in the fruiting body life cycle stage. These 2 CKs had differing trends over the 72-hour time course; DA increased in concentration from 166 pmol/ 10^6 cells to 919 pmol/ 10^6 cells, whereas, iP concentrations decreased slightly from 485 pmol/ 10^6 cells at the 24-hour time point to 426 pmol/ 10^6 cells at the 72-hour time point (Figure 3.2C). Similar to DA, iPRP concentration also had an increasing trend over the 72-hour germination period, where the initial concentration of 7 pmol/ 10^6 cells nearly tripled to 20 pmol/ 10^6 cells. 2MeSiP was only detected at the final 72-hour time point, when over 75% of the spores had germinated. Lastly, cZ and iPR concentrations were detected at low, unchanging levels (< 6 pmol/ 10^6 cells; Figure 3.2C).

***N*⁶-Isopentenyladenine prolongs the stationary phase of *D. discoideum* growth**

Considering the detection of CKs during *D. discoideum* growth, the effect of exogenously applied CKs on the rate of cell proliferation in axenic culture was assessed (Figure 3.3). HL5 medium was supplemented with iP, DA, or BA at five different

concentrations: 1 nM, 10 nM, 100 nM, 500 nM, and 1 μ M. In order to test the CK effect at physiologically relevant concentrations, we did not exceed concentrations over 1 μ M. Proliferation of the CK-treated AX3 cells was assessed over 6 days and compared against the proliferation of untreated cells. Interestingly, the CK analyte detected endogenously at the highest concentration during growth, iP, was the only CK to have an effect on cell proliferation, when supplemented to the medium (Figure 3.3). A significant difference in cell density was observed for the 100 nM iP-treated cells at the 120- and 144-hour time points compared to untreated cells ($p < 0.05$) (Figure 3.3). No significant differences in cell proliferation were observed for cells treated with DA or BA at any of the 5 concentrations tested (data not shown).

DISCUSSION

This study provides insight into the nature of CK biosynthesis, secretion, and function during *D. discoideum* growth, development, and spore germination. While the presence of CKs in *D. discoideum* has been known for almost 40 years, CK detection within *D. discoideum* was limited to only the fruiting body life cycle stage (Obata et al., 1973). Considering the dominant presence of iP and DA within *D. discoideum* and that iP CKs are the precursor molecules from which other CK types can be formed, HPLC-(ESI+)-HRMS/MS was used in this study to determine whether additional CK forms are present in *D. discoideum* throughout the other, not previously investigated life cycle stages. This study reveals that CK metabolites are synthesized by *D. discoideum* during growth and development, beyond what has been previously documented. Specifically, the CK analytes *cZ*, DA, iP, iPR, iPRP, and 2MeSiP were detected. To our knowledge, endogenous

production of *cZ*, *iPR*, *iPRP*, and *2MeSiP* has never been documented in *D. discoideum*, and we are the first to document the production of CKs outside of the fruiting body life cycle stage. These CK profiling results expand our understanding of CK metabolism in *D. discoideum* and allow us to propose a model of CK biosynthesis (Figure 3.4).

Of the *iP*-type CKs identified in this study, the free base, *iP*, was the most abundant CK analyte, with the exception of the mound stage. The presence of the nucleotide, riboside, and free base *iP* forms suggests that *D. discoideum* follows a similar isoprenoid CK biosynthesis pathway, as found in plants and other CK-producing organisms (Figure 3.4) (Kamada-Nobusada and Sakakibara, 2009; Frébort et al., 2011; Spíchal, 2012; Morrison et al., 2015; Morrison et al., 2017). An early report on the cell free CK biosynthesis in *D. discoideum* was conducted by Taya et al. (1978b) who utilized crude extracts harvested from the late stages of *D. discoideum* culmination to determine that 5'AMP was the acceptor molecule of the isopentenyl group onto the N^6 position of the adenine. Radio-labeled AMP and unlabeled isopentenyl pyrophosphate (IPP) were assayed with crude *D. discoideum* extracts, in which *iPRP*, *iPR*, and *iP* were formed as products and were identified through thin-layer chromatography. *iPRP* was shown to be the first reaction product; however, the authors concluded that further studies were necessary to determine whether *iP* is formed directly from *iPRP* or if *iPR* acts as an intermediate. While that early study demonstrated that *D. discoideum* extracts possess the enzymes responsible for CK biosynthesis, it did not detect endogenous levels of *iPRP* or *iPR*. The detection of the nucleotide and riboside fractions of *iP* in the present study, in all life cycle stages where *iP* is detected, suggests that *iP*-biosynthesis in *D. discoideum* utilizes *iPR* as an intermediate

form between the nucleotide and free base iP forms, as shown in our proposed biosynthesis figure (Figure 3.4).

It is established that iP acts as the precursor molecule from which DA is synthesized (Taya et al., 1978a). The presence of the iP nucleotide, riboside, and free base forms during growth and aggregation, even when no presence of DA was detected, suggests iP-type CK have additional biological functions beyond acting as the substrate for DA production. In support of this finding, iP was the only one of the exogenously applied CKs to stimulate the *in vitro* growth of AX3 cells. This coincides with our CK metabolite results, which showed the free base iP concentration considerably increased from growth to aggregation. We would expect to see an enhanced effect of exogenous iP treatment on *in vitro* growth in IPT knockout strains in the absence of endogenous CK production. Within CK-producing organisms, there are often many functions carried out by a single CK molecule; for instance, in fungi, endogenously produced CKs affect nutrient uptake and water and ion transport (LeJohn and Stevenson, 1973; Gogala, 1991). Within *D. discoideum*, further investigations looking at interactions between iP, cAMP, and nitric oxide (NO) may determine if CKs play a role in regulating either of these important molecules that facilitate the transition to multicellularity.

cZ was detected during growth and early development at low levels in the EC and the IC samples ($< 1 \text{ pmol}/10^6 \text{ cells}$). During germination, the level of *cZ* was slightly elevated compared to that detected during growth and development. Of the isoprenoid-type CKs, the role of *cZ* is the least understood owing to its lower activity in many classical CK bioassays compared to its *trans*-zeatin (*tZ*) isomer (Shäfer et al., 2015). Synthesis of *cZ* is believed to originate from the mevalonate pathway via tRNA-IPTs (Kasahara et al., 2004).

Specifically, tRNA-IPTs prenylate position A37 of a specific subset of tRNA molecules forming iP-bound tRNA. A hydroxylating enzyme further modifies the iP side chain to form cZ-bound tRNA molecules, which is depicted as number 2 in the proposed CK biosynthesis pathway (Figure 3.4). Considering that the *D. discoideum* genome contains two putative tRNA-IPTs (*iptB* and *iptC*), it follows that the detected levels of cZ are likely a result of degradation of the tRNA molecules modified through tRNA-IPT and a hydroxylating enzyme. However, further research is necessary to confirm the source of cZ synthesis and whether these low levels are of biological significance to *D. discoideum* growth and development.

Along with cZ, 2MeSiP was detected during growth, aggregation, and germination. The levels of 2MeSiP were lower during growth and aggregation (< 2 pmol/10⁶ cells) compared to germination (between 2–55 pmol/10⁶ cells). In comparison to other CK-types, the role of methylthio-CKs (2MeSCKs) is the most obscure. These CKs are found in a subset of tRNAs as secondary modifications to tRNA-bound iP in plants, fungi, bacteria, and mammals. Upon tRNA degradation, the 2MeSCKs contribute to the free CK pool within the organism (Burrows et al., 1970; Kisiala et al., 2013; Morrison et al., 2015; Seegobin et al., 2018). Collectively, CK-tRNA modifications are strongly linked to translation fidelity, but the activities of free, tRNA-derived CKs have never been characterized (see reviews Persson et al., 1994; Schweizer et al., 2017). In bacteria, the product of the *miaB* gene is responsible for methylthiolation of tRNA-bound iP, whereas the product of the less common gene, *miaE*, first isolated from *Salmonella typhimurium* is responsible for hydroxylation of 2MeSiP to 2MeSZ (Persson and Björk, 1993). In mammals, the gene responsible for 2MeSiP modifications in tRNA is known as

CDK5RAPI (Reiter et al., 2012). Interestingly, the *D. discoideum* genome encodes a putative ortholog of *CDK5RAPI* (depicted as enzyme 2 in the CK biosynthesis pathway, Figure 3.4), but the gene itself remains to be characterized (*DDB_G0287079*; <http://www.dictybase.org>). Based on this information, it is possible that 2MeSiP is produced via a pathway that is similar to the pathways observed in other CK-producing organisms.

CK profiles and metabolomic data support previous literature on the presence of DA in the fruiting body life cycle stage. Low levels of DA were detected in the mound and slug stages at concentrations 38-fold lower than those detected in the fruiting body. Interestingly, the data obtained from the metabolomics study suggest that DA is one of the most upregulated small molecules during development, which speaks to the importance of its tight regulation leading to rapid encapsulation of spores and maintenance of spore dormancy (Taya et al., 1980; Anjard and Loomis, 2008). Similar to the spore dormancy effects of DA, a hypersporulation phenotype is observed in the fungi, *Claviceps purpurea*, following knockout of the CK-specific hydroxylating enzyme, Cpp450, which forms *tZ* (Hinsch et al., 2015). As such, the role of CKs in the regulation of sporulation extends beyond what is observed in the Amoebozoa phylum.

Lastly, the spore germination assay expands upon previous research illustrating the continued production of DA during the process of germination. The increasing extracellular concentrations of DA support previous studies regarding the role of DA in germination inhibition; accordingly, the spores should cease intracellular DA production in the presence of available nutrients and, thereby, allow for DA secretion into the surrounding environment to rid the inhibition signal and allow germination of amoeba.

This is supported by the IC data for DA, as the highest DA levels were detected at the 24-hour time point and production decreased as germination occurred. The extracellular DA levels increased consistently over 72-hour with the final time-point containing the highest level of CKs detected at any life cycle stage. From this data, there are many questions to pursue regarding the expanded roles of CKs and respective signal transduction pathways in *D. discoideum*. This becomes especially pertinent following the identification of novel CK forms during *D. discoideum* growth and development in the present study.

CONCLUSION

Collectively, the present results are the first to identify CKs in *D. discoideum* beyond the fruiting body life cycle stage. In addition to iP and DA, four more CK analytes were identified in this study (*cZ*, iPR, iPRP, and 2MeSiP) defining the pathway by which *D. discoideum* can synthesize multiple CK types and explains the origins of the two previously documented CK forms. The increase in iP free base during the transition from growth to development suggests a potentially wider role of CKs in the transition to multicellularity. Indeed, our experiments show that iP is the only tested CK form capable of increasing cell proliferation in liquid culture. Furthermore, the detection of the high CK levels during germination with distinct trends in DA synthesis support previous literature regarding the role of DA as a spore germination inhibitor. While much remains to be explored in *D. discoideum* regarding the role of CKs throughout the life cycle, this study provides unique evidence of the CK production and supports previous literature on the involvement of CKs in the metabolism of non-plant organisms. This study expands our understanding of CK-producing organisms, thus highlighting the utility of the social amoeba in the research on

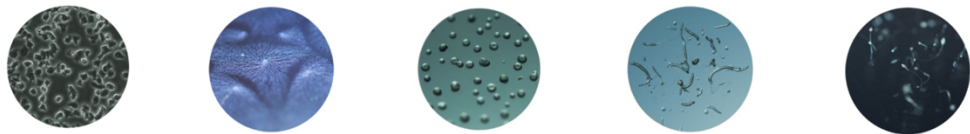
this group of growth regulating hormones. Knockout experiments of the three isopentenyltransferase genes (*iptA*, *iptB*, and *iptC*) are underway to better resolve the biological roles of CKs in *D. discoideum*.

TABLES AND FIGURES

Table 3.1. Endogenous and ²H-labeled cytokinins (CKs) scanned for by high-performance liquid chromatography-positive electrospray ionization-high resolution tandem mass spectrometry (HPLC-(ESI+)-HRMS/MS) in *Dictyostelium discoideum* intracellular (IC) and extracellular (EC) samples. Labeled internal standards obtained from OlChemim Ltd. (Olomouc, Czech Republic) were used to identify and quantify CKs.

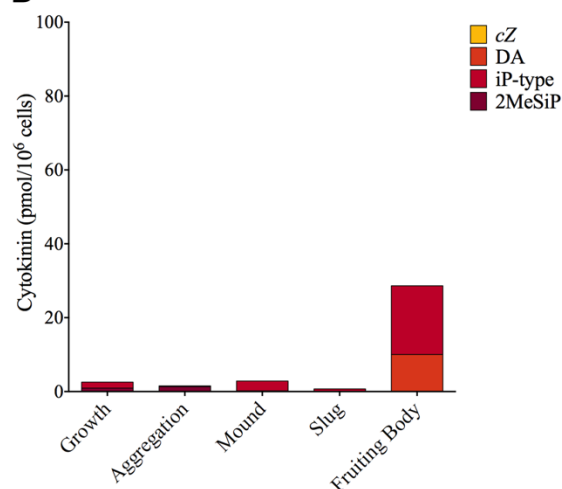
Endogenous CK Fractions	² H-labeled Internal Standard
Nucleotides (RP)	
<i>trans</i> -zeatin riboside-5'-monophosphate (<i>tZRP</i>)	² H ₆ [9RMP]DZ
<i>cis</i> -zeatin riboside-5'-monophosphate (<i>cZRP</i>)	² H ₆ [9RMP]DZ
Dihydrozeatin riboside-5'-monophosphate (DZRP)	² H ₆ [9RMP]DZ
<i>N</i> ⁶ -benzyladenosine-5'-monophosphate (BARP)	² H ₆ [9RMP]DZ
<i>N</i> ⁶ -isopentyladenosine-5'-monophosphate (iPRP)	² H ₆ [9RMP]iP
Ribosides (R)	
<i>trans</i> -zeatin riboside (<i>tZR</i>)	² H ₅ [9R] <i>tZ</i>
<i>cis</i> -zeatin riboside (<i>cZR</i>)	² H ₅ [9R] <i>tZ</i>
Dihydrozeatin riboside (DZR)	² H ₃ [9R]DZ
<i>N</i> ⁶ -isopentyladenosine (iPR)	² H ₆ [9R]iP
<i>N</i> ⁶ -benzyladenosine (BAR)	² H ₇ [9R]BA
Free bases (FB)	
<i>trans</i> -zeatin (<i>tZ</i>)	² H ₃ DZ
<i>cis</i> -zeatin (<i>cZ</i>)	² H ₃ DZ
Discadenine (DA)	² H ₃ DZ
Dihydrozeatin (DZ)	² H ₃ DZ
<i>N</i> ⁶ -isopentyladenine (iP)	² H ₆ iP
<i>N</i> ⁶ -benzyladenine (BA)	² H ₇ BA
Glucosides (GLUC)	
<i>trans</i> -zeatin-O-glucoside (<i>tZOG</i>)	² H ₅ <i>tZOG</i>
<i>cis</i> -zeatin-O-glucoside (<i>cZOG</i>)	² H ₅ <i>tZOG</i>
Dihydrozeatin-O-glucoside (DZOG)	² H ₇ DZOG
<i>trans</i> -zeatin-O-glucoside riboside (<i>tZROG</i>)	² H ₅ <i>tZROG</i>
<i>cis</i> -zeatin-O-glucoside riboside (<i>cZROG</i>)	² H ₅ <i>tZROG</i>
Dihydrozeatin-O-glucoside riboside (DZROG)	² H ₇ DZROG
<i>trans</i> -zeatin-7-glucoside (<i>tZ7G</i>)	² H ₅ <i>tZ7G</i>
<i>trans</i> -zeatin-9-glucoside (<i>tZ9G</i>)	² H ₅ <i>tZ9G</i>
<i>cis</i> -zeatin-9-glucoside (<i>cZ9G</i>)	² H ₅ <i>tZ9G</i>
Dihydrozeatin-9-glucoside (DZ9G)	² H ₃ DZ9G
Methylthiols (2MeS)	
2-Methylthio-zeatin (2MeSZ)	² H ₅ 2MeS <i>tZ</i>
2-Methylthio-zeatin riboside (2MeSZR)	² H ₅ 2MeS <i>tZR</i>
2-Methylthio- <i>N</i> ⁶ -isopentenyladenine (2MeSiP)	² H ₆ 2MeSiP
2-Methylthio- <i>N</i> ⁶ -isopentenyladenosine (2MeSiPR)	² H ₆ 2MeSiPR

A



	Growth (pmol/10 ⁶ cells)		Aggregation (pmol/10 ⁶ cells)		Mound (pmol/10 ⁶ cells)		Slug (pmol/10 ⁶ cells)		Fruiting Body (pmol/10 ⁶ cells)	
	IC	EC	IC	EC	IC	EC	IC	EC	IC	EC
cZ	n.d.	0.49±0.03	n.d.	0.84±0.08	0.02±0.01	0.04±0.01	n.d.	0.01±0.001	n.d.	n.d.
DA	n.d.	n.d.	n.d.	n.d.	0.15±0.03	1.32±0.11	0.04±0.01	1.11±0.09	10.05±0.62	46.37±3.73
iP	0.07±0.00	8.88±0.36	0.11±0.01	14.09±1.29	n.d.	0.69±0.09	n.d.	n.d.	2.64±0.15	41.12±4.60
iPR	0.14±0.02	0.38±0.02	0.10±0.02	0.58±0.05	n.d.	n.d.	n.d.	n.d.	n.d.	n.d.
iPRP	1.41±0.33	n.d.	n.d.	3.79±1.04	2.69±1.56	n.d.	0.69±0.35	n.d.	15.97±3.85	0.61±0.15
2MeSiP	0.94±0.09	1.09±0.15	1.34±0.25	1.25±0.15	n.d.	n.d.	n.d.	n.d.	n.d.	n.d.

B



C

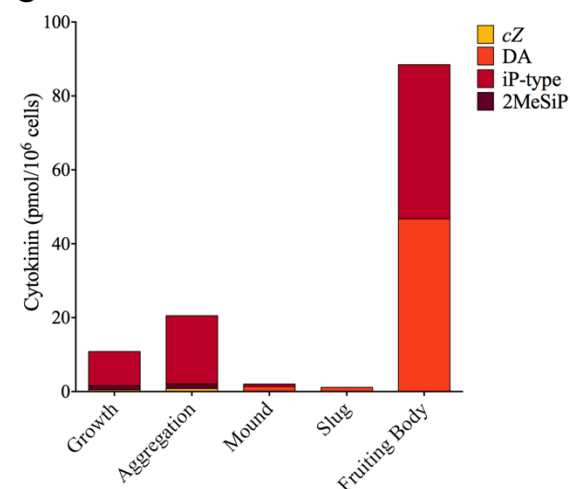


Figure 3.1. Cytokinin (CK) production (pmol/10⁶ cells) detected by high-performance liquid chromatography-positive electrospray ionization-high resolution tandem mass spectrometry (HPLC-(ESI+)-HRMS/MS) during five stages of the *Dictyostelium discoideum* life cycle. (A) Individual CK analyte concentrations detected intracellularly (IC) and extracellularly (EC) during the life cycle. Values presented as means ± standard error of the mean (SEM; n = 4); n.d. represents CKs not detected. (B) Total concentrations of CK-types detected within the IC samples during the five life cycle stages. (C) Total concentrations of CK-types detected within the EC samples. iP-type CKs encompass the free base (iP), riboside (iPR), and nucleotide (iPRP).

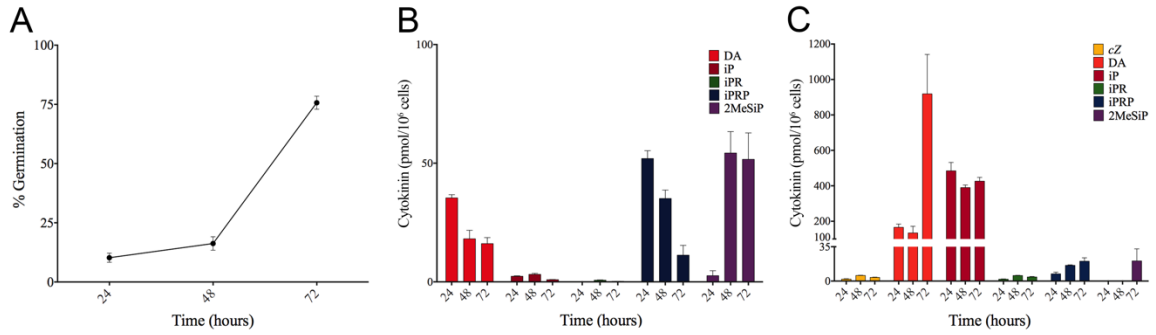


Figure 3.2. *Dicytostelium discoideum* germination rate (%) and cytokinin (CK) production over a 72-hour time course. (A) The percentage of germinated spores was determined for each of the sampled time points. (B) IC CK analyte concentrations detected by high-performance liquid chromatography-positive electrospray ionization-high resolution tandem mass spectrometry (HPLC-(ESI+)-HRMS/MS) during a 72-hour germination period. (C) EC CK analyte concentrations detected by HPLC-(ESI+)-HRMS/MS during a 72-hour germination period. The presented values are means \pm SEM (n = 4). The experiment shown was a typical response that was confirmed by other independently replicated trials.

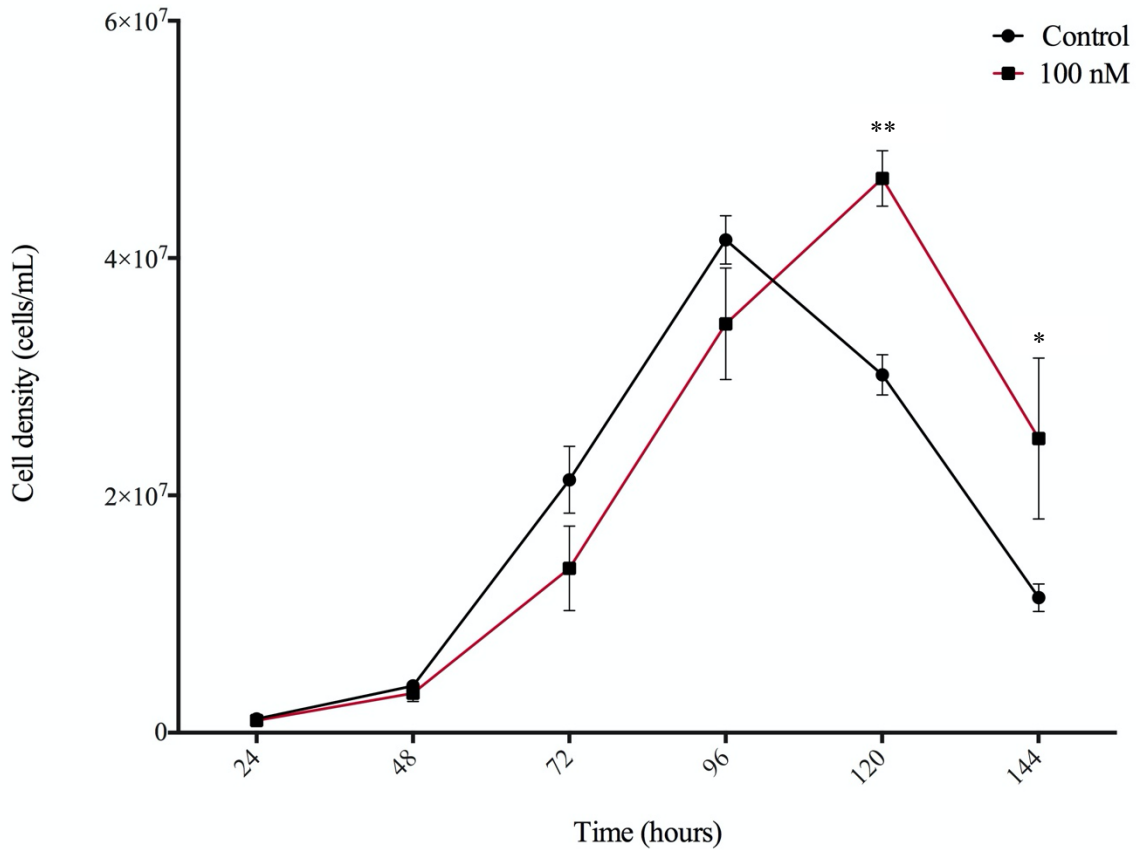


Figure 3.3. Effect of 100 nM *N*⁶-isopentenyladenine (iP) treatment on AX3 cell proliferation in HL5 medium over a 144-hour growth period. Data are presented as mean concentration (cells/mL) ± SEM (n = 6). Statistical significance was assessed using two-way ANOVA ($p < 0.05$) followed by the Bonferroni multiple comparisons test. This analysis revealed a significant effect of CK treatment on growth for the 100 nM concentration of iP at the 120-hour and 144-hour time points (** $p < 0.01$, and * $p < 0.05$). This finding was replicated in two independent experiments.

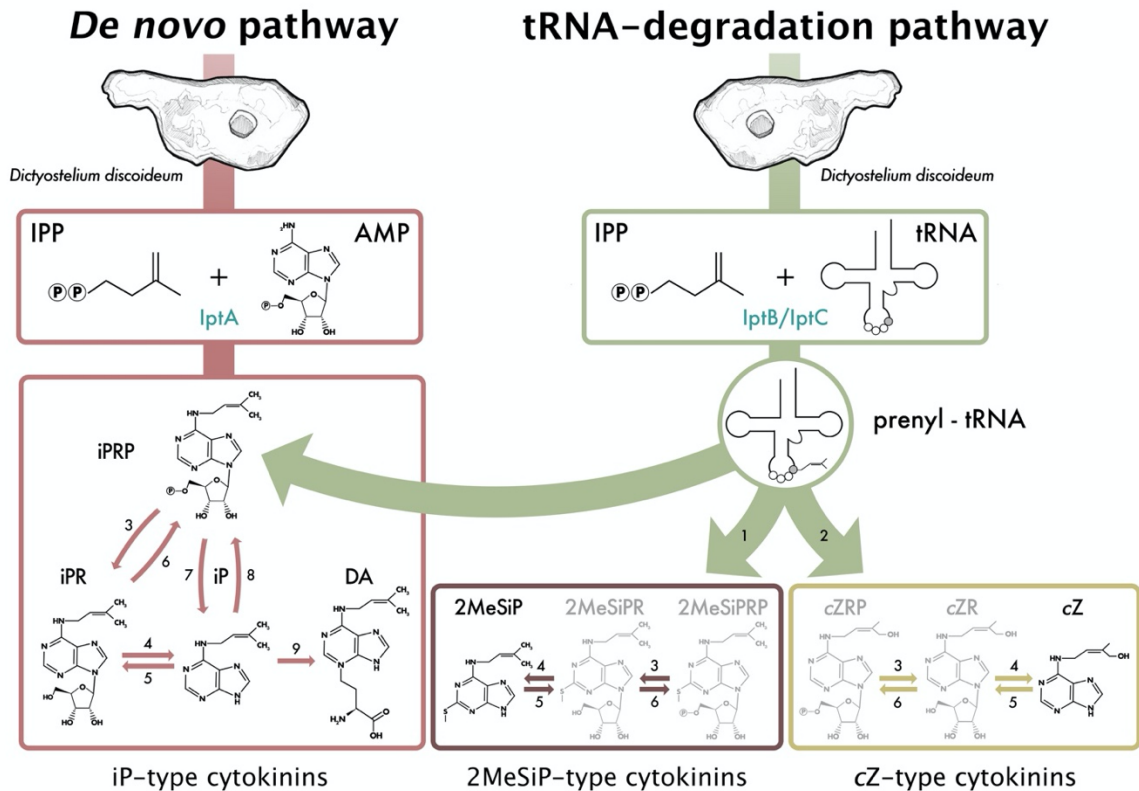
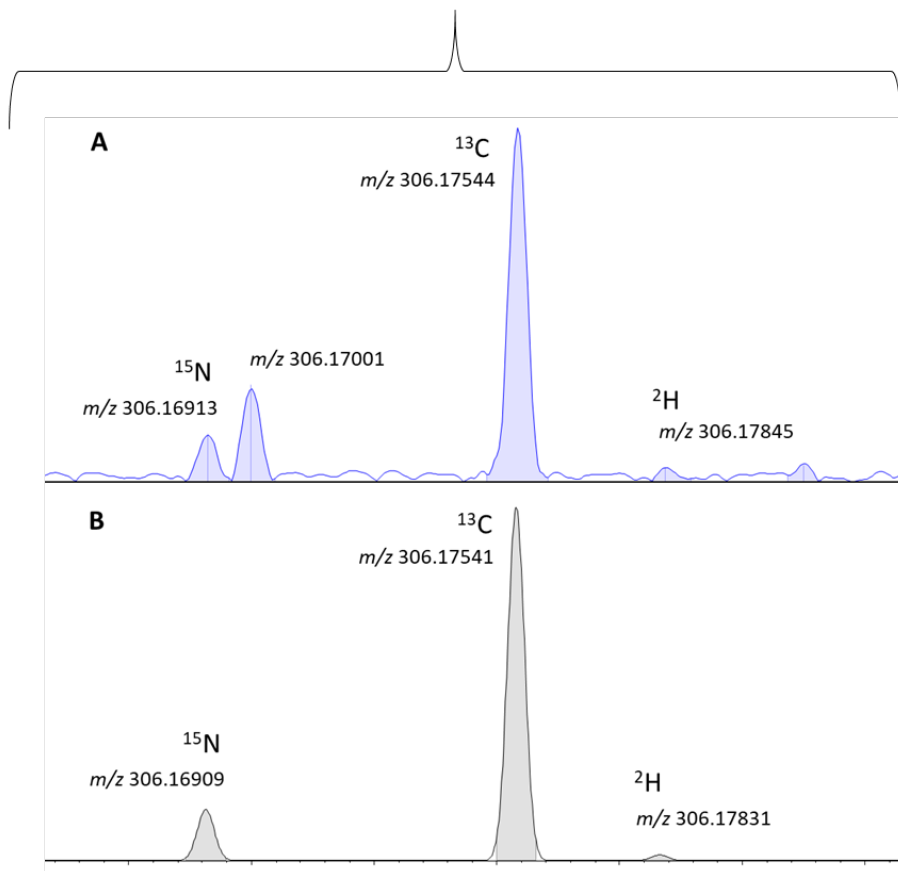
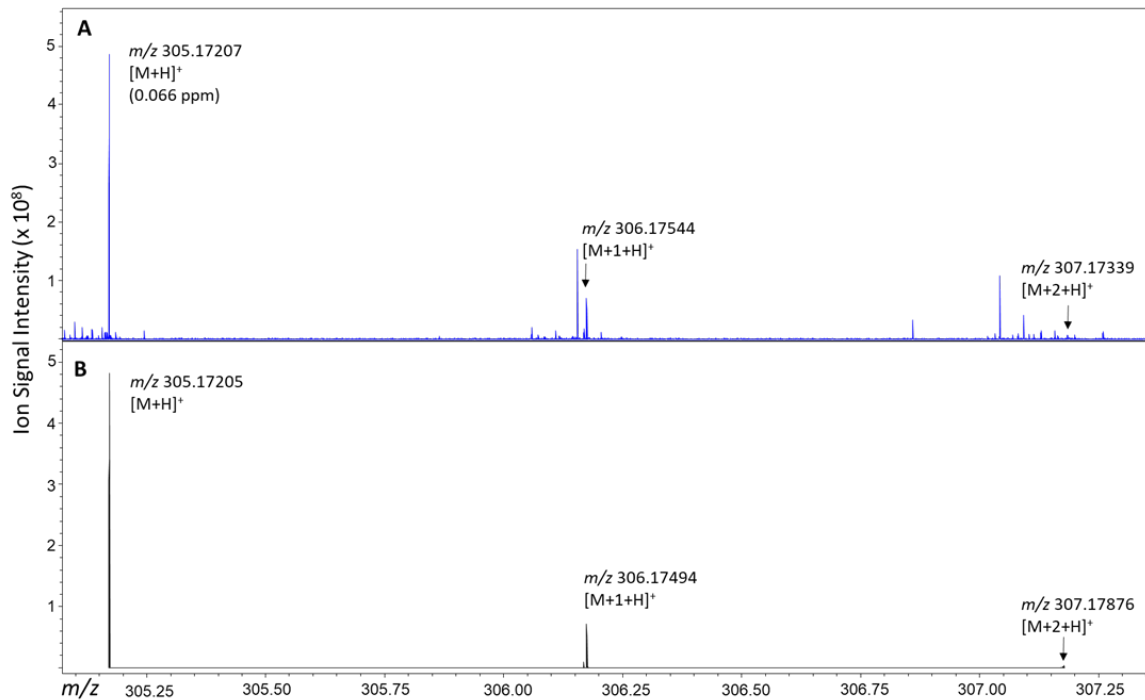


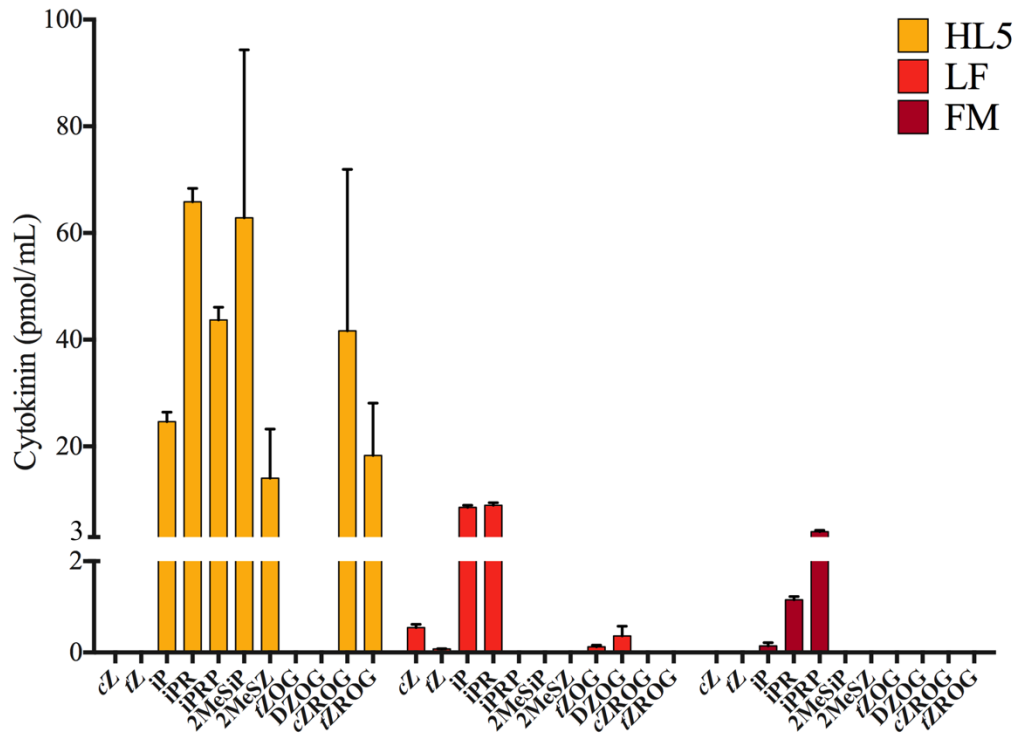
Figure 3.4. Proposed model of cytokinin (CK) biosynthesis in *Dictyostelium discoideum* consisting of two activation pathways—*de novo* and tRNA degradation. The information presented in the pathway was inferred from the current study and previous *D. discoideum*, plant, and fungi studies (Taya et al., 1978a; Taya et al., 1978b; Anjard and Loomis, 2008; Kamada-Nobusada and Sakakibara, 2009; Frébort et al., 2011; Spichal, 2012; Morrison et al., 2015; Morrison et al., 2017; Nishii et al., 2018). Isopentenyltransferase (IptA) catalyzes the addition of a prenyl group from isopentenyl pyrophosphate (IPP) to adenosine monophosphate (AMP) to form free N⁶-isopentenyladenine-type (iP-type) CKs and discadenine (DA) via the *de novo* biosynthesis pathway (Taya et al., 1978a; Taya et al., 1978b). IptB and IptC are proposed tRNA isopentenyltransferases which catalyze prenylation of tRNA molecules that can be further modified to form 2-methylthio-N⁶-isopentenyladenine-type (2MeSiP-type) CKs or *cis*-zeatin-type (*cZ*-type) CKs via the tRNA degradation pathway (Anjard and Loomis, 2008; Nishii et al., 2018). Degradation from the tRNA molecule contributes to the pool of free CKs, depicted by the three green arrows coming off of the prenyl-tRNA molecule. Expression data for the three isopentenyltransferase genes can be found in the Supplementary Figure 3.4 (Rot et al., 2009). Black CK molecules depict the six CKs synthesized by *D. discoideum* in the present study, while gray CK molecules represent CKs typical of CK biosynthesis pathways, but not detected in this study. Numbers represent inferred enzymes as follows: 1. *cdk5rap1*-like ortholog (*DDB_G0287079*); 2. *cis*-hydroxylase; 3. 5'-ribonucleotide phosphohydrolase; 4. adenosine nucleosidase; 5. purine nucleoside phosphorylase; 6. adenosine kinase; 7. CK phosphoribohydrolase (LOG-like ortholog, *DDB_G0281309*); 8. adenine phosphoribosyltransferase; 9. discadenine synthase.

SUPPLEMENTARY MATERIALS

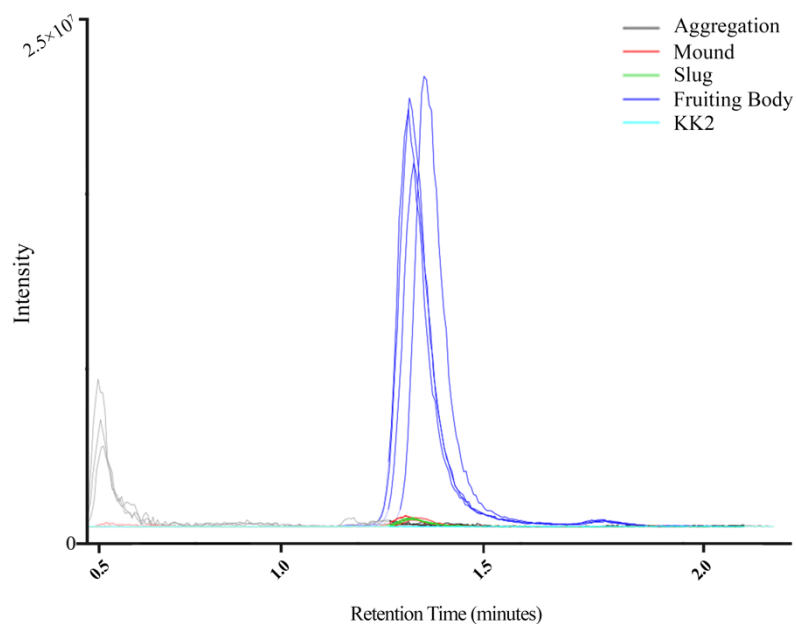
Supplementary Materials: Fourier transform ion cyclotron resonance mass spectrometer (FTICR-MS) Analysis: The presence of DA in sample extracts was investigated using a 7 T Bruker Solarix XR, FTICR-MS equipped with an electrospray ionization source operated in positive ion mode (Billerica, MA, USA). Sodium trifluoroacetic acid (0.1 mg/mL in methanol) was used to externally calibrate the instrument. Samples were infused at a rate of 180 $\mu\text{L}/\text{h}$ and source parameters included capillary voltage of 5500 V, nebulizer gas pressure 1 bar, drying gas flow rate of 4 L/min and drying temperature of 200 $^{\circ}\text{C}$. Accumulation time was optimized for 1×10^9 ions in the ion cyclotron resonance (ICR) cell. Mass spectra were acquired from m/z 54 to 1100 for 100 scans; 16 M data points were collected per scan with a free ion decay (FID) of 4.1943 s. Spectra were acquired using Bruker fms Control software (version 2.1.0) and analyzed using Bruker Compass DataAnalysis software (version 5.0). As indicated in Figure S1, the mass spectra obtained from a sample extract is in good agreement with the theoretical mass spectrum of discadenine (DA, $\text{C}_{14}\text{H}_{20}\text{N}_6\text{O}_2$), mass accuracy 0.066 ppm. Examination of the isotopic fine structure of the M^{+1} isotope (insert) is also in agreement with the theoretical mass spectrum of DA. The peak observed at m/z 306.17001 was not identified and is likely another analyte in the sample extract.



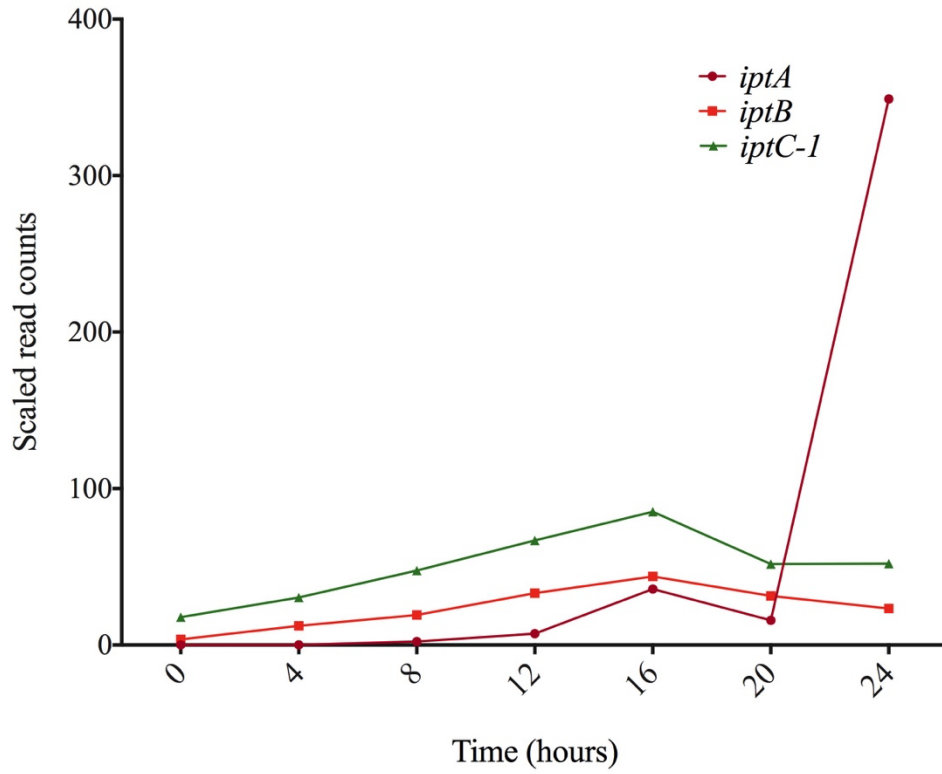
Supplementary Figure 3.1. Observed mass spectrum of *Dictyostelium discoideum* sample extract (A) and the theoretical mass spectrum of discadenine (DA, C₁₄H₂₀N₆O₂) (B). Magnification of the isotopic fine structure of the M+1 isotope is shown.



Supplementary Figure 3.2. Cytokinin (CK) profiles of three common *Dictyostelium discoideum* culture media: HL5, Lo-Flo (LF), and FM minimal medium. Values presented as means \pm standard error of the mean (SEM; n = 4).



Supplementary Figure 3.3. Extracted ion chromatogram for DA showing the peak intensity for each of the developmental life cycle stages of *Dictyostelium discoideum* analyzed using a multigroup analysis performed through XCMS Online (Gowda et al., 2014). KK2 buffer was used as a negative control in the multigroup analysis to exclude features present in the buffer during statistical analysis. DA was eluted at 1.38 min at m/z 305.1705.



Supplementary Figure 3.4. Gene expression analysis of the three isopentenyltransferase genes in *Dictyostelium discoideum*. RNA-Seq data was obtained from dictyExpress (www.dictyexpress.biolab.si) (Rot et al., 2009).

REFERENCES

- Abe, H., Hashimoto, K., and Uchiyama, M. (1981). Discadenine distribution in cellular slime molds and its inhibitory activity on spore germination. *Agric. Biol. Chem.* 45, 1295–1296. doi:10.1080/00021369.1981.10864699.
- Abe, H., Uchiyama, M., Tanaka, Y., Saito, H. (1976). Structure of discadenine, a spore germination inhibitor from the cellular slime mold *Dictyostelium discoideum*. *Tetrahedron Lett.* 17, 3807–3810. doi: 10.1016/S0040-4039(00)93115-0.
- Anjard, C. and Loomis, W. F. (2008). Cytokinins induce sporulation in *Dictyostelium*. *Development* 135, 819-827. doi: 10.1242/dev.018051.
- Burrows, W. J., Armstrong, D. J., Kamínek, M., Skoog, F., Bock, R. M., Hecht, S. M., et al. (1970). Isolation and identification of four cytokinins from wheat germ transfer ribonucleic acid. *Biochemistry* 1970, 9, 1867–1872. doi: 10.1021/bi00811a001.
- Chen, C., Li, C., Wang, Y., Renaud, J., Tian, G., Kambhampati, S., et al. (2017). Cytosolic acetyl-CoA promotes histone acetylation predominantly at H3K27 in *Arabidopsis*. *Nat. Plants* 3, 814–824. doi: 10.1038/s41477-017-0023-7.
- Eichinger, L., Pachebat, J. A., Glöckner, G., Rajandream, M.-A., Sugang, R., Berriman, M., et al. (2005). The genome of the social amoeba *Dictyostelium discoideum*. *Nature* 435, 43–57. doi: 10.1038/nature03481.
- Emery, R. J. N., Ma, Q., and Atkins, C. A. (2000). The forms and sources of cytokinins in developing white lupine seeds and fruits. *Plant Physiol.* 123, 1593–1604. doi: 10.1104/pp.123.4.1593.
- Farrow, S. C. and Emery, R. J. N. (2012). Concurrent profiling of indole-3-acetic acid, abscisic acid, and cytokinins and structurally related purines by high-performance-liquid-chromatography tandem electrospray mass spectrometry. *Plant Methods* 8, 42. doi: 10.1186/1746-4811-8-42.
- Fey, P., Kowal, A. S., Gaudet, P., Pilcher, K. E., and Chisholm, R. L. (2007). Protocols for growth and development of *Dictyostelium discoideum*. *Nat. Protoc.*, 2, 1307–1316.
- Frébort, I., Kowalska, M., Hluska, T., Frébortová, J., and Galuszka, P. (2011). Evolution of cytokinin biosynthesis and degradation. *J. Exp. Bot.* 62, 2431–2452. doi: 10.1093/jxb/err004.
- Gerisch, G. and Wick, U. (1975). Intracellular oscillations and release of cyclic AMP from *Dictyostelium* cells. *Biochem. Biophys. Res. Commun.* 65, 364–370. doi: 10.1016/s0006-291x(75)80102-1.
- Gogala, N. (1991). Regulation of mycorrhizal infection by hormonal factors produced by

- hosts and fungi. *Experientia* 47, 331–340. doi: 10.1007/BF01972074.
- Gowda, H., Ivanisevic, J., Johnson, C. H., Kurczy, M. E., Benton, H.P., Rinehart, D., et al. (2014). Interactive XCMS Online: Simplifying advanced metabolomic data processing and subsequent statistical analyses. *Anal. Chem.* 86, 6931-6939. doi: 10.1021/ac500734c.
- Hinsch, J., Vrabka, J., Oeser, B., Novák, O., Galuszka, P., and Tudzynski, P. (2015). *De novo* biosynthesis of cytokinins in the biotrophic fungus *Claviceps purpurea*. *Environ. Microbiol.* 17, 2935–2951. doi: 10.1111/1462-2920.12838.
- Hoyerová, K., Gaudinová, A., Malbeck, J., Dobrev, P. I., Kocábek, T., Šolcová, B., et al. (2006). Efficiency of different methods of extraction and purification of cytokinins. *Phytochemistry* 67, 1151–1159. doi: 10.1016/j.phytochem.2006.03.010.
- Ihara, M., Taya, Y., and Nishimura, S. (1980). Developmental regulation of cytokinin, spore germination inhibitor discadenine and related enzymes in *Dictyostelium discoideum*. *Exp. Cell Res.* 126, 273–278. doi: 10.1016/0014-4827(80)90265-7.
- Ihara, M., Taya, Y., Nishimura, S., and Tanaka, Y. (1984). Purification and some properties of Δ^2 -isopentenylpyrophosphate:5'AMP Δ^2 -isopentenyltransferase from the cellular slime mold *Dictyostelium discoideum*. *Arch. Biochem. Biophys.* 230, 652–660. doi: 10.1016/0003-9861(84)90446-6.
- Kamada-Nobusada, T. and Sakakibara, H. (2009). Molecular basis for cytokinin biosynthesis. *Phytochemistry* 70, 444–449. doi: 10.1016/j.phytochem.2009.02.007.
- Kasahara, H., Takei, K., Ueda, N., Hishiyama, S., Yamaya, T., Kamiya, Y., et al. (2004). Distinct isoprenoid origins of *cis*- and *trans*-Zeatin biosyntheses in *Arabidopsis*. *J. Biol. Chem.* 279, 14049–14054. doi: 10.1074/jbc.M314195200.
- Kisiala, A., Laffont, C., Emery, R.J.N., and Frugier, F. (2013). Bioactive cytokinins are selectively secreted by *Sinorhizobium meliloti* nodulating and nonnodulating strains. *Mol. Plant Microbe Interact.* 26, 1225–1231. doi: 10.1094/MPMI-02-13-0054-R.
- Kisiala, A., Kambhampati, S., Stock, N. L., Aoki, M., and Emery, R. J. N. (2019). Quantification of cytokinins using high-resolution accurate-mass orbitrap mass spectrometry and parallel reaction monitoring (PRM). *Analytical Chemistry* 91, 15049-15056. doi: 10.1021/acs.analchem.9b037.
- Konijn, T. M., Van De Meene, J. G., Bonner, J. T., and Barkley, D. S. (1967). The acrasin activity of adenosine-3',5'-cyclic phosphate. *Proc. Natl. Acad. Sci. U.S.A.* 58, 1152-1154. doi: 10.1073/pnas.58.3.1152.
- LeJohn, H. B. and Stevenson, R. M. (1973). Cytokinins and magnesium ions may control the flow of metabolites and calcium ions through fungal cell membranes. *Biochem.*

- Biophys. Res. Commun.* 54, 1061–1066. doi: 10.1016/0006-291X(73)90801-2.
- Lindner, A. C., Lang, D., Seifert, M., Podlešáková, K., Novák, O., Strnad, M., et al. (2014). Isopentenyltransferase-1 (IPT1) knockout in *Physcomitrella* together with phylogenetic analyses of IPTs provide insights into evolution of plant cytokinin biosynthesis. *J. Exp. Bot.* 65, 2533–2543. doi: 10.1093/jxb/eru142.
- Loomis, W. F. (2014). Cell signaling during development of *Dictyostelium*. *Dev. Biol.* 391, 1–16. doi: 10.1016/j.ydbio.2014.04.001.
- Mik, V., Mičková, Z., Doležal, K., Frébort, I., and Pospíšil, T. (2017). Activity of (+)-discadenine as a plant cytokinin. *J. Nat. Prod.* 80, 2136–2140. doi: 10.1021/acs.jnatprod.6b01165.
- Mok, D. W., and Mok, M. C. (2001). Cytokinin metabolism and action. *Annu. Rev. Plant Physiol. Plant Mol. Biol.* 52, 89–118. doi: 10.1146/annurev.arplant.52.1.89.
- Morrison, E. N., Emery, R. J. N., and Saville, B. J. (2017). Fungal derived cytokinins are necessary for normal *Ustilago maydis* infection of maize. *Plant Pathol.* 66, 726–742. doi: 10.1111/ppa.12629.
- Morrison, E. N., Knowles, S., Hayward, A., Thorn, R. G., Saville, B. J., and Emery, R. J. N. (2015). Detection of phytohormones in temperate forest fungi predicts consistent abscisic acid production and a common pathway for cytokinin biosynthesis. *Mycologia* 107, 245–257. doi: 10.3852/14-157.
- Nishii, K., Wright, F., Chen, Y. Y., and Möller, M. (2018). Tangled history of a multigene family: The evolution of ISOPENTENYLTRANSFERASE genes. *PLoS One* 13, 1–23. doi: 10.1371/journal.pone.0201198.
- Obata, Y., Abe, H., Tanaka, Y., Yanagisawa, K., and Uchiyama, M. (1973). Isolation of a spore germination inhibitor from a cellular slime mold *Dictyostelium discoideum*. *Agric. Biol. Chem.* 37, 1989–1990. doi: 10.1080/00021369.1973.10860941.
- Persson, B. C. and Björk, G.R. (1993). Isolation of the gene (miaE) encoding the hydroxylase involved in the synthesis of 2-methylthio-*cis*-ribozeatin in tRNA of *Salmonella typhimurium* and characterization of mutants. *J. Bacteriol.* 175, 7776–7785. doi: 10.1128/jb.175.24.7776-7785.1993.
- Persson, B. C., Esberg, B., Ólafsson, Ó., and Björk, G. R. (1994). Synthesis and function of isopentenyl adenosine derivatives in tRNA. *Biochimie* 76, 1152–1160. doi: 10.1016/0300-9084(94)90044-2.
- Prince, J. T. and Marcotte, E. M. (2006). Chromatographic alignment of ESI-LC-MS proteomics data sets by ordered bijective interpolated warping. *Anal. Chem.* 78, 6140–6152. doi: 10.1021/ac0605344.

- Quesnelle, P. E. and Emery, R. J. N. (2007). *cis*-cytokinins that predominate in *Pisum sativum* during early embryogenesis will accelerate embryo growth *in vitro*. *Can. J. Bot.* 85, 91–103. doi: 10.1139/b06-149.
- Reiter, V., Matschkal, D. M. S., Wagner, M., Globisch, D., Kneuttinger, A. C., Müller, M. et al. (2012). The CDK5 repressor CDK5RAP1 is a methylthiotransferase acting on nuclear and mitochondrial RNA. *Nucleic Acids Res.* 40, 6235–6240. doi: 10.1093/nar/gks240.
- Rot, G., Parikh, A., Curk, T., Kuspa, A., Shaulsky, G., and Zupan, B. (2009). dictyExpress: A *Dictyostelium discoideum* gene expression database with an explorative data analysis web-based interface. *BMC Bioinformatics* 10, 265. doi: 10.1186/1471-2105-10-265.
- Sakakibara, H. (2006). Cytokinins: Activity, biosynthesis, and translocation. *Annu. Rev. Plant Biol.* 57, 431–449. doi:10.1146/annurev.arplant.57.032905.105231.
- Schweizer, U., Bohleber, S., and Fradejas-Villar, N. (2017). The modified base isopentenyladenosine and its derivatives in tRNA. *RNA Biol.* 14, 1197-1208. doi: 10.1080/15476286.2017.1294309.
- Schaap, P., Winckler, T., Nelson, M., Alvarez-Curto, E., Elgie, B., Hagiwara, H., et al. (2006). Molecular phylogeny and evolution of morphology in the social amoebas. *Science* 314, 661–663. doi: 10.1126/science.1130670.
- Schäfer, M., Brütting, C., Canales, I. M., Großkinsky, D. K., Vankova, R., Baldwin, I. T., et al. (2015). The role of *cis*-zeatin-type cytokinins in plant growth regulation and mediating responses to environmental interactions. *J. Exp. Bot.* 66, 4873-4884. doi: 10.1093/jxb/erv214.
- Schilde, C., and Schaap, P. (2013). “The Amoebozoa.” In; *Humana Press*, Totowa, NJ, USA 2013; pp. 1–15. doi: 10.1007/978-1-62703-302-2_1.
- Seegobin, M., Kisiala, A., Noble, A., Kaplan, D., Brunetti, C., and Emery, R. J. N. (2018). *Canis familiaris* tissues are characterized by different profiles of cytokinins typical of the tRNA degradation pathway. *FASEB J.* 32, 6575–6581. doi: 10.1096/fj.201800347.
- Siegert, F. and Weijer, C. J. (1995). Spiral and concentric waves organize multicellular *Dictyostelium* mounds. *Curr. Biol.* 5, 937–943. doi: 10.1016/s0960-9822(95)00184-9.
- Spíchal, L. (2012). Cytokinins - recent news and views of evolutionally old molecules. *Funct. Plant Biol.* 39, 267. doi: 10.1071/FP11276.
- Tanaka, Y.-M., Hashimoto, Y., Yanagisawa, K., Abe, H., and Uchiyama, M. (1975). Partial

structure of a spore germination inhibitor from a cellular slime mold, *Dictyostelium discoideum*. *Agric. Biol. Chem.* 39, 1929–1932. doi: 10.1080/00021369.1975.10861883.

Tanaka, Y., Abe, H., Uchiyama, M., Taya, Y., and Nishimura, S. (1978). Isopentenyladenine from *Dictyostelium discoideum*. *Phytochemistry* 17, 543–544.

Tautenhahn, R., Patti, G. J., Rinehart, D., and Siuzdak, G. (2012). XCMS Online: A web-based platform to process untargeted metabolomic data. *Anal. Chem.* 84, 5035–5039. doi: 10.1021/ac3000698c.

Taya, Y., Tanaka, Y., and Nishimura, S. (1978a). 5'-AMP is a direct precursor of cytokinin in *Dictyostelium discoideum*. *Nature* 271, 545–547. doi: 10.1038/271545a0

Taya, Y., Tanaka, Y., and Nishimura, S. (1978b). Cell-free biosynthesis of discadenine, a spore germination inhibitor of *Dictyostelium discoideum*. *FEBS Lett.* 89, 326–328. doi: 10.1016/0014-5793(78)80247-6

Taya, Y., Yamada, T., and Nishimura, S. (1980). Correlation between acrasins and spore germination inhibitors in cellular slime molds. 143, 715–719. doi: 10.1128/jb.143.2.715-719.1980.

CHAPTER 4

PREFACE

- Title:** From biosynthesis and beyond – Loss or overexpression of the cytokinin synthesis gene, *iptA*, alters cytokinesis and mitochondrial and amino acid metabolism in *Dictyostelium discoideum*
- Authors:** Megan M. Aoki, Anna B. Kisiala, Sabateeshan Mathavarajah, Jared Treverton, Elias Habib, Graham Dellaire, R. J. Neil Emery, Craig R. Brunetti, and Robert J. Huber
- Reference:** The chapter is currently under preparation for submission. The published version of this manuscript will appear different from the chapter presented here.
- Contributions:** Conceptualization M.M.A., C.R.B., R.J.N.E and R.J.H.; Formal analysis, M.M.A. generated the *iptA*⁻ strain and performed all experiments beyond what is listed by the individuals hereafter, A.B.K. assisted with mass spectrometry and metabolomics analysis, S.M. performed the qPCR analysis, cytokinesis analysis in HL5, and assisted with the TEM analysis, J.T. performed data analysis from the TEM images, and E.H. prepared and performed the TEM analysis; Methodology, M.M.A., A.B.K., S.M., and E.H.; Supervision, C.R.B., R.J.N.E and R.J.H.; Writing—original draft, M.M.A.; Writing—review and editing, M.M.A., A.B.K., S.M., G.D., R.J.N.E., C.R.B., and R.J.H.

CHAPTER 4

From biosynthesis and beyond – Loss or overexpression of the cytokinin synthesis gene, *iptA*, alters cytokinesis and mitochondrial and amino acid metabolism in *Dictyostelium discoideum*

ABSTRACT

Cytokinins (CKs) are a class of growth-promoting signaling molecules that affect many different cellular and developmental processes. These phytohormones are well-studied in plants, but their detection continues to be uncovered in organisms spanning all kingdoms, which poses many new questions about their roles and functions outside of plant systems. Cytokinin production is initiated by one of two different biosynthetic enzymes, adenylate isopentenyltransferases (IPTs) or tRNA isopentenyltransferases (tRNA-IPTs). In this study, the simple eukaryotic model, *Dictyostelium discoideum*, was used to study the role of CKs by generating deletion and overexpression strains of its single adenylate-IPT gene, *iptA*. Previous research determined that *D. discoideum* produces CKs throughout its life cycle stages and that CKs are necessary for proper development, specifically in the induction of sporulation and maintenance of spore dormancy. The current study focuses on vegetative growth and early development to investigate potential expanded roles of CKs. We found that *iptA*-deficiency resulted in cytokinesis defects, and *iptA*-deficiency and overexpression resulted in dysregulated TCA cycle and amino acid metabolism, as well as increased levels of AMP. Collectively, these findings suggest that *iptA* loss and overexpression alter biological processes in vegetative growth that are different from those affected in the later stages of multicellular development. Moreover, the combined phenotypes are indicative of mitochondrial-associated dysfunction during vegetative growth.

KEYWORDS: adenylate isopentenyltransferase, IptA, mitochondrial function, cytokinesis, amino acid metabolism, TCA cycle, metabolomics, *Dictyostelium discoideum*

INTRODUCTION

Cytokinins (CKs) are most well-known in plants as phytohormones and are essential plant growth regulators (Kieber and Schaller, 2018). CKs act as signaling molecules coordinating all aspects of growth and development, and they enable plants to sense and respond to environmental signals. CKs, therefore, provide the means to communicate at both the cellular and whole-plant levels with widespread roles in cell division, differentiation, vascular and gametophyte development, senescence, nutrient sensing, and responses to both biotic and abiotic stresses (Kieber and Schaller, 2018). Impactful roles of CKs are not exclusive to plants – in fact, several have been documented in many CK-producing organisms spanning several kingdoms. For example, CKs control: the cell cycle in apicomplexan parasites, fungi, and pathogenic nematodes (Siddique et al., 2015; Andrabi et al., 2018; Gupta et al., 2021), virulence of bacteria and fungi (Pertry et al., 2010; Morrison et al., 2016; Chanclud et al., 2016; Hinsch et al., 2016; Samanovic et al., 2018; Kabbara et al., 2020), spore germination in amoebae and fungi (Anjard and Loomis, 2008; Hinsch et al., 2015; Aoki et al., 2019), and cellular trafficking in fungi (Gupta et al., 2021). Owing to the pleiotropic nature of CKs, much remains to be understood regarding the mechanisms by which CKs influence cellular and developmental processes.

The production of cytokinins (CKs) is initiated by a first and rate-limiting step involving one of two biosynthetic enzymes, adenylate isopentenyltransferases (IPTs) or tRNA isopentenyltransferases (tRNA-IPTs) (Kakimoto et al., 2000; Takei et al., 2001). Disruption of *IPT* genes (including tRNA-IPTs) in both plant- and non-plant organisms results in drastic reductions in CK levels, with a variety of phenotypes including: decreased

shoot growth and increased root growth in *Arabidopsis thaliana* (Miyawaki et al., 2006), decreased colony growth in *Physcomitrella patens* (Lindner et al., 2014), decreased virulence in *Claviceps purpurea* (Hinsch et al., 2016), decreased drought tolerance in *Triticum aestivum* (wheat) (Wang et al., 2022), and spore viability defects in the amoeba, *Dictyostelium discoideum* (Anjard and Loomis, 2008). In plants, studying the roles of individual *IPT* genes can prove difficult owing to gene redundancy from the multiple whole-genome duplications that have occurred throughout plant evolution (Panchy et al., 2016). For instance, there are 24 putative *IPT* genes in *Triticum aestivum* (wheat) (18 *IPT*, 6 tRNA-*IPT*; Wang et al., 2022), 9 in *A. thaliana* (7 *IPT* and 2 tRNA-*IPT*s; Kakimoto, 2000; Takei et al., 2001), and 10 in *Oryza sativa* (rice) (8 *IPT* and 2 tRNA-*IPT*s; Sakamoto et al., 2006). By contrast, we employed a simple eukaryotic model, *Dictyostelium discoideum*, to exploit its genetic tractability to expand our understanding of CKs outside of plant systems by investigating the role of its only adenylate-*IPT* gene, *iptA*, through gene knockout and overexpression.

D. discoideum is a motile, soil-dwelling amoeba that can be studied at both the single- and multicellular levels. Starvation triggers multicellular development, where tens of thousands of cells merge together to form distinct morphological structures over its 24-hour life cycle (Kessin, 2001). In *D. discoideum*, it is straightforward to study a variety of different cellular and developmental processes throughout its life cycle, which has contributed to its usefulness as a model organism and has expanded our understanding of various biological processes (Bozzaro, 2019). Evolutionarily, *D. discoideum* belongs to the Amoebozoa phylum that diverged shortly after the line leading from plants to animals and has both plant- and animal-like characteristics (Eichinger et al., 2005).

Previous studies using *D. discoideum* established CKs as key signaling molecules necessary for spore production during the later stages of multicellular development (Anjard and Loomis, 2008; Loomis, 2014). Disruption of *iptA* reduces CK levels by 90% with visible morphological phenotypes in the final fruiting body life cycle stage (Anjard and Loomis, 2008). Recently, we profiled CKs throughout the life cycle stages of *D. discoideum* and found that six different CK forms were produced in varying amounts (Aoki et al., 2019). The highest CK levels were detected in the fruiting body stage, but there were also considerable CK levels detected in the vegetative growth and early development (aggregation) life cycle stages. Moreover, there was a profile shift in the dominant CK forms between the vegetative growth and aggregation life cycle stages compared to those found in the fruiting body life cycle stage (Aoki et al., 2019). These findings prompted us to investigate what roles, if any, CKs may have in vegetative growth and early development in *D. discoideum*. Here, we generated an *iptA* knockout mutant through CRISPR/Cas9 mediated genome editing and investigated the effects of *iptA*-deficiency on *D. discoideum* proliferation, pinocytosis, and cytokinesis. We then observed the subcellular morphology of our mutant and wild-type (WT) strains through transmission electron microscopy (TEM). Lastly, we generated a *GFP-iptA* overexpression strain in addition to the *iptA*-deficient strain to assess the metabolic consequences from altered CK dynamics using a metabolomics approach. We found that *iptA*-deficiency results in a defect in cytokinesis and abnormal mitochondria morphology; furthermore, both *iptA*-deficiency and overexpression result in a downregulation of several TCA cycle metabolites and amino acid metabolism, as well as increased levels of the energy metabolite, AMP, during vegetative growth. Collectively, these results expand our understanding of CKs to include

new roles of IptA in *D. discoideum* vegetative growth that are different from those previously established in late multicellular development.

MATERIALS & METHODS

Culture conditions and chemicals

Strains were thawed from frozen stocks onto SM/2 agar (10 g/L glucose, 10 g/L protease peptone, 1 g/L yeast extract, 1 g/L MgSO₄·7H₂O, 1.9 g/L KH₂PO₄, and 0.6 g/L K₂HPO₄) with *Klebsiella aerogenes* (KA; Fey et al., 2007) and incubated at room temperature (22°C). HL5 containing glucose, Lo-Flo, FM minimal medium, and FM minimal medium without arginine and lysine, and FM minimal medium without amino acids were all purchased from Formedium (Hunstanton, Norfolk, United Kingdom). Cells were grown axenically in HL5 routinely supplemented with 100 µg/mL ampicillin and 300 µg/mL streptomycin on an orbital shaker at 150 rpm. G418 was used at a concentration of 20 µg/mL for knockout and overexpression strains, as appropriate. For all experiments, cells were harvested during the mid-log phase of growth (2-5×10⁶ cells/mL) and washed twice in cold KK2 buffer (2.2 g/L KH₂PO₄, .7 g/L K₂HPO₄). All primers or single-guide RNAs were ordered from Integrated DNA Technologies (Coralville, Iowa, USA).

Strains and plasmids

All experiments were conducted with the *D. discoideum* parental strain, AX3, which is denoted as either AX3 or wild-type (WT) throughout the manuscript. The *D. discoideum* *iptA* mutant strain was previously determined to have a spore viability defect (Anjard and Loomis, 2008); therefore, all strains (WT, mutant, and overexpression strains) used for experiments were thawed fresh prior to the start of each experiment from frozen

stocks onto SM/2 agar with KA for consistency. Once plaques appeared, and before multicellular structures developed, cells were scraped from the agar plates and cultured axenically in HL5 medium. Spores were never used for culturing owing to the spore viability defect in the mutant *iptA* strain. We were unable to obtain the previously generated *iptA*⁻ strain from Anjard and Loomis (2008), therefore, we generated a new strain through CRISPR/Cas9 mediated gene editing to assess the effects of *iptA*-deficiency in vegetative amoebae considering it is the key enzyme responsible for CK biosynthesis in *D. discoideum*.

To generate the *iptA* knockout (KO) strain, we used the pTM1285 all-in-one sgRNA CRISPR/Cas9 expression vector, as previously described (Sekine et al., 2018). The pTM1285 vector was kindly provided by the University of Tsukuba through the National Bio Resource Project (NBRP) of the MEXT Japan. Candidate single guide-RNA (sgRNA) sequences for the *iptA* gene were designed using CRISPOR and ordered containing overhangs specific to BpiI (Concordet and Haeussler, 2018; Supplementary Table 4.1A). Single sgRNAs were cloned into the pTM1285 vector using BpiI according to manufacturer's instructions (New England Biolabs, Whitby, ON, Canada; Sekine et al., 2018). Ligation of the sgRNA was confirmed through PCR with the sense oligo sgRNA 5'-agcaACCAA AATAT TCGCT TTCAT-3' and the tracrRV primer 5'-AAGCT TAAAA AAAGC ACCGA CTCGG TGCC-3'. Sanger sequencing was conducted prior to transformation into *D. discoideum* with the tracrRV primer (Supplementary Table 4.1B-C).

Validated pTM1285-sgRNA constructs were transformed into AX3 cells via electroporation using established *D. discoideum* protocols (Knecht and Pang, 1995; Gaudet

et al., 2007). Cells in the mid-log phase of growth were pelleted at 500g for five minutes and washed twice in ice-cold H50 buffer (20 mM HEPES, 50 mM KCl, 10 mM NaCl, 1 mM Mg₂SO₄, 5 mM NaHCO₃, 1 mM Na₂HPO₄). The cells were resuspended in a total volume of 100 µL ice-cold H50 buffer containing 6 µg of validated pTM1285-sgRNA construct. A 0.1 cm cuvette was pre-chilled prior to use, and the cell suspension was added to the cuvette, incubated on ice for 5 minutes and then electroporated using a MicroPulser electroporator (Bio-Rad Laboratories Canada, Mississauga, ON, Canada) with the *Dic* settings according to the Bio-Rad instruction manual (1 kV, 2 pulses, 1 ms time constant; Knecht and Pang, 1995). The cuvette was placed immediately back into ice and let sit for 15 minutes after adding a solution of CaCl₂ and MgCl₂ to a final concentration of 1 mM for each respective compound. The cells were then plated in 100 mm Petri dishes with 10 mL HL5 containing ampicillin (100 µg/mL) streptomycin (300 µg/mL) and left to sit at room temperature for 8 hours. G418 was added to each Petri dish at a final concentration of 20 µg/mL, and the plate was left for four days. Following the four-day incubation, the remaining cells were counted, washed, serially diluted, and plated (65-150 cells) onto SM/2 agar plates with KA. Individual clones (plaques) were isolated from the SM plates and transferred to 12-well plates containing HL5 with only ampicillin and streptomycin (between four to seven days following plating on SM). Once sufficient growth in the 12-well plate was achieved, the cells were transferred to 100 mm Petri dishes and were scaled up to flasks once the Petri dish was over 70% confluent. A 200 µL aliquot of cells from the confluent Petri dish was washed and then lysed for DNA extraction using 48 µL LyseB buffer (10 mM Tris, pH 8.3, 50 mM KCl, 2.5 mM MgCl₂, 0.45% NP40, and 0.45% Tween) and 2 µL Proteinase K (Charette and Cosson, 2004). To detect indels generated from

CRISPR/Cas9, a 764 bp region spanning the sgRNA cut site was amplified via PCR and ran on an agarose gel (Supplementary Table 4.1D). PCR amplicons from clones with visible indels were sent for Sanger sequencing, and we selected a clone with a 32 base-pair mutation that resulted in a frameshift and early truncation of the gene product as our *iptA* knockout strain for all further experiments (Figure 4.1; Supplementary Table 4.1E). A custom antibody was ordered to validate the knockout through western blot; however, we were unable to detect IptA or GFP-IptA with the antibody. Therefore, RT-qPCR and CK production screens, detailed in the following sections, were used to validate knockout of *iptA*, as similarly performed by Lindner et al. (2014) to validate knockout of an *ipt* gene in *Physcomitrella patens*. The full length *iptA* nucleotide sequence and the selected *iptA* knockout strain nucleotide sequence with their corresponding amino acid translations can be found in Supplementary Table 4.2.

An N-terminal *GFP-iptA* overexpression construct using the pTX-GFP extrachromosomal vector was generated, as previously described (Huber et al., 2014; Levi et al., 2000). A pTX-GFP empty vector was used as a control for the GFP-IptA strain for the ADP/ATP and NAD⁺/NADH assays. Strains expressing this vector were supplemented with G418 (20 µg/mL), and the primers used for amplifying the full-length *iptA* gene can be found in Supplementary Table 4.3. The *GFP-iptA* overexpression strain is also denoted as the overexpression strain or OE throughout the manuscript.

RT-qPCR

To confirm knockout of *iptA*, we assessed its relative mRNA expression through RT-qPCR. WT and knockout (KO) strains were starved for 24 hours in flasks, and replicates of 2×10^7 cells were lysed and homogenized using Trizol reagent (Thermo Fisher,

Mississauga, ON, Canada) according to manufacturer's instructions to be used for RNA extraction. RNA was isolated according to manufacturer's instructions using the Ambion PureLink RNA Mini Kit, which included an on-column DNaseI digestion (Thermo Fisher, Mississauga, ON, Canada). Both RNA quantity and quality were measured using a Nanodrop 2000 spectrophotometer (Thermo Fisher, Mississauga, ON, Canada), and absorbance measurements A260/A280 and A260/A230 with ratios ~2.0 were accepted as pure for RNA. One microgram of RNA was reverse-transcribed to cDNA using the Bio-Rad 5X iScript RT supermix kit (Bio-Rad Laboratories Canada; Mississauga, ON, Canada) for RT- qPCR, after which samples were diluted 1:1 with nuclease free water. Samples without reverse transcriptase were included to confirm no genomic DNA contamination. Quantitative PCR (qPCR) was performed on cDNA samples using the 2X SsoAdvanced Universal SYBR Green Supermix (Bio-Rad Laboratories Canada; Mississauga, ON, Canada). A Bio-Rad CFX Connect was used to perform the reactions in triplicate, and gene expression data were normalized to the reference genes, *rn1A* (mitochondrial large subunit) and *gpdA* (glyceraldehyde-3-phosphate dehydrogenase). The Bio-Rad CFX Maestro Software was used to analyze the data. All primers used were designed using NCBI Primer Blast (<https://www.ncbi.nlm.nih.gov/tools/primer-blast/>) (Supplementary Table 4.4), and data were collected and analyzed as per the MIQE guidelines.

Cytokinin analysis

Total cytokinin (CK) levels were quantified to confirm direct effects of gene knockout and to assess the overall contribution of CK levels of *iptA* among the other tRNA-CK biosynthesis genes present in *D. discoideum* (*iptB* and *iptC*). A total of 7.5×10^7 cells were plated onto four individual 100 mm 1% KK2 agar Petri dishes and were incubated at

21°C for 24 hours in a humidity chamber, as previously described (Aoki et al., 2019). Fruiting bodies were harvested from the agar and separated into extracellular (supernatant from KK2 washes used to collect sample off the plate) and intracellular samples (pelleted fruiting body structures). The samples were flash frozen in liquid nitrogen and transferred immediately to a -80°C freezer. Samples were subjected to a CK hormone extraction and purification to process samples for CK analysis using high-performance liquid chromatography-positive electrospray ionization-high resolution tandem mass spectrometry (UHPLC-(ESI+)-HRMS/MS), as previously described (Aoki et al., 2019). Total CK levels for both extracellular (EC) and intracellular (IC) samples from the four most abundant CK forms detected (*N*⁶-isopentenyl adenine, *N*⁶-isopentenyladenosine (iPR), *N*⁶-isopentenyladenine-9-ribose-5' phosphate (iPRP), and discadenine) were quantified individually and combined to determine total CK content for each strain.

Fruiting body morphology and count

Fruiting body morphology was examined after multicellular development on 1% KK2 agar plates to avoid CK contamination from organic ingredients used in SM agar and CKs potentially produced by bacteria (Aoki et al., 2021). 3×10^7 cells were pelleted, washed, and resuspended in 1 mL of KK2. From this cell suspension, 25 μ L droplets containing 7.5×10^5 cells were deposited onto KK2 agar and incubated at room temperature (22°C) for 24 hours. Images were taken from above using a Leica EZ4W stereomicroscope equipped with an internal 5MP CMOS camera. The same magnification was used for all strains, and the sori area was quantified using the Fiji/ImageJ measuring tool. From these same images, the total number of fruiting bodies formed and the number of fruiting bodies that contained sori reaching the average sori area of WT were counted (>500 pixels). This

experiment was independently replicated five times with three technical replicates per experiment.

Cell proliferation (liquid culture and solid plates)

Cell proliferation was assessed in liquid culture through cell counts over a 144-hour time course as previously described (Aoki et al., 2019) and on solid bacterial plates through measurements of plaque diameter (mm) at 12-hour intervals. For both experiments, cells in the mid-log phase of growth were collected and washed twice in KK2 buffer, and all cells were incubated at room temperature (22°C). For liquid culture measurements, the cells were resuspended to a density of 2×10^5 cells/mL in HL5 medium or 5×10^5 cells/mL in FM minimal medium. Cell counts were then taken every 24-hours over a 144-hour growth period using a hemocytometer. For solid culture measurements, serial dilutions were performed on the washed cells to plate a total of 15 cells in 15 μ L on each plate with *Klebsiella aerogenes* on SM/2 agar plates. Imaging of plaques occurred every 12 hours once the plaques were visible to the eye, starting at 48 hours after plating and ending at 84 hours after plating. Images of the plaques were captured at the respective timepoints using a Leica EZ4W stereomicroscope equipped with an internal 5MP CMOS camera (Leica Microsystems Incorporated, Concord, ON, Canada) and were quantified using Fiji/ImageJ. Both experiments were independently replicated three times with three technical replicates per experiment.

Pinocytosis

Pinocytosis was assessed as previously described (Rivero and Maniak, 2006), measuring both uptake and release of the fluorescent marker, fluorescein isothiocyanate (FITC)-dextran. Axenic cultures were harvested and resuspended in 5 mL of fresh HL5

medium at a density of 5×10^6 cells/mL. Cultures were then incubated at 21°C and shaken at 150 rpm. 100 μ L of a 20 mg/mL FITC-dextran stock solution was added to the suspension. Endocytosis was assessed every 15 minutes, starting from the addition of FITC-dextran, over a 90-minute time course. Prior to the addition of FITC-dextran, a background measurement of cells was sampled to subtract background fluorescence and control for differences in protein content. For all sampling periods, a 250 μ L cell suspension was collected, washed twice with 750 μ L ice-cold Sorenson's buffer (2 mM Na_2HPO_4 , 14.6 mM KH_2PO_4 , pH 6.0) and lysed with 500 μ L lysis buffer (50 mM Na_2HPO_4 , 0.2% Triton-X, pH 9.3). Triplicates of 100 μ L of lysate were added to separate wells of black, clear bottom 96-well plates. Fluorescence measurements were obtained using a BioTek Synergy HTX plate reader using the following filters: 485/20 nm for excitation and 528/20 nm for emission (BioTek Instruments Incorporated, Winooski, VT, USA). For assessing exocytosis, cells were immediately washed with fresh HL5 medium following the 90-minute time course and were resuspended in the same volume of HL5 remaining after sampling (without FITC-dextran) and covered in aluminum foil (Rivero and Maniak, 2006). A time-zero measurement was taken using the same sampling method described above to be used as a 100% relative fluorescence measurement for the remaining sample, which was collected after 120 minutes of incubation. The decrease in fluorescence indicates the amount of FITC-dextran released following the 90-minute FITC-dextran pre-incubation. The experiment was independently replicated three times with three technical replicates per experiment.

Cytokinesis

To assess cytokinesis, a total of 3×10^5 vegetative cells were harvested and deposited on individual coverslips to be incubated overnight at 22°C in Lo-Florescence HL5 medium, FM minimal medium, FM minimal medium without arginine and lysine, or FM minimal medium without amino acids for 36 hours. Following the respective incubation times, the coverslips were fixed in -80°C methanol for one hour and then mounted on slides using Dako mounting solution with DAPI (Sigma-Aldrich, Oakville, ON, Canada). Fluorescent micrographs were captured with a Prime BSI scientific complementary metal oxide semiconductor (sCMOS) camera (Teledyne Photometrics, Tucson, AZ, USA) on a custom-built Zeiss Cell Observer Microscope (Intelligent Imaging Innovations, Denver, CO, USA) using a 1.4 NA 63X immersion oil objective lens and LED illumination via a Spectra light engine (Lumencor, Beaverton, OR, USA). Images were processed and analyzed using Adobe Photoshop v. 21.2.12. Three independent replicates were performed, and at least 100 cells were analyzed per replicate.

Transmission electron microscopy (TEM) and mitochondrial size metrics

Transmission electron microscopy (TEM) was used to assess any aberrant ultrastructural phenotypes as a result of *iptA* knockout. Vegetative WT and KO cells were cultured in either FM minimal medium or starved in FM minimal medium without amino acids for 36 hours in 100 mm Petri dishes, as previously described (Otto et al., 2003). Cells were harvested, washed, and fixed in 2.5% glutaraldehyde (pH 7.2) diluted with 0.1M of sodium cacodylate buffer for two hours. The fixed cells were rinsed three times (10 minutes per wash) with 0.1M sodium cacodylate buffer. The supernatant was removed, and the cells were post-fixed in 1% osmium tetroxide for two hours. The cells were rinsed again in distilled water and placed in 0.25% uranyl acetate at 4°C overnight. Following this, the

cells were dehydrated in a graded aqueous-acetone series, which were then embedded in 100% epon-araldite resin in a 60°C oven for 48 hours, which allows the sample to harden correctly. To obtain ultrathin sections, a Reichert Jung Ultracut E Ultramicrotome fitted with a diamond knife was used (approximately 100 nm thick). Sections were retrieved on 300 uncoated copper mesh grids. The sections were stained with 2% aqueous uranyl acetate for approximately 10 minutes, which was followed by a series of five-minute rinses with distilled water. Samples were stained with lead citrate for four minutes and rinsed two times with distilled water for five minutes. Finally, the samples were observed using a JEOL JEM 1230 transmission electron microscope at 80kV, and images were taken using a Hamamatsu ORCA-HR digital camera. Mitochondrial area and circularity were measured using Fiji/ImageJ.

Metabolomic profile of mitochondrial-related metabolites

Samples from WT, *iptA*⁻, and the *GFP-iptA* overexpression strains were harvested under the same conditions as used for assessing ultrastructural phenotypes via TEM, with the addition of a 24-hour fruiting body sample for each strain. For the vegetative samples, a total of 2×10^6 cells were seeded into four individual 100 mm Petri dishes with 7 mL HL5 and incubated overnight. The medium was disposed of, and the adherent cells were washed twice with cold KK2 buffer followed by the addition of 7 mL fresh medium – either FM minimal medium or FM minimal medium without arginine and lysine. The cells were incubated at room temperature for 36 hours. For the 24-hour fruiting body samples, 7.5×10^7 cells were plated onto four individual 1% KK2 agar Petri dishes and collected after a 24-hour incubation period as described in the CK analysis methodology above. All sample

types were harvested, washed, pelleted, and flash frozen in liquid nitrogen and kept at -80°C until they were processed for metabolite extraction and purification.

Samples were freeze-dried and endogenous metabolites were extracted with ice-cold 50% acetonitrile (ACN) and purified by solid phase extraction (SPE) using HLB cartridges as previously described (Šimura et al., 2018). The mitochondrial-related metabolites were assessed using a customized quantification method and grouped into the following categories: amino acids and derivatives, nucleotide metabolites, and energy metabolism which encompasses metabolites from the glycolysis/gluconeogenesis pathways, TCA cycle pathway, and pentose phosphate pathway, as previously described (Chen et al., 2016; Supplementary Table 4.5). All samples were spiked with 10 µL of a stable-isotope labeled canonical amino acid mix (0.25 µM final concentration of amino acids; Cambridge Isotope Laboratories, Tewksbury, MA, USA; Supplementary Table 4.6). Samples were evaporated to dryness at ambient temperature in a speed vacuum concentrator. The sample residues were redissolved in 500 µL of 90% acetonitrile (acetonitrile:water, v/v). Pooled sample mixtures from each strain (WT/KO/OE) or treatment type (FM/FM-AL/24-hour) composed of 20 µL of each sample extract was used to generate MS/MS for compound identification. For this, the top 10 data-dependent acquisition experiments were performed separately in positive and negative ionisation mode for each of the pooled samples to obtain MS/MS spectra of the most abundant compounds (Chen et al., 2017). All samples were filtered using 0.2 µm PVDF spin filter with 2 mL receiver tubes (InnoSep Spin, Canadian Life Sciences, Peterborough, Canada) and transferred to 2 mL vials containing 350 µL inserts for high performance liquid

chromatography-high resolution accurate mass-full scan mass spectrometry (HPLC-(HRAM)-FS-MS) analysis.

Samples were resolved with a Kinetex C18 column (2.1 × 50 mm, 2.6 μm). A volume of 25 μL of each sample was injected into a Dionex UltiMate 3000 HPLC (ThermoFisher, Mississauga, Canada) coupled to a QExactive Orbitrap mass spectrometer (ThermoFisher, Mississauga, Canada). A flow rate of 0.3 mL/min was used with a mobile phase of 0.08% acetic acid in water (A) and 0.08% acetic acid in acetonitrile (B). The following gradient was used to elute the analytes: mobile phase B was held at 0% for 1.25 min to retain the compounds on the column and avoid the metabolite elution in the void volume before increasing to 50% over 2.75 min and to 100% over the next 0.5 min. Solvent B was then held at 100% for 2 min before returning to 0% over 0.5 min for 4 minutes of column re-equilibration.

Orbitrap QExactive was operated with a heated electrospray ionization (HESI) probe in positive and negative mode (Kisiala et al., 2019). Each sample was analyzed using a mass range of m/z 70–900, and data were acquired at 70,000 resolution, automatic gain control (AGC) target of 1×10^6 , and maximum injection time (IT) of 100 ms.

Metabolite processing and identification of all full scan and ddMS2 data was performed in Xcalibur 4.1 software, using a customized quantification method for our list of mitochondrial-related metabolites (Supplementary Table 4.5). Metabolites were identified by accurate mass (with a 10 ppm mass error) and comparison of retention times to authentic or labeled standards (authentic standards were a mix of unlabeled, high purity compounds for HPLC analysis including sugars, organic acids, and amino acids; additionally, labeled amino acids were spiked into each sample as specified above; Level

1 and highest confidence for metabolite identification according to Schrimpe-Rutledge et al., 2016), or by accurate mass and comparison of fragmentation patterns to MS/MS databases (METLIN, PubChem; Level 2 confidence), or lastly by accurate mass and MS1 m/z database match (Level 3 confidence) (Supplementary Table 4.5). To determine the relative concentration of mitochondrial metabolites in the three different strains and treatment types, the peak areas were first normalized based on the median recovery of the 20 stable-isotope labeled canonical amino acid mix in each analyzed sample (Supplementary Table 4.6). The relative metabolite content of the KO or OE strains was compared to WT to assess any metabolic consequences in mitochondrial-related metabolism as a result of *iptA*-deficiency or overexpression for each of the three treatment types.

ADP/ATP and NAD⁺/NADH measurement

ADP and ATP content were measured using the ADP/ATP Ratio Luminescent Assay Kit according to manufacturer's directions (mak135; Sigma-Aldrich, Oakville, ON, Canada). 5×10^5 axenic vegetative cells were washed twice in phosphate buffered saline (PBS), resuspended in 10 μ L PBS, and plated in white 96-well plates. A total of three independent experiments were performed, each with two replicates for measuring ATP, ADP, and residual ATP background luminescence. The ADP/ATP ratio was calculated by the following equation: (RLU of ADP – RLU of residual ATP)/RLU of ATP, where RLU represents relative light units. NAD⁺ and NADH content were measured using the NAD⁺/NADH Fluorometric Assay Kit according to manufacturer's instructions (ab176723; Abcam, Toronto, ON, Canada). 9×10^7 vegetative cells were washed twice in PBS, resuspended in 225 μ L warm lysis buffer from the kit and incubated at room

temperature for 15 minutes in the dark. 25 μ L of lysed cell suspension was plated in individual wells in a black, clear bottom 96-well plate, and the assay continued according to manufacturer's instructions. A total of three independent experiments were performed, each with two replicates for measuring NAD⁺, NADH, and total NAD⁺/NADH. A standard curve for NADH was used to calculate concentrations of the compounds for each reaction, which was provided with the kit. The BioTek Synergy HTX plate reader was used to measure luminescence for the ADP/ATP kit, and fluorescence for the NAD⁺/NADH kit (excitation: 528/20 nm and emission: 590/35 nm) (BioTek Instruments Incorporated, Winooski, VT, USA).

Statistical analyses and software

All statistical analyses were performed using GraphPad Prism v. 9.5.0 (GraphPad Software, La Jolla, California, USA). For pairwise comparisons, two-tailed *t*-tests were performed, and for multiple comparisons, either a one-way ANOVA with the Dunnett's multiple comparison test or a two-way ANOVA with the Tukey multiple comparison's test was performed, unless otherwise specified. MetaboAnalyst v. 5.0 was used to generate heatmaps for the metabolomics analysis to show clustering of samples with the Euclidean distance measure, Ward clustering method, and the one-way ANOVA statistical test (Pang et al., 2022). Graphs were generated using Prism v. 9.5.0, Adobe Photoshop v. 21.2.12, and Adobe Illustrator v. 25.2.

RESULTS

Confirmation of *iptA* knockout and aberrant developmental phenotypes

To investigate the role of *iptA* in vegetative growth and early development of *D. discoideum*, CRISPR/Cas9 mediated genome editing was used to disrupt the *iptA* gene and generate a knockout strain. We screened multiple different knockout clones through PCR and Sanger sequencing with various indels and selected a clone with a 32 base pair deletion from nucleotides 118-149 of the *iptA* genomic sequence for all further experiments (Figure 4.1A-C; Supplementary Figure 4.2). Translation of the selected clone results in a 44 amino acid (aa) protein product, where the first 39 aa's align with the native IptA aa sequence before a frameshift in the reading frame occurs and two stop codons are encountered resulting in early truncation of the protein. qPCR data of the resultant *iptA*⁻ cells confirm successful disruption of the gene (Figure 4.1D). Furthermore, we observed aberrant fruiting body morphology and a 99% reduction in total cytokinin (CK) levels after 24 hours of development, which is consistent with previous work conducted with a *D. discoideum iptA*⁻ cells during the later stages of multicellular development (Figure 4.1E-F; Anjard and Loomis, 2008). We quantified the aberrant morphology of *iptA*⁻ fruiting bodies, looking at average sori area, number of fruiting bodies formed, and number of fruiting bodies formed with an average sori area similar to WT (Figure 4.2A-C). In all cases, we saw a significant reduction in these fruiting body metrics in the *iptA*⁻ cells (*t*-test, two-tailed; **p*< 0.05, ***p*<0.01).

***iptA*⁻ does not affect vegetative growth or pinocytosis**

Considering that CKs are named after their roles in promoting cell division, we first assessed the effects of *iptA* loss on vegetative growth in axenic culture and on solid medium with bacteria (Figure 4.3A-C). We assessed growth in both nutrient rich conditions, cultured in HL5 (Figure 4.3A), and in minimal nutrient conditions, cultured in FM minimal

medium (Figure 4.3B). In both cases, there was a minimal effect of *iptA* loss on growth, and the knockout strain had slightly higher cell densities at all time points until the final 144-hour time point. On solid medium, there were no differences observed between WT and *iptA*⁻ growth rates, as measured through plaque expansion (Figure 4.3C).

We evaluated the effects of *iptA*⁻ on pinocytosis to determine if loss of *iptA* affects the uptake or release of nutrients through measurement of the fluorescent marker, FITC-dextran (Figure 4.3D-E). Knockout of *iptA* does not appear to have any effect on endocytosis or exocytosis, as the relative % fluorescence of FITC-dextran uptake and release was similar to WT.

***iptA*⁻ reduces cytokinesis**

To assess cytokinesis, we compared the numbers of nuclei per cell between *iptA*⁻ and WT cells by staining with DAPI under nutrient rich and minimal nutrient conditions, including autophagy stimulating environments in minimal medium without arginine and lysine or without amino acids altogether (Figure 4.4A-E). Despite there being no effects of *iptA*⁻ on cell proliferation, there was a reduction in cytokinesis following knockout of *iptA* in nutrient rich and minimal environments, and this manifested as significant increases in the number of nuclei per cell in the knockout strain compared to WT in both HL5 and FM minimal medium (Figure 4.4B-C; $p < 0.0001$). There was a more pronounced effect on multinucleated cells in nutrient rich conditions, in which *iptA*⁻ cultures contained 30% more cells with 2 or more nuclei and 10% more cells containing 3 or more nuclei compared to WT (Figure 4.4A and Figure 4.4B). In FM minimal medium, *iptA*⁻ cultures contained 20% more cells with 2 or more nuclei and 10% more cells containing 3 or more nuclei compared to WT (Figure 4.4A and 4.4C). Notably, the impairment in cytokinesis is negated when

cultured under autophagy stimulating environments in FM minimal medium without arginine and lysine or FM minimum medium without amino acids altogether (Figure 4.4D-E).

Loss of *iptA* results in abnormal mitochondria and altered TCA cycle metabolism

We used transmission electron microscopy (TEM) to examine possible ultrastructural phenotypes as a result of *iptA*-deficiency during vegetative growth (36-hour incubation in FM minimal medium) and early development (36-hour incubation in FM minimal medium without amino acids) (Figure 4.5A; Supplementary Figure 4.1). Visually, the *iptA*⁻ mitochondria had a rounded appearance compared to those of WT in the vegetative growth samples cultured in FM minimal medium (Figure 4.5A). Mitochondria are easily distinguished from other organelles owing to their higher electron density, which makes them appear darker, and their visible and distinct internal cristae structures. From the vegetative growth TEM images, we quantified the number of mitochondria per cell and the mitochondrial circularity (Figure 4.5B-C). There was a significant increase in the number of mitochondria per cell in the *iptA*⁻ strain (unpaired, two tailed *t*-test, $p < 0.05$), as well as a significant increase in the mitochondrial circularity (unpaired, two tailed *t*-test, $p < 0.0001$). For our circularity metric, a value of 1.0 indicates a perfect circle. The average circularity of the *iptA*-deficient strain was 0.91, indicating a much higher proportion of rounded mitochondria compared to the WT strain, which had an average circularity of 0.83 (Figure 4.5C). During early development, *iptA*⁻ samples cultured in FM minimal medium without amino acids displayed impaired turnover of organelles, as visualized through decreased formation in recycling organelles, and cytoplasmic proteins under autophagy stimulating conditions compared to WT (Supplementary Figure 4.1).

The results from the TEM images prompted us to explore the metabolic consequences of *iptA*-deficiency as well as *iptA*-overexpression on mitochondrial metabolism using a metabolomics approach (Figure 4.6). We employed full scan mass spectrometry to analyze endogenous metabolites and focused on 70 mitochondrial-related metabolites making up the “mitobolome” described by Chen et al. (2016), which we grouped into the following categories: amino acids and derivatives, nucleotide metabolites, and energy metabolism. The latter encompasses metabolites from the glycolysis/gluconeogenesis pathways, TCA cycle pathway, and pentose phosphate pathway (Supplementary Table 4.5). The metabolomics samples were cultured under the same conditions as those used for the TEM analyses with the addition of a 24-hour fruiting body life cycle stage sample (three life cycle stages assessed: FM minimal medium (vegetative amoebae), FM minimal medium without arginine and lysine (early development), and 24-hour development (fruiting bodies)). Heatmap analyses of the top 400 significantly different metabolites for each respective treatment type show clustering of the individual replicates for each strain, indicating consistency of strain effects and thus validity in our sampling methods and downstream analyses (MetaboAnalyst v 5.0, Pang et al., 2022; Supplementary Figures 4.3-5). Among the top 400 metabolites assessed in each of the three treatments, the metabolite levels of the WT and KO strains were more similar to each other than the OE strain in the vegetative amoebae treatment (Supplementary Figure 4.3). In the early development treatment, the metabolite levels of the WT and OE strains were more similar to each other than those in the KO strain (Supplementary Figure 4.4), and in the 24-hour development treatment, the metabolite levels of the KO and OE strains were more similar to each other than those in the WT strain (Supplementary Figure

4.5). The trends in metabolite abundance for the mitochondrial-related metabolites we assessed were similar in *iptA* knockout and overexpression strains (typically both lower than WT) but were more pronounced in the OE strain (Supplementary Figure 4.2).

Among all three treatments analyzed for mitochondrial-related metabolic changes, the vegetative amoebae were the most affected. Specifically, the TCA cycle was the most affected pathway from loss or overexpression of *iptA* (Figure 4.6; Supplementary Figure 4.2A). There were significant decreasing trends in metabolite abundance in succinate and fumarate in both strains compared to WT (two-way ANOVA with a false discovery rate of $p < 0.05$; Figure 4.6; Supplementary Figure 4.2A). In the glycolysis pathway, a significant decrease in lactate was observed in both knockout and overexpression strains compared to WT (Figure 4.6; Supplementary Figure 4.2A). In only the overexpression strain, there was a significant decrease in the levels of glucose/fructose (isomers that were indiscernible with our LC-MS method) and malate ($p < 0.01$ and $p < 0.0001$, respectively) compared to WT. There were no clear trends observed in the early development samples cultured in FM minimal medium without arginine and lysine for any of the energy metabolism metabolites we assessed from the glycolysis pathway, TCA cycle, or the pentose phosphate pathway (Supplementary Figure 4.2B). However, in the 24-hour development fruiting body samples, a similar decreasing trend in succinate levels was observed in the knockout and overexpression strains compared to WT (Supplementary Figure 4.2C; $p < 0.05$ and $p < 0.001$ respectively). The combined energy metabolism pathway metabolite analyses align with the abnormal mitochondrial morphology visualized through TEM (Figure 4.5).

Mitochondrial dysfunction is well-studied in *D. discoideum*, owing to the fact that mitochondrial disease phenotypes are known to be conserved in this organism (Francione

et al., 2011). As such, a set of “readouts” consistent in mitochondrial disease phenotypes have been established in *D. discoideum* to assess dysregulated intracellular signaling pathways. In many cases, mitochondrial disease phenotypes affect energy metabolism which result in the chronic activation of the AMP-activated protein kinase (AMPK) (Francione et al., 2011). Therefore, we assessed the effects of *iptA*-deficiency and overexpression on energy and redox metabolism. Using commercially available kits, we assessed ATP and ADP content as well as NAD⁺ and NADH content in *iptA*-deficient cells relative to WT, and *iptA*-overexpression cells relative to a pTX-GFP empty vector control during vegetative growth (Figure 4.7). The levels of ATP were relatively similar in *iptA*-deficient cells compared to WT cells, but the ADP levels were significantly reduced, resulting in a significant decrease in the ADP/ATP ratio in the knockout strain (Figure 4.7A). For the *GFP-iptA* overexpression strain, both ATP and ADP levels were significantly and unequally increased relative to the pTX-GFP empty vector strain, in such a way that created a significant increase in the ADP/ATP ratio (Figure 4.7A). Interestingly, AMP levels, as assessed in our metabolomics analyses, were significantly elevated in both the *iptA*-deficient strain and the overexpression strain compared to WT (unpaired, two-tailed *t*-test; ***p*<0.01, ****p*<0.001; Figure 4.7B). These findings point to *iptA*-deficiency and/or overexpression being associated with mitochondrial function, as AMPK is activated by elevated AMP/ADP and AMP/ATP ratios and oxidative stress. This chronic activation of AMPK is able to restore ATP levels but leads to characteristic aberrant phenotypic outcomes that have been associated with mitochondrial dysfunction in *D. discoideum* (Bokko et al., 2007; Francione et al., 2011). Our results point to elevated AMP/ADP or

AMP/ATP ratios as the activators of AMPK over oxidative stress, as our measurements of NAD⁺ and NADH were relatively similar across the tested strains (Figure 4.7C).

***iptA*-deficiency and overexpression down-regulates amino acid metabolism**

Within our metabolomics analysis, we assessed amino acid levels and their derivatives as a result of loss or overexpression of *iptA* (Figure 4.8). Interestingly, the amino acid levels in the 24-hour development were the most affected by *iptA*-deficiency or overexpression compared to the vegetative and early development treatments (Figure 4.8A-C). Specifically, alanine/sarcosine (isomers that were not resolvable with our LC-MS method), aspartate, glutamate, glutamine, serine, tyrosine, and GABA were all significantly downregulated in both the KO and OE strains compared to WT (Figure 4.8C). In only the overexpression strain, there was a significant decrease in the levels of threonine/homoserine (isomers that were not resolvable with our LC-MS method) (Figure 4.8C). Similar decreasing trends in the KO and OE strains for many of these same amino acid and derivative levels were observed in the vegetative amoebae cells; however, only arginine levels were significantly downregulated in both the KO and OE strain (Figure 4.8A). Additionally, leucine/isoleucine, methionine, and tyrosine were significantly downregulated in the OE strain compared to WT (Figure 4.8A). Similar to the results of the energy metabolism pathways in the early development samples, there were no clear trends in amino acid or derivative levels observed in the cells cultured in FM minimal medium without arginine or lysine (Figure 4.8B).

DISCUSSION

CKs are necessary for proper development of *D. discoideum* and act as key intercellular signals for terminal differentiation during fruiting body formation (Anjard and Loomis, 2008; Loomis, 2014). The induction of sporulation and the maintenance of spore dormancy are two roles governed by precise regulation of CK production through the primary CK biosynthetic enzyme, IptA (Ihara et al., 1980; Anjard and Loomis, 2008). Expression levels of *iptA* continue to rise throughout late development and are highest during fruiting body development; therefore, previous research on *iptA* and CK production in *D. discoideum* had focused on the later developmental life cycle stages (Ihara et al., 1980; Anjard and Loomis, 2008). In this study, we were particularly interested in dissecting the role of CK during the vegetative and early development stages of *D. discoideum* based on our initial research documenting CK levels during both of these stages, in addition to the fruiting body stage of development (Aoki et al., 2019). Therefore, we generated a knockout of the primary CK-biosynthesis gene, *iptA*, focusing our attention on aberrant vegetative growth and early developmental phenotypes in *D. discoideum*. We examined classical roles of CKs by assessing proliferation, cytokinesis, and nutrient acquisition and found that *iptA*-deficiency decreases cytokinesis by a mechanism that does not alter proliferation or nutrient uptake. To gain further insight into CK dynamics, we generated a *GFP-iptA* overexpression strain for the remaining analyses. TEM and metabolomics analyses revealed altered mitochondrial morphology and the downregulation of several TCA cycle metabolites and amino acids, in addition to an increase in the energy metabolite, AMP.

CKs were named after their earliest established role in promoting cell division or cytokinesis (Amasino, 2005). Considering this classical role, we assessed cytokinesis in

our *iptA*-deficient strain under both nutrient rich and autophagy stimulating environments. We found that cytokinesis is decreased following loss of *iptA*, but only when nutrients are sufficient (HL5 or FM minimal medium). In *Arabidopsis*, the molecular mechanism underlying mitotic CK-activated cell division was recently discovered (Yang et al., 2021). CKs were shown to spike precisely at the G2/M transition coincident with rapid nuclear accumulation of the MYB3R4 transcription factor that activates mitotic gene expression. Interestingly, *iptA* expression in *D. discoideum* is altered during the early development of both *mybB*⁻ and MybB-GFP overexpression strains obtained from a publicly available RNAseq dataset by Katoh-Kurasawa et al. (2021) and visualized on dictyExpress (<http://www.dictyExpress.org>, Stajdohar et al., 2017). *mybB*⁻ cells are unable to differentiate and cannot aggregate, whereas the cells overexpressing MybB-GFP act similar to WT (Katoh-Kurasawa et al., 2021). In the *mybB*⁻ RNAseq dataset, *iptA* has two peaks in expression at the early stages of starvation (at the 2-hour and 4-hour stages) followed by a complete absence in expression during cAMP-mediated chemotaxis and aggregation (between hours 4-6), and then a stable plateau from the beginning of mound formation to fruiting body formation (between hours 8-24). The final *iptA* expression levels in the *mybB*⁻ RNAseq dataset are 50-fold lower than normal *iptA* transcript levels in WT at its peak expression during fruiting body formation (24 hours; <http://www.dictyExpress.org>, Stajdohar et al., 2017). In the MybB-GFP overexpression RNAseq dataset, the expression levels from the onset of starvation to initiation of aggregation (from 0-hours to 5-hours) are stable and low (0.07-0.15), and similar to what is normally observed in *iptA* expression in WT; but this is followed by a sharp increase in expression during aggregation (6-hour time point) from 0.12 to 5.07. A decline back to a typical expression level of 0.27 from the

beginning of mound formation followed by a gradual climb in expression until its peak expression during fruiting body formation is observed (between hours 8-24). This combined evidence suggests that CKs may act on the MybB transcription factor in *D. discoideum* to initiate a transcriptional cascade controlling mitosis and cytokinesis, perhaps in a similar manner to that observed in *Arabidopsis*. Assessing interactions with CKs and MybB under both nutrient rich and autophagy stimulating conditions may help determine the variation observed in the cytokinesis defect under varying conditions.

Dictyostelium discoideum is a well-established model for studying mitochondrial disease for two primary reasons: 1) its unique life cycle consisting of two mutually exclusive stages (vegetative growth and multicellular development), has allowed researchers to reveal a variety of distinct phenotypes associated with mitochondrial disease in *D. discoideum*, and 2) the *D. discoideum* genome contains many genes orthologous to those in other prokaryotic and eukaryotic systems (including humans), for which researchers have consistently shown conserved functions, thus allowing for research to be translated beyond *D. discoideum* (Barth et al., 2007; Francione et al., 2011; Pearce et al., 2019). Phenotypes associated with mitochondrial dysfunction include those with and without defects in oxidative phosphorylation (OXPHOS) (Francione et al., 2011). The classical mitochondrial disease phenotypes involve defects in OXPHOS, which include: delayed growth in liquid and/or solid medium; altered transition from growth to development resulting in impaired chemotactic aggregation; impaired phototaxis and thermotaxis of slugs; impaired differentiation of cells into stalk and spore cells which results in fruiting bodies with short, thick stalks; and *Legionella* susceptibility (Francione et al., 2011). Observable mitochondrial-associated dysfunctions that do not affect

OXPHOS are rare and have varied phenotypes depending on the gene studied. Many different phenotypes have been observed through gene disruption, which include elongated mitochondria (in the mitochondrial fission genes *fszA* and *fszB*), slowed movement of vegetative amoeba and impaired chemotaxis (in the mitochondrial-associated gene, *torA*), impaired cytokinesis and slightly impaired growth (in the nuclear gene essential for proper mitochondrial localization, *cluA*), and slow growth and impaired development under cyanide stress (in the alternative oxidase gene, *aoxA*, which provides an alternative pathway for electron flow) (Francione et al., 2011; Pearce et al., 2019). In both mitochondrial disease (disease related to respiration) and mitochondrial-associated dysfunction (mitochondrial dysfunction that does not affect respiration), disruptions in intracellular signaling leads to the chronic activation of the energy sensing protein kinase, AMPK, which underlies many of the aberrant mitochondrial disease phenotypes described above (Bokko et al., 2007; Francione et al., 2009).

The combined data from our analyses of *iptA*-deficiency and overexpression strains provide a unique subset of phenotypes that are not typical of those described in classical mitochondrial disease in *D. discoideum*, but, rather, more in line with those described in cases of mitochondrial-associated dysfunction. From the TEM data, *iptA*-deficiency results in abnormal mitochondrial morphology and increased numbers of mitochondria in vegetative amoebae. The rounded mitochondrial morphology in the *iptA*-deficient cells was the first indication that *iptA* may be involved in aspects of mitochondrial function, which has not been a well-established role of CKs or their biosynthetic enzymes in plants or any other CK-producing organisms. A similarly rounded mitochondrial phenotype with increased content of mitochondrial DNA was observed in calcineurin-silenced vegetative

cells in *D. discoideum*, which was speculated to be associated with oxidative stress (Kobel-Höller et al., 2018). To verify, the authors assessed gene expression in several oxidative stress-related genes (*sodA*, *sodB*, *sodC*, *sod2*, and *catA*) and reported an up-regulation in all but one of the measured genes. This indicates that increased intracellular oxidative stress was a result of calcineurin silencing. It was concluded that calcineurin is involved in the interplay between mitochondria and reactive oxygen species in vegetative growth in *D. discoideum* (Kobel-Höller et al., 2018). While we did not assess redox metabolites beyond NAD⁺ and NADH, there are numerous articles that report on protective effects of CKs against oxidative stress in mammalian cells (Othman et al., 2016; Naseem et al., 2020), plants (Rubio-Wilhelmi et al., 2011; Zwack et al., 2016; Arnaud et al., 2017; Gujjar and Supaibulwatana, 2019), and bacteria (Samanovic et al., 2015; Wang et al., 2017). Taken together, it would be of interest to assess oxidative stress in our *iptA*-deficient and overexpression strains to determine if CK and/or *iptA* exerts any protective effects in *D. discoideum*.

To further assess the potential role of IptA in mitochondrial function during vegetative growth and early development, we employed a metabolomics approach with a focus on mitochondrial associated metabolites in our downstream analyses. Interestingly, the TCA cycle was the most affected pathway we analyzed during vegetative growth. Succinate, fumarate, and malate were downregulated in both the *iptA*-deficient and overexpression strains compared to wild-type. Moreover, there were increases in the levels of AMP in both the knockout and overexpression strains compared to WT, despite ATP levels remaining similar among all strains assessed. In cases of either classical mitochondrial dysfunction or mitochondrial-associated dysfunction, the chronic signaling

of AMPK, as a result of altered intracellular signaling, appears to be a common feature underlying the similar or unique phenotypes observed within mitochondrial dysfunction in *D. discoideum* (Pearce et al., 2019; Chen et al., 2021). The higher levels of AMP would, in turn, activate AMPK, leading to downstream signaling that shifts metabolism from an anabolic to a catabolic state and, thereby, stimulating glucose consumption (Hardie, 2004). Furthermore, AMPK is likewise activated by decreased glucose levels, which is observed in our study in both the knockout and overexpression strains compared to WT. To further support our metabolomic analyses, it would be informative to look at gene expression of the *snfA/ampka* (encodes the alpha subunit of AMPK) and other mitochondrial genes in *iptA*-deficient and overexpression cells.

As part of the metabolomic analysis, we assessed the levels of amino acids in the *iptA*-deficient and overexpression strains. Similar to the observed decreasing trends in metabolites of the TCA cycle, we observed decreasing amino acids levels in the vegetative amoebae and 24-hour fruiting body knockout and overexpression samples compared to WT. Interestingly, there were many more significantly decreased amino acids in the 24-hour samples, which were different than those decreased in vegetative amoebae samples. These findings support the idea of temporally separated dual roles of IptA in early growth versus late development, which aligns with the differing CK profiles observed at the same two stages (Aoki et al., 2019). In vegetative cells, there were decreasing trends in the levels of arginine, leucine/isoleucine, methionine, and tyrosine in the knockout and overexpression strains compared to WT. On the contrary, there were decreasing trends in alanine/sarcosine, aspartate, glutamine, glutamate, glycine, serine, threonine/homoserine, tyrosine, and GABA in the 24-hour development knockout and overexpression strains

compared to WT. From a mitochondrial perspective, a decrease in various amino acids would be expected as they directly participate in the synthesis of the 13 mitochondrially encoded proteins necessary for proper function of the respiratory chain (Tang et al., 2020). They are also directly involved in various aspects of mitochondrial metabolism, and mitochondria biosynthesize several of these amino acids – glutamine, glutamate, alanine, proline, and aspartate (Spinelli and Haigis, 2018). Lussey-Lepoutre et al. (2015) showed that the loss of succinate dehydrogenase, which is an integral component of the mitochondrial respiratory chain complex II and is responsible for oxidizing succinate to fumarate, dysregulates non-essential amino acid metabolism. Alanine, aspartate, glutamate, asparagine, and serine were among the most down-regulated amino acids in their analyses. Accompanying these changes were also decreased levels of TCA cycle metabolites, including fumarate, malate, and citrate. Another study used a metabolomics approach to assess the metabolic consequences of fumarate-hydratase-deficiency (the enzyme that catalyzes the conversion of fumarate to malate in the TCA cycle) in mammalian cells and found that the cells became auxotrophic for arginine (Zheng et al., 2013). Similar to these findings in mammalian cells, a study in yeast observed that disruption of mitochondrial respiration resulted in decreased arginine levels, as well as other amino acids derived from the TCA cycle (Malecki et al., 2020). These studies, among many others, illustrate that perturbations in the TCA cycle can result in altered metabolic activity affecting amino acid metabolism, and numerous other pathways (see reviews and references therein - Spinelli and Haigis, 2018; Sainero-Alcolado et al., 2022).

In the mitochondrial-related metabolites assessed, there were no trends found in the early development samples cultured in FM minimal medium without arginine and lysine.

This result was unexpected, as increasing levels of total CKs were observed from vegetative growth to early development (Aoki et al., 2019). However, we did notice impaired turnover of organelles and cytoplasmic proteins in our TEM data, which could be further investigated through staining for p80 or VatC (late endosomal and contractile vacuole markers) to assess changes in recycling components under starvation as a result of *iptA*-deficiency or overexpression. In this study, early development was simulated through the onset of nitrogen stress by culturing cells in FM minimal medium without arginine and lysine for 36-hours, as previously described (Otto et al., 2003). This method was different from our earlier CK profiling work that took place during early development, for which cells were starved for 6 hours in KK2 and samples were collected with distinct streams and aggregation centers (Aoki et al., 2019). A recent publication assessing mitochondrial dynamics in vegetative growth and early development in *D. discoideum* through bioenergetics and proteomics found that the main mitochondrial processes are downregulated during early development and that there was less mitochondrial yield overall in early developmental samples compared to vegetative cells (Mazur et al., 2021). Therefore, sampling a larger population of cells in early development may have helped make our findings in mitochondrial content more comparable to what was analyzed in our vegetative samples. Sampling after the initiation of streaming and aggregation centers have formed would provide an insightful follow up to this analysis. Moreover, performing mitochondrial isolation in both sampled stages may be a better method to account for variation in mitochondrial yield between the sampled life cycle stages. This approach has been validated in mammalian cells where it was found that analyzing isolated mitochondria

rather than whole-cells is better for revealing mitochondrial-related metabolite changes and depicting mitochondrial dynamics (Chen et al., 2016).

It is important to note that, in our combined data, we cannot distinguish whether the aberrant phenotypes are a direct result of the lack or excess of CKs produced through knockout or overexpression of the *iptA* gene or whether the lack or excess of the IptA protein impacts biological processes beyond its catalytic role. A comparable example of this comes from Frej et al. (2016) who highlighted distinct roles of the biosynthetic enzyme, inositol-3-phosphate synthase, in *D. discoideum*, beyond its catalytic role that were not rescued by inositol supplementation (Frej et al., 2016). As such, supplementation or depletion of CKs in the *iptA*-deficient and overexpression strains, respectively, would be necessary to distinguish which of the observed phenotypes are associated with a lack/excess of CK versus a lack/excess of IptA.

CONCLUSION

In summary, IptA appears to have temporally separated roles during vegetative growth and the later stages of multicellular development validating our hypothesis that the profile shift in dominant CK forms we observed during growth and early development have a separate function compared to those found during later development. This is the first *D. discoideum* study to report on an *iptA* overexpression strain and to conduct a metabolomics analysis in response to altered CK dynamics. While there are no macro-scale phenotypes from loss or overexpression of *iptA* during vegetative growth, such as those seen in late development, we documented many impactful biochemical changes at the cellular and molecular level. We conclude that *iptA*-deficiency affects cytokinesis and both *iptA*-

deficiency and overexpression results in unique sub-cellular phenotypes in line with mitochondrial-associated dysfunction, including altered mitochondrial morphology, dysregulated TCA cycle and amino acid metabolism, and increased AMP levels during vegetative growth.

FIGURES

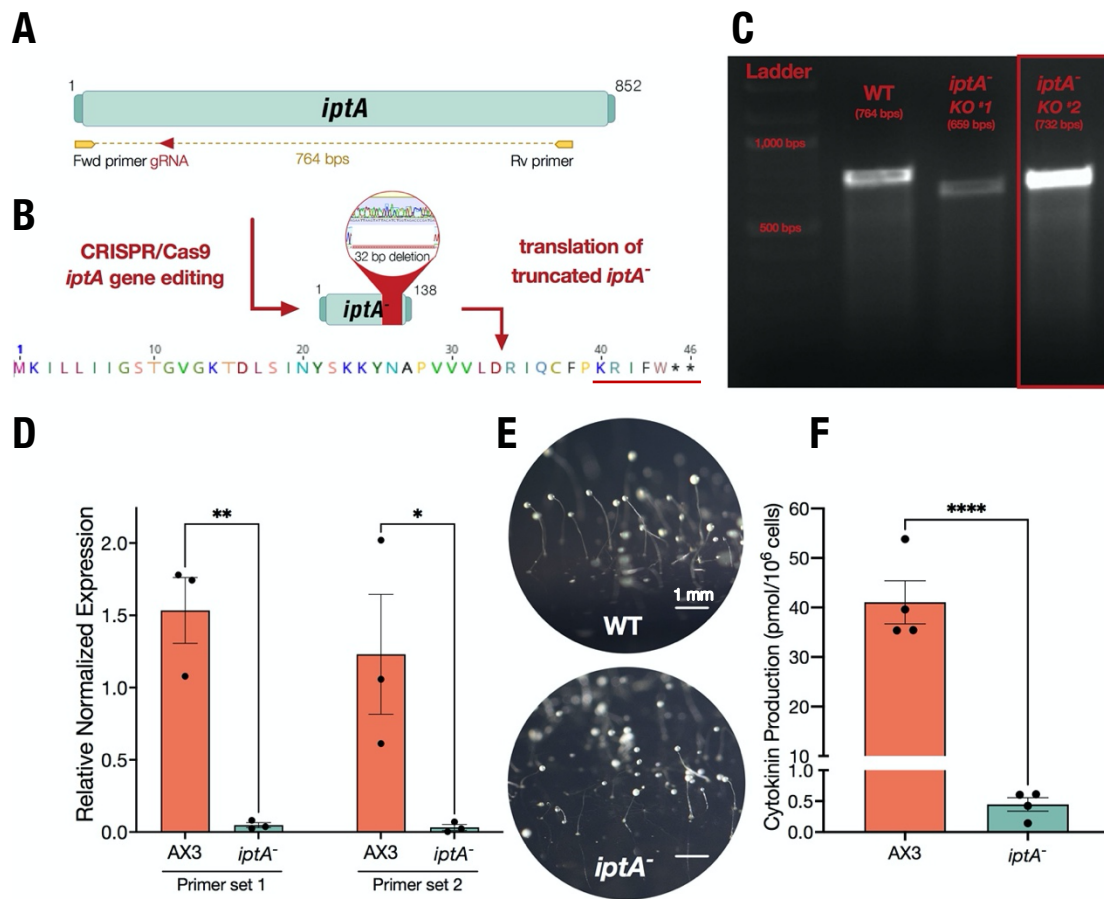


Figure 4.1. Knockout of *iptA* results in a 99% reduction of total cytokinin (CK) levels and fruiting bodies with small sori (suspended spore mass) and thin stalks. (A) *iptA* schematic indicating the CRISPR guide RNA cut site (gRNA; red) showing the region of the gene that was targeted for knockout (KO) and the genomic primers used (yellow) for verification of diagnostic *iptA* KO products. Fwd indicates forward primer, and Rv indicates reverse primer. (B) Sanger sequencing schematic of the selected *iptA* KO clone used in all experiments. This clone has a 32 base pair deletion from nucleotides 118-149 of the genomic *iptA* sequence, which results in a shift in the reading frame and early truncation of the gene product. The translation of the truncated *iptA* gene product is shown beneath the cartoon *iptA* truncated product; the red line underneath the translation indicates where the sequence deviates from wild-type (WT) because of the deletion (see nucleotide and amino acid sequence in Supplementary Table 2). (C) Verification of *iptA* KO by PCR from genomic DNA. The red box around *iptA* KO #2 indicates the clone selected for all further experimentation. (D) Confirmation of gene KO through quantitative PCR (qPCR) analysis of *iptA* gene mRNA expression using two different primer sets spanning the *iptA* gene. Wild-type (AX3) and *iptA*⁻ vegetative cells were harvested from flasks after 24 hours in FM Minimal Medium. Data was normalized to *gpdA* and *rmlA* (data are presented as individual values (dots) and mean \pm standard error for 3 independent). (E) *iptA*⁻ fruiting

bodies have decreased sori size and thin stalks. WT fruiting bodies are shown in the upper image, and *iptA*⁻ fruiting bodies are shown in the lower image. The scale bar represents 1 mm. (F) Total CK levels are 99% lower in KO than in WT. Fruiting bodies were harvested from KK2 agar as previously described (Aoki et al., 2019), and both intra- and extracellular CK concentrations were analyzed and pooled (data are presented as individual values (dots) and mean ± standard error for 4 independent replicates). For panels D and F, the statistical significance was determined by a *t*-test (two-tailed; **p*<0.05, ***p*<0.01, *****p*<0.0001).

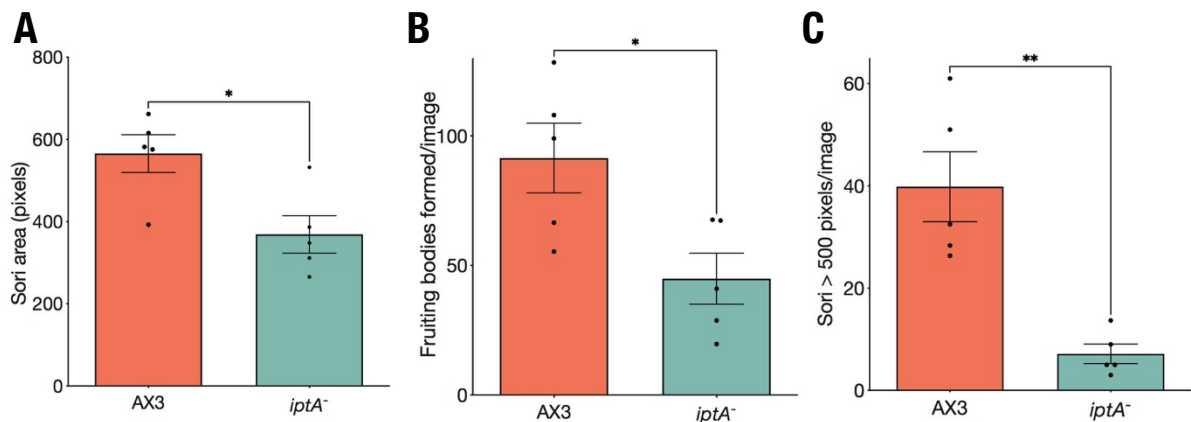


Figure 4.2. *iptA*-deficiency results in aberrant developmental morphology. (A) Disruption of *iptA* generates fruiting bodies containing smaller sori, (B) fewer fruiting bodies formed per number of cells plated, and (C) an overall reduction in sori reaching the average area of WT (AX3). Fiji/ImageJ was used to assess sori area. Data are presented as individual values (dots) and mean ± standard error for 5 independent experiments, and statistical significance was determined by a *t*-test (two-tailed; **p*<0.05, ***p*<0.01).

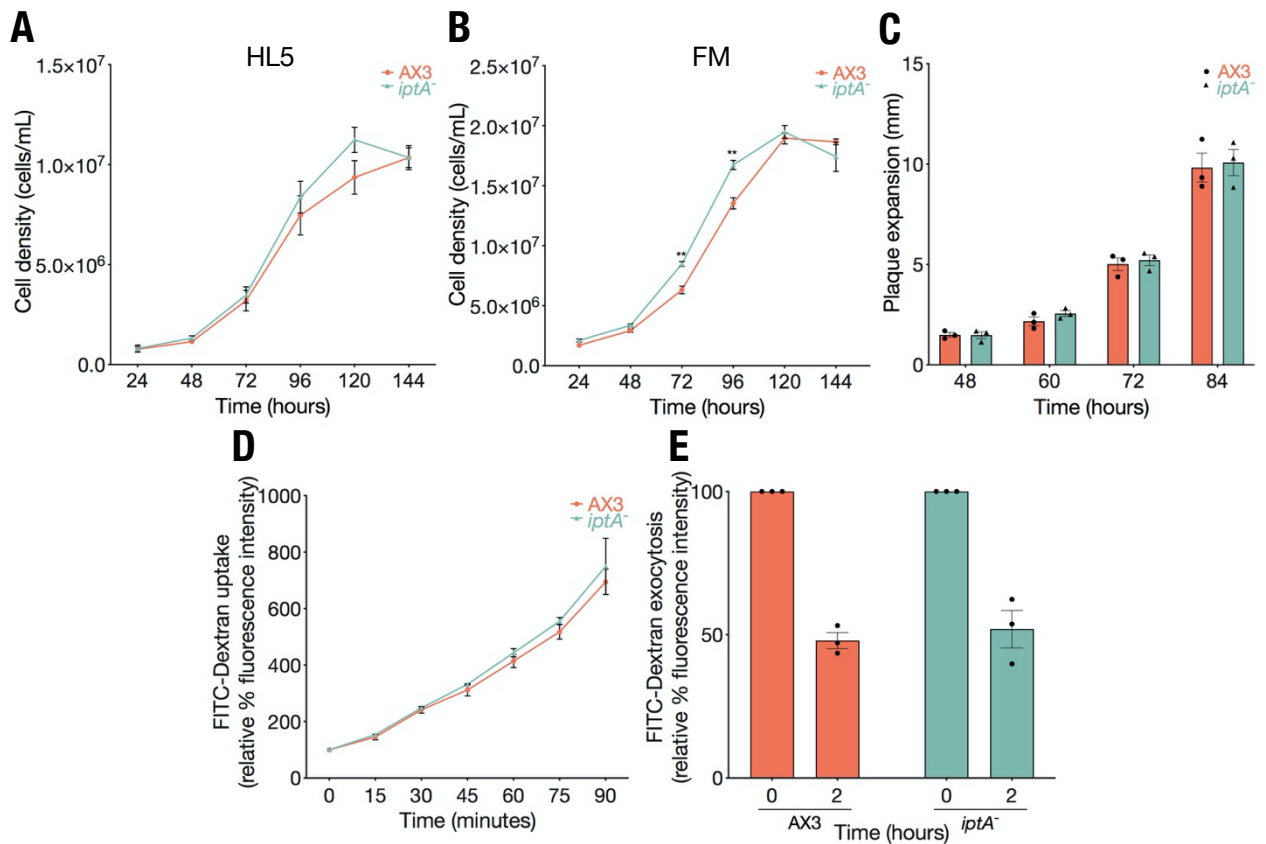


Figure 4.3. *iptA*-deficiency does not affect vegetative growth or pinocytosis. (A) The loss of *iptA* has a minimal effect on vegetative growth in axenic culture under nutrient rich conditions (HL5) and (B) minimal nutrient conditions (FM). Cell density was determined every 24 hours using a hemocytometer. (C) *iptA*⁻ cells grow similarly to WT (AX3) on agar plates seeded with bacteria, as measured through plaque expansion (mm) over an 84-hour time course. (D) Relative pinocytosis rates are unaffected by the loss of *iptA*. WT and *iptA*⁻ cells were incubated in HL5 containing FITC-Dextran, and the uptake of FITC-Dextran was assessed every 15 minutes. The data were corrected for background signal and expressed as the mean fluorescence change (%) relative to the 0-minute time point. (E) Relative exocytosis was assessed using the same flask of cells culture over a 90-minute time course. The 2-hour time point was normalized to the time 0 reading for each strain. For all panels, the data are presented as mean ± standard error for 3 independent experiments, and statistical significance comparing *iptA*⁻ to WT (AX3) was determined by an unpaired *t*-test (two-tailed; ***p*<0.01).

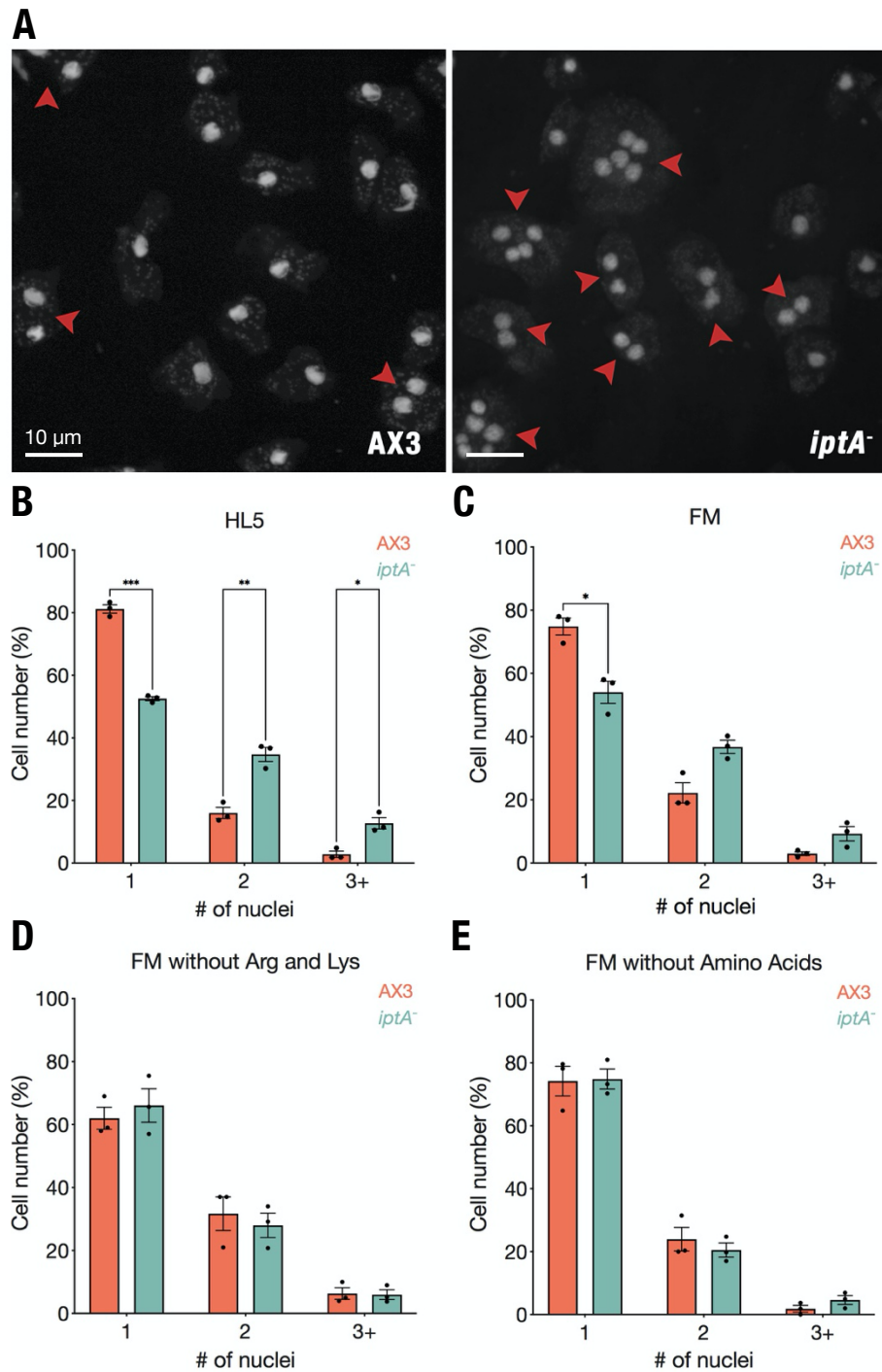


Figure 4.4. Loss of *iptA* impairs cytokinesis. (A) Representative images from WT (AX3) and *iptA*⁻ cells stained with DAPI nuclear stain to assess cytokinesis. Red arrows indicate multinucleated cells in each image. The scale bars represent 10 μ m. (B-E) The number of nuclei was quantified under both nutrient rich conditions (HL5; B), minimal nutrient conditions (FM; C), minimal nutrient conditions without arginine and lysine (FM without Arg/Lys; D), and minimal nutrient conditions without amino acids (E). Data are presented as individual values (dots) and mean \pm standard error for 3 independent replicates, where at least 300 cells were analyzed per condition. Statistical significance was determined by

an unpaired *t*-test with the Bonferroni-Dunn multiple comparisons test (two-tailed; **p*<0.05, ***p*<0.01, ****p*<0.001).

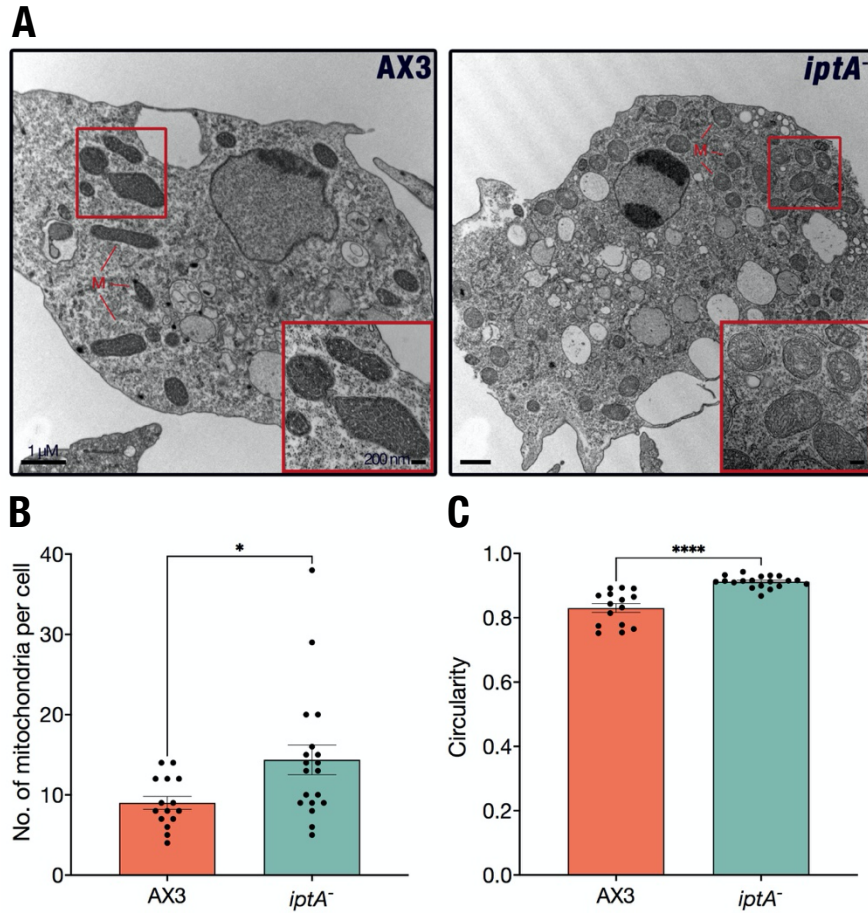


Figure 4.5. *iptA*-deficiency alters the morphology and numbers of mitochondria during vegetative growth. (A) TEM images of representative WT (AX3) and *iptA*⁻ vegetative amoebae cultured in FM minimal medium for 36 hours showing altered mitochondria morphology in the KO (*iptA*⁻) strain compared to WT. The inset shows a zoomed in section of the mitochondria highlighting the rounded mitochondrial morphology present in the KO strain. (B) *iptA*⁻ cells have a greater number of mitochondria per cell and (C) the mitochondria area is significantly more rounded/circular. For panels B and C, data are presented as individual values (dots) and mean ± standard error for 2 independent experiments, and statistical significance was determined by an unpaired *t*-test (two-tailed; **p*<0.05, *****p*<0.0001). The large scale bars on the bottom left of the TEM images represent 1 μm, and the smaller scale bars in the bottom right panels represent 200 nm. Fiji/ImageJ was used to assess circularity.

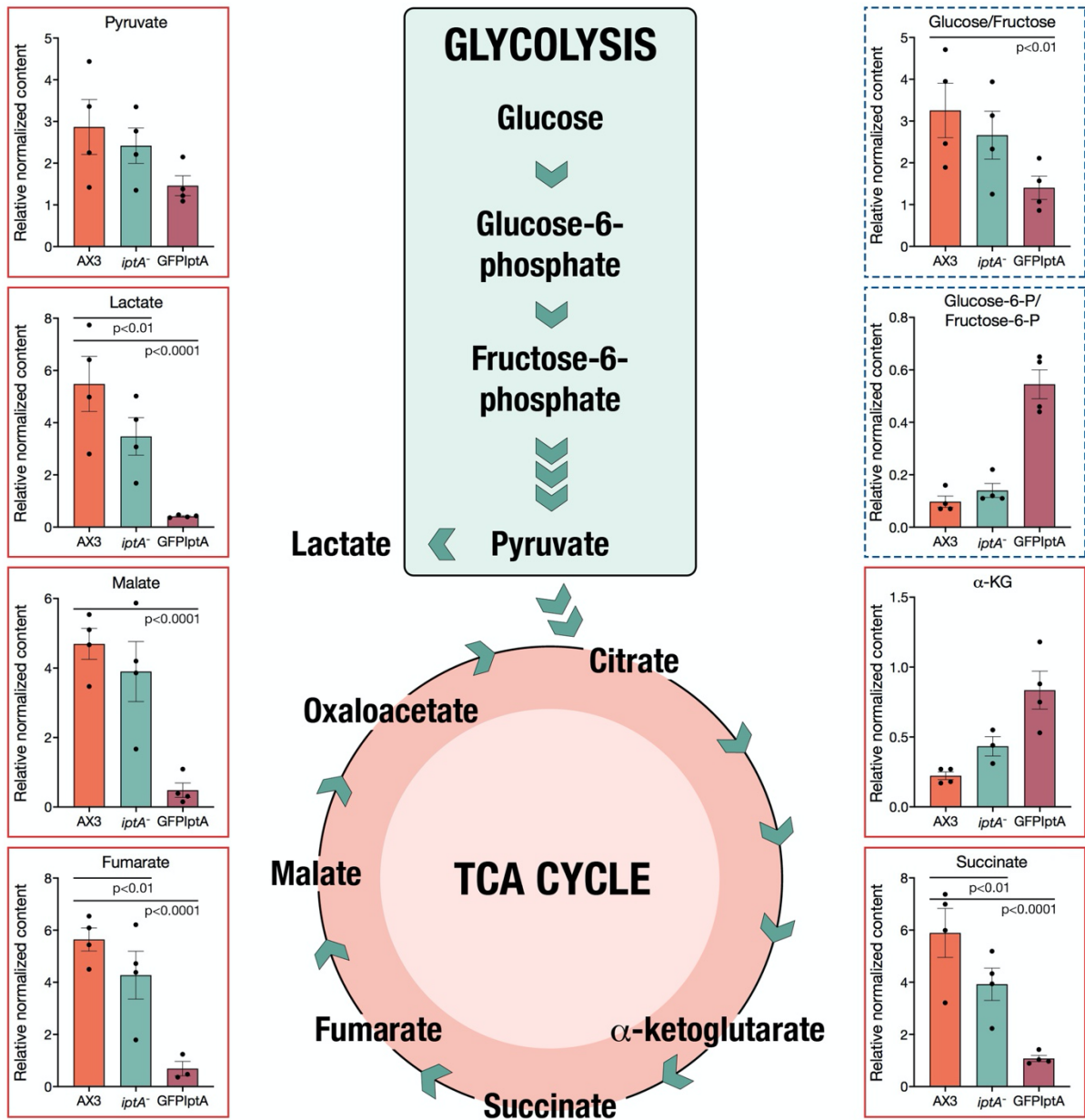


Figure 4.6. *iptA*-deficiency (*iptA*⁻) and overexpression (*GFP-iptA*) dysregulates the tricarboxylic acid (TCA) cycle in vegetative amoebae. High performance liquid chromatography-high resolution accurate mass-full scan mass spectrometry HPLC-(HRAM)-FS-MS was used to detect changes in mitochondrial-related metabolites as a result of *iptA*-deficiency and overexpression. *D. discoideum* WT (AX3), *iptA*⁻, and *GFP-iptA* vegetative cells were cultured under the same FM minimal medium conditions used for the TEM images (n = 4). Abundance of succinate, fumarate, and lactate were all significantly decreased in both the *iptA* knockout (KO) and overexpression (OE) strains compared to WT. In the *GFP-iptA* strain, the levels of glucose/fructose and malate were significantly decreased compared to WT and were similarly decreased in the *iptA*⁻ strain compared to WT. This analysis revealed that *iptA*-deficiency and/or overexpression significantly affects key metabolites in the TCA cycle, supporting the altered mitochondrial

morphology in the TEM images. Data from the individual metabolite plots were normalized relative to labeled amino acid standards added to each sample and are presented as individual values (dots) and mean \pm standard error for 4 independent replicates. Statistical significance comparing *iptA*⁻ and *GFP-iptA* strains to WT for all quantified metabolites was determined through a two-way ANOVA with the Benjamini, Krieger, and Yekutieli-correction controlling for multiple comparisons with false discovery rate (FDR) of <0.05 – *p*-values are listed above the bar graph with a line spanning between WT and *iptA*⁻ or between WT and *GFP-iptA* to indicate when there was a significant difference in metabolite abundance. Solid red boxes around the individual metabolite plots indicate the metabolite was validated by MS² data and have no known isomers, and dashed blue boxes indicate the metabolite has an isomer that was unable to be differentiated in our LC-MS method (isomer names included in the figure titles). Metabolites that were unable to be detected in our method were either excluded from the shown pathways or were included in the pathway and do not have individual metabolite plots shown alongside the pathway.

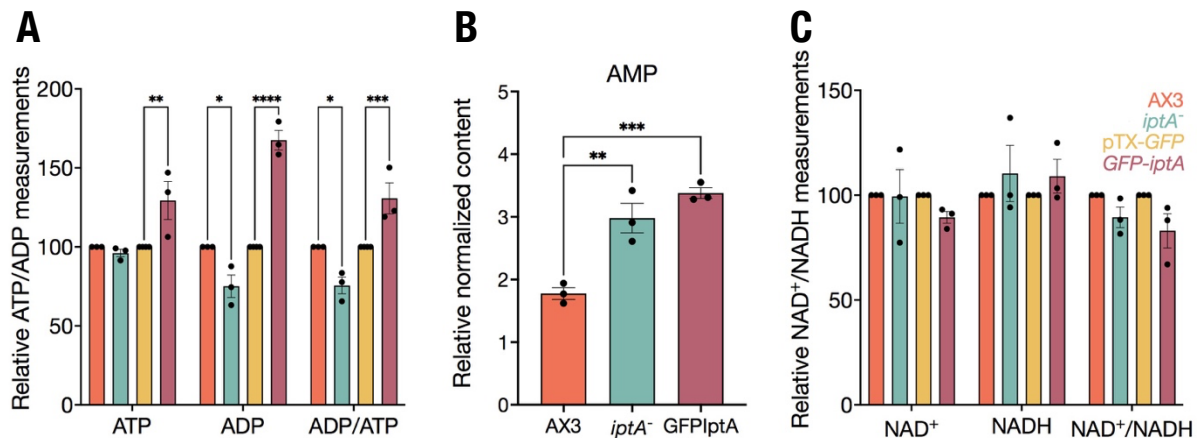


Figure 4.7. *iptA*-deficiency and overexpression affect energy metabolite levels (AMP/ADP/ATP) but do not affect NAD⁺/NADH levels. (A) ATP and ADP content is reduced in the *iptA*⁻ (KO) strain relative to WT (AX3) during vegetative growth resulting in a significant decrease in the ADP/ATP ratio. In the *GFP-iptA* (OE) strain, ATP and ADP content is significantly increased relative to the pTX-GFP empty vector control during vegetative growth, resulting in a significant increase in the ADP/ATP ratio. (B) AMP levels were significantly increased in both the KO and OE strains compared to WT. (C) NADH content was slightly elevated in both the KO and OE strains relative to WT and empty vector strains during vegetative growth, respectively, resulting in a slightly decreased NAD⁺/NADH ratio. For panels A and C, metabolite content was determined through commercial kits and analyzed with a plate reader to acquire relative readings compared to WT or empty vector strains, and data are presented as individual values (dots) and \pm standard error for 3 independent experiments. Statistical significance was determined through a two-way ANOVA with the Tukey multiple comparisons test (* $p < 0.05$, ** $p < 0.01$, *** $p < 0.001$, **** $p < 0.0001$). For panel B, AMP content was determined through the LC-MS/MS targeted metabolomic analysis and was normalized relative to labeled amino acid standards added to each sample. Data are presented as individual values (dots) and mean \pm standard error of the mean for 4 independent replicates, and statistical significance was determined through a one-way ANOVA with the Dunnett's multiple comparison test (** $p < 0.01$, *** $p < 0.001$).

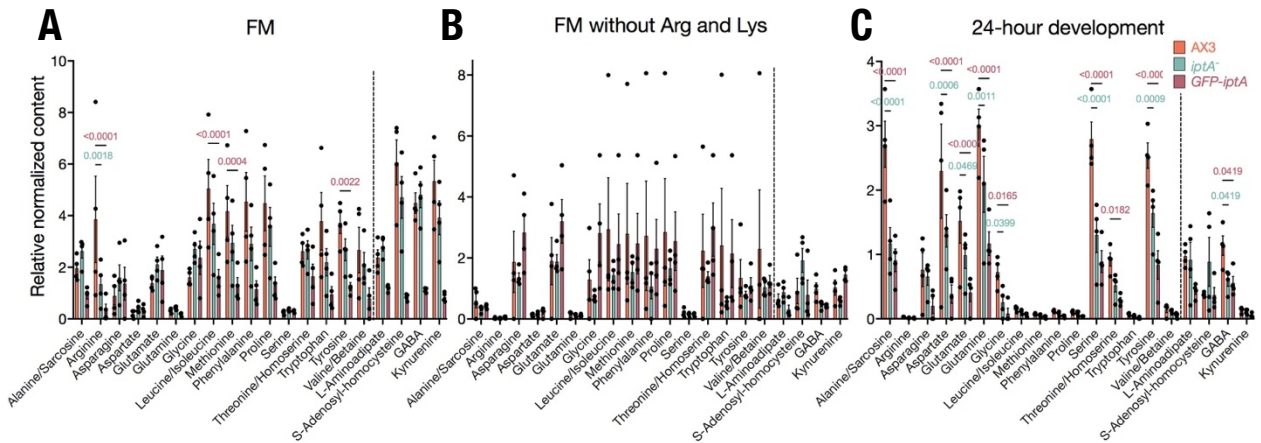


Figure 4.8. Amino acid and derivatives decrease in abundance in *iptA*-deficient and overexpression strains in vegetative growth and 24-hour development. (A) Amino acid and amino acid derivative metabolite levels detected in vegetative amoebae cultured in FM minimal medium, (B) in early development amoebae cultured in FM minimal medium without arginine and lysine, and (C) in 24-hour development fruiting bodies cultured on 1% KK2 agar. High performance liquid chromatography-high resolution accurate mass-full scan mass spectrometry HPLC-(HRAM)-FS-MS was used to detect amino acids and amino acid derivatives, which are separated by a dashed line on each figure. Individual metabolite levels were normalized relative to labeled amino acid standards added to each sample and are presented as individual values (dots) and mean \pm standard error for 4 independent replicates. Statistical significance comparing *iptA*⁻ and *GFP-iptA* strains to WT (AX3) for all detected metabolites was determined through a two-way ANOVA with the Benjamini, Krieger, and Yekutieli-correction controlling for multiple comparisons with false discovery rate (FDR) of <0.05 – *p*-values are listed above the bar graph with a line spanning between WT and *iptA*⁻ (blue font) or between WT and *GFP-iptA* (pink font) to indicate when there was a significant difference in metabolite abundance. Isomers that were not able to be differentiated in our method are both listed under the metabolite plots and are separated with a slash.

SUPPLEMENTARY MATERIALS

Supplementary Table 4.1. *iptA* primer sequences used for cloning, PCR, or sanger sequencing. All uppercase nucleotides refer to the genomic/coding region. Lowercase nucleotides are specified below the sequence.

A. sgRNA primer sequences used for cloning into the pTM1285 CRISPR/Cas 9 vector	
Primer Sequence (5' – 3')	
sgRNA sense	agcaACCAAAATATTCGCTTTCAT
sgRNA	aaacATGAAAGCGAATATTTTGGT
antisense	*lowercase regions refer to the BpiI overhangs corresponding to the pTM1285 vector
B. PCR primers used for amplifying/confirming ligation of sgRNAs	
Primer Sequence (5' – 3')	
sgRNA sense	agcaACCAAAATATTCGCTTTCAT
tracrRV	AAGCTTAAAAAAGCACCGACTCGGTGCC
C. Sanger sequencing primer used for confirming proper insert of sgRNAs	
Primer Sequence (5' – 3')	
tracrRV	AAGCTTAAAAAAGCACCGACTCGGTGCC
D. PCR primers used for amplifying indels in <i>D. discoideum</i> clones	
Primer Sequence (5' – 3')	
<i>iptAF</i>	ATGAAGATTTTATTAATTATCGGTTC
<i>iptAR</i>	GCATAATTATAGTGAGCCAATG
E. Sanger sequencing primer used for sequencing indels	
Primer Sequence (5' – 3')	
<i>iptAR</i>	GCATAATTATAGTGAGCCAATG

Supplementary Table 4.2. Nucleotide and amino acid sequences of full length *iptA* and our selected *iptA* knockout strain (full length sequence was obtained from <http://dictyBase.org>). Red font indicates where the KO strain deviates from the WT sequence at the nucleotide or amino acid level.

A. Gene sequence for full length <i>iptA</i> and <i>iptA</i> knockout		
	Gene Sequence (5' – 3')	Sequence length
<i>iptA</i>	ATGAAGATTTTATTAATTATCGGTTCTACTGGAGTTG GCAAACAGACTTGTCAATAAATTATTCAAAAAAAT ATAATGCCCTGTTGTAGTTTTAGATAGAATTCAATG TTTCCAGAATTAAGTATTACATCTGGTAGACCCGAT GAAAGCGAATATTTTGGTAGTAAAAGGATTTACTTAA CCGATTTATTGGTAGAACCAGGGAATGAAAATATAA AAAAACTTTTTATGTTAATAAATTAATAAACATTTT AAATGAAATAAGAATAATTATGACACCCAAAATTT ACCAAATGAAAAGGTTATGGCTGTATATTTGAAGG AGGCTCAATAAGTTTGTAAAAGAGCTACTCACAAA AATTAATAAACTTCCCTATAAAATCACCTGTGTAATA TATATTAGACCCAGCGATTCCATTGATAATCATAAAT TATATAAGCTAAAATTTTTAAAAGAGTCTCTCAAAT GTTATCCCAACAGAAGAAGGAAATGACTCTCAAATT TTAGAAGTTAAAAGAATTTTAAATAAAGGTAAAAC GTTAATGCTCAAGGAGAAATTAATTTAGAATATTATG AAAAAATTAACAAGTTTTAATATCTTTAGTTGGTTT GGTTGGTATTGAAGATGTTATTCATTTTTAGATAAG CAATATGATCAGAAAAATATAACATCAAAGTTGGAT CCAAATTATTTAAATGAAATTCAATCACAATTGATTG AAATAATAACATTGGCTCACTATAATTATGCACTATC ACAATTGAATTAATCGATAGCTTGATTAACAATTA CCAAATCAATTGAATATTGTTTAAAAAATATTGAAA TTAATTAA	852 bp
<i>iptA⁻</i>	ATGAAGATTTTATTAATTATCGGTTCTACTGGAGTTG GCAAACAGACTTGTCAATAAATTATTCAAAAAAAT ATAATGCCCTGTTGTAGTTTTAGATAGAATTCAATG TTTCCAAAGCGAATATTTTGGTAGTAA	138 bp
B. Amino acid sequence for full length IptA and the truncated IptA knockout		
	Amino Acid Sequence	Sequence length
IptA	MKILLIIGSTGVGKTDLSINYSKKYNAPVVLDRIQCFPE LSITSGRPDESEYFGSKRIYLDLLVEPGNENIKKTFYVN KLINILNEIKNNYDTQNLPNKGYGCIFEGGSISLLKELL TKINKLPYKITCVIYIRPSDSIDNHKLYKAKIFKRVSQML FPTEEGNDSQILEVKRILNKGKTVNAQGEINLEYEYKIK QVLISLVGLVGIEDVIHFLDKQYDQKNITSKLDPNYLNEI	283 aa

	QSQLIETITLAHYNYSLSQIELIDSLIKQLPKSIEYCLKNIE IN*	
IptA ⁻	MKILLIIGSTGVGKTDLSINYSKKYNAPVVVLDRIQCFPK RIFW**	44 aa
	**Stop codons are UAG and UAA respectively	

Supplementary Table 4.3. Primer sequences used for amplifying the full-length *iptA* gDNA and cloning into the N-terminal GFP tag pTX-GFP extrachromosomal vector. Uppercase nucleotides refer to the *iptA* coding region, and the underlined portion is the restriction enzyme site overhang used to facilitate directional cloning (SacI: 5' – gagctc – 3'; XhoI: 5' – ctcgag – 3').

Primer Sequence (5' – 3')	
<i>pTX-iptAF</i>	gaactt <u>gagctc</u> caaaATGAAGATTTTATTAATTATCGG
<i>pTX-iptAR</i>	taatcc <u>ctcgag</u> TTAATTAATTTCAATATTTTTTAAAC

Supplementary Table 4.4. qPCR primer sequences for *iptA* and two reference genes: *rnlA* and *gpdA*.

A. <i>iptA</i> qPCR primer sequences (2 different sets)	
	Primer Sequence (5' – 3')
<i>iptAF</i>	TGGCTGTATATTTGAAGGAGGCT
<i>iptAR</i>	TCAATGGAATCGCTGGGTCT
<i>iptAF2</i>	AGACCCAGCGATTCCATTGAT
<i>iptAR2</i>	AGTCATTTCTTCTTCTGTTGGGA
B. <i>rnlA</i> qPCR primers	
	Primer Sequence (5' – 3')
<i>rnlAF</i>	TTACATTTATTAGACCCGAAACCAAGCG
<i>rnlAR</i>	TTCCCTTTAGACCTATGGACCTTAGCG
C. <i>gpdA</i> qPCR primers	
	Primer Sequence (5' – 3')
<i>gpdAF</i>	GTTGTCCCAATTGGTATTAATG
<i>gpdAR</i>	GTTGGGTTGAATCATATTTGAAC

Supplementary Table 4.5. Customized list of mitochondrial-related metabolites from various pathways involved in mitochondrial function. This is a summary of the list of mitochondrial-related metabolites we assessed in our method. The metabolites were analyzed by high performance liquid chromatography-high resolution accurate mass-full scan mass spectrometry HPLC-(HRAM)-FS-MS and are separated by the pathway they belong to. For each metabolite, we indicate their experimental formula, the ion mode we used for detection, the observed m/z for that ion mode, and the confidence level of compound identification as defined by Schrimpe-Rutledge et al. (2016), with Level 1 indicating a validated metabolite identification and the highest level of confidence. The comprehensive list of mitochondrial-related metabolites was adapted from Chen et al. (2016). Metabolites that were not consistently detected in at least 3 of our 4 replicates were not included in our final analysis (labeled not included in the last column of the table), and metabolites that were not detected above background in our method are labeled not detected (n.d.). P is short form for phosphate. Isomers that were indiscernible with our LC-MS method are listed together as one compound with a slash between the isomer names.

Compound	Experimental Formula	Selected ion	Observed <i>m/z</i>	Confidence level of compound ID
AMINO ACIDS and DERIVATIVES				
GABA	C4H9NO2	[M+H]	104.07060	Level 1
Phenylalanine	C9H11NO2	[M+H]	166.08625	Level 1
Kynurenine	C10H12N2O3	[M+H]	209.09206	Level 2
Leucine/Isoleucine	C6H13NO2	[M+H]	132.10190	Level 1
Methionine	C5H11NO2S	[M+H]	150.05832	Level 1
Tryptophan	C11H12N2O2	[M+H]	182.08116	Level 1
Arginine	C6H14N4O2	[M+H]	175.11894	Level 1
Tyrosine	C9H11NO3	[M+H]	182.08116	Level 1
Valine/Betaine	C5H11NO2	[M+H]	118.08625	Level 1
Aspartate	C4H7NO4	[M+H]	134.04478	Level 1
Glutamate	C5H9NO4	[M+H]	148.06043	Level 1
S-Adenosyl-homocysteine	C14H20N6O5S	[M-H]	383.11429	Level 2
L-Aminoadipate	C6H11NO4	[M-H]	160.06153	Level 2
Threonine/Homoserine	C4H9NO3	[M+H]	120.06551	Level 1
Proline	C5H9NO2	[M+H]	116.07060	Level 1
Asparagine	C4H8N2O3	[M+H]	133.06076	Level 1
Glutamine	C5H10N2O3	[M+H]	147.07641	Level 1
Alanine/Sarcosine	C3H7NO2	[M+H]	90.05495	Level 1
Citrulline	C6H13N3O3	[M+H]	176.10295	Level 2
Serine	C3H7NO3	[M+H]	106.04986	Level 1
Glycine	C3H7NO3	[M+H]	76.03930	Level 1
Cystathionine	C7H14N2O4S	[M+H]	223.07470	Level 2
NUCLEOTIDES				
Adenosine monophosphate	C10H14N5O7P	[M+H]	348.07034	Level 1
Cytidine monophosphate	C9H14N3O8P	[M-H]	322.04456	Level 1
5-Methyluridine	C10H14N2O6	[M+H]	259.09245	Level 1
Uridine/Pseudouridine	C9H12N2O6	[M-H]	243.06225	Level 1

Adenosine	C10H13N5O4	[M+H]	268.10401	Level 1
Adenine	C5H5N5	[M+H]	136.06175	Level 1
Guanosine	C10H13N5O5	[M+H]	284.09892	Level 1
Adenosine diphosphate ribose	C15H23N5O14P2	[M-H]	558.06438	Level 1
Inosine	C10H12N4O5	[M-H]	267.07348	Level 1
Uridine diphosphate	C9H14N2O12P2	[M+H]	405.00947	Level 1
Uridine monophosphate	C9H13N2O9P	[M-H]	323.02858	Level 1
5-deoxyadenosine	C10H13N5O3	[M+H]	252.10909	Level 1

GLYCOLYSIS/GLUCONEOGENESIS METABOLITES

Glucose/Fructose	C6H12O6	[M-H]	179.05611	Level 1
Glucose/Fructose-6-phosphate	C6H13O9P	[M-H]	259.02244	Level 1
B-D-Fructose-1,6P ₂	C6H14O12P ₂	[M-H]	338.98877	not included
Glyceraldehyde-3-P	C3H7O6P	[M-H]	168.99075	n.d.
Glycerate-1/2,3P ₂	C3H8O10P ₂	[M-H]	264.95199	n.d.
Glycerate-2/3P	C3H7O7P	[M-H]	184.98566	Level 3
Phosphoenolpyruvate	C3H5O6P	[M-H]	166.97506	not included
Pyruvate	C3H4O3	[M-H]	87.00877	Level 1
Lactate	C3H6O3	[M-H]	89.02442	Level 1

TRICARBOXYLIC ACID (TCA) CYCLE METABOLITES

Acetyl-CoA	C23H38N7O17P3S	[M+H]	810.13302	n.d.
Citrate	C6H8O7	[M-H]	191.01973	n.d.
Cis-aconitrate	C6H6O6	[M-H]	173.00916	not included
Isocitrate	C6H8O7	[M-H]	191.01973	n.d.
α-Ketoglutarate	C5H6O5	[M-H]	145.01425	Level 1
2-Hydroxyglutarate	C5H8O5	[M-H]	147.02990	Level 1
Succinate	C4H6O4	[M-H]	117.01933	Level 1
Fumarate	C4H4O4	[M-H]	115.00368	Level 1
Malate	C4H6O5	[M-H]	133.01425	Level 1

PENTOSE PHOSPHATE PATHWAY METABOLITES

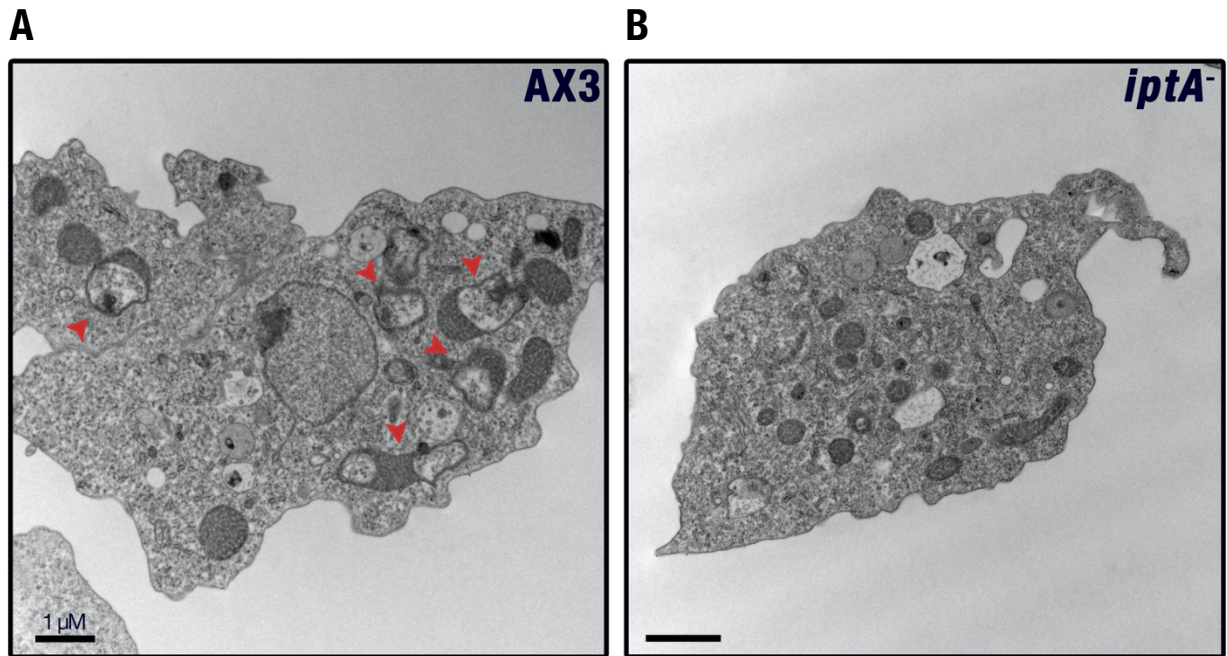
Glucose/Fructose-6-P	C6H13O9P	[M-H]	259.02244	Level 1
----------------------	----------	-------	-----------	---------

6-phosphogluconolactone	C6H11O9P	[M-H]	257.00679	Level 3
6-phosphogluconate	C6H13O10P	[M-H]	275.01732	Level 3
Ribose/Ribulose/Xylulose-5-P	C5H11O8P	[M-H]	229.01188	Level 1
Glyceraldehyde-3-P	C3H7O6P	[M-H]	168.99075	not included
Sedoheptulose-7-P	C7H15O10P	[M-H]	289.03301	Level 1
Erythrose-4-P	C4H9O7P	[M-H]	199.00131	not included

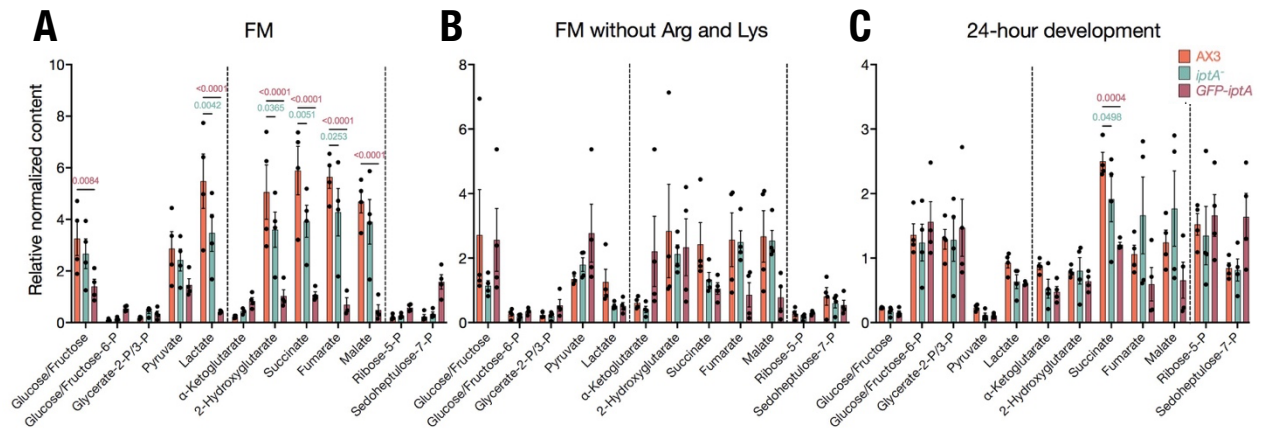
Supplementary Table 4.6. Stable-isotope labeled amino acid internal standards obtained from Cambridge Isotope Laboratories Ltd. (Tewksbury, MA, USA) used to determine the relative concentration of metabolites for all analyses obtained through high performance liquid chromatography-high resolution accurate mass-full scan mass spectrometry (HPLC-(HRAM)-MS).

Labeled Amino Acid Standards	Abbreviation	Label and Enrichment
Glycine*	Gly	$^{13}\text{C}_2$, 99%; ^{15}N , 99%
L-Alanine	Ala	$^{13}\text{C}_3$, 99%; ^{15}N , 99%
L-Arginine·HCl*	Arg	$^{13}\text{C}_6$, 99%; $^{15}\text{N}_4$, 99%
L-Asparagine·H ₂ O	Asn	$^{13}\text{C}_4$, 99%; $^{15}\text{N}_2$, 99%
L-Aspartic Acid	Asp	$^{13}\text{C}_4$, 99%; ^{15}N , 99%
L-Cysteine*	Cys-Cys	$^{13}\text{C}_6$, 99%; $^{15}\text{N}_2$, 99%
L-Glutamic Acid	Glu	$^{13}\text{C}_5$, 99%; ^{15}N , 99%
L-Glutamine	Gln	$^{13}\text{C}_5$, 99%; $^{15}\text{N}_2$, 99%
L-Histidine·HCl·H ₂ O*	His	$^{13}\text{C}_6$, 97-99%; $^{15}\text{N}_3$, 97-99%
L-Isoleucine	Iso	$^{13}\text{C}_6$, 99%; ^{15}N , 99%
L-Leucine	Leu	$^{13}\text{C}_6$, 99%; ^{15}N , 99%
L-Lysine·2HCl*	Lys	$^{13}\text{C}_6$, 99%; $^{15}\text{N}_2$, 99%
L-Methionine	Met	$^{13}\text{C}_5$, 99%; ^{15}N , 99%
L-Phenylalanine	Phe	$^{13}\text{C}_9$, 99%; ^{15}N , 99%
L-Proline	Pro	$^{13}\text{C}_5$, 99%; ^{15}N , 99%
L-Serine	Ser	$^{13}\text{C}_3$, 99%; ^{15}N , 99%
L-Threonine	Thr	$^{13}\text{C}_4$, 97-99%; ^{15}N , 97-99%
L-Tryptophan	Trp	$^{13}\text{C}_{11}$, 99%; $^{15}\text{N}_2$, 99%
L-Tyrosine	Tyr	$^{13}\text{C}_9$, 99%; ^{15}N , 99%
L-Valine	Val	$^{13}\text{C}_5$, 99%; ^{15}N , 99%

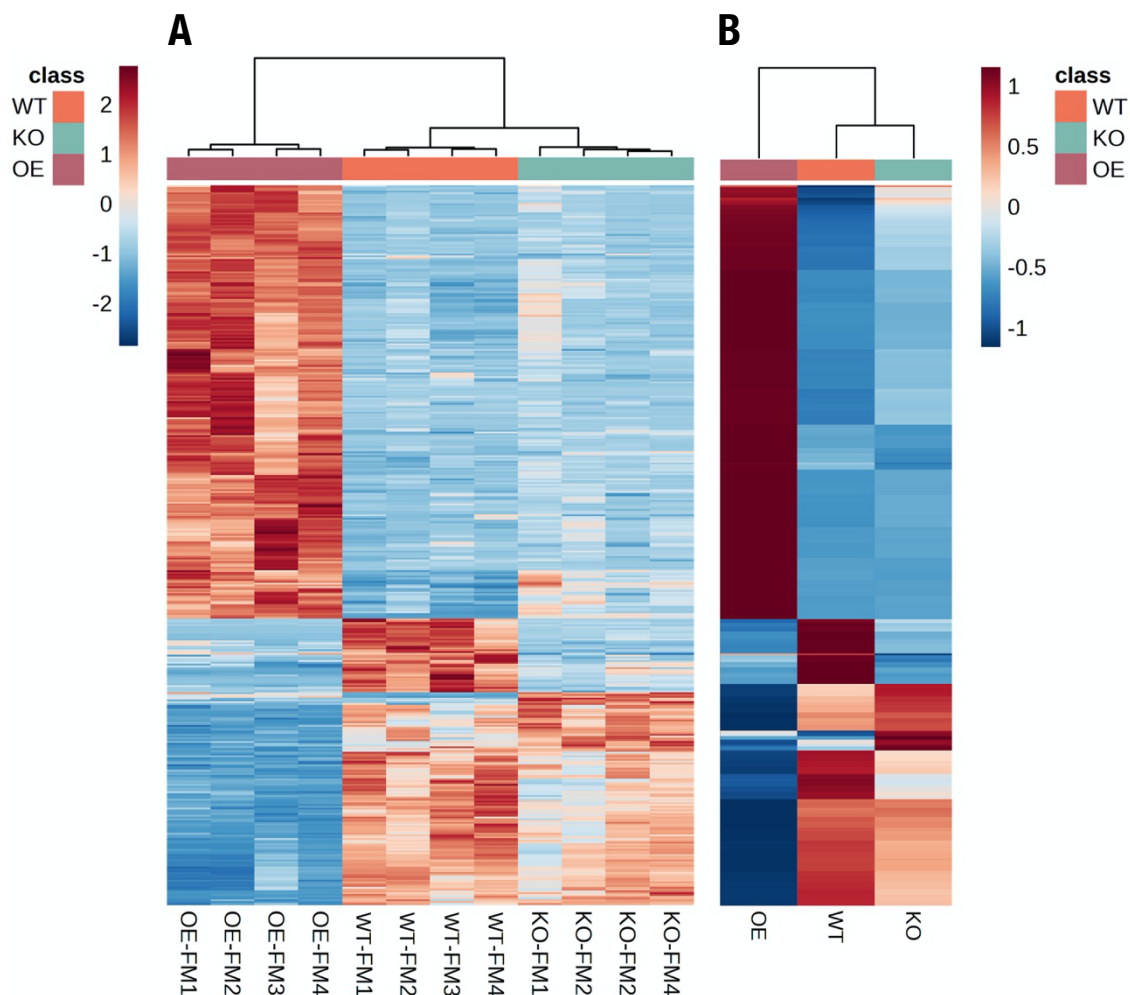
*indicates low recovery of labeled standard with our LC-MS method, so these compounds were not used to normalize relative peak areas



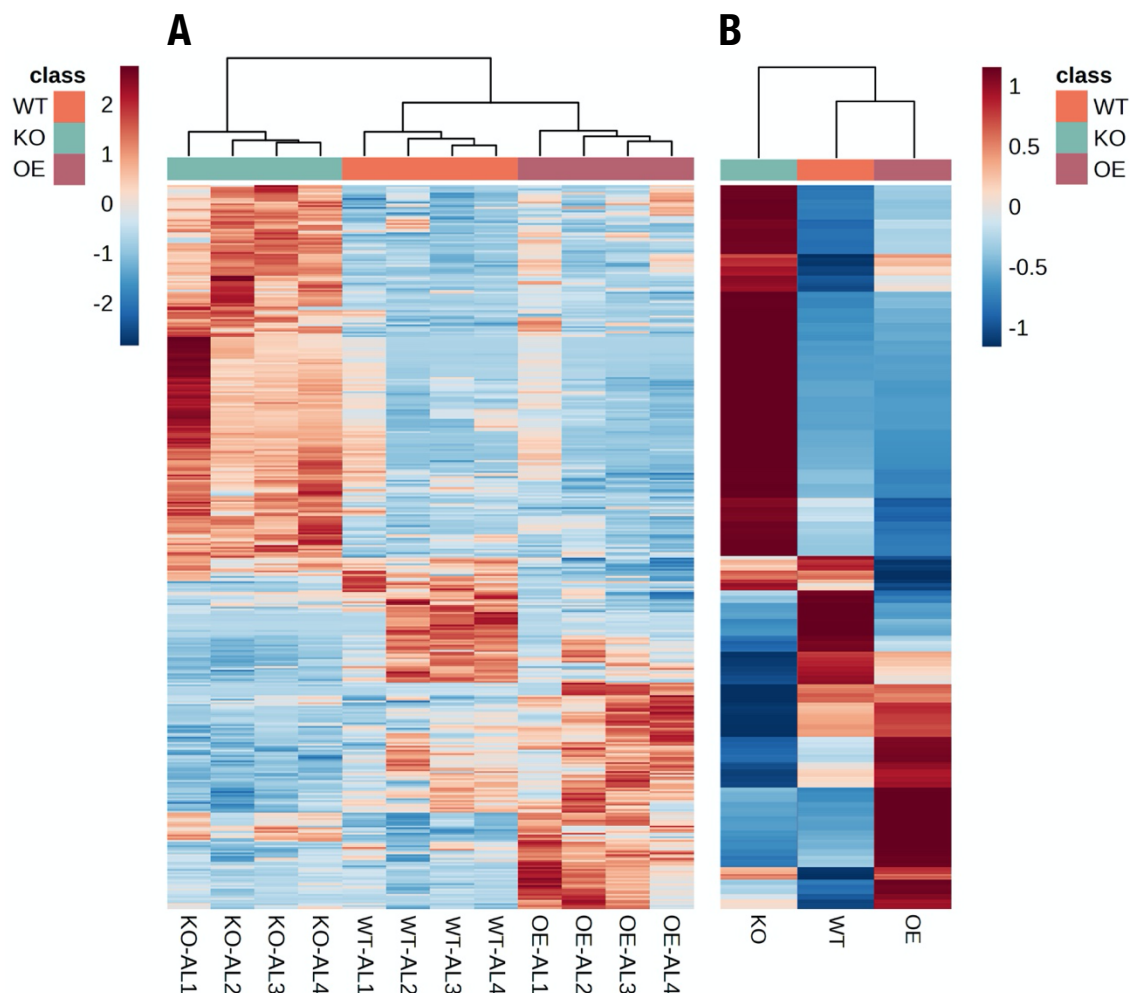
Supplementary Figure 4.1. TEM images of representative wild-type (AX3) and *iptA*⁻ (KO) early development amoebae cultured in FM minimal medium lacking arginine and lysine for 36 hours. (A) WT cells show recycling of organelles as visualized through characteristic formation of double membraned recycling components (indicated by red arrows) and reduced cytoplasmic proteins (less granular cytoplasm) when cultured under autophagy stimulating conditions. (B) KO cells retain the rounded mitochondria phenotype visualized in the FM vegetative amoebae samples and appear to be delayed in their response of protein turnover under autophagy stimulating conditions because of the loss of *iptA*.



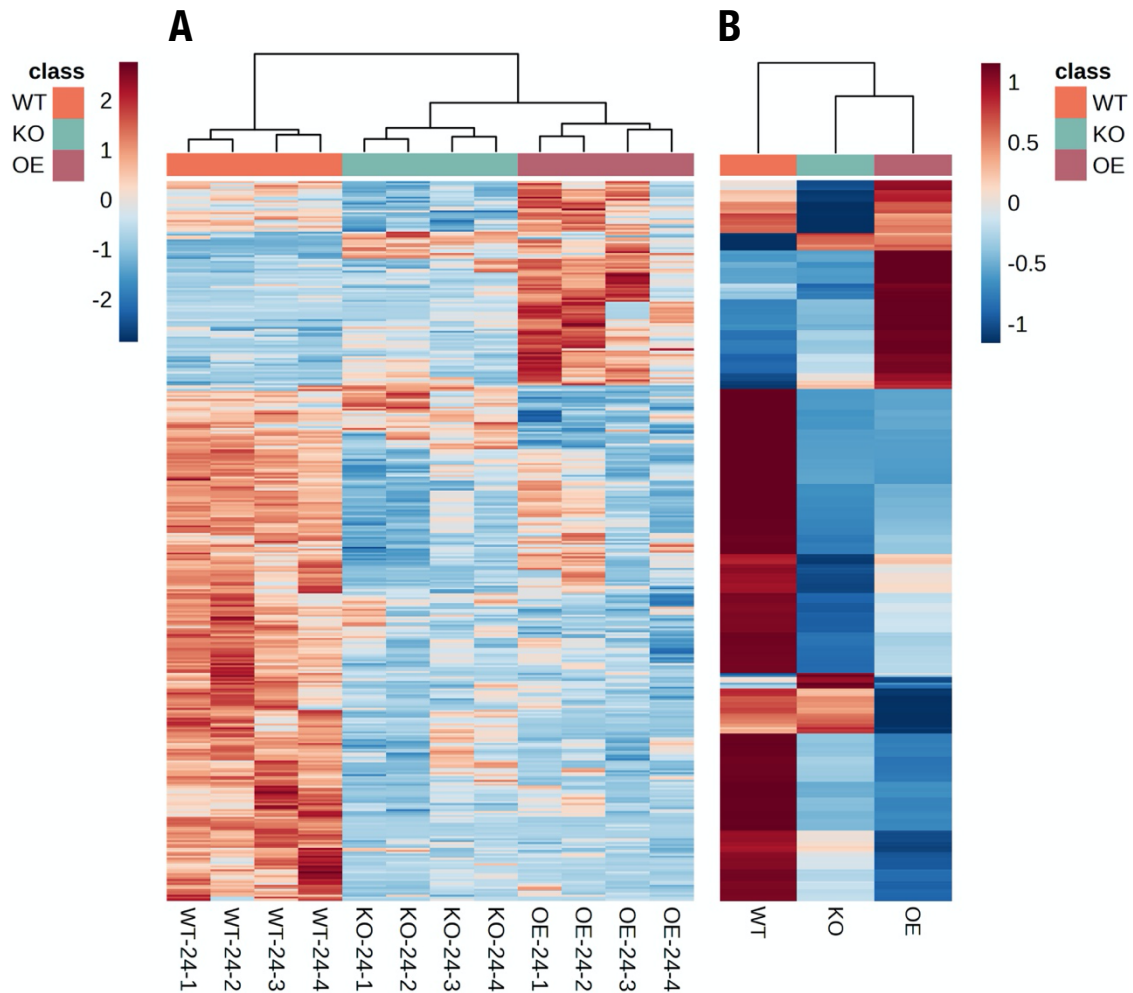
Supplementary Figure 4.2. Energy metabolism pathway analysis in *iptA*-deficient and overexpression cells during vegetative growth, early development, and late development in *D. discoideum*. High performance liquid chromatography-high resolution accurate mass-full scan mass spectrometry HPLC-(HRAM)-FS-MS was used to detect changes in metabolite levels in the glycolysis pathway (left side of each figure), TCA cycle (middle of each figure), and pentose phosphate pathway (right side of each figure) in (A) vegetative amoebae cultured in FM minimal medium, (B) in early development amoebae cultured in FM minimal medium without arginine and lysine, and (C) in 24-hour development fruiting bodies cultured on 1% KK2 agar. Individual metabolite levels were normalized relative to labeled amino acid standards added to each sample and are presented as individual values (dots) and mean \pm standard error for 4 independent replicates. Statistical significance comparing *iptA*⁻ and *GFP-iptA* strains to WT (AX3) for all detected metabolites was determined through a two-way ANOVA with the Benjamini, Krieger, and Yekutieli-correction controlling for multiple comparisons with false discovery rate (FDR) of <0.05 – *p*-values are listed above the bar graph with a line spanning between WT and *iptA*⁻ (blue font) or between WT and *GFP-iptA* (pink font) to indicate when there was a significant difference in metabolite abundance. Isomers that were not able to be differentiated in our method are both listed under the metabolite plots and are separated by a slash. Any metabolite that included a phosphate in its name has been abbreviated to P.



Supplementary Figure 4.3. Heatmap visualization of the top 400 metabolites in the vegetative amoebae samples cultured in FM minimal medium. (A) The top 400 significantly different metabolites for each individual replicate. **(B)** Averages of top 400 metabolites from the individual replicates shown in the A panel. Metaboanalyst v. 5.0 was used to generate a heatmap to visualize clustering of the individual replicates for each strain with the Euclidean distance measure, Ward clustering method, and the one-way ANOVA statistical test (Pang et al., 2022). Wild-type cells (AX3) are labeled WT, *iptA*-deficient cells are labeled KO, and the *GFP-iptA* overexpression cells are labeled OE.



Supplementary Figure 4.4. Heatmap visualization of the top 400 metabolites in the early development amoebae samples cultured in FM minimal medium without arginine and lysine. (A) The top 400 significantly different metabolites for each individual replicate. **(B)** Averages of top 400 metabolites from the individual replicates shown in the A panel. Metaboanalyst v. 5.0 was used to generate a heatmap to visualize clustering of the individual replicates for each strain with the Euclidean distance measure, Ward clustering method, and the one-way ANOVA statistical test (Pang et al., 2022). Wild-type cells (AX3) are labeled WT, *iptA*-deficient cells are labeled KO, and the *GFP-iptA* overexpression cells are labeled OE.



Supplementary Figure 4.5. Heatmap visualization of the top 400 metabolites in the 24-hour development fruiting bodies cultured on 1% KK2 agar. (A) The top 400 significantly different metabolites for each individual replicate. **(B)** Averages of top 400 metabolites from the individual replicates shown in the A panel. Metaboanalyst v. 5.0 was used to generate a heatmap to visualize clustering of the individual replicates for each strain with the Euclidean distance measure, Ward clustering method, and the one-way ANOVA statistical test (Pang et al., 2022). Wild-type cells (AX3) are labeled WT, *iptA*-deficient cells are labeled KO, and the *GFP-iptA* overexpression cells are labeled OE.

REFERENCES

- Amasino, R. (2005). 1955: kinetin arrives: the 50th anniversary of a new plant hormone. *Plant Physiol.* 138, 1177-84. doi: 10.1104/pp.104.900160.
- Andrabi, S. B. A., Tahara, M., Matsubara, R., Toyama, T., Aonuma, H., Sakakibara, H., et al. (2018). Plant hormone cytokinins control cell cycle progression and plastid replication in apicomplexan parasites. *Parasitol Int.* 67, 47-58. doi: 10.1016/j.parint.2017.03.003.
- Anjard, C. and Loomis, W. F. (2008). Cytokinins induce sporulation in *Dictyostelium*. *Development* 135, 819-827. doi: 10.1242/dev.018051.
- Aoki, M. M., Kisiala, A. B., Li, S., Stock, N. L., Brunetti, C. R., Huber, R. J., et al. (2019). Cytokinin detection during the *Dictyostelium discoideum* life cycle: Profiles are dynamic and affect cell growth and spore germination. *Biomolecules* 9. doi: 10.3390/biom9110702.
- Aoki, M. M., Kisiala, A. B., Rahman, T., Morrison, E. N., and Emery, R. J. N. (2021). Cytokinins are pervasive among common in vitro culture media: An analysis of their forms, concentrations and potential sources. *J Biotechnol.* 334, 43-46. doi: 10.1016/j.jbiotec.2021.05.005.
- Arnaud, D., Lee, S., Takebayashi, Y., Choi, D., Choi, J., Sakakibara, H., and Hwang, I. (2017). Cytokinin-mediated regulation of reactive oxygen species homeostasis modulates stomatal immunity in *Arabidopsis*. *Plant Cell* 29, 543-559. doi: 10.1105/tpc.16.00583.
- Barth, C., Le, P., and Fisher, P. R. (2007). Mitochondrial biology and disease in *Dictyostelium*. *Intern. Rev. Cytol.* 263, 207–52. doi: 10.1016/S0074-7696(07)63005-8.
- Bokko, P. B., Francione, L., Bandala-Sanchez, E., Ahmed, A. U., Annesley, S. J., Huang, X., et al. (2007). Diverse cytopathologies in mitochondrial disease are caused by AMP-activated protein kinase signaling. *Mol. Biol. Cell* 18, 1874–1886. doi: 10.1091/mbc.e06-09-0881.
- Bozzaro, S. (2019). The past, present and future of *Dictyostelium* as a model system. *Int. J. Dev. Biol.* 63, 321-331. doi: 10.1387/ijdb.190128sb.
- Charette, S. J. and Cosson, P. (2004). Preparation of genomic DNA from *Dictyostelium discoideum* for PCR analysis. *BioTechniques* 36, 574–575. doi: 10.2144/04364bm01.
- Chen, S., Annesley, S. J., Jasim, R. A. F., and Fisher, P. R. (2021). The Parkinson's disease-associated protein DJ-1 protects *Dictyostelium* cells from AMPK-dependent outcomes of oxidative stress. *Cells* 10, 1874. doi: 10.3390/cells10081874.

- Chen, W. W., Freinkman, E., Wang, T., Birsoy, K., and Sabatini, D.M. (2016). Absolute quantification of matrix metabolites reveals the dynamics of mitochondrial metabolism. *Cell* 166, 1324–1337.e11. doi: 10.1016/j.cell.2016.07.040.
- Chen, C., Li, C., Wang, Y., Renaud, J., Tian, G., Kambhampati, S., et al. (2017). Cytosolic acetyl-CoA promotes histone acetylation predominantly at H3K27 in *Arabidopsis*. *Nat. Plants* 3, 814–824. doi: 10.1038/s41477-017-0023-7.
- Concordet, J.-P. and Haeussler, M. (2018). CRISPOR: intuitive guide selection for CRISPR/Cas9 genome editing experiments and screens. *Nucleic Acids Research* 46, W242–W245, doi: 10.1093/nar/gky354.
- Chanclud, E., Kisiala, A., Emery, R. J. N., Chalvon, V., Ducasse, A., Romiti-Michel, C., et al. (2016). Cytokinin production by the rice blast fungus is a pivotal requirement for full virulence. *PLoS Pathog.* 12, e1005457. doi: 10.1371/journal.ppat.1005457.
- Eichinger, L., Pachebat, J. A., Glöckner, G., Rajandream, M.-A., Sucgang, R., Berriman, M., et al. (2005). The genome of the social amoeba *Dictyostelium discoideum*. *Nature* 435, 43–57. doi: 10.1038/nature03481.
- Fey, P., Kowal, A. S., Gaudet, P., Pilcher, K. E., and Chisholm, R. L. (2007). Protocols for growth and development of *Dictyostelium discoideum*. *Nat. Protoc.*, 2, 1307–1316.
- Francione, L. M., Annesley, S. J., Carilla-Latorre, S., Escalante, R., and Fisher, P. R. (2011). The *Dictyostelium* model for mitochondrial disease. *Semin. Cell Dev. Biol.* 22, 120–130. doi:10.1016/j.semcdb.2010.11.004.
- Francione, L., Smith, P. K., Accari, S. L., Taylor, P. E., Bokko, P. B., Bozzaro, S., et al. (2009). *Legionella pneumophila* multiplication is enhanced by chronic AMPK signalling in mitochondrially diseased *Dictyostelium* cells. *Dis Model Mech.* 2, 479–89. doi: 10.1242/dmm.003319.
- Frej, A. D., Clark, J., Le Roy, C. I., Lilla, S., Thomason, P. A., Otto, G. P., et al. (2016). The inositol-3-phosphate synthase biosynthetic enzyme has distinct catalytic and metabolic roles. *Mol Cell Biol.* 36, 1464–79. doi: 10.1128/MCB.00039-16.
- Gaudet, P., Pilcher, K., Fey, P., and Chisolm, R. L. (2007). Transformation of *Dictyostelium discoideum* with plasmid DNA. *Nat Protoc.* 2, 1317–1324. doi: 10.1038/nprot.2007.179.
- Gujjar, R. S. and Supaibulwatana, K. (2019). The mode of cytokinin functions assisting plant adaptations to osmotic stresses. *Plants* (Basel, Switzerland) 8, 542. doi: 10.3390/plants8120542.

- Gupta, R., Anand, G., Pizarro, L., Laor, D., Kovetz, N., Sela, N., et al. (2021). Cytokinin inhibits fungal development and virulence by targeting the cytoskeleton and cellular trafficking. *mBio* 12, e0306820. doi: 10.1128/mBio.03068-20.
- Hardie, D. G. (2004). The AMP-activated protein kinase pathway—new players upstream and downstream. *J. Cell Sci.* 117, 5479–5487. doi: 10.1242/jcs.01540.
- Hinsch, J., Galuszka, P., and Tudzynski, P. (2016). Functional characterization of the first filamentous fungal tRNA-isopentenyltransferase and its role in the virulence of *Claviceps purpurea*. *New Phytol.* 211, 980–992. doi: 10.1111/nph.13960.
- Hinsch, J., Vrabka, J., Oeser, B., Novák, O., Galuszka, P., and Tudzynski, P. (2015). *De novo* biosynthesis of cytokinins in the biotrophic fungus *Claviceps purpurea*. *Environ. Microbiol.* 17, 2935–2951. doi: 10.1111/1462-2920.12838.
- Huber, R. J., Myre, M. A., and Cotman, S. L. (2014). Loss of Cln3 function in the social amoeba *Dictyostelium discoideum* causes pleiotropic effects that are rescued by human CLN3. *PLoS One* 9, e110544. doi: 10.1371/journal.pone.0110544.
- Ihara, M., Taya, Y., and Nishimura, S. (1980). Developmental regulation of cytokinin, spore germination inhibitor discadenine and related enzymes in *Dictyostelium discoideum*. *Exp. Cell Res.* 126, 273–278. doi: 10.1016/0014-4827(80)90265-7.
- Kabbara, S., Bidon, B., Kilani, J., Osman, M., Hamze, M., Stock, A. M., et al. (2020). Cytokinin sensing in bacteria. *Biomolecules* 10, 186. doi: 10.3390/biom10020186.
- Kakimoto, T. (2001). Identification of plant cytokinin biosynthetic enzymes as dimethylallyl diphosphate:ATP/ADP isopentenyltransferases. *Plant Cell Physiol.* 42, 677–685. doi: 10.1093/pcp/pce112.
- Katoh-Kurasawa, M., Hrovatin, K., Hirose, S., Webb, A., Ho, H. I., Zupan, B., et al. (2021). Transcriptional milestones in *Dictyostelium* development. *Genome Res.* 8, 1498-1511. doi: 10.1101/gr.275496.121.
- Kessin, R. H. (2001). *Dictyostelium*: evolution, cell biology, and development of multicellularity. Cambridge, UK: Cambridge University Press.
- Kieber, J. J., and Schaller, G. E. (2018). Cytokinin signaling in plant development. *Development* 145, dev149344. doi: 10.1242/dev.149344.
- Kisiala, A., Kambhampati, S., Stock, N. L., Aoki, M., and Emery, R. J. N. (2019). Quantification of cytokinins using high-resolution accurate-mass orbitrap mass spectrometry and parallel reaction monitoring (PRM). *Analytical Chemistry* 91, 15049-15056. doi: 10.1021/acs.analchem.9b037.

- Knecht D and Pang KM (1995). Electroporation of *Dictyostelium discoideum*. *Methods Mol. Biol.* 47, 321–330. doi: 10.1385/0-89603-310-4:321.
- Kobel-Höller, K., Gley, K., Jochinke, J., Heider, K., Fritsch, V. N., Nguyen, H. V. D., et al. (2018). Calcineurin silencing in *Dictyostelium discoideum* leads to cellular alterations affecting mitochondria, gene expression, and oxidative stress response. *Protist* 169, 584–602. doi: 10.1016/j.protis.2018.04.004.
- Lindner, A. C., Lang, D., Seifert, M., Podlešáková, K., Novák, O., Strnad, M., et al. (2014). Isopentenyltransferase-1 (IPT1) knockout in *Physcomitrella* together with phylogenetic analyses of IPTs provide insights into evolution of plant cytokinin biosynthesis. *J. Exp. Bot.* 65, 2533–2543. doi: 10.1093/jxb/eru142.
- Levi, S., Polyakov, M., and Egelhoff, T. T. (2000). Green fluorescent protein and epitope tag fusion vectors for *Dictyostelium discoideum*. *Plasmid* 44, 231–238. doi: 10.1006/plas.2000.1487.
- Loomis, W. F. (2014). Cell signaling during development of *Dictyostelium*. *Dev. Biol.* 391, 1–16. doi: 10.1016/j.ydbio.2014.04.001.
- Lussey-Lepoutre, C., Hollinshead, K. E., Ludwig, C., Menara, M., Morin, A., Castro-Vega, L. J., et al. (2015). Loss of succinate dehydrogenase activity results in dependency on pyruvate carboxylation for cellular anabolism. *Nat Commun.* 6, 8784. doi: 10.1038/ncomms9784.
- Malecki, M., Kamrad, S., Ralser, M., and Bähler, J. (2020). Mitochondrial respiration is required to provide amino acids during fermentative proliferation of fission yeast. *EMBO Rep.* 21, e50845. doi: 10.15252/embr.202050845.
- Mazur, M., Wojciechowska, D., Sitkiewicz, E., Malinowska, A., Świdarska, B., Kmita, H., et al. (2021). Mitochondrial Processes during early development of *Dictyostelium discoideum*: From bioenergetic to proteomic studies. *Genes* 12, 638. doi: 10.3390/genes12050638.
- Miyawaki, K., Tarkowski, P., Matsumoto-Kitano, M., Kato, T., Sato, S., Tarkowska, D., et al. (2006). Roles of *Arabidopsis* ATP/ADP isopentenyltransferases and tRNA isopentenyltransferases in cytokinin biosynthesis. *Proc. Natl. Acad. Sci. U.S.A.* 103, 16598–16603. doi: 10.1073/pnas.0603522103.
- Morrison, E. N., Emery, R. J. N., and Saville, B. J. (2016). Fungal derived cytokinin are necessary from normal *Ustilago maydis* infection of maize. *Plant Pathology*, 66, 726–742.
- Naseem, M., Othman, E. M., Fathy, M., Iqbal, J., Howari, F. M., AlRemeithi, F. A., et al. (2020). Integrated structural and functional analysis of the protective effects of kinetin

- against oxidative stress in mammalian cellular systems. *Sci Rep.* 10, 13330. doi: 10.1038/s41598-020-70253-1.
- Othman, E. M., Naseem, M., Awad, E., Dandekar, T., and Stopper, H. (2016). The plant hormone cytokinin confers protection against oxidative stress in mammalian cells. *PLoS One.* 11, e0168386. doi: 10.1371/journal.pone.0168386.
- Otto, G. P., Wu, M. Y., Kazgan, N., Anderson, O. R., and Kessin, R. H. (2003). Macroautophagy is required for multicellular development of the social amoeba *Dictyostelium discoideum*. *J. Biol. Chem.* 278, 17636-17645. doi: 10.1074/jbc.M212467200.
- Panchy, N., Lehti-Shiu, M., and Shiu, S.-H. (2016). Evolution of gene duplication in plants, *Plant Physiology* 171, 2294–2316. doi: 10.1104/pp.16.00523.
- Pang, Z., Zhou, G., Ewald, J., Chang, L., Hacariz, O., Basu, N., et al. (2022). Using MetaboAnalyst 5.0 for LC–HRMS spectra processing, multi-omics integration and covariate adjustment of global metabolomics data. *Nat Protoc.* 17, 1735–1761 doi: 10.1038/s41596-022-00710-w.
- Pearce, X. G., Annesley, S. J., and Fisher, P. R. (2019). The *Dictyostelium* model for mitochondrial biology and disease. *Int. J. Dev. Biol.* 63, 497-508. doi: 10.1387/ijdb.190233pf.
- Pertry, I., Václavíková, K., Gemrotová, M., Spíchal, L., Galuszka, P., Depuydt, S., et al. (2010). *Rhodococcus fascians* impacts plant development through the dynamic fas-mediated production of a cytokinin mix. *Mol. Plant Microbe Interact.* 23, 1164-74. doi: 10.1094/MPMI-23-9-1164.
- Rivero, F., and Maniak, M. (2006). Quantitative and microscopic methods for studying the endocytic pathway. *Methods Mol. Biol.* 346, 423-38. doi: 10.1385/1-59745-144-4:423.
- Rubio-Wilhelmi, M. M., Sanchez-Rodriguez, E., Rosales, M. A., Begona, B., Rios, J. J., Romero, L., et al. (2011). Effect of cytokinins on oxidative stress in tobacco plants under nitrogen deficiency. *Environ. Exp. Bot.* 72, 167–173. doi: 10.1016/j.envexpbot.2011.03.005.
- Sakamoto, T., Sakakibara, H., Kojima, M., Yamamoto, Y., Nagasaki, H., Inukai, Y., et al. (2006). Ectopic expression of KNOTTED1-like homeobox protein induces expression of cytokinin biosynthesis genes in rice. *Plant Physiol.* 142, 54-62. doi: 10.1104/pp.106.085811.
- Samanovic, M. I., Hsu, H. C., Jones, M. B., Jones, V., McNeil, M. R., Becker, S. H., et al. (2018). Cytokinin signaling in *Mycobacterium tuberculosis*. *mBio* 9, e00989-18. doi: 10.1128/mBio.00989-18.

- Samanovic, M. I., Tu, S., Novák, O., Iyer, L. M., McAllister, F. E., Aravind, L., et al. (2015). Proteasomal control of cytokinin synthesis protects *Mycobacterium tuberculosis* against nitric oxide. *Mol. Cell* 57, 984-994. doi: 10.1016/j.molcel.2015.01.024.
- Sainero-Alcolado, L., Liaño-Pons, J., Ruiz-Pérez, M. V., and Arsenian-Henriksson, M. (2022). Targeting mitochondrial metabolism for precision medicine in cancer. *Cell Death Differ.* 29, 1304-1317. doi: 10.1038/s41418-022-01022-y.
- Schrimpe-Rutledge, A. C., Codreanu, S. G., Sherrod, S. D., and McLean, J. A. (2016). Untargeted metabolomics strategies-challenges and emerging directions. *J. Am. Soc. Mass Spectrom.* 27, 1897-1905. doi: 10.1007/s13361-016-1469-y.
- Sekine, R., Kawata, T., and Muramoto, T. (2018). CRISPR/Cas9 mediated targeting of multiple genes in *Dictyostelium*. *Sci Rep.* 8, 8471. doi: 10.1038/s41598-018-26756-z.
- Siddique, S., Radakovic, Z. S., De La Torre, C. M., Chronis, D., Novák, O., Ramireddy, E., et al. (2015). A parasitic nematode releases cytokinin that controls cell division and orchestrates feeding site formation in host plants. *Proc. Natl. Acad. Sci. U.S.A.* 112, 12669-74. doi: 10.1073/pnas.1503657112.
- Šimura, J., Antoniadi, I., Široká, J., Tarkowská, D., Strnad, M., Ljung, K., et al. (2018). Plant hormonomics: Multiple phytohormone profiling by targeted metabolomics. *Plant Physiol.* 177, 476-489. doi: 10.1104/pp.18.00293.
- Spinelli, J. B. and Haigis, M. C. (2018). The multifaceted contributions of mitochondria to cellular metabolism. *Nat. Cell Biol.* 20, 745-754. doi: 10.1038/s41556-018-0124-1.
- Stajdohar, M., Rosengarten, R. D., Kokosar, J., Jeran, L., Blenkus, D., Shaulsky, G., et al. (2017). dictyExpress: a web-based platform for sequence data management and analytics in *Dictyostelium* and beyond. *BMC bioinformatics* 18, 291. doi: 10.1186/s12859-017-1706-9.
- Takei, K., Sakakibara, H., and Sugiyama, T. (2001). Identification of genes encoding adenylate isopentenyltransferase, a cytokinin biosynthesis enzyme, in *Arabidopsis thaliana*. *J. Biol. Chem.* 276, 26405-26410. doi: 10.1074/jbc.M102130200.
- Tang, J. X., Thompson, K., Taylor, R. W., and Oláhová, M. (2020). Mitochondrial OXPHOS biogenesis: Co-regulation of protein synthesis, import, and assembly pathways. *Int J Mol Sci.* 21, 3820. doi: 10.3390/ijms21113820.
- Wang, F. F., Cheng, S. T., Wu, Y., Ren, B. Z., and Qian, W. (2017). A bacterial receptor PcrK senses the plant hormone cytokinin to promote adaptation to oxidative stress. *Cell Rep.* 21, 2940-2951. doi: 10.1016/j.celrep.2017.11.017.

- Wang, N., Chen, J., Gao, Y., Zhou, Y., Chen, M., Xu, Z., et al. (2022). Genomic analysis of isopentenyltransferase genes and functional characterization of TaIPT8 indicates positive effects of cytokinins on drought tolerance in wheat, *The Crop Journal*, 11, 46-56. doi: 10.1016/j.cj.2022.04.010.
- Yang, W., Cortijo, S., Korsbo, N., Roszak, P., Schiessl, K., Gurzadyan, A., et al. (2021). Molecular mechanism of cytokinin-activated cell division in *Arabidopsis*. *Science* 371, 1350-1355. doi: 10.1126/science.abe2305.
- Zheng, L., MacKenzie, E. D., Karim, S. A., Hedley, A., Blyth, K., Kalna, G., et al. (2013). Reversed arginosuccinate lyase activity in fumarate hydratase-deficient cancer cells. *Cancer Metab.* 1, 12. doi: 10.1186/2049-3002-1-12.
- Zwack, P. J., De Clercq, I., Howton, T. C., Hallmark, H. T., Hurny, A., Keshishian, E. A., et al. (2016). Cytokinin response factor 6 represses cytokinin-associated genes during oxidative stress. *Plant Physiol.* 172, 1249-1258. doi: 10.1104/pp.16.00415.

CHAPTER 5

PREFACE

- Title: Functional characterization of a Lonely Guy protein in *Dictyostelium discoideum*
- Authors: Megan M. Aoki, Anna B. Kisiala, Scott C. Farrow, Craig R. Brunetti, Robert J. Huber, and R. J. Neil Emery
- Reference: The chapter is currently under preparation for submission. The published version of this manuscript will appear different from the chapter presented here.
- Contributions: Conceptualization M.M.A., C.R.B., R.J.H., and R.J.N.E; Formal analysis, M.M.A. was responsible for all cloning experiments, expression and purification of recombinant protein, enzyme assays, and preparing of samples for mass spectrometry analysis, A.B.K. assisted with mass spectrometry methods, and S.C.F assisted with methodology for cloning, purification of protein, and analysis of enzyme kinetics; Methodology, M.M.A., A.B.K., S.C.F; Supervision, C.R.B., R.J.H., and R.J.N.E.; Writing—original draft, M.M.A.; Writing—review and editing, M.M.A., A.B.K., C.R.B., R.J.H., and R.J.N.E

CHAPTER 5

Functional characterization of a Lonely Guy protein in *Dictyostelium discoideum*

ABSTRACT

Lonely guy (LOG) proteins are phosphoribohydrolases (PRHs) that have been well established as key cytokinin (CK)-activating enzymes within both plant and non-plant CK-producing organisms. During CK biosynthesis, CK-nucleotides (CK-NTs) are the precursors that give rise to the biologically active free base CK form through the one-step reaction catalyzed by LOGs. Putative LOG proteins have been identified in organisms spanning all domains of life. Studies assessing the functional and biochemical characterization of these putative LOGs in bacteria, archaea, algae, and fungi have confirmed LOG/PRH activity in these organisms - many of which had not yet been shown to produce CKs. In many cases, LOG/PRH activity has been assessed only with one subset of NT – either only CK-NTs or non-CK-NTs. Therefore, there is limited knowledge on the substrate specificity of LOGs. In this study, we performed bioinformatic analyses and biochemical characterization of a LOG ortholog (DDB0305758) in the soil-dwelling amoeba, *Dictyostelium discoideum*, which has been shown to produce CKs and is dependent upon CKs for unicellular growth and multicellular development. Here, the *Dd*LOG recombinant protein exhibited LOG/PRH activity on the two tested CK-NTs, *N*⁶-isopentenyladenosine-5'-monophosphate (iPMP) and *N*⁶-benzyladenosine-5'-monophosphate (BAMP), and on one of the non-CK-NTs, adenosine 5'-monophosphate (AMP), but not on 3', 5'-cyclic adenosine-monophosphate (cAMP). There was a higher rate of turnover for CK-NTs over AMP confirming that *Dd*LOG acts as a CK-activating

enzyme; however, it maintains a broader specificity for substrates (AMP) than LOGs found in plants.

KEYWORDS: cytokinin metabolism, LOG protein, PRH activity, cytokinin-activating enzyme, *Dictyostelium discoideum*, kinetics

INTRODUCTION

Cytokinins (CKs) comprise a major class of plant hormones that are best known for their critical roles in plant growth and development (Mok and Mok, 1994; Kieber and Schaller, 2018; Li et al., 2020). Naturally occurring CKs are adenine derivatives with either isoprenoid or aromatic side chains added to the N^6 position of the adenine. The majority of what is documented about these hormones, in relation to their roles in biosynthesis and signaling, is mostly known from plant systems; however, it is becoming increasingly clear that CKs are synthesized by all organisms. The repertoire of CKs continues to be expanded as there is an increasing number of both non-plant and plant-associated organisms from which researchers have documented the production of CKs and the conservation of key CK biosynthesis enzymes – e.g., isopentenyltransferase (IPT) and Lonely Guy (LOG) (Naseem et al., 2015; Nishii et al., 2018). IPTs initiate CK biosynthesis through the addition of an isoprenoid side chain to the N^6 position of AMP/ADP/ATP to form a presumably inactive CK nucleotide (Kakimoto et al., 2001; Takei et al., 2001). The CK nucleotides (CK-NTs) can then be converted into their biologically active free base forms via dephosphoribosylation in a one-step reaction catalyzed by the CK-activating LOG enzymes (Kurakawa et al., 2007; Kuroha et al., 2009).

The first LOG enzyme was discovered in rice, *Oryza sativa*, and was named lonely guy (LOG) after its loss-of-function phenotype for which the rice mutant only had one stamen and no pistil (Kurakawa et al., 2007). Functional characterization of LOGs in two plant species, *Oryza sativa* and *Arabidopsis thaliana*, revealed that these proteins react specifically with CK nucleoside 5'-monophosphates, but not with their di- or tri-phosphate derivatives, nor do they react with AMP (Kurakawa et al., 2007; Kuroha et al., 2009). As

such, researchers refer to LOG proteins as selective towards only CK-NTs as classical LOGs. LOG genes belong to a superfamily (IPR031100) containing a highly conserved PGG_xGT_{xx}E motif which encode phosphoribohydrolases (PRHs) that vary in their substrate specificity. An initial LOG-family protein possessing a PGG_xGT_{xx}E motif was inaccurately annotated as a lysine decarboxylase (LDC), which has resulted in widespread misannotations of putative LOG proteins as LDCs (Pfam: PF03641; Naseem et al., 2018). Recent studies in bacteria, archaea, algae, and fungi assessing the functional and biochemical characterization of putative LOGs, which contained lysine decarboxylase (LDC) annotations, have all shown LOG/PRH activity rather than LDC activity (Hinsch et al., 2015; Seo et al., 2016; Seo and Kim, 2018A; Seo and Kim, 2018B; Moramarco et al., 2019; Mayaka et al., 2019; Nayar, 2021). The misannotation of LOG proteins within databases is starting to be corrected, and there are now two different classifications for the LOG protein family on InterPro: LOG proteins that are selective towards either purine/pyrimidine riboside 5'-monophosphates (NTs) (IPR031100) and LOG proteins selective towards cytokinin riboside 5'-monophosphates (CK-NTs) (IPR005269). Beyond the misannotations of LOGs, some concerns remain about classifying a PRH as a LOG protein if it has not yet been tested with a CK substrate to show specific activity towards CK-NTs (Naseem et al., 2018; Chen et al., 2022). With this in mind, we performed a BLASTp search and identified a single LOG candidate in the soil-dwelling amoeba, *Dictyostelium discoideum* (DDB0305758). We then assessed the CK-activating activity of the protein.

The soil-dwelling amoeba, *D. discoideum*, is a well-established eukaryotic model organism for studying a wide variety of cellular processes, including chemotaxis, cell

motility, autophagy, and differentiation (Kessin, 2001; Bozzaro, 2013). As a model organism, *D. discoideum* is rare in that researchers can study processes during single- and multicellular life cycle stages. *D. discoideum* belongs to the Dictyostelia class within the Amoebozoa phylum, which evolved shortly after the line leading from plants to animals, but before fungi (Bapteste et al., 2002; Eichinger et al., 2005). *D. discoideum* is a rare example with a documented ability to produce cytokinins (CKs) across all life cycle stages with key conserved genes for CK biosynthesis and metabolism that are largely understudied among members of this class of organisms (Anjard and Loomis, 2008; Aoki et al., 2020). It is among a select group of non-plant associated CK producers that have established roles for CK production (Aoki et al., 2019). Even more rare is its production of a novel CK, discadenine, that, to date, has only been documented among the later diverged group 4 species of dictyostelids (Aoki et al., 2020; Schapp, 2011).

In this study, we employed *D. discoideum* as a model organism to study CK metabolism to further understand the possible roles of CKs and conservation of key CK biosynthesis genes beyond plant systems. We combined bioinformatic analyses and biochemical characterization of the DDB0305758 protein to confirm its identity as the only LOG ortholog and CK-activating enzyme in *D. discoideum*. Using multiple CK-NTs and non-CK-NTs as substrates, we show that the protein encoded by *DDB_G0281309* has LOG activity and we furthermore characterize *in vitro* attributes of the recombinant enzyme, which we hereafter name *DdLOG*.

MATERIALS & METHODS

Sequence and bioinformatic analysis

The *DDB_G0281309* DNA and protein sequences were obtained from dictyBase, and homology with other known and putative LOGs was assessed through the dictyBase BLASTp server (E-value, 0.1; Matrix, BLOSUM62; Filter, no; <http://dictybase.org>). The predicted monomeric 3D structure was obtained through AlphaFold, and the proposed dimeric structure was generated through the SWISS-Model server using PDB 5.its.1.A as a template (Jumper et al., 2021; Varadi et al., 2021). Both 3D structures were visualized using the Mol* software (Sehnal et al., 2021; RCSB PDB). Multiple sequence alignment was conducted with the MUSCLE alignment software (Edgar, 2004) using the default parameters in the Lasergene MegAlignPro v. 17.4 program (DNASTAR, Madison, WI, USA).

Cloning of *DDB_G0281309* - *DdLOG*

The *Escherichia coli* strain DH5 α was used for cloning (New England Biolabs, Whitby, Ontario, Canada). Phusion High-Fidelity polymerase (Fisher Scientific, Ottawa, Ontario, Canada) was used for all PCR amplifications. The *DDB_G0281309* gene sequence was obtained from dictyBase, codon optimized, and synthesized for expression in *E. coli* at TWIST Biosciences with adapters (San Francisco, California, USA; Supplementary Table 5.1A). Primers with overhangs were used to facilitate directional cloning into *E. coli* expression vector pOPINF (Fwd primer: 5'-AAGTT CTGTT TCAGG GCCCG GAGAC CGTCA ACAAG ATTAA CAAC-3'; Rev primer: 5'-ATGGT CTAGA AAGCT TTACG CCTGG CTCGA GGTC-3') (Berrow et al., 2007; Supplementary Table 5.1B). The synthetic gene fragment was ligated into the pOPINF vector using the In-Fusion HD cloning kit according to manufacturer's instructions (TakaraBio, San Jose, California,

USA). Sanger sequencing was used to confirm identities of the inserted sequences (Supplementary Table 5.1C).

Protein expression and purification

Constructs were transformed into *E. coli* BL21-Codon Plus(DE3)-RIL cells (Fisher Scientific, Ottawa, Ontario, Canada). Cells were grown overnight at 37°C in 50 mL LB broth supplemented with ampicillin (100 µg/mL) and chloramphenicol (50 µg/mL). Cultures were diluted 1:20 in 2xYT medium (750 mL final volume) supplemented with ampicillin (100 µg/mL) and chloramphenicol (50 µg/mL) and grown to an OD_{600nm} of 0.6-0.8. The cultures were adjusted to room temperature (22°C), and protein expression was induced with isopropyl β-D-thiogalactopyranoside (IPTG) to obtain final concentration of 1 mM IPTG (Fisher Scientific, Ottawa, Ontario, Canada). The cells were allowed to grow at room temperature with shaking (200 rpm) for four hours. Cells were pelleted via centrifugation (5,000 g, 10 minutes) and lysed by sonication in binding buffer (50 mM Tris-HCl pH 8, 50 mM glycine, 500 mM NaCl, 5% v/v glycerol, 20 mM imidazole) supplemented with EDTA-free protease inhibitor (Millipore Sigma, Oakville, Ontario, Canada), 50 µL DNase (New England Biolabs, Whitby, Ontario, Canada), and 0.2 mg/mL lysozyme (Sigma-Aldrich, Oakville, Ontario, Canada). Cell debris was removed by centrifugation (5,000 g, 50 minutes), and the resulting supernatant was filtered through a 0.45 µM glass fiber syringe membrane (Millipore Sigma, Oakville, Ontario, Canada). Soluble proteins were purified with Ni-NTA agarose (Fisher Scientific, Ottawa, Ontario, Canada) and eluted stepwise using a 20 to 400 mM imidazole gradient in elution buffer (50 mM Tris-HCl pH 8, 50 mM glycine, 500 mM NaCl, 5% v/v glycerol). Proteins were buffer-exchanged into 38 mM Tris-HCl pH 7.5, and protein concentrations were quantified with

a Qubit 2.0 Fluorometer (Fisher Scientific, Ottawa, Ontario, Canada) and used immediately for enzyme assays. Recombinant protein was separated by SDS-PAGE to verify the purity and yield (loaded 20 μg); Additionally, western blotting was performed using rabbit polyclonal anti-His primary antibodies (1:1000 dilution; Cell Signaling Technologies, Danvers, Massachusetts) and anti-rabbit IgG secondary antibodies linked to horseradish peroxidase (HRP; 1:2000 dilution; New England Biolabs, Whitby, Ontario).

Biochemical properties and phosphoribohydrolase assays

Optimal conditions for the assay including pH, temperature, and incubation time (within the linear range) were determined using 20 μM N^6 -isopentenyladenosine-5'-monophosphate (iPMP). For pH, standard buffers were used to assess *Dd*LOG activity over a pH range from 3.0-9.0. For temperature, eight different temperatures were assessed ranging from 5°C to 60°C. Lastly to determine an incubation time within the linear range of product formation for the enzyme, three different enzyme concentrations were tested ranging from 10 nM to 500 nM over a 64-minute incubation period assessing product formation every doubling time from 0 to 64 minutes. The optimal conditions from each of these experiments were used for all other enzyme assays described below; Specifically, 500 nM of purified and desalted recombinant protein was incubated with 20 μM of the candidate substrate in a total reaction volume of 40 μl in Tris-HCl buffer (pH 7.5, 38 mM) for 15 minutes at 25°C. Four different substrates were selected to assess classical LOG and standard PRH activity and were screened in triplicate. The substrates were: one isoprenoid cytokinin-nucleotide (CK-NT) previously detected in *D. discoideum* (N^6 -isopentenyladenosine-5'-monophosphate, iPMP; Olchemim Ltd., Olomouc, Czech Republic) (Aoki et al., 2019), one aromatic, non-endogenous CK-NT (N^6 -benzyladenosine-

5'-monophosphate, BAMP; Olchemim Ltd., Olomouc, Czech Republic), and two non-CK-NTs in *D. discoideum* (adenosine 5'-monophosphate, AMP; 3', 5'-cyclic adenosine-monophosphate, cAMP – both from Sigma-Aldrich, Oakville, Ontario, Canada) (Taya, Tanaka, and Nishimura, 1978; Saran et al., 2002). The reaction was stopped by the addition of two volumes of ice-cold methanol and stored at -20°C. The quenched reaction was centrifuged at 20,000 g for 10 minutes and transferred to a new microcentrifuge tube. Denatured proteins and/or no-enzyme reactions were used as negative controls. Identical conditions as described above were used to determine relative PRH activity through % turnover for all substrates accepted by *DdLOG*. The relative PRH enzyme activity was calculated by using the following formula: $\text{product peak area}/(\text{substrate peak area} + \text{product peak area}) \times 100$. Kinetic curves were calculated using the optimal enzyme conditions described above while substituting various concentrations of substrate. GraphPad Prism v. 9 was used to calculate the kinetic constants based on Michaelis-Menten kinetics (GraphPad Software, La Jolla, California, USA). Kinetic experiments were repeated twice for iPMP and AMP with the same results, and thrice for BAMP with consistent irregularity for various substrate concentrations, which is discussed below as a likely solubility issue.

Reaction product identification using HPLC-(ESI+)-HRMS/MS

Samples were either dried down in a vacuum concentrator and resuspended in water-acetonitrile [95:5], v/v with 0.08% glacial acetic acid or diluted directly with that solvent. Prior to processing, all samples were spiked with 20 ng of isotopically labeled CK internal standards (IS) for compound identification or quantification through isotope dilution assay calculations: $^2\text{H}_6\text{iP}$, $^2\text{H}_7\text{BA}$, (Olchemim Ltd., Olomouc, Czech Republic) and/or $^{15}\text{N}_5\text{Ade}$ (Toronto Research Chemicals; Table 5.1). The reaction products for each

substrate were analyzed by high-performance liquid chromatography-positive electrospray ionization-high resolution tandem mass spectrometry (HPLC-(ESI+)-HRMS/MS) using a Dionex UltiMate 3000 HPLC (Thermo Scientific, San Jose, California, USA) coupled to a QExactive Orbitrap HRMS system (Thermo Scientific, San Jose, California, USA). All samples were diluted to a final concentration of 1 μ M to be within the linear range of detection for each substrate and product, determined through a nine-point calibration curve (128 pM to 50 μ M).

Chromatographic separation of both substrates and reaction products was achieved on either an Acclaim RSLC 120 C18 column (2.2 μ m, 3.0 \times 100 mm; Fisher Scientific, Ottawa, Ontario, Canada) or a HALO C18 column (2.7 μ m, 2.1 \times 50 mm; Canadian Life Sciences, Peterborough, Ontario, Canada). For AMP, cAMP, and Ade detection, the Thermo Acclaim C18 column was used at a 0.2 mL/min flow rate with a binary gradient of water (A) and acetonitrile (B), both with 0.08% glacial acetic acid. The initial gradient (0% B) was held for 1.25 min, increased linearly to 50% B over 2.75 min, increased again to 100% B over 0.5 min and held at 100% B for 2.5 min, before returning to initial conditions for 6 min of column re-equilibration, resulting in a total run time of 13.3 min. For BAMP, BA, iPMP, and iP, the HALO C18 column was used at a 0.5 mL/min flow rate with a binary gradient of water (A) and acetonitrile (B), both with 0.08% glacial acetic acid (Kisiala et al., 2019). The initial gradient (5% B) was held for 0.25 min, increased linearly to 40% B over 3.75 min, increased again to 95% B over 0.1 min and held at 95% B for one minute before returning to initial conditions for 2 min of column re-equilibration, resulting in a total run time of 8.2 min. The injection volume for all samples was 25 μ l, and HPLC columns were operated at room temperature (22°C). Samples were kept at 4°C during the

analysis. The eluted substrates and reaction products were analyzed with the QExactive Orbitrap-HRMS equipped with a heated electrospray ionization source (HESI-II) using a modified method optimized for CKs (Kisiala et al., 2019). Auxiliary gas heater and capillary temperatures were 450 and 300°C, respectively; spray voltage was 3.9 kV; sheath, auxiliary, and sweep gases were operated at 30, 8, and 0 respectively; S-lens RF level was 60. Acquisition was performed in positive ion mode simultaneously acquiring data in both full scan (FS) and parallel reaction monitoring (PRM) modes. FS data were acquired at a resolution of 140,000 with automatic gain control (AGC) of 3×10^6 , a maximum injection time (IT) of 524 ms, and a m/z range of 100 to 400 for AMP, cAMP, and Ade, or a m/z range 200 to 450 for BAMP, BA, iPMP, and iP. Parallel Reaction Monitoring (PRM) data was acquired at a resolution of 35,000 with AGC of 3×10^6 , IT of 128 ms, and the normalized collision energy (NCE) was optimized for each individual substrate and reaction product to retain at least 10% of the unfragmented precursor ion. Targeted scan windows were optimized to enhance ion signal intensity for each analyzed compound.

RESULTS and DISCUSSION

Identification of a Lonely Guy ortholog in *Dictyostelium discoideum*

We searched the *D. discoideum* genome (<http://dictybase.org>) for LOG candidates based on amino acid similarity of the previously characterized LOGs in bacteria, archaea, plants, and fungi. These analyses revealed a single putative LOG ortholog in *D. discoideum* with high sequence similarity (35-50% identity) to selected LOG proteins in various CK-producing organisms (Figure 5.1A-D; Supplementary Table 5.2). The single *D. discoideum* LOG (*DdLOG*) candidate is encoded by the gene *DDB_G0281309* and comprised of two

exons (Supplementary Table 5.1A). The encoded protein is 200 amino acids in length. Conserved domain analyses of *Dd*LOG in Pfam databases revealed the presence of a lysine decarboxylase (LDC) domain owing to the highly conserved PGG_xGT_{xx}E motif, while InterPro classifies it within the LOG family as a cytokinin riboside 5'-monophosphate phosphoribohydrolase LOG (InterPro ID: IRP005269). The LDC domain prediction is consistent with those found in other putative LOG proteins that were investigated and characterized as phosphoribohydrolases (PRHs) after showing no experimental LDC activity (Naseem et al., 2018).

Structurally, the predicted *Dd*LOG monomer exhibits a typical Rossmann α - β fold and is made up of seven parallel β -sheets and nine surrounding α -helices (Figure 5.1A; AlphaFold ID: AF-Q54UC5-F1; Jumper et al., 2021; Varadi et al., 2021). Using the SWISS-Model homology modelling platform, *Dd*LOG was searched against experimentally validated crystal structures to predict its *in vitro* conformation. This search resulted in 485 different templates as hits from various LOG and LDC-like proteins. The top 15 hits had at least 90% coverage and 40% sequence similarity to *Dd*LOG. These top hits included characterized LOGs from *Corynebacterium glutamicum*, *Claviceps purpurea*, and *Mycobacterium tuberculosis* – all of which were classified as type-I LOGs, indicating they were dimeric *in vitro* (Figure 5.1B; Seo et al., 2016; Dzurová et al., 2015; Seo and Kim, 2017; Shang et al., 2022). LOGs have been previously separated into two main clusters, each containing a sub-group, based on the phylogenetic analysis of over 120 different LOG-like proteins (Seo and Kim, 2017). Analysis of the amino acid compositions indicate a structural basis for LOG proteins, with type-I proteins comprising dimeric structures and type-II proteins comprising hexameric structures. The subgroups are further

categorized by differences in the amino acid composition at key residues involved in enzyme catalysis, substrate binding, and in the PGG_xGT_{xx}E motif (Seo and Kim, 2017). When comparing the sequence of *Dd*LOG to the key residues of type-Ia/b and type-IIa/b LOGs, *Dd*LOG is classified as a type-Ia. This is consistent with the predicted homo-dimer oligo-state from the SWISS-MODEL homology modelling report (Figure 5.1B).

Multiple sequence alignment of *Dd*LOG with 12 other organisms with either putative or characterized LOG proteins showed numerous conserved residues, previously determined to be critical for PRH catalysis, AMP binding, and prenyl-binding (Seo et al., 2016; Figure 5.1C-D). *Dd*LOG shares the highest sequence identities with the classical LOG proteins of plants, ranging from non-vascular bryophytes like *Marchantia polymorpha* (48%) and *Physcomitrella patens* (50%) to vascular seed plants like *Arabidopsis thaliana* (48%) and *Oryza sativa* (49%) (Supplementary Table 5.2). This is noteworthy as *Dd*LOG accepts substrates that are more typical of the LOG proteins characterized in non-plant organisms (discussed below). A consensus cladogram highlights the conserved domain architecture of the LOG protein family across all domains of life and shows no major expansions of the protein either across species or throughout evolution (Figure 5.2; GenBank Accession numbers, Supplementary Table 5.2).

Biochemical properties of *Dd*LOG

His-tagged *Dd*LOG was expressed in *E. coli* and purified with Ni-NTA agarose to assess its PRH and CK-activating activity. The purified recombinant protein had the expected theoretical mass as determined through SDS-PAGE and western blot (Figure 5.3). To determine the reaction conditions optimal for *Dd*LOG, iPMP substrate was used at a 20 μ M concentration, and conversion from substrate to product was assessed using HPLC-

(ESI+)-HRMS/MS. *DdLOG* activity was the most stable between 20-30°C, with a clear temperature optimum at 25°C (Figure 5.4A). *DdLOG* showed the highest activity between pH 7.0 and 8.0 in Tris-HCl buffer, with a pH optimum of 7.5 (Figure 5.4B). Under these conditions, we assessed product turnover with enzyme concentrations ranging from 10 nM to 500 nM to select an incubation time within the linear product formation range of the enzyme (data not shown). A 500 nM enzyme concentration had the clearest linear range of product formation tested over a 64-minute incubation period. We selected an incubation time of 15-minute for all subsequent *DdLOG* experiments based on the product formation plot (Figure 5.4C).

***DdLOG* is a cytokinin-activating enzyme**

Two CK-NTs, iPMP (isoprenoid CK produced in *D. discoideum*) and BAMP (aromatic CK-NT), and two non-CK-nucleotides, AMP and cAMP, were screened in triplicate as potential substrates for *DdLOG*. These various substrate types served as an assessment of the protein's LOG or PRH activities (Figure 5.5A). Full scan HPLC-(ESI+)-HRMS/MS analysis was used to detect conversion of each substrate to their respective FB reaction products, and labeled internal standards were used to enable accurate compound identification for each free base product assessed (Table 5.1). A no-enzyme reaction and a boiled enzyme reaction were used as negative controls in all the experiments.

Of the tested substrates, *DdLOG* was able to hydrolyze iPMP, BAMP, and AMP, but not cAMP. These results support our hypothesis that it acts as a LOG but also retains the ability to hydrolyze non-CK-NTs (Figure 5.5B; and discussed below). The turnover rates of the two CK-NT substrates, iPMP and BAMP, were higher than that of AMP at

each of the four incubation times assessed (Figure 5.5B). At 30 minutes, iPMP, had almost 95% product turnover, BAMP had 90%, while AMP had only 57%.

Kinetic analysis of *Dd*LOG showed substrate affinities that were comparable, yet somewhat unexpected considering the rate of turnover obtained for the three tested substrates (Figure 5.5B; Figure 5.6). *Dd*LOG exhibited a K_m value of 98 μM with iPMP as a substrate, 16 μM with BAMP, and 59 μM with AMP (Figure 5.6). In all other known cases where both iPMP and AMP were used as substrates for assaying PRH activity in LOGs of both plant and non-plant organisms, the enzyme affinity for iPMP was consistently higher than for AMP in *A. thaliana* (*At*LOG3 iPMP K_m : 14 μM ; AMP: no binding), *O. sativa* (*Os*LOG iPMP K_m : 12 μM ; AMP: no binding), *C. purpurea* (*Cp*LOG iPMP K_m : 4 μM ; AMP: 28 μM), and *M. tuberculosis* (*Mt*LOG iPMP K_m : 6 μM ; AMP: 73 μM) (Kurakawa et al., 2007; Kuroha et al., 2009; Hirsch et al., 2015; Samanovic et al., 2015). Unfortunately, in many recent studies that characterized LOGs in non-plant organisms, CK-NTs were not tested as substrates; thus, we have no such values to use as a comparison to our results. Our relative PRH activity data, as measured by % turnover for all three substrates, supports the previous aforementioned findings indicating LOGs have a higher affinity towards CK-NTs than AMP (Figure 5.5B). For both iPMP and BAMP, at least 90% product turnover was achieved by the 30-minute incubation period, whereas AMP was at 57%. In our kinetic curves, we have reason to believe there may have been some interference in product turnover due to the hydrophobic nature of both BAMP and iPMP over AMP (Figure 5.6). We did not detect any product or substrate inhibition for any of the tested substrates; however, the increasingly high substrate concentrations necessary for obtaining kinetic curves may have been confounded by some insolubility of the

substrates, which would largely affect the final K_m values obtained from BAMP and iPMP (Figure 5.6). According to our supplier information from our three tested substrates, AMP is 5-times more soluble than iPMP in water, and over 100-times more soluble than BAMP. The CK free base products are hydrophobic in nature, which is well known in the CK research community, and has led to researchers synthesizing novel water-soluble CK derivatives that retain their CK properties to be used in large scale agricultural applications (Klos et al., 2022). From the combined data, we conclude that *Dd*LOG acts as a hybrid LOG enzyme, encompassing a broader substrate specificity than previously tested LOGs with activity for both CK-NTs and non-CK-NTs (e.g., AMP).

Insight into the nature of our hybrid *Dd*LOG may come from the proposed dual function of LOG proteins in other organisms. For example, a putative LOG ortholog was identified in *Saccharomyces cerevisiae* during a screen for genes that confer resistance to the mutagenic effects of certain base analogs (Stepchenkova et al., 2005; Carlsson et al., 2018). Completely unrelated to the function of LOG as a CK-activating enzyme, a putative LOG has been studied in *S. cerevisiae* for its role in nucleotide sensing and metabolic detoxification of base analogs that could be misincorporated into RNA or DNA, resulting in possible lethal interference of nucleic acids (Ko, Nishihama, and Pringle, 2008; Carlsson et al., 2013; Burroughs et al., 2015; Carlsson et al., 2018). The yeast LOG protein (YJL055W; referred to as LOG1 in paper) conferred resistance against two commonly used base analogs that have toxic effects on either DNA or RNA – 6-N-hydroxylaminopurine (HAP; purine analogue) and 5-fluorouracil (5-FU; pyrimidine analogue) (Carlsson et al., 2018). These same researchers show that the resistance of LOG1 against 5-FU is partially dependent upon *HAMI*, which is the gene that encodes inosine triphosphate

pyrophosphatase and lies upstream from *LOG1*. The authors conclude that Ham1 and LOG1 likely serve as gatekeepers against non-canonical bases, thus protecting against the misincorporation of a broad range of toxic base analogues into nucleic acids. In that process, Ham1 dephosphorylates bases and LOG1 dephosphoribosylates bases – which, together, mitigates potential harm caused by DNA or RNA misincorporations. This combined evidence paired with the known role of LOG proteins as CK-activating enzymes prompted the authors to propose that LOGs initially had roles in nucleotide sensing and metabolic detoxification, and that the CK activation roles of LOGs were a more recent development (Carlsson et al., 2018).

STRING analysis of *DdLOG* against the *D. discoideum* proteome identified an ortholog to human and yeast inosine triphosphate pyrophosphatase (*D. discoideum* gene ID: DDB_G0286495; protein ID: DDB0238062 – denoted ItpA) as the most highly predicted functional partner to *DdLOG* (database version 11.5, <https://string-db.org/>; von Mering et al., 2005). Therefore, it would be of interest to further assess the relationship between *DdLOG* and ItpA in nucleotide sensing and metabolic detoxification. While it seems the LOG proteins in *A. thaliana* and *O. sativa* are CK-specific and have diverged away from this proposed original function of metabolic detoxification based on their specificity towards CK-NTs, *D. discoideum* may have retained this original function whilst it expanded its binding capacity for CK-NTs so that it now possesses dual functions.

CONCLUSION

Cytokinins (CKs) play a critical role during the life cycle of *D. discoideum*, yet much of their biosynthesis and mechanism of action remain to be characterized and

understood. Through biochemical and bioinformatic analyses, we have characterized a key enzyme involved in CK activation in *D. discoideum*, *DdLOG* (*DDB_G0281309*). We showed that *DdLOG* functions as a classical LOG protein, hydrolyzing BAMP and iPMP, but also as a standard PRH with non-CK-NTs, such as AMP. Our structural analyses indicate *DdLOG* adopts a homo-dimer oligostate *in vitro*, and sequence data supports a type Ia classification. These findings leave many areas to explore in the future with *DdLOG*. Specifically, work is needed to confirm the importance of *DdLOG* in CK activation through gene knockout, as well as investigate any interactions with ItpA for roles in nucleotide sensing and metabolic detoxification. It would be informative to perform evolutionary genomic analyses from *D. discoideum* sister species to identify signatures of natural selection that could give insight into selective pressures acting on CK genes in *D. discoideum* and provide important insights into protein function.

TABLES AND FIGURES

Table 5.1. Free base (FB) products and their respective labeled internal standard compounds scanned for by high-performance liquid chromatography-positive electrospray ionization-high resolution tandem mass spectrometry (HPLC-(ESI+)-HRMS/MS) in all enzyme assay samples. Labeled internal standards obtained from OlChemim Ltd. (Olomouc, Czech Republic) and Toronto Research Chemicals (Toronto, Canada – indicated by *) were used to enable accurate compound identification.

Compound	Molecular Weight	Labeled Internal Standard	Molecular Weight
Product (FB)			
<i>N</i> ⁶ -benzyladenine (BA)	226.10872	² H ₇ BA	233.15266
<i>N</i> ⁶ -isopentyladenine (iP)	204.12437	² H ₆ iP	210.16003
Adenine (Ade)	136.06175	¹⁵ N ₅ Ade*	141.04695

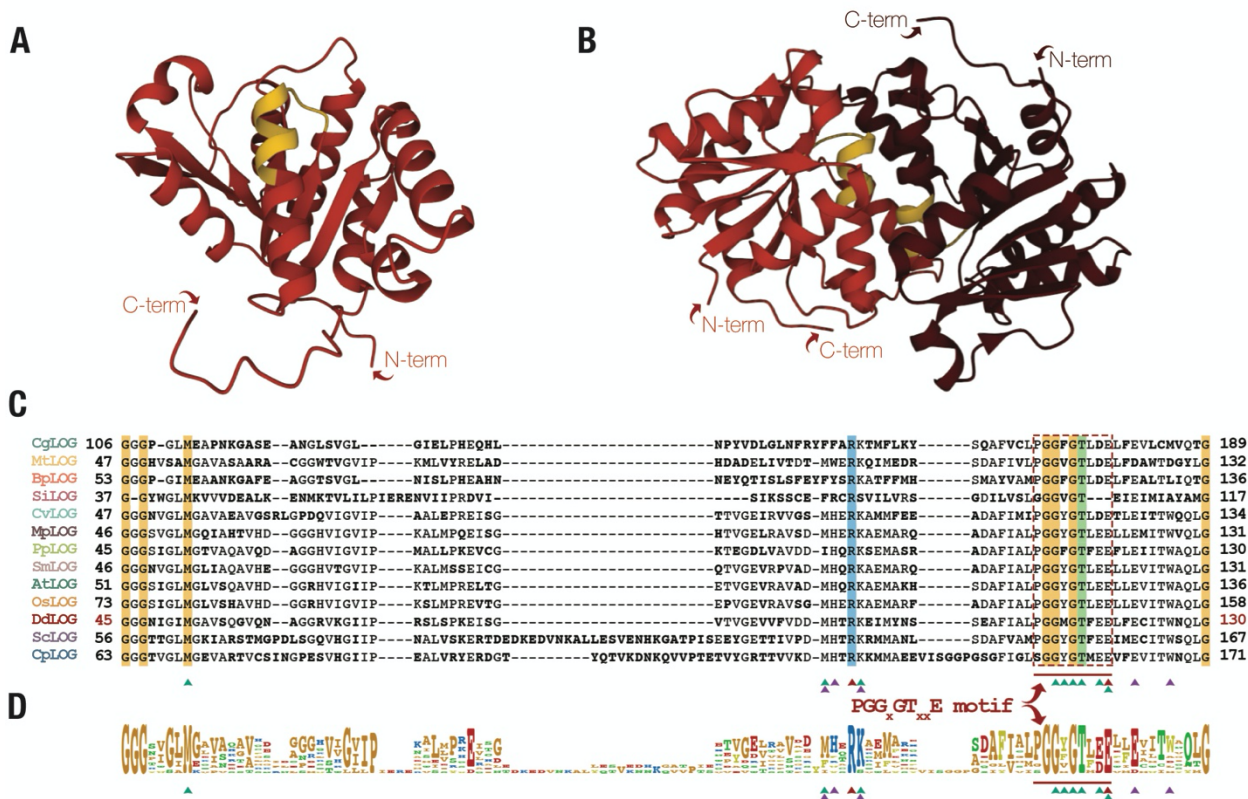


Figure 5.1. Structural and conserved features of *DdLOG*. **A)** The predicted monomeric structure presented as a cartoon diagram (AlphaFold ID: AF-Q54UC5-F1; Jumper et al., 2021; Varadi et al., 2021). **B)** Proposed dimeric structure of *DdLOG* generated through SWISS-Model using PDB: 5its.1.A as the template. The classic PGG_xGT_{xx}E motif of LOG proteins is highlighted in yellow in **A** and **B**, and both structures were visualized using Mol* (Sehna et al., 2021; RCSB PDB). **C)** MUSCLE alignments were performed using *D. discoideum* and 12 representative species from all domains ranging from bacteria to fungi (full names below in E caption) with characterized or putative LOG orthologs. The alignments were made and visualized with DNASTAR MegAlignPro and conserved functional residues across all 13 species are highlighted corresponding to their amino acid chemistry. The PGG_xGT_{xx}E motif is indicated by the dashed red box and red line. The red, teal, and purple triangles represent residues involved in catalysis, AMP binding, and prenyl-binding respectively (Seo et al., 2016). Dashes indicate gaps within the sequence alignment between orthologs. **D)** Sequence logo for the multiple alignment. The figure was generated with DNASTAR MegAlignPro and colors are representative of the amino acid chemistry.

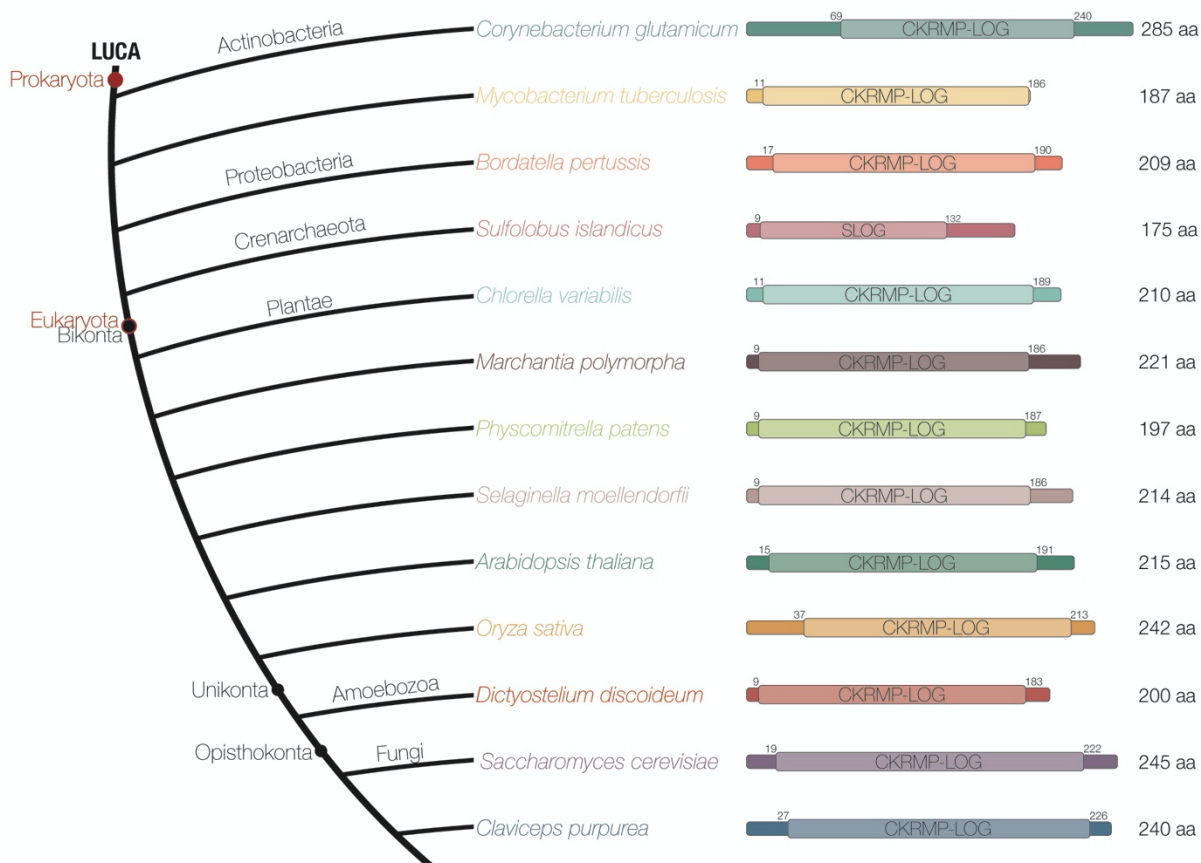


Figure 5.2. Consensus cladogram of the highly conserved LOG protein family. The cladogram shows 13 representative organisms spanning all domains of life (Bacteria: *Corynebacterium glutamicum*, *Mycobacterium tuberculosis*, and *Bordetella pertussis*; Archaea: *Sulfolobus islandicus*; Eukaryota: *Chlorella variabilis*, *Marchantia polymorpha*, *Physcomitrella patens*, *Selaginella mollendorffii*, *Arabidopsis thaliana*, *Oryza sativa*, *Dictyostelium discoideum*, *Saccharomyces cerevisiae*, and *Claviceps purpurea*). The cladogram topology is based on the proposed phylogenetic relationships of organisms as described in Rodriguez-Ezpeleta et al., 2007, Guy and Ettema, 2011, Katz, 2012, and Forterre, 2015, and branch lengths are not intended to describe phylogenetic relationships. The InterPro domain ID, IPR005269, was shared among 12 of the 13 presented species in the cladogram and is named cytokinin riboside 5'-monophosphate phosphoribohydrolase LOG, which was abbreviated to CKRMP-LOG in the domain illustrations in the figure (Blum et al., 2021). Domain sequence positions are listed above the domain, and amino acid lengths are listed to the right of the protein. The archaeal LOG protein from *Sulfolobus islandicus* used in this cladogram was experimentally determined to use AMP as a substrate but was not tested with a CK-NT substrate (Mayaka et al., 2019). It was the only species of the 13 to have the InterPro Domain SLOG cluster4 (ID: IPR041164), which has minimal information on the domain.

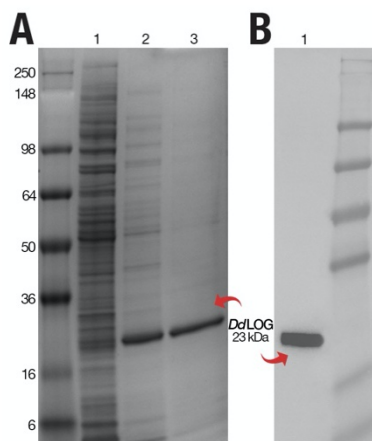


Figure 5.3. SDS-PAGE and western blot of purified *DdLOG* protein from *E. coli* culture. (A) Lanes 1-3 represent the supernatant fraction (1), 100 mM imidazole purified *DdLOG* recombinant protein (2), and 400 mM imidazole purified *DdLOG* recombinant protein (3). The gel was stained with Safety Stain. (B) Western blot using anti-His primary antibody and the 400 mM imidazole purified *DdLOG* recombinant protein (1).

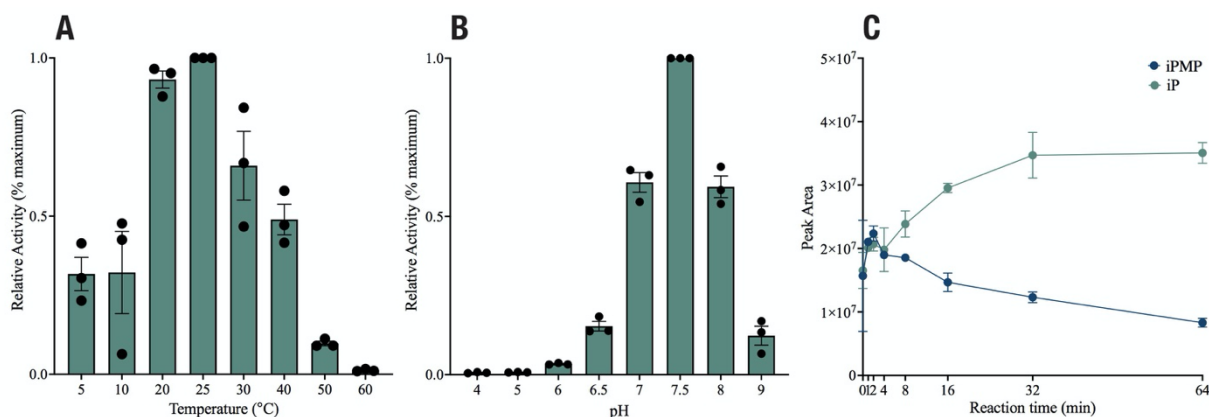


Figure 5.4. *In vitro* characterization of purified and desalted recombinant *DdLOG* using iPMP as a substrate. A) Temperature optimum. B) pH optimum. C) Linear product formation of iP over a 64-minute incubation period using 500 nM *DdLOG* concentration. Values represent the mean product formation of iP from iPMP \pm standard error of 3 independent replicates as measured by HPLC-(ESI+)-HRMS/MS. A and B panels are shown as % maximum based relative to the temperature of pH with the highest iP production. Panel C shows peak area of product and substrate over a 64-minute incubation period. All assays used an initial 20 μ M iPMP substrate concentration.

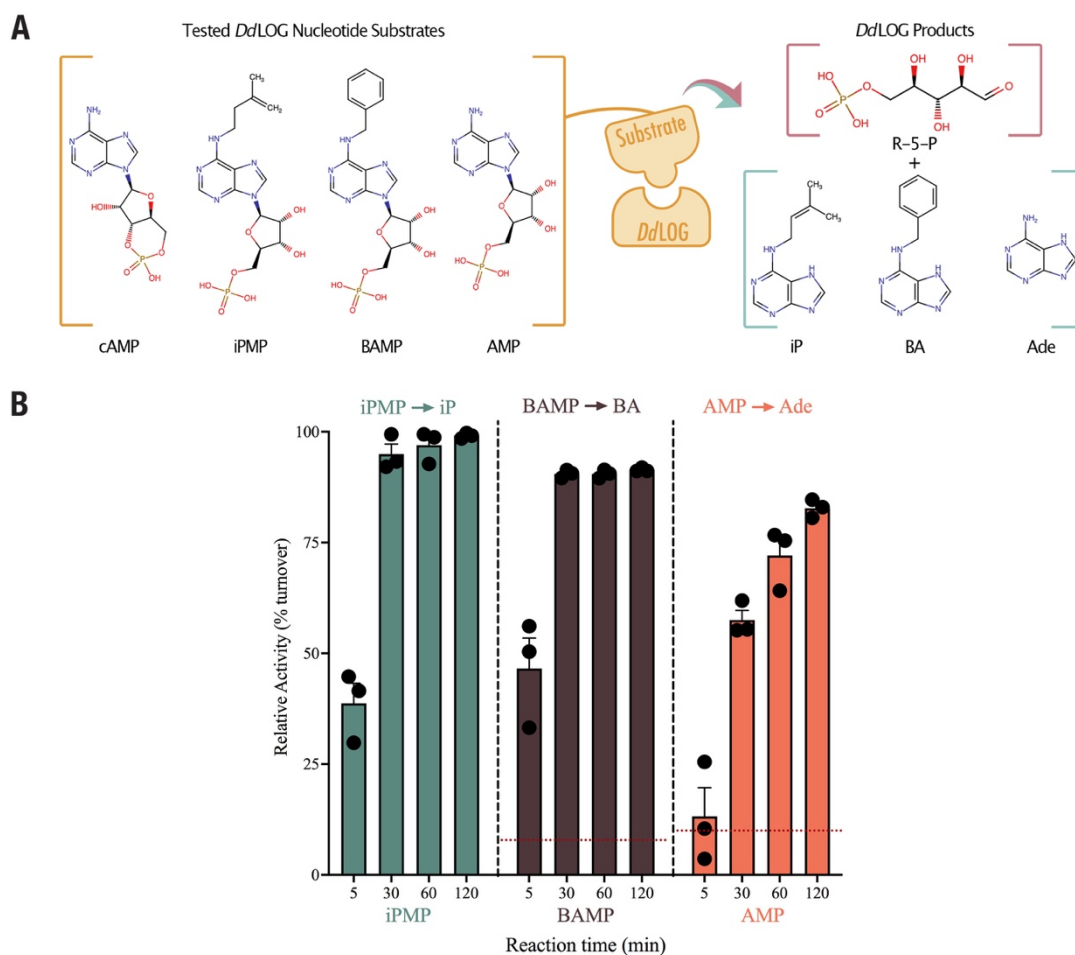


Figure 5.5. Reaction scheme and relative phosphoribohydrolase activity of *DdLOG*. **A)** Reaction scheme of a phosphoribohydrolase (PRH) enzyme. Two cytokinin nucleotides (iPMP and BAMP) and two non-cytokinin nucleotides (AMP and cAMP) were tested to determine whether the putative *DdLOG* acted as a cytokinin riboside 5'-monophosphate phosphoribohydrolase (LOG) or, non-specifically, as a PRH. Ribose-5-phosphate and the respective free base derivatives (BA, iP, or Ade) of the tested substrates are the breakdown products of the reaction. Adenine is the breakdown product for both cAMP and AMP. **B)** Relative PRH activity. Values represent the mean % turnover \pm standard error of 3 independent replicates for each product as measured using HPLC-MS/MS. cAMP is not shown as it was not accepted as a substrate by *DdLOG*. A no-enzyme control was used for each substrate and the levels of the products obtained in each negative control reaction were subtracted as background at each respective time point. The red dotted line indicates the boiled enzyme control turnover for each substrate; iPMP had less than 1% turnover, so a line is not shown.

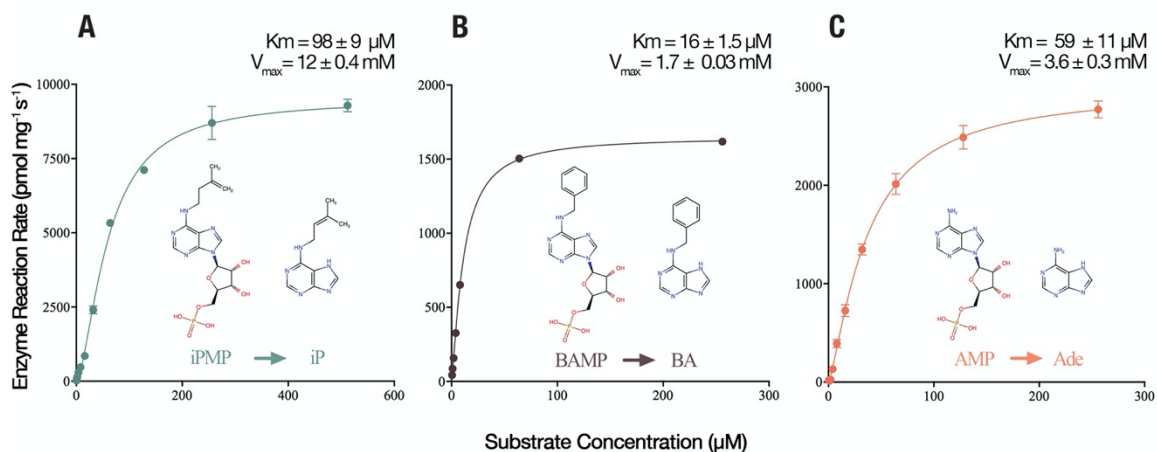


Figure 5.6. Enzyme kinetics of *DdLOG*. A-C are enzyme kinetics of recombinant *DdLOG* using iPMP (A), BAMP (B), and AMP (C) as substrates. Incubation time (15 minutes), protein concentration (500 nM, *DdLOG*), and pH (7.5) were optimized before kinetics. Values represent the mean product formation ($\text{pmol mg}^{-1} \text{ s}^{-1}$) \pm SE for three independent measurements. Any error bars that appear to be missing are smaller than the size of the symbol and are therefore not shown. K_m and V_{max} values are mean \pm SE for three independent measurements and were determined based on Michaelis-Menten kinetics using Prism v. 9.

SUPPLEMENTARY MATERIALS

Supplementary Table 5.1. Gene and primer sequences used for cloning *DdLOG*. All uppercase nucleotides refer to coding region of LOG or primers designed for the coding region. Lowercase nucleotides are specified below the sequence.

A. Native and codon optimized gene sequences used for cloning <i>DdLOG</i> into <i>E. coli</i> .		
	Gene Sequence (5' – 3')	Sequence length
<i>DdLOG</i>	ATGGAAACAGTTAATAAAAATCAATAATATTTGTGTATTTTG TGGAAGTAGAAAAGGAAATGATGAAGTATATATTCAAGTA ACAGAAGTATTAGCTAAAGAAATGGCAAAAAGAAATTATG GATTAATTTATGGTGGTGGTAATATTGGTATTATGGGAGCA GTTTCACAAGGTGTTCAAAATGCCGGTGGAAAGAGTTAAAGG TATCATTCCAAGATCATTATCACCAAAGAAATTTTCAGGTG TAACTGTTGGTGAAGTTGTATTTGTTGATGATATGCACACCA GAAAAGAAATTATGTATAATTCATCCGAAGCTTTTATTGCA TTACCAGGTGGTATGGGTACTTTTGAGGAATTATTTGAATG CATTACATGGAATCAATTAGGTATTCCTCAAACCAGTTG GTATTTTAAATATAAATGGTTATTATGATCCATTAGTAGCAT TATTAACAACAAGTGTGGTAGTGGTTTTGTTGATAGTGATT TTGCAAAATCAATTATTGTTAGTCCGATCCAATTGAATTAT TAAATAAATTAGAATCAACTCCGTCATATAAAAAGTCAATTA AAATGGTTAACATCTTCACAAGCATAA	603 bp
TWIST E. coli codon optimized LOG	gaagtgccattccgctgacctATGGAGACCGTCAACAAGATTAACAAC ATCTGCGTTTTCTGCGGCAGCCGTAAGGGCAACGACGAGGT TTACATCCAGGTCACTGAGGTTTTGGCCAAGGAGATGGCCA AGCGTAACTACGGCCTGATCTACGGCGGCGGAAACATCGG AATCATGGGTGCCGTGTCCAGGGCGTGCAGAACGCTGGCG GCCGCGTAAAGGGCATTATCCCTCGCTCTGTCTCCTAAG GAAATCTCGGGAGTTACCGTGGGCGAGGTGGTCTTCGTAGA CGACATGCATACTCGCAAGGAGATCATGTACAACAGCTCTG AGGCGTTCATCGCGCTCCCGGGCGGCATGGGCACATTGCAA GAGCTGTTGAGTGTATCACCTGGAACCAGCTTGGAATCCA TAGCAAGCCTGTAGGCATCCTTAACATCAACGGCTACTACG ACCCTCTCGTCTCCTGAAGACCTCAGTGGGCTCGGGC TTCGTCGACTCGGACTTCGCGAAGTCGATCATCGTAAGCTC GGACCCGATCGAGCTGTTGAACAAGTTGGAGAGCACCCCAT CTTACAAGTCGCAGCTGAAGTGGTTGACCTCGAGCCAGGCG TGAaggctaggtggaggctcagtg *lowercase regions refer to the TWIST adaptor sequences that were added to the sequence for stability by TWIST Biosciences	646 bp
B. Primers used for amplifying open reading frame for ligation into pOPINF		
	Primer Sequence (5' – 3')	Sequence length
LOG Fwd primer	aagttctgttcaggccccGAGACCGTCAACAAGATTAACAAC	44 bp
LOG Rv primer	atggtctagaagctttaCGCCTGGCTCGAGGTC *lower case regions refer to vector specific overhangs that were added to facilitate directional cloning	34 bp
C. Gene specific primers used for confirming sequence identity with Sanger sequencing		

	Primer Sequence (5' – 3')	Sequence length
LOG Fwd primer	GGGCATTATCCCTCGCTC	18 bp
LOG Rv primer	TTCAGGAGAGCGACGAGA	18 bp

Supplementary Table 5.2. GenBank protein accession numbers and % sequence identity of LOG proteins used to identify *Dd*LOG.

Organism	Accession Number	% Sequence Identity
<i>Dictyostelium discoideum</i>	EAL66951.1	-
<i>Corynebacterium glutamicum</i>	BAB98503.1	26%
<i>Mycobacterium tuberculosis</i>	CCP43961.1	37%
<i>Bordetella pertussis</i>	CAE41549.1	24%
<i>Sulfolobus islandicus</i>	ADX84516.1	-
<i>Chlorella variabilis</i>	EFN51355.1	41%
<i>Marchantia polymorpha</i>	OAE35142.1	48%
<i>Physcomitrium patens</i>	EDQ53599.1	50%
<i>Selaginella moellendorffii</i>	EFJ14638.1	46%
<i>Arabidopsis thaliana</i>	AAD18138.2	48%
<i>Oryza sativa</i>	BAD52880.1	49%
<i>Saccharomyces cerevisiae</i>	CAA89346.1	38%
<i>Claviceps purpureum</i>	CCE28582.1	35%

The amino acid sequences of LOG proteins were inputted into the BLASTp server of dictyBase with the following parameters: E-value, 0.1; Matrix, BLOSUM62; Filter, no (<http://dictybase.org>).

REFERENCES

- Anjard, C. and Loomis, W. F. (2008). Cytokinins induce sporulation in *Dictyostelium*. *Development* 135, 819-827. doi: 10.1242/dev.018051.
- Aoki, M. M., Emery, R. J. N., Anjard, C., Brunetti, C. R., and Huber, R. J. (2020). Cytokinins in *Dictyostelia* – A unique model for studying the functions of signaling agents from species to kingdoms. *Front. Cell Dev. Biol.* 8, 511. doi: 10.3389/fcell.2020.00511.
- Aoki, M. M., Kisiala, A. B., Li, S., Stock, N. L., Brunetti, C. R., Huber, R. J., et al. (2019). Cytokinin detection during the *Dictyostelium discoideum* life cycle: Profiles are dynamic and affect cell growth and spore germination. *Biomolecules* 9, 702. doi: 10.3390/biom9110702.
- Bapteste, E., Brinkmann, H., Lee, J. A., Moore, D. V., Sensen, C. W., Gordon, P., et al. (2002). The analysis of 100 genes supports the grouping of three highly divergent amoebae: *Dictyostelium*, *Entamoeba*, and *Mastigamoeba*. *Proc. Natl. Acad. Sci. U.S.A.* 99, 1414-1419. doi: 10.1073/pnas.032662799.
- Berrow, N. S., Alderton, D., Sainsbury, S., Nettleship, J., Assenberg, R., Rahman, N., et al. (2007). A versatile ligation-independent cloning method suitable for high-throughput expression screening applications. *Nucleic Acids Res.* 35, e45. doi: 10.1093/nar/gkm047.
- Blum, M., Chang, H. Y., Chuguransky, S., Grego, T., Kandasamy, S., Mitchell, A., et al. (2021). The InterPro protein families and domains database: 20 years on. *Nucleic Acids Res.* 49, D344-D354. doi: 10.1093/nar/gkaa977.
- Bozzaro, S. (2013). The Model Organism *Dictyostelium discoideum*. *Methods Mol. Biol.* 983, 17–37. doi: 10.1007/978-1-62703-302-2_2.
- Burroughs, A. M., Zhang, D., Schäffer, D. E., Iyer, L. M., and Aravind, L. (2015). Comparative genomic analyses reveal a vast, novel network of nucleotide-centric systems in biological conflicts, immunity and signaling. *Nucleic Acids Res.* 43, 10633–10654. doi: 10.1093/nar/gkv1267.
- Carlsson, M., Gustavsson, M., Hu, G. Z., Murén, E., and Ronne, H. A. (2013). Ham1p-dependent mechanism and modulation of the pyrimidine biosynthetic pathway can both confer resistance to 5-fluorouracil in yeast. *PLoS One* 8, e52094. doi: 10.1371/journal.pone.0052094.
- Carlsson, M., Hu, G. Z., and Ronne, H. (2018). Gene dosage effects in yeast support broader roles for the LOG1, HAM1 and DUT1 genes in detoxification of nucleotide analogues. *PLoS One* 13, e0196840. doi: 10.1371/journal.pone.0196840.

- Chen, L., Jameson, G. B., Guo, Y., Song, J., and Jameson, P. E. (2022). The LONELY GUY gene family: from mosses to wheat, the key to the formation of active cytokinins in plants. *Plant Biotechnol. J.* 20, 625-645. doi: 10.1111/pbi.13783.
- Dzurová, L., Forneris, F., Savino, S., Galuszka, P., Vrabka, J., and Frébort, I. (2015). The three-dimensional structure of “Lonely Guy” from *Claviceps purpurea* provides insights into the phosphoribohydrolase function of Rossmann fold-containing lysine decarboxylase-like proteins. *Proteins: Struct. Funct., Genet.* 83, 1539–1546. doi:10.1002/prot.24835.
- Edgar, R.C. (2004). MUSCLE: A multiple sequence alignment method with reduced time and space complexity. *BMC Bioinform.* 5, 113. doi: 10.1186/1471-2105-5-113
- Eichinger, L., Pachebat, J. A., Glöckner, G., Rajandream, M.-A., Sucgang, R., Berriman, M., et al. (2005). The genome of the social amoeba *Dictyostelium discoideum*. *Nature* 435, 43–57. doi: 10.1038/nature03481.
- Forterre P. (2015). The universal tree of life: an update. *Front Microbiol.* 6, 717. doi: 10.3389/fmicb.2015.00717.
- Guy, L. and Ettema, T. J. (2011). The archaeal 'TACK' superphylum and the origin of eukaryotes. *Trends Microbiol.* 19, 580-587. doi: 10.1016/j.tim.2011.09.002.
- Hinsch, J., Vrabka, J., Oeser, B., Novák, O., Galuszka, P., and Tudzynski, P. (2015). *De novo* biosynthesis of cytokinins in the biotrophic fungus *Claviceps purpurea*. *Environ. Microbiol.* 17, 2935–2951. doi: 10.1111/1462-2920.12838.
- Jumper, J., Evans, R., Pritzel, A., Green, T., Figurnov, M., Ronneberger, O., et al. (2021). Highly accurate protein structure prediction with AlphaFold. *Nature* 596, 583–589. doi: 10.1038/s41586-021-03819-2.
- Katz, L. A. (2012). Origin and diversification of eukaryotes. *Annu. Rev. Microbiol.* 66, 411-427. doi: 10.1146/annurev-micro-090110-102808.
- Kessin, R. H. (2001). *Dictyostelium*: evolution, cell biology, and development of multicellularity. Cambridge, UK: Cambridge University Press.
- Kieber, J. J., and Schaller, G. E. (2018). Cytokinin signaling in plant development. *Development* 145, dev149344. doi: 10.1242/dev.149344.
- Kisiala, A., Kambhampati, S., Stock, N. L., Aoki, M., and Emery, R. J. N. (2019). Quantification of cytokinins using high-resolution accurate-mass orbitrap mass spectrometry and parallel reaction monitoring (PRM). *Analytical Chemistry* 91, 15049-15056. doi: 10.1021/acs.analchem.9b037.
- Klos, D., Dušek, M., Samol'ová, E., Zatloukal, M., Nožková, V., Nesnas, N., et al. (2022).

- New water-soluble cytokinin derivatives and their beneficial impact on barley yield and photosynthesis. *J. of Agric. Food Chem.* 70, 7288-7301. doi: 10.1021/acs.jafc.2c00981.
- Ko, N., Nishihama, R., and Pringle, J. R. (2008). Control of 5-FOA and 5-FU resistance by *Saccharomyces cerevisiae* YJL055W. *Yeast* 25, 155–160. doi:10.1002/yea.1554.
- Kurakawa, T., Ueda, N., Maekawa, M., Kobayashi, K., Kojima, M., Nagato, Y., et al. (2007). Direct control of shoot meristem activity by a cytokinin-activating enzyme. *Nature* 445, 652–655. doi: 10.1038/nature05504.
- Kuroha, T., Tokunaga, H., Kojima, M., Ueda, N., Ishida, T., Nagawa, S., et al. (2009). Functional analyses of LONELY GUY cytokinin-activating enzymes reveal the importance of the direct activation pathway in *Arabidopsis*. *Plant Cell* 21, 3152–3169. doi: 10.1105/tpc.109.068676.
- Li, S.-M., Zheng, H.-X., Zhang, X.-S., and Sui, N. (2020). Cytokinins as central regulators during plant growth and stress response. *Plant Cell Reports.* 40, 271-282. doi: 10.1007/s00299-020-02612-1.
- Mayaka, J. B., Huang, Q., Xiao, Y., Zhong, Q., Ni, J., and Shen, Y. (2019). The Lonely Guy (LOG) homologue SiRe_0427 from the thermophilic archaeon *Sulfolobus islandicus* REY15A is a phosphoribohydrolase representing a novel group. *Appl. Environ. Microbiol.* 85. doi: 10.1128/AEM.01739-19.
- Mok, D. W., and Mok, M. C. (2001). Cytokinin metabolism and action. *Annu. Rev. Plant Physiol. Plant Mol. Biol.* 52, 89–118. doi: 10.1146/annurev.arplant.52.1.89.
- Moramarco, F., Pezzicoli, A., Salvini, L., Leuzzi, R., Pansegrau, W., and Balducci, E. (2019). A LONELY GUY protein of *Bordetella pertussis* with unique features is related to oxidative stress. *Sci. Rep.* 9, 1–12. doi: 10.1038/s41598-019-53171-9.
- Naseem, M., Bencurova, E., and Dandekar, T. (2018). The cytokinin-activating LOG-family proteins are not lysine decarboxylases. *Trends in Biochemical Sciences* 43, 232–236. doi: 10.1016/j.tibs.2018.01.002.
- Naseem, M., Sarukhanyan, E., and Dandekar, T. (2015). LONELY-GUY knocks every door: Crosskingdom microbial pathogenesis. *Trends Plant Sci.* 20, 781-783. doi: 10.1016/j.tplants.2015.10.017.
- Nayar, S. (2021). Exploring the role of a cytokinin-activating enzyme LONELY GUY in unicellular microalga *Chlorella variabilis*. *Front. Plant Sci.* 11, 611871. doi: 10.3389/fpls.2020.611871.
- Nishii, K., Wright, F., Chen, Y. Y., and Möller, M. (2018). Tangled history of a multigene family: The evolution of ISOPENTENYLTRANSFERASE genes. *PLoS One* 13, 1–

23. doi: 10.1371/journal.pone.0201198.

- Rodríguez-Ezpeleta, N., Brinkmann, H., Burger, G., Roger, A. J., Gray, M. W., Philippe, H., et al. (2007). Toward resolving the eukaryotic tree: The phylogenetic positions of jakobids and cercozoans. *Current Biology*, 17, 1420–1425. doi: 10.1016/j.cub.2007.07.036.
- Samanovic, M. I., Tu, S., Novák, O., Iyer, L. M., McAllister, F. E., Aravind, L., et al. (2015). Proteasomal control of cytokinin synthesis protects *Mycobacterium tuberculosis* against nitric oxide. *Mol. Cell* 57, 984-994. doi: 10.1016/j.molcel.2015.01.024.
- Saran, S., Meima, M. E., Alvarez-Curto, E., Weening, K. E., Rozen, D. E., and Schaap P. (2002). cAMP signaling in *Dictyostelium*. Complexity of cAMP synthesis, degradation and detection. *J. Muscle Res. Cell Motil.* 23, 793-802. doi: 10.1023/a:1024483829878.
- Sehnal, D., Bittrich, S., Deshpande, M., Svobodová, R., Berka, K., Bazgier, V., et al. (2021). Mol* Viewer: Modern web app for 3D visualization and analysis of large biomolecular structures. *Nucleic Acids Res.* 49, W431-W437. doi: 10.1093/nar/gkab314.
- Seo, H. and Kim, K.-J. (2017). Structural basis for a novel type of cytokinin-activating protein. *Sci. Rep.* 7, 45985. doi: 10.1038/srep45985.
- Seo, H. and Kim, K.-J. (2018a). Structural and biochemical characterization of the type-II LOG protein from *Streptomyces coelicolor* A3. *Biochem. Biophys. Res. Commun.*, 499, 577–583. doi: 10.1016/j.bbrc.2018.03.193.
- Seo, H. and Kim, K.-J. (2018b). Structural insight into molecular mechanism of cytokinin activating protein from *Pseudomonas aeruginosa* PAO1. *Environ. Microbiol.* 20, 3214-3223. doi: 10.1111/1462-2920.14287.
- Seo, H., Kim, S., Sagong, H.-Y., Son, H. F., Jin, K. S., Kim, H.-K., et al. (2016). Structural basis for cytokinin production by LOG from *Corynebacterium glutamicum*. *Sci. Rep* 6, 31390. doi: 10.1038/srep31390.
- Shang, L., Li, G., Lin, Q., Ou, M., Liang, J., Xiao, G., et al. (2022). Crystal structure of the cytokinin-producing enzyme "lonely guy" (LOG) from *Mycobacterium tuberculosis*. *Biochem. Biophys. Res. Commun.* 598, 113-118. doi: 10.1016/j.bbrc.2022.01.103.
- Stepchenkova, E. I., Kozmin, S. G., Alenin, V. V., and Pavlov, Y. I. (2005). Genome-wide screening for genes whose deletions confer sensitivity to mutagenic purine base analogs in yeast. *BMC Genet.* 6, 31. doi: 10.1186/1471-2156-6-31.

- Taya, Y., Tanaka, Y., and Nishimura, S. (1978). 5'-AMP is a direct precursor of cytokinin in *Dictyostelium discoideum*. *Nature* 271, 545–547. doi: 10.1038/271545a0.
- Varadi, M., Anyango, S., Deshpande, M., Nair, S., Natassia, C., Yordanova, G., et al. (2022). AlphaFold Protein Structure Database: massively expanding the structural coverage of protein-sequence space with high-accuracy models. *Nucleic Acids Res.* 50, D439–D444. doi: 10.1093/nar/gkab1061.
- von Mering, C., Jensen, L. J., Snel, B., Hooper, S. D., Krupp, M., Foglierini, M., et al. (2005) STRING: known and predicted protein–protein associations, integrated and transferred across organisms. *Nucleic Acids Res.* 33, D433- D437. doi: 10.1093/nar/gki005.

CHAPTER 6

GENERAL DISCUSSION

Prior to this thesis, only two cytokinins (CKs) had been identified in *Dictyostelium discoideum* (*N*⁶-isopentenyladenine and discadenine), and these were implicated in the induction of sporulation and maintenance of spore dormancy (Obata et al., 1973; Taya et al., 1978-cell free; Anjard and Loomis, 2008). All previous research investigating CKs in *D. discoideum* explored roles of CKs during the later stages of multicellular development, leaving questions about whether CKs were involved in regulating growth or other developmental life cycle stages. Therefore, this thesis aimed to capture the full spectrum of CK involvement during the entirety of the *D. discoideum* life cycle with the overarching objective to expand our understanding of the pleiotropic nature of CKs in a non-plant system. The chapters presented in this thesis cover two main themes aimed at further characterizing 1) the *D. discoideum* CK biosynthesis pathway (Chapters 3 and 5), and 2) the pleiotropic roles of CKs (Chapter 4). In this general discussion, important findings related to each experimental chapter are highlighted and future research directions are discussed.

THE *Dictyostelium discoideum* CK BIOSYNTHESIS PATHWAY

The foundation of this thesis was built upon the findings of Chapter 3, which involved comprehensive mass spectrometric screening of over 30 naturally occurring CKs to determine the CK profile during all stages of the *D. discoideum* life cycle. This study revealed that CK production is not solely restricted to the later developmental stages of the *D. discoideum* life cycle. Significant findings in this study were:

1. CKs are produced during each stage of the *D. discoideum* life cycle: growth, aggregation, mound, slug, fruiting body, and spore germination.
2. *D. discoideum* produces six different CKs, representing four more than were previously known: *cis*-zeatin (*cZ*), discadenine (DA), *N*⁶-isopentenyladenine (iP), *N*⁶-isopentenyladenine-9-ribose (iPR), *N*⁶-isopentenyladenine-9-ribose-5' phosphate (iPRP), and 2-methylthio-*N*⁶-isopentenyladenine (2MeSiP).
3. The CK profiles are dynamic, and there is a switch in the dominant CK forms between vegetative growth and early development (iP-type CKs) compared to the DA-centric CK profiles of later development (fruiting body) and germination.
4. *N*⁶-isopentenyladenine (iP) supplementation prolongs the stationary phase of *D. discoideum*, whereas DA has no effect on vegetative growth.

The overall findings presented in Chapter 3 helped to define a pathway by which *D. discoideum* produces CKs and explained the origins of the two previously identified CK forms. The proposed biosynthesis model mapped the six detected *D. discoideum* CKs onto two different activation pathways – the *de novo* pathway catalyzed by adenylate isopentenyltransferases (IPTs), and the tRNA degradation pathway catalyzed by tRNA-isopentenyltransferases (tRNA-IPTs). These two pathways are characteristic of those found in plants (Kamada-Nobusada and Sakakibara, 2009; Spíchal et al., 2012). The preservation of these CK biosynthesis pathways across a wide range of both plant and non-plant organisms speaks to the significance of CKs as key signals. More importantly, the findings laid out in this chapter indicate that there is more to the CK story in *D. discoideum* than the state of knowledge suggested before the start of this thesis. The production of dominant CK forms that differ between early growth and development led to the hypothesis

that CKs perform expanded functions during growth and development, which formed the basis of Chapter 4.

Following the discovery of an expanded CK profile in *D. discoideum*, we wrote an exhaustive review summarizing previous publications that investigated CK-related topics in *D. discoideum* (Chapter 2). This review framed what is known regarding CK biosynthesis and metabolism, CK secretion and translocation, and CK signal transduction in *D. discoideum* and highlighted the utility of the social amoeba as a model eukaryote for studying CKs. From analyses conducted for the review, several orthologs of CK biosynthesis enzymes were identified, including an ortholog of the CK-activating enzyme, Lonely Guy or CK-phosphoribohydrolase. In plants, a phosphoribohydrolase is designated the name Lonely Guy only if it possesses CK-specific phosphoribohydrolase activity against CK substrates (CK- nucleotides; CK-NTs) in light of a loss-of-function phenotype identified in the first characterized CK-specific phosphoribohydrolase enzyme in rice (Kurakawa et al., 2007; Naseem et al., 2018; Chen et al., 2022). In Chapter 5, we functionally characterized the single *D. discoideum* Lonely Guy candidate, *DDB_G0281309*, through recombinant protein expression. As part of this research, we identified a gap in literature surrounding the naming convention of characterized phosphoribohydrolases relating to whether the protein has CK-specific phosphoribohydrolase activity. Therefore, we assessed both CK-NT and non-CK-NT substrates to definitively test the CK-specific activity of the protein encoded by the uncharacterized gene, *DDB_G0281309*. The key findings from this study (Chapter 5) include:

1. The protein encoded by the uncharacterized gene, *DDB_G0281309*, has CK-specific phosphoribohydrolase activity, which merits the designation of *DdLOG*.
2. *DdLOG* has a broader substrate range than plant LOG proteins, whereby it accepts both CK-NTs and the non-CK NT, AMP.
3. STRING analysis identified an ortholog to human/yeast inosine triphosphate pyrophosphatase (ItpA) as the most likely functional partner of *DdLOG*, and this has implications for expanded roles of the protein in nucleotide sensing and metabolic detoxification that remains unexplored.

The combined results from Chapter 5 clarify the assumptions from the proposed CK biosynthesis pathway in Chapter 3 (Figure 3.4) that *DdLOG* acts as CK-phosphoribohydrolase and is responsible for the activation of CKs in *D. discoideum* into their biologically active free base forms. Therefore, these findings establish that *DdLOG*, similar to IptA, is essential for optimal development of *D. discoideum*. Moreover, *DdLOG* encompasses a broader substrate specificity than its plant ortholog counterparts. This further suggests that *DdLOG* retains more functions beyond the unique role of CK activation that is typical of plants.

THE PLEIOTROPIC ROLES OF CYTOKININS

Within the CK research community, it is well-established that CKs are involved in a diverse range of biological processes at both the cellular and developmental level (Kieber and Schaller, 2018; Aoki et al., 2020; Wu et al., 2021; Anand et al., 2022). Novel CK-producing organisms continue to be discovered, and the list of new roles for CKs continues to expand among old and new-CK-producing organisms. Following the expanded CK

profiles in Chapter 3, we developed the hypothesis that CKs have differing roles during the vegetative growth and later multicellular development life cycle stages. To test this hypothesis, knockout and overexpression strains were generated for the primary CK biosynthesis gene, *iptA*, and the effects of *iptA*-deficiency and overexpression were investigated using cell-based assays, transmission electron microscopy, and metabolomics. This multi-tiered approach allowed for the identification of novel CK roles in *D. discoideum* vegetative amoebae that would have not been uncovered by studies that only relied on observable macro-scale phenotypes. The significant findings from this study (Chapter 4) include:

1. IptA has unique roles during vegetative growth and the fruiting body stage of multicellular development in *D. discoideum*.
2. Loss of *iptA* results in impaired cytokinesis.
3. *iptA*-deficiency and overexpression elicits unique sub-cellular phenotypes in line with mitochondrial-associated dysfunction, including altered mitochondrial morphology, dysregulated TCA cycle and amino acid metabolism, and increased AMP levels during vegetative growth.
4. A novel CK-mitochondrial role was established in *D. discoideum* that has not been revealed in other CK-producing organisms.
5. The methodology and research approach for this chapter can be used as a template for uncovering similar subtle biochemical and sub-cellular CK roles in other CK-producing organisms.

The comprehensive approach used in this study allowed for the detection of subtle sub-cellular phenotypes (altered mitochondrial morphology and dysregulation of TCA

cycle and amino acid metabolism) and the establishment of a novel role for CKs in mitochondrial function that would not have been uncovered by cellular-based assays alone. This is the first study, to our knowledge, to identify a link between CKs and mitochondrial and amino acid metabolism. Moreover, this study established that IptA in *D. discoideum* is involved in the classical CK role of cytokinesis.

FUTURE DIRECTIONS

The combined analyses from this thesis yielded new insights in the field of CK research, as well as the *D. discoideum* research community. Prior to the onset of this thesis, CKs were established as one of the few intercellular signals regulating terminal differentiation in late multicellular development (Anjard and Loomis, 2008; Loomis, 2014). In a review of cell signaling during *D. discoideum* development, Loomis (2014) stated that there is a strong advantage for an already established biological signal to be adapted to regulate new biological processes. This is particularly evident when we look at the small subset of molecules that contribute to biological signaling in *D. discoideum* and other organisms. In the case of CKs, this statement provides context for their wide-ranging pleiotropic roles and suggests that they are established biological signals across the wide range of organisms that produce them. The findings of this thesis yielded new insights regarding CK function, but also poses many new questions surrounding the regulation of CK biosynthesis and the molecular mechanisms governing CK involvement in cytokinesis and mitochondrial function in vegetative amoebae.

In Chapter 3, a proposed model of CK biosynthesis was established from our newly identified CK profiles during the life cycle of *D. discoideum* (Figure 3.4; Aoki et al., 2019).

The production of various CK forms requires specific enzymes, which were proposed in the CK biosynthesis pathway. One of the key CK-activating enzymes in the pathway, *DdLOG*, was functionally characterized as a part of this thesis (Chapter 5), but several remain that require similar characterization, including: discadenine synthase responsible for discadenine (putative candidate gene, *DDB_G0267868*), a hydroxylating enzyme of unknown origin responsible for the production of *cis*-zeatin CKs, the tRNA-methylthiolation enzyme responsible for MeSiP-type CKs (putative candidate gene, *DDB_G0287079*), and the two tRNA-IPT enzymes (IptB and IptC). To comprehensively characterize the involvement of these respective CK biosynthesis enzymes, the methodologies laid out in Chapters 4 and 5 should be undertaken to assess both *in vitro* function of the enzymes and *in vivo* function of knockout and overexpression strains in *D. discoideum*.

In Chapter 4, the hypothesis that CKs perform unique functions during growth and development was supported. The distinctive subset of mitochondrial-associated phenotypes requires further study to determine the molecular targets of CKs and the signaling pathways regulating CK-mitochondrial interactions. Investigating *ampka* expression in response to *iptA*-deficiency or overexpression would be a good starting point to determine if AMPK dysregulation occurs and underlies the aberrant mitochondrial phenotypes described in Chapter 4 (Pearce et al., 2019). Furthermore, the MybB transcription factor should be investigated to see if CK promotes the nuclear shuttling of MybB in *D. discoideum* to regulate cell division similarly to that observed in *Arabidopsis thaliana* (Yang et al., 2021).

A central theme of this thesis is the idea of dual or expanded roles for the studied CKs or CK biosynthesis genes in question. As alluded to in the introduction of this section, CKs appear to be well-established biological signals spanning all kingdoms of life, which explains their pleiotropic nature. A question that arose from Chapter 5 involves the potential role of *DdLOG* in nucleotide sensing and metabolic detoxification through interactions with inosine triphosphate pyrophosphatase (ItpA) (Carlsson et al, 2018). For *DdLOG*, as well as the other discussed CK biosynthesis enzymes, it would be of interest to perform evolutionary genomic analyses from *D. discoideum* sister species to identify signatures of natural selection that could give insight into selective pressures acting on these genes in *D. discoideum*.

CONCLUSIONS

With the completion of this Ph.D. thesis comes a greater knowledge of the pleiotropic roles of CKs in the social amoeba, *D. discoideum*. The findings in this thesis confirmed that CKs have temporally separated roles during vegetative growth and the later stages of multicellular development of *D. discoideum*. A new role for CKs was discovered associating these conserved signaling molecules with mitochondrial and amino acid metabolism that raises the question if this is a role unique to *D. discoideum* or is conserved and still to be revealed across other CK-producing organisms. Lastly, a key CK-activating enzyme, *DdLOG*, was characterized, and the remaining enzymes involved in CK biosynthesis were identified for future investigations. The methods established as part of this thesis can be used as a foundation for characterizing the remaining biosynthesis

enzymes and as a guide for detecting subtle sub-cellular phenotypes for CK-related metabolism and beyond.

REFERENCES

- Anand, G., Gupta, R., Marash, I., Leibman-Markus, M., and Bar, M. (2022). Cytokinin production and sensing in fungi. *Microbiological Research* 262, 127103. doi: 10.1016/j.micres.2022.127103.
- Anjard, C. and Loomis, W. F. (2008). Cytokinins induce sporulation in *Dictyostelium*. *Development* 135, 819-827. doi: 10.1242/dev.018051.
- Aoki, M. M., Emery, R. J. N., Anjard, C., Brunetti, C. R., and Huber, R. J. (2020). Cytokinins in Dictyostelia – A unique model for studying the functions of signaling agents from species to kingdoms. *Front. Cell Dev. Biol.* 8, 511. doi: 10.3389/fcell.2020.00511.
- Aoki, M. M., Kisiala, A. B., Li, S., Stock, N. L., Brunetti, C. R., Huber, R. J., et al. (2019). Cytokinin detection during the *Dictyostelium discoideum* life cycle: Profiles are dynamic and affect cell growth and spore germination. *Biomolecules* 9, 702. doi: 10.3390/biom9110702.
- Carlsson, M., Hu, G. Z., and Ronne, H. (2018). Gene dosage effects in yeast support broader roles for the LOG1, HAM1 and DUT1 genes in detoxification of nucleotide analogues. *PLoS One* 13, e0196840. doi: 10.1371/journal.pone.0196840.
- Chen, L., Jameson, G. B., Guo, Y., Song, J., and Jameson, P. E. (2022). The LONELY GUY gene family: from mosses to wheat, the key to the formation of active cytokinins in plants. *Plant Biotechnol. J.* 20, 625-645. doi: 10.1111/pbi.13783.
- Kamada-Nobusada, T. and Sakakibara, H. (2009). Molecular basis for cytokinin biosynthesis. *Phytochemistry* 70, 444–449. doi: 10.1016/j.phytochem.2009.02.007.
- Kieber, J. J. and Schaller, G. E. (2018). Cytokinin signaling in plant development. *Development* 145, dev149344. doi: 10.1242/dev.149344.
- Kurakawa, T., Ueda, N., Maekawa, M., Kobayashi, K., Kojima, M., Nagato, Y., et al. (2007). Direct control of shoot meristem activity by a cytokinin-activating enzyme. *Nature* 445, 652–655. doi: 10.1038/nature05504.
- Loomis, W. F. (2014). Cell signaling during development of *Dictyostelium*. *Dev. Biol.* 391, 1–16. doi: 10.1016/j.ydbio.2014.04.001.
- Naseem, M., Bencurova, E., and Dandekar, T. (2018). The cytokinin-activating LOG-family proteins are not lysine decarboxylases. *Trends in Biochemical Sciences* 43, 232–236. doi: 10.1016/j.tibs.2018.01.002.
- Obata, Y., Abe, H., Tanaka, Y., Yanagisawa, K., and Uchiyama, M. (1973). Isolation of a spore germination inhibitor from a cellular slime mold *Dictyostelium discoideum*.

Agric. Biol. Chem. 37, 1989–1990. doi: 10.1080/00021369.1973.10860941.

Pearce, X. G., Annesley, S. J., and Fisher, P. R. (2019). The *Dictyostelium* model for mitochondrial biology and disease. *Int. J. Dev. Biol.* 63, 497-508. doi: 10.1387/ijdb.190233pf.

Spíchal, L. (2012). Cytokinins - recent news and views of evolutionally old molecules. *Funct. Plant Biol.* 39, 267. doi: 10.1071/FP11276.

Taya, Y., Tanaka, Y., and Nishimura, S. (1978). Cell-free biosynthesis of discadenine, a spore germination inhibitor of *Dictyostelium discoideum*. *FEBS Lett.* 89, 326–328. doi: 10.1016/0014-5793(78)80247-6

Wu, W., Du, K., Kang, X., and Wei, H. (2021). The diverse roles of cytokinins in regulating leaf development. *Hortic. Res.* 8, 118. doi: 10.1038/s41438-021-00558-3.

Yang, W., Cortijo, S., Korsbo, N., Roszak, P., Schiessl, K., Gurzadyan, A., et al. (2021). Molecular mechanism of cytokinin-activated cell division in *Arabidopsis*. *Science* 371, 1350-1355. doi: 10.1126/science.abe2305.

APPENDIX I

Permission from copyright holders

CHAPTERS 1 and 2: Cytokinins in Dictyostelia – A unique model for studying the functions of signaling agents from species to kingdoms.
Published in: *Front. Cell Dev. Biol.* (2020) 8, 511
doi: 10.3389/fcell.2020.00511



Megan Aoki <meganaoki@trentu.ca>
to Frontiers, cellbiology ▾

Sat, Mar 19, 2022, 7:19 PM ☆ ↶ ⋮

Dear **Frontiers** Editorial Office,

I am writing in regards to my 2020 article published in **Frontiers Cell and Developmental Biology** entitled "Cytokinins in Dictyostelia – A unique model for studying the functions of signaling agents from species to kingdoms" (doi: 10.3389/fcell.2020.00511). I would like to include this article in my Ph.D. dissertation. Would you be able to advise me on how to obtain the rights to do so under the current Creative Commons license?

Kind regards,
Megan Aoki



Frontiers in Cell and Developmental Biology <cellbiology@frontiersin.org>
to me ▾

Mon, Mar 21, 2022, 5:20 AM ☆ ↶ ⋮

Dear Megan,

Thank you for your email.

Under a Creative Commons license the authors retain ownership of the work they produce and anyone may use, build upon and redistribute the unmodified work provided they reference it correctly. Providing you reference the article correctly, I don't see there being a problem with including it in your thesis.

Congratulations on nearing the end of your PhD journey, I wish you all the best.

Kind regards,
Reece

Frontiers | Editorial Office - Publishing Development
Journal Manager: Roberta Callari, PhD

CHAPTER 3: Cytokinin detection during the *Dictyostelium discoideum* life cycle: Profiles are dynamic and affect cell growth and spore germination.

Published in: *Biomolecules* 9, 702

doi: 10.3390/biom9110702



Megan Aoki <meganaoki@trentu.ca>
to Biomolecules ▾

Sat, Mar 19, 2022, 7:12 PM ☆ ↶ ⋮

Dear **Biomolecules** Editorial Office,

I am writing in regards to my 2019 article published in **Biomolecules** entitled "Cytokinin detection during the *Dictyostelium discoideum* life cycle: Profiles are dynamic and affect cell growth and spore germination" (doi: 10.3390/biom9110702). I would like to include this article in my Ph.D. dissertation. Would you be able to advise me on how to obtain the rights to do so under the current Creative Commons license?

Kind regards,
Megan Aoki



Biomolecules <biomolecules@mdpi.com>
to me ▾

Mon, Mar 21, 2022, 2:45 AM ☆ ↶ ⋮

Dear Dr. Aoki,

Thank you for your e-mail. Regarding the article below, please note that, it is an open access article, distributed under the Creative Commons Attribution Licence which permits unrestricted use, distribution and reproduction in any medium, provided the original work is properly cited.

Please find more information at the following link:
<https://www.mdpi.com/openaccess>

If any questions, please feel free to contact us.

Kind regards,
Billie Jiao